

COMPLEX DYNAMICS IN THE SPREAD OF COVID-19

Dissertation
for the award of the degree
"Doctor rerum naturalium" (Dr.rer.nat.)
of the Georg-August-Universität Göttingen

within the doctoral program IMPRS Physics of Biological and Complex Systems
of the Georg-August University School of Science (GAUSS)

submitted by
Sebastian Antonio Contreras Gonzalez

From Recoleta, Chile.
Göttingen, 2023

THESIS COMMITTEE:

Prof. Dr. Viola Priesemann, Max Planck Institute for Dynamics and Self-Organization, Göttingen

Prof. Dr. Stefan Klumpp, Institut für Dynamik komplexer Systeme, Georg-August-Universität Göttingen

Prof. Dr. Dr. h.c. Eberhard Bodenschatz, Max Planck Institute for Dynamics and Self-Organization, Göttingen

MEMBERS OF THE EXAMINATION BOARD:

Reviewer: Prof. Dr. Viola Priesemann, Max Planck Institute for Dynamics and Self-Organization, Göttingen

Second Reviewer: Prof. Dr. Stefan Klumpp, Institut für Dynamik komplexer Systeme, Georg-August-Universität Göttingen, Göttingen

FURTHER MEMBERS OF THE EXAMINATION BOARD:

Prof. Dr. Dr. h.c. Eberhard Bodenschatz, Max Planck Institute for Dynamics and Self-Organization, Göttingen

Prof. Dr. Michael Wilczek, Physikalisches Institut Universität Bayreuth, Bayreuth

Jun-Prof. Dr. Anne Wald, Institute for Numerical and Applied Mathematics, Georg-August-Universität Göttingen, Göttingen

Prof. Dr. Theo Geisel, Max Planck Institute for Dynamics and Self-Organization, Göttingen

DATE OF THE ORAL EXAMINATION: 28 April 2023.

*Hay que luchar, luchar y seguir luchando, aunque en ello se nos vaya
la vida.*

— Gladys Marin

Dedicated to Sonia Brunel, Sandra Jara, Ninna Barría, Mónica Álvarez,
María Elena Salazar, my former teachers at the public high-school
Liceo Juan Bautista Contardi, Punta Arenas, Chile. Thank you for
sparkling curiosity and dreams in so many young hearts like mine.

ACKNOWLEDGMENTS

I want to thank my family for their love, which distance nor time has managed to wear. Thanks to my mom, Pilar, and my dad, Ricardo, for their unconditional support. To my siblings, Conita, Vicho, and Mati, for the joy of having them in my life. To my husband, Alvo, for supporting me through the good, the bad, and the ugly of my Ph.D. journey and life in general. Thank you for never doubting my abilities (even in the times I did), for your patience and love, for building a home full of cats with me, and for always giving me something to look forward to in our future.

Thanks to my supervisor, Viola Priesemann, for giving me this unique opportunity of doing science with her and her wonderful group. Thank you for teaching me so much about science, giving me space and tools to build my scientific path, and always caring about us beyond science. Thanks to Jonas, Paul, Simon, Philipp, Joel, Sebastian, Emil, Johannes, and all the members of Viola's Group, for the joy that's doing science and sharing time with you. Special thanks (again) to Philipp, Simon, Álvaro, Martín, Johannes, and Emil for all their help and support in discussing and proofreading this manuscript.

Thank you, Andrés, for your love and constant support. Thank you for inspiring me to study compartmental models and apply them to COVID-19; I've gotten this far only because of you. Thank you, Álvaro, David, Karen, and Anita, for supporting me so much at the beginning of my scientific career. It is a pleasure to have the excuse of doing science together just to see you more often. Thank you, Cata and Joaquin, for always cheering me up and being an endless source of fun. Thanks to Claudia, my dearest friend, for motivating me to always go for more. Thank you for teaching me to believe in myself and to fight for my dreams. Thanks, Cordero, Andrés, and Omar, my *Clan Cui*, for your support and love. Every time I think of my family, I think of you too.

Thanks to the friends I have known here in Germany, Jens, Britta, Alvaro, Robert, Werner, Marc, Andreas, Volki, Heiko, Meile, Ine, Rudi, and most especially to the Member's Club: Jenny, Julius, Nelson, Maite. Thank you for making me feel at home being so far from my roots.

Thank you to everyone who is part of my life, for giving me countless reasons to be grateful.

FUNDING

I gratefully acknowledge support from the Max Planck Society and funding from the German Federal Ministry for Education and Research through the RESPINOW project (031L0298).

ABSTRACT

The COVID-19 pandemic is the most recent example that infectious diseases can disrupt and permanently alter how societies work and interact. This manuscript builds around a series of papers studying disease spread from the point of view of dynamical systems, using the COVID-19 pandemic as a working example. We first study the effect of including test-trace-and-isolate policies in compartmental models and describe their dynamical regimes. We find two tipping points between controlled and uncontrolled spread, defining a novel stable regime at low case numbers where long-term pandemic control is feasible with fewer restrictions. This regime, dependent on the contact behavior and the maximum contact tracing capacity, also maximizes freedom when rolling out a vaccine. Besides, in a minimal model with delayed contact tracing, we found that the delay can induce sustained oscillations through a Hopf bifurcation. We then explored the effects of including behavior as an effective feedback loop between incidence, and both contact rates and vaccination willingness. We found that if the leeway for voluntary action is large enough, a major surge in case numbers is prevented through the behavioral feedback loop. This suggests that societies implicitly agree on an incidence level they tolerate, which in the end constitutes the endemic equilibrium of the disease, and dynamically adapt their behavior to keep case numbers around this level. However, the stability of this equilibrium can be lost through Hopf bifurcations and period-doubling cascades to chaos. This points to the next major research question: How do agents, on average, make decisions with partial information from widely unobserved complex systems? We finish this manuscript proposing a hybrid methodology combining deterministic models for disease spread and stochastic sampling to assess the efficacy of sample selection protocols for, e.g., genomic surveillance, which is adaptable to general dynamical systems that are not in equilibrium.

ZUSAMMENFASSUNG

Die COVID-19-Pandemie ist das aktuellste Beispiel dafür, dass Infektionskrankheiten die Funktionsweise von Gesellschaften dauerhaft verändern können. Dieses Manuskript baut auf einer Reihe von Publikationen auf, in denen die Ausbreitung von Infektionskrankheiten aus der Sicht dynamischer Systeme untersucht wird, wobei die COVID-19-Pandemie als Musterbeispiel dient. Wir untersuchen zunächst die Auswirkungen von Test-Trace-and-Isolate-Maßnahmen (Testen, Kontaktverfolgung und Isolation) in Kompartiment-Modellen und beschreiben deren dynamische Regime. Wir finden zwei Kippunkte zwischen kontrollierter und unkontrollierter Ausbreitung und definieren ein neues stabiles Regime bei niedrigen Fallzahlen, in dem eine langfristige Pandemiekontrolle mit weniger Einschränkungen möglich ist. Dieses Regime, das vom Kontaktverhalten und der maximalen Kapazität der Kontaktverfolgung abhängt, maximiert auch die Freiheit während einer Impfkampagne. In einem minimalen Modell mit verzögerter Kontaktverfolgung fanden wir außerdem, dass die Verzögerung durch eine Hopf-Bifurkation anhaltende Oszillationen hervorrufen kann. Anschließend untersuchten wir die Auswirkungen des menschlichen Verhaltens als effektive Rückkopplungsschleife zwischen Inzidenz und Kontaktverhalten und Impfbereitschaft. Wir fanden heraus, dass ein starker Anstieg der Fallzahlen durch die Verhaltensrückkopplungsschleife verhindert wird, wenn der Spielraum für freiwilliges Handeln groß genug ist. Dies deutet darauf hin, dass sich Gesellschaften implizit auf ein von ihnen toleriertes Inzidenzniveau einigen, das letztlich zum endemischen Gleichgewicht der Krankheit wird, und ihr Verhalten dynamisch anpassen, um die Fallzahlen um dieses Niveau herum zu halten. Die Stabilität dieses Gleichgewichts kann jedoch durch Hopf-Bifurkationen und Periodenverdoppelungskaskaden bis hin zum Chaos verloren gehen. Dies wirft die nächste wichtige Forschungsfrage auf: Wie treffen Agenten im Mittel Entscheidungen auf Basis von Teilinformationen aus weitgehend unbeobachteten komplexen Systemen? Am Ende dieses Manuskripts schlagen wir eine hybride Methode vor, die deterministische Modelle für die Ausbreitung von Krankheiten und stochastische Stichproben kombiniert, um die Wirksamkeit von Stichprobenauswahlprotokollen, z.B. für die genomische Überwachung, zu bewerten. Diese Methode kann an allgemeine dynamische Systeme angepasst werden, die sich nicht im Gleichgewicht befinden.

PUBLICATIONS

This dissertation is the result of research at the Max Planck Institute for Dynamics and Self-Organization, carried out in close collaboration with scientists in Chile (at Universidad de Chile, Universidad de Talca, and Universidad de Magallanes) and worldwide. Some ideas and figures have appeared previously in the research articles, notes, commentaries, and reviews listed below. I also supervised the BSc thesis of Mr. Joel Wagner (jointly with Prof. Dr. Viola Priesemann) and the MSc thesis of Mr. Philipp Dönges.

- [1] Sebastian Contreras*, Jonas Dehning*, Matthias Loidolt*, Johannes Zierenberg, F Paul Spitzner, Jorge H Urrea-Quintero, Sebastian B Mohr, Michael Wilczek, Michael Wibrál, and Viola Priesemann. “The challenges of containing SARS-CoV-2 via test-trace-and-isolate.” In: *Nature communications* 12.1 (2021), pp. 1–13. DOI: <https://doi.org/10.1038/s41467-020-20699-8>.
- [2] Sebastian Contreras*, Jonas Dehning*, Sebastian B Mohr*, Simon Bauer*, F Paul Spitzner*, and Viola Priesemann*. “Low case numbers enable long-term stable pandemic control without lockdowns.” In: *Science advances* 7.41 (2021), eabg2243. DOI: <https://doi.org/10.1126/sciadv.abg2243>.
- [3] Simon Bauer*, Sebastian Contreras*, Jonas Dehning, Matthias Linden, Emil Iftekhar, Sebastian B Mohr, Alvaro Olivera-Nappa, and Viola Priesemann. “Relaxing restrictions at the pace of vaccination increases freedom and guards against further COVID-19 waves.” In: *PLoS computational biology* 17.9 (2021), e1009288. DOI: <https://doi.org/10.1371/journal.pcbi.1009288>.
- [4] Philipp Dönges* et al. “Interplay Between Risk Perception, Behavior, and COVID-19 Spread.” In: *Frontiers in Physics* 10 (2022). ISSN: 2296-424X. DOI: [10.3389/fphy.2022.842180](https://doi.org/10.3389/fphy.2022.842180).
- [5] Karen Y Oróstica*, Sebastian Contreras*, Sebastian B Mohr*, Jonas Dehning*, Simon Bauer, David Medina-Ortiz, Emil N Iftekhar, Karen Mujica, Paulo C Covarrubias, Soledad Ulloa, et al. “Mutational signatures and transmissibility of SARS-CoV-2 Gamma and Lambda variants.” In: *arXiv preprint arXiv:2108.10018* (2021). DOI: <https://doi.org/10.48550/arXiv.2108.10018>.

- [6] Karen Y Oróstica, Sebastian Contreras, Anamaria Sanchez-Daza, Jorge Fernandez, Viola Priesemann, and Álvaro Olivera-Nappa. “New year, new SARS-CoV-2 variant: Resolutions on genomic surveillance protocols to face Omicron.” In: *The Lancet Regional Health–Americas* 7 (2022). DOI: <https://doi.org/10.1016/j.lana.2022.100203>.
- [7] Sebastian Contreras and Viola Priesemann. “Risking further COVID-19 waves despite vaccination.” In: *The Lancet Infectious Diseases* (2021). DOI: [https://doi.org/10.1016/S1473-3099\(21\)00167-5](https://doi.org/10.1016/S1473-3099(21)00167-5).
- [8] Sebastian Contreras, Álvaro Olivera-Nappa, and Viola Priesemann. “Rethinking COVID-19 vaccine allocation: it is time to care about our neighbours.” In: *The Lancet Regional Health–Europe* 12 (2022). DOI: <https://doi.org/10.1016/j.lanepe.2021.100277>.
- [9] Sebastian Contreras, Karen Y Oróstica, Anamaria Daza-Sanchez, Joel Wagner, Philipp Dönges, David Medina-Ortiz, Matias Jara, Ricardo Verdugo, Carlos Conca, Viola Priesemann, et al. “Model-based assessment of sampling protocols for infectious disease genomic surveillance.” In: *Chaos, Solitons & Fractals* 167 (2023), p. 113093. DOI: <https://doi.org/10.1016/j.chaos.2022.113093>.
- [10] Jonas Dehning, Sebastian B. Mohr, Sebastian Contreras, Philipp Dönges, Emil N. Iftekhhar, Oliver Schulz, Philip Bechtle, and Viola Priesemann. “Impact of the Euro 2020 championship on the spread of COVID-19.” In: *Nature Communications* 14.1 (2023), p. 122. ISSN: 2041-1723. DOI: [10.1038/s41467-022-35512-x](https://doi.org/10.1038/s41467-022-35512-x).
- [11] Sebastian Contreras, Jonas Dehning, and Viola Priesemann. “Describing a landscape we are yet discovering.” In: *AStA Advances in Statistical Analysis* (2022), pp. 1–4. DOI: <https://doi.org/10.1007/s10182-022-00449-5>.

Note: Asterisks denote shared first authorship.

CONTENTS

I Background

- 1 Introduction 3
 - 1.1 Infectious diseases and the COVID-19 pandemic 3
 - 1.2 Organization of this manuscript 6
- 2 Mathematical background 11
 - 2.1 Dynamical systems 11
 - 2.1.1 Stability of fixed points 11
 - 2.2 Limit cycles in the plane 12
 - 2.2.1 Poincaré-Bendixson Theorem 13
 - 2.3 Hopf bifurcations 13
 - 2.3.1 Hopf bifurcation in single delay DDEs 14
- 3 Physics of infection and contagion 17
 - 3.1 Pathogens and infection 17
 - 3.2 Contagion 18
 - 3.3 Compartmental models for disease spread 19
 - 3.4 Test-Trace-and-Isolate in ODE compartmental models 22
 - 3.4.1 Linear SIR-TTI model 23
 - 3.4.2 A nonlinear SEIR-TTI model for intermittent interventions 35
 - 3.4.3 A nonlinear minimal SIR-TTI model 36
 - 3.5 Self-regulation of contagious contacts and vaccination willingness 43
 - 3.5.1 Behavioral feedback loops 45
 - 3.5.2 Long-term wave patterns and predictability 46
 - 3.5.3 Short-term rebound waves 46

II Complex dynamics in the spread of COVID-19

- 4 The challenges of containing SARS-CoV-2 via test-trace-and-isolate[†] 49
- 5 Low case numbers enable long-term stable pandemic control without lockdowns[†] 63
- 6 Relaxing COVID-19 restrictions at the pace of vaccination 81
- 7 Interplay Between Risk Perception, Behavior, and COVID-19 Spread[†] 121
- 8 Model-based assessment of sampling protocols for infectious disease genomic surveillance[†] 135

III Discussion and outlook

9	Discussion and outlook	151
9.1	A tale of tipping points	151
9.1.1	TTI-induced tipping points	151
9.1.2	New mechanistic insights to empirical evidence	152
9.2	Endemicity as a social agreement	153
9.3	On the use of compartmental models in disease spread	155
9.4	Ten principles for disease mitigation and control	157
9.5	Future research directions	164
9.5.1	Short-term research projects	164
9.5.2	Long-term research projects	165
9.6	Closing remarks	166
	Bibliography	167

LIST OF FIGURES

Figure 3.1	Linear SIR model including test-trace-and-isolate.	24
Figure 3.2	Fixed points and linear stability of the SIR-TTI model.	34
Figure 3.3	Block diagram of the SEIR-TTI model in Chapter 5.	36
Figure 3.4	Minimal non-linear SIR-TTI model with waning immunity and delayed contact tracing.	37
Figure 3.5	Stability boundary and onset of Hopf bifurcation in the minimal SIR-TTI model.	41
Figure 3.6	Stability of the endemic equilibrium \mathcal{E}_* in the minimal SIR-TTI model.	43
Figure 3.7	Validity of the SIR-TTI model in the unstable regime.	44
Figure 9.1	Our model offers a mechanism for different exponential asymptotic modes of exponential growth.	153
Figure 9.2	Point 1: Mind the tipping points.	157
Figure 9.3	Point 2: Exploit the tipping points.	158
Figure 9.4	Point 3: Mind the distance to criticality.	159
Figure 9.5	Point 4: Hit early.	159
Figure 9.6	Point 5: Hit hard.	160
Figure 9.7	Point 6: Plan your interventions.	160
Figure 9.8	Point 7: Characterize the levels of mixing in the population.	161
Figure 9.9	Point 8: There is no single herd immunity.	162
Figure 9.10	Point 9: Look out for variants.	163

LIST OF TABLES

Table 3.1	Model parameters and values for simulations (linear SIR-TTI model).	33
Table 3.2	Model parameters and values for simulations (minimal nonlinear SIR-TTI model).	42

ACRONYMS

TTI	Test-trace-and-isolate
NPI	Non-pharmaceutical intervention
SIR	Susceptible-Infectious-Removed
SIRS	Susceptible-Infectious-Recovered-Susceptible
SEIR	Susceptible-Exposed-Infectious-Removed
RSV	Respiratory Syncytial Virus
HRV	Human Rhinovirus
ODE	Ordinary Differential Equation
DDE	Delay Differential Equation
LAS	Locally Asymptotically Stable
ABM	Agent Based Model

Part I

BACKGROUND

INTRODUCTION

1.1 INFECTIOUS DISEASES AND THE COVID-19 PANDEMIC

Infectious diseases have posed substantial challenges to societies. The COVID-19 pandemic is only the most recent example, where, besides the high toll of deaths and disease burden, the whole world saw modern lifestyles disrupted and permanently changed. Understanding basic principles on the spreading dynamics of infectious diseases is critical for the well-being of societies. However, this is not an easy task: human behavior, and thus contagion, is complex. Further adding to this complexity, contact networks are plastic, the probability of contagion given contact may not be constant, pathogens causing diseases can evolve and change their properties, and not all variables and parameters can be observed from data. Consequently, statistical physics and the theory of nonlinear dynamical systems find broad applications in revealing, understanding, and quantifying the drivers and mechanisms behind such complexity [1–5].

Part of the complexity of contagion can be understood as a competition between the pathogen’s potential for spread and the awareness of the disease in the population [6–10]. As contagion occurs, newly infected individuals can infect others, thereby contributing to the replication and spread of the pathogen. Conversely, with more infected individuals that become ill or die, other individuals gain awareness and reduce their exposure, thereby reducing their contribution to contagion [11–15]. Mandatory governmental interventions, either pharmaceutical or non-pharmaceutical, can also accompany this response and limit even further disease spread. In that way, the pathogen is subject to a selective pressure that favors their evolution towards more transmissible variants [6, 16]. This co-dependence between adaptation of social patterns and pathogen evolution suggests that diseases have shaped societies as much as societies have filtered which diseases they tolerate [17].

Diseases that are common to a population or region are referred to as *endemic diseases*, and their typical incidence (i.e., number of active cases relative to the total population at the time), as the *endemic equilibrium*. Examples of these diseases are influenza and other respiratory diseases caused by, e.g., Respiratory Syncytial Virus (RSV) or Human Rhinovirus

(HRV). Around their endemic equilibrium, these diseases pose a burden that societies are implicitly willing to accept—a cost which paradoxically often surpasses the costs of eradicating them back in their epidemic phase [17]. Variations of the endemic equilibrium can follow seasonal patterns due to temporal variations on pathogen persistence or population contact patterns [18, 19]. The endemic equilibrium corresponds to a fixed point in the equivalent dynamical system, and thus analyzing its stability and bifurcations can inform epidemiological risk assessment [3, 20–22].

Diseases new to a population are said to "emerge" (or re-emerge if previously eliminated from an area). These epidemic diseases are typically more dangerous than endemic diseases and thus trigger an immediate response to curb their spread [17]. Examples of such are Ebola, Marburg virus disease, and COVID-19. In addition, new diseases can emerge due to zoonosis, i.e., pathogens affecting other species mutating to infect humans, or being endemic to isolated regions and imported to others. Disregarding the source, and compared to endemic diseases, societies invest a substantial effort in controlling outbreaks before they affect a significant part of the population [17, 23]. Mechanistically, mitigation efforts can be included in epidemiological models as feedback loops (e.g., as in [11]), featuring rich long-term dynamics, such as high-periodic wave patterns and period-doubling cascades to chaos [9, 21, 22, 24, 25].

Once a deviation from the endemic equilibrium or the emergence of a new disease with epidemic potential has been reported, policymakers and health authorities deploy a portfolio of interventions to mitigate or contain the spread. These interventions can be pharmaceutical (e.g., distributing vaccines or a functional cure for the disease among the population) or non-pharmaceutical. The latter is essential for a novel disease, as developing vaccines or finding a cure requires time. Non-pharmaceutical intervention (NPI)s can aim to limit the number of contacts in the population (e.g., lockdowns and curfews [20]), reduce the probability of transmission upon contact (e.g., mask mandates, and enforcement of hygiene measures [26, 27]), or produce an ecological interference to disease spread by "removing" individuals from the pool of susceptible individuals (e.g., isolation of risk groups [12]) or infectious individuals (e.g., by Test-trace-and-isolate (TTI) [28–31]). Altogether, the objective is the same: to reduce the spreading rate of the disease.

However, what ultimately determines how effectively these NPI reduce the spreading rate of a disease is the adherence of individuals to them [11, 17, 32]. Individuals adapt their adherence to mandatory NPIs depending on their economic possibilities and needs and their perception of risk [17,

33, 34]. As information about an outbreak becomes available, individuals update their attitude toward the disease and the risk they perceive, which changes their behavior. These behavioral changes can be reflected on different timescales: Individuals decide whether (and how properly) they wear a mask daily and act accordingly [11], but would take longer before accepting a vaccine if hesitant [1, 35]. On the one hand, increased risk perception will motivate individuals to actively engage in protective measures. On the other hand, if they do not feel at risk, complying with seemingly absurd mandates would not appeal to them and thus would increase their rate of contagious contact. This behavior-driven modulation of the spreading rate results from the interplay between information, opinion, behavior, and disease spread and opens a wide variety of dynamical regimes [11, 21, 24, 25].

On a larger timescale, the evolutionary dynamics of the pathogen can play a major role, e.g., new variants with increased transmissibility or partial escape from current immunity could emerge [6, 36–38]. One of the mechanisms used to monitor this evolution is genomic surveillance, where the mutational dynamics of a particular pathogen (and variants thereof) are tracked and quantified [39, 40]. Over time, this allows keeping track of the evolutionary patterns and mutational signatures of pathogens with large epidemic potential, such as influenza (as per the GISAID: Global initiative on sharing all influenza data [41]). However, the reliability of this information depends on i) the strategy to select which samples would be analyzed (sequenced), and ii) the total number of samples that can be analyzed given the installed capacity [40]. Limited sampling challenges the inference of properties in dynamical systems [42, 43] and may introduce systematic bias to observations [44–47]. Despite decreasing costs for sequencing, the high equipment and training costs still pose economic barriers to low-to-middle income countries [39, 48]. This factor, for example, had overarching consequences in the context of the COVID-19 pandemic [49–53].

The COVID-19 pandemic provides an example where all these sources of complexity converge. Here, the world faced an emerging infectious disease, highly transmissible, with marked seasonality, moderate fatality risk, asymptomatic transmission, and a quickly evolving pathogen (SARS-CoV-2), so that containment was challenged due to logistic limitations and misinformation across multiple epidemic waves. Pharmaceutical interventions also took place, but the insufficient protection against infection and the high rate at which new SARS-CoV-2 variants with partial immune escape emerged made it impossible to eradicate

COVID-19 by vaccination. In this manuscript, we seek to answer the following questions:

- Which dynamical regimes can we observe when including [TTI](#) in simple models for COVID-19 spread?
- Is there a sweet spot for long-term policy planning defined by these dynamical regimes?
- How do vaccination and increased immunity expand these regimes?
- How does information about the disease affect contact rates and the willingness to get vaccinated, and thereby the spread itself?
- How does one maximize the information gathered through genomic surveillance of emerging SARS-CoV-2 variants in settings with limited resources?

Answers to these questions find direct application in health policy, especially in the context of the ongoing pandemic. However, we will show that these questions are also exciting and challenging from a physicist's perspective.

1.2 ORGANIZATION OF THIS MANUSCRIPT

This manuscript is divided into three parts, containing nine Chapters in total. The first part, *Background*, presents the context of this research and the mathematical principles of infectious disease modeling. Specific epidemiological concepts will be explained in detail where required. Chapter 2 provides the mathematical foundations required for this work. Chapter 3 goes deeper into the modeling and analysis (i.e., the physics) of infection and contagion. The first sections provide a brief overview of the mechanics of infection and considerations modelers need to have when building epidemiological models. Then, it provides a detailed analysis of the Susceptible-Infectious-Removed ([SIR](#)) model and a study of its variations. Here, we analyze disease spread from the point of view of dynamical systems theory, describing fixed points, their stability, bifurcations, and their implications for epidemiology. This chapter contains original results on the theoretical analysis of simplified versions of the models in Contreras et al. [[20](#), [28](#)].

The second part of this manuscript, *Complex Dynamics in the Spread of COVID-19*, summarizes the papers encompassed in this doctoral dissertation. It contains five Chapters that are identical to the corresponding five publications.

In Chapter 4 (Contreras et al. [28]), we propose a modified version of a linear SIR model to include TTI and use it to analyze the impact of different challenges regarding testing and contact tracing. We first find that including TTI expands the parameter range for which the system is virtually stable, but conditionally; the new zones require the new cases to be within the handling capacity of health authorities (what we call TTI capacity limit), and the linear approximation of the model would deviate as infections increase. We refer to this regime as *a metastable regime at low case numbers*, where TTI helps slow down and eventually stop the spread of the disease. We also identify two tipping points between controlled and uncontrolled spread: (1) the behavior-driven reproduction number of the hidden infections becomes too large to be compensated by TTI, and (2) the number of new infections exceeds the tracing capacity. Finally, our results suggest that TTI alone is insufficient to fully contain outbreaks. This implies that complementary measures like social distancing and improved hygiene remain necessary in the considered period.

In Chapter 5 (Contreras et al. [20]), we demonstrate that the metastable regime at low case numbers in [28] persists in more complex (non-linear) models and provides a sweet-spot for policy planning. In this regime where TTI promptly breaks infection chains and allows for more freedoms, daily cases stabilize around ten or fewer new infections per million people. We further explore the benefits and costs of two different strategies of stabilization that include imposing a short lockdown aiming to drive the current incidence below a given threshold: (i) stabilizing around the TTI capacity (profiting from the slow-down effect that TTI has when efficient), or (ii) stabilizing around the hospital capacity limit (with the excuse of immediate freedom for some of the population). We see that only the first alternative maximizes this freedom and minimizes lockdown time and total cases.

In Chapter 6 (Bauer et al. [54]), we study how to profit from the metastable regime at low case numbers to minimize total mandatory measures when a working vaccine is rolled out. We show that in contrast to strategies lifting all restrictions early, maintaining case numbers at a level where TTI can promptly break chains of infections allows for more freedom in a sustained way, quickly surpassing that of those strategies—which unavoidably implying reintroducing strong measures, such as lockdowns, to control cases. We demonstrate this using a control-theoretical approach. At each time step, we assess whether the current level of infectious contacts can be marginally increased (i.e., lifting restrictions by just a bit) without endangering case numbers surpassing

the **TTI** limit. Here we introduce the effects of interventions acting differently on different age groups, e.g., closing schools or hardening compulsory hygiene measures. Here a new question arises: What would happen if different groups had differing opinions on engaging with mandatory measures based on their perceived risk?

In Chapter 7 (Dönges et al. [11]), we further explore the latter question, changing the focus of mitigation from mandatory measures to voluntary actions. To that end, we model people's voluntary actions as an effective feedback loop between ICU occupancy and i) the current spreading rate and ii) their willingness to accept a vaccine if offered. Including any of these feedback loops plus seasonality has been reported to produce rich long-term dynamics, from highly periodic wave patterns to period-doubling cascades to chaos. See, e.g., [21, 22, 24, 25] and references therein. Here we explore a more practical question: Given current immunity levels and in the face of adverse seasonality, which combination of mandatory interventions produces, in the end, the greater public health outcome? In a scenario analysis, we found that cases where mandatory **NPIs** were too strong to allow for individual action, or not strong at all, had the worst outcomes. On the one hand, if individuals do not feel at risk and do not accumulate naturally acquired immunity, the excess susceptibility fuels rebound waves (see more on this in Dönges [55]). On the other hand, if individuals were forced to continue with their normal contact patterns (i.e., going to work, school, and other non-essential contacts), they could not react sufficiently and protect themselves. Only scenarios where individuals had enough leeway to react voluntarily to moderate levels of risk had the best outcomes, both in winter and spring. However, this occurs where no new SARS-CoV-2 variants would have emerged. If this were the case, how long would it take to detect a novel variant and prepare to counteract it?

In Chapter 8 (Contreras et al. [47]), we propose a hybrid approach to assess the effectiveness of different sampling protocols for genomic surveillance of infectious diseases at a country scale. Using a deterministic ODE model for the simultaneous spread of an arbitrarily large number of SARS-CoV-2 variants, we build a stochastic sampling framework that retrieves a simulated "observed" vector of labels which we use to estimate the share of cases corresponding to each variant. We study two strategies for sample collection between communities and points of entry to the country. We demonstrate that adaptive sampling, i.e., dynamically adapting the limited sequencing capacity to analyze samples collected in the community or at points of entry, outperforms those strategies where a constant number of samples from each source

is always analyzed. In fact, in situations with limited sequencing capacity, adaptive sampling can reduce the expected detection delay of new variants by up to five weeks. Altogether, we quantify the improvement achieved by following the intuitive CARD (Coordinated, Adaptive, Representative, and Differential) rules for sampling protocols for genomic surveillance [40]. Finally, our methodology can be readily adapted to study undersampling (see, e.g., [43]) in other dynamical systems.

Finally, the last part, *Discussion and outlook*, presents a comprehensive analysis of our findings and their implications for the physics of infectious diseases. We summarize these in a few principles for effective mitigation and outline future research directions to continue the results of this PhD thesis.

In this chapter, we provide some basic notions of nonlinear systems and bifurcations required for some demonstrations in Chapter 3. Chapters 4-8 include a in-depth methods section and online appendixes. For a more comprehensive introduction to nonlinear dynamical systems please refer to Strogatz [56].

2.1 DYNAMICAL SYSTEMS

We will define a *dynamical system* as a system with functional dependence on time. Although the definition is less restrictive, for this work we will focus on dynamical systems represented by Ordinary Differential Equation (ODE) and Delay Differential Equation (DDE). The general form for an ODE dynamical system is given by:

$$\dot{\vec{x}} = F(\vec{x}, t) \quad (2.1)$$

We will say that the system is autonomous when $F(\vec{x}, t) = F(\vec{x})$. Note that we can convert a non-autonomous system into an autonomous one by increasing the order of the system by one:

$$\vec{z} = \begin{pmatrix} \vec{x} \\ t \end{pmatrix}, \quad \frac{d}{dt}\vec{z} = \begin{pmatrix} \dot{\vec{x}} \\ 1 \end{pmatrix} = \tilde{F}(\vec{z}) \quad (2.2)$$

We will understand as *fixed points* of an autonomous dynamical system those vectors $\vec{x}_0 \in \mathbb{R}^n$ where $F(\vec{x}_0) = 0$, and thus $\dot{\vec{x}}|_{x=x_0} = 0$. In other words, the state of the system does not vary over time if starting at the fix point. However, how do trajectories starting slightly away from it behave?

2.1.1 Stability of fixed points

Assume that x_0 is a fixed point of the autonomous system $\dot{x} = F(x)$, i.e., that $F(x_0) = 0$. How do solutions starting close to x_0 behave? For a perturbed trajectory starting arbitrarily close to the fix point, i.e., at $x_0 + \epsilon$, we can do Taylor expansion:

$$\frac{d}{dt}(x_0 + \epsilon) = \underbrace{F(x_0)}_{=0} + JF(x_0)\epsilon + o(\epsilon^2) \Leftrightarrow \frac{d\epsilon}{dt} = JF(x_0)\epsilon + o(\epsilon^2). \quad (2.3)$$

(note that $\epsilon \in \mathbb{R}^n$, and thus the exponent in ϵ^2 is not directly the square but denotes higher order terms). Disregarding higher order terms for ϵ , the linear stability of the system (i.e., whether perturbations will grow or decay) is determined by the eigenvalues of the Jacobian matrix of F evaluated at the fixed point $JF(x_0)$.

We will say that the fixed point is *hyperbolic* if the real part of all eigenvalues is different than zero. In virtue of the *Hartman-Grobman* theorem, the local phase portrait (i.e., dynamical regimes of a nonlinear dynamical system) near a hyperbolic fixed point is topologically equivalent to the phase portrait of the linearization [56]; the classification of the linear system holds for the nonlinear system.

We will say that a fixed point is a *stable attractor* if the real part of all eigenvalues of the linearized system evaluated on it is strictly negative. If the real part of all eigenvalues is strictly positive, then the fixed point is an *unstable attractor* (or a repeller). If there is a pair of eigenvalues with different sign, then the fixed point is a *saddle*.

Some systems with a single fixed point can have different pathways to instability. Consider, for example, a system of coupled reactors where a certain quantity could be amplified or damped depending on a single control parameter. If one of them is in an amplifying condition, then the slightest coupling with other compartments even in damping conditions can drive the whole system unstable.

2.2 LIMIT CYCLES IN THE PLANE

A limit cycle is an isolated closed trajectory [56]. Closed implies periodicity, and isolated implies that neighboring trajectories are not closed and approach or diverge from the limit cycle. They are easier to understand in polar coordinates, where they are represented by fixed points on the differential equation of the radius.

Linear systems allow for oscillatory behavior, but the only solution that is closed is not isolated. We illustrate that in the following example. Consider the 2D system:

$$\frac{dx}{dt} = \begin{pmatrix} \alpha & -\beta \\ \beta & \alpha \end{pmatrix} x. \quad (2.4)$$

The eigenvalues of the system's matrix are $\alpha \pm i\beta$, thus all solutions will spiral inwards or outwards depending on whether α is smaller or larger than zero. If $\alpha = 0$, then trajectories are closed, but so are all those in a neighborhood of the solution. Therefore, these are not isolated. We can thus conclude that limit cycles are a non-linear phenomena.

2.2.1 Poincaré-Bendixson Theorem

This theorem proves the existence of limit cycles in certain conditions. As enunciated in Strogatz [56], a trajectory C confined in a closed, bounded subset of the plane R is a closed orbit (or spirals towards it as $t \rightarrow \infty$) if:

- $\dot{x} = f(x)$ is a continuously differentiable vector field on an open set containing R
- R does not contain any fixed points.

The intuition behind this is the following: First, we find an unstable fixed point, i.e., trajectories starting close to it escape from it. Then we construct a "trapping region", i.e., a bounded subset of the plane where the vector field $f(x)$ always points inwards that has "a hole" where the fixed point is. Then, we call this trapping region R and we can conclude that there is a limit cycle therein. References to the subtleties and formalities of the proof are given in Strogatz [56].

Although the definition of limit cycles seems restrictive, there is a particular kind of bifurcation that generates them; the Hopf bifurcation.

2.3 HOPF BIFURCATIONS

Consider a 2D dynamical system, where the eigenvalues of its linearized version around a fixed point depend on a control parameter. As we vary it, the system can turn unstable in different ways. Unlike 1D systems, 2D systems can already feature oscillatory solutions. Hopf bifurcations are a particular case of those, when a stable fixed point turns unstable and features a limit cycle. For this, two complex conjugate eigenvalues simultaneously cross the imaginary axis (from left to right) with nonzero

speed, and turn unstable. As other bifurcations, these come in super and subcritical variants, which are thoroughly described in Strogatz [56]. Here, we analyze the necessary and sufficient conditions to have a Hopf bifurcation (of any kind) in a single delay DDE.

2.3.1 Hopf bifurcation a 2D DDE system with a single delay τ

Consider a 2D DDE system and its linearization around a fixed point

$$x'(t) = Ax(t) + Bx(t - \tau). \quad (2.5)$$

We can study the linear stability of this system as in ODE, using the trial solutions $x(t) = \vec{v} \exp(\mu t)$. Note that the notation is not the classical one and we use μ instead of λ , which we reserve for model parameters throughout the next chapters. Plugging this ansatz into eq. 2.5, we obtain the condition

$$\begin{aligned} \mu \vec{v} \exp(\mu t) &= A \vec{v} \exp(\mu t) + B \exp(-\mu \tau) \vec{v} \exp(\mu t), \\ \Leftrightarrow 0 &= (A - \mu I_{2 \times 2} + B \exp(-\mu \tau)) \vec{v}, \end{aligned}$$

implying that nontrivial solutions must be found by solving the transcendental equation

$$p(\mu, \tau) = \det(A - \mu I_{2 \times 2} + B \exp(-\mu \tau)) = 0. \quad (2.6)$$

The system above undergoes a Hopf bifurcation at $\tau = \tau_{\text{crit}}$ if:

- The eigenvalues are purely imaginary, i.e.,

$$\mu_{\text{crit}} = i\phi. \quad (2.7)$$

- The imaginary axis is crossed with a nonzero speed, i.e.,

$$\text{Re} \left(\frac{d\mu}{d\tau} \right) \Big|_{\tau=\tau_{\text{crit}}} \neq 0. \quad (2.8)$$

Note that these conditions are simplified from the general case as our system is 2D, thus has only a pair of complex conjugates as eigenvalues. For more general cases, the reader is referred to Orosz [57] and Strogatz [56].

Imposing the first condition into the transcendental equation eq. 2.6 generates two nonlinear equations which we need to solve for τ and ϕ :

$$\operatorname{Re}(p(\mu = i\phi, \tau = \tau_{\text{crit}})) = 0, \quad (2.9)$$

$$\operatorname{Im}(p(\mu = i\phi, \tau = \tau_{\text{crit}})) = 0. \quad (2.10)$$

The second condition can be obtained by implicit derivation of eq. 2.6 with respect to τ ;

$$\frac{dp}{d\tau} = \frac{\partial p}{\partial \mu} \frac{d\mu}{d\tau} + \frac{\partial p}{\partial \tau} = 0, \quad \Rightarrow \frac{d\mu}{d\tau} = -\frac{\frac{\partial p}{\partial \tau}}{\frac{\partial p}{\partial \mu}}. \quad (2.11)$$

We then have

$$\operatorname{Re}\left(\frac{d\mu}{d\tau}\right)\Big|_{\mu=i\phi, \tau=\tau_c} = \operatorname{Re}\left(-\frac{\frac{\partial p}{\partial \tau}}{\frac{\partial p}{\partial \mu}}\right)\Big|_{\mu=i\phi, \tau=\tau_c}. \quad (2.12)$$

However, we can also calculate the total derivative of eq. 2.6 with respect to μ ;

$$\frac{dp}{d\mu} = \frac{\partial p}{\partial \mu} + \frac{\partial p}{\partial \tau} \frac{d\tau}{d\mu} = 0, \quad \Rightarrow \left(\frac{d\mu}{d\tau}\right)^{-1} = -\frac{\frac{\partial p}{\partial \tau}}{\frac{\partial p}{\partial \mu}}. \quad (2.13)$$

Therefore, we can also write the second condition for a Hopf bifurcation as

$$\operatorname{Re}\left(\frac{d\mu}{d\tau}\right)\Big|_{\mu=i\phi, \tau=\tau_c} = \operatorname{Re}\left(\left(\frac{d\mu}{d\tau}\right)^{-1}\right)\Big|_{\mu=i\phi, \tau=\tau_c}. \quad (2.14)$$

In this chapter, we provide a very brief overview of and links to some relevant literature on the physics of the different phenomena involved at the different scales relevant to infection and contagion. For a topic-specific survey of the state-of-the-art, the reader is referred to the Introduction section in Chapters 4–8. This chapter also contains original results exploring the physics of the model in Chapter 4 (Section 3.4.1) and of a simpler version of the model in Chapter 5 (Section 3.4).

3.1 PATHOGENS AND INFECTION

The game of life occurs at all scales, and pathogens are certainly part of it. The principle is the same; they hijack part of the machinery of host organisms/ecosystems to complete their life cycle. Among the most common pathogens, we find bacteria and viruses. Bacterial infections are typically aggressive but have been largely controlled since the discovery of penicillin and other antibiotics. On the other hand, viruses, in most cases, coexist peacefully with their hosts. However, they can also parasitize them and cause diseases and even take over entire ecosystems [6]. At all these scales, complex physical phenomena occur, from protein folding and docking when viruses infect cells to the plasticity of social networks when coupling opinion and disease dynamics. We will again use the COVID-19 pandemic as an example, and in this context, the SARS-CoV-2 coronavirus.

After infecting a host, the natural immune response of the organism is triggered. Here, antibodies aiming to impede viral replication or actively clear it from the bloodstream compete with the virus's vital cycle in a dynamical equilibrium—which the antibodies not always can win. See Perelson [58] and references therein for an in-depth analysis of the physics of the immune response before viral infection. Another route to immunization, this time without requiring being infected, is through vaccination or prophylaxis (see Wang et al. [1] for an in-depth analysis of the physics of vaccination). Just to illustrate the complexity behind immune responses, there are several layers of immune memory; it does matter which kind of immunity an individual has and when was their last inoculation or exposure to the infectious agent (as, e.g., for dengue

[59] and COVID-19 [60]). Either way, immunity can wane over time [61, 62], and thus individuals become susceptible again.

On the other hand, viruses evolve, and viral variants may emerge. Evolutionary processes in viruses are complex by nature; the apparent simplicity of their genome masks higher-order interactions between and within genes, such that the effect of mutations is conditioned to others occurring in different loci [6, 63]. Every time the virus replicates, it has a chance to mutate and generate variants; when larger fractions of the population get infected (in the context of a pandemic), the odds of generating variants are higher. This evolutionary process is further accelerated by the host's immune response, especially when it is insufficient to counteract viral replication [64–66]. While variants with enhanced transmissibility, partial immune escape, and producing fewer symptoms are likelier to be more successful in replacing current dominant variants, this does not warrant that more lethal variants will not emerge or persist [67]. Genomic surveillance, i.e., the tracking of the mutational signatures of the variants driving an epidemic, is thus crucial for an opportune enacting of restrictions [16, 40, 47, 68].

3.2 CONTAGION

Contagion is the process of transmitting the pathogen causing infection. It is, by definition, a stochastic process resulting from the probability of having contagious contact, its duration, and the infectiousness of the pathogen. Contagion can be direct when individuals infect individuals through contagious contact or indirect when individuals are infected through environmental reservoirs or asynchronous contacts with infectious hosts. For a modeling guide separating direct from indirect transmission the reader is referred to Benson et al. [69]. Respiratory infectious diseases are typically transmitted by direct contagion through droplets generated while breathing or talking, which after drying, are inhaled as aerosols by the susceptible individual. While typical models assume that a single copy of the pathogen per aerosol particle, in some cases (for the largest aerosols), there can be thousands of copies and thus have a non-negligible effect on the results. For a general model for the risk of infection indoors, tailored but not limited to SARS-CoV-2, see Nordsiek, Bodenschatz, and Bagheri [70].

Understanding aerosol dynamics was critical to assess the effectiveness of physical distancing and mask-wearing. Note that these cannot be evaluated in real settings, i.e., through randomized trials; not providing

protective elements to the population is unethical. In particular, masks were proved to outperform physical distancing in reducing the risk of infection [71], and together with natural and mechanical ventilation, could make office activities and classes safe in the context of a pandemic [72].

Modelling the spreading dynamics of infectious diseases requires capturing both the spreading mechanisms of the pathogen and the characteristics of the contact network where the disease spreads. In the following sections, we explore and analyze different models for disease spread where contagion occurs in a compartmentalized population.

3.3 COMPARTMENTAL MODELS FOR DISEASE SPREAD

One of the most popular approaches to studying disease spread is using ODE compartmental models, as the SIR model [73]. These models partition the total population into disjoint states representing different levels of disease and health. For the SIR model, these states are susceptible, infectious, and removed. Upon contact with an infectious individual, susceptible individuals may also become infectious. They contribute to spreading the disease until recovering or dying, being either way removed from the dynamics. The transitions between these states are governed by mass-action-like rules leading to first-order kinetics and exponential residence times in the infectious state. This model assumes that once recovered/removed, individuals cannot be infected again and thus do not take place in the dynamics anymore.

While useful, the information gathered through these models must always be analyzed in context; many implicit hypotheses might not always hold. For example, some diseases might have markedly long latent and incubation periods, so the assumption of individuals turning infectious upon contagion does not hold anymore. In that case, modelers find it useful to include an extra compartment E for exposed individuals [74]. Another hypothesis is that the whole population remains constant at the time. This, however, is not true for diseases whose timescales are similar to birth/death processes (e.g., measles) or for diseases so severe that susceptible individuals are protected from contagion by being curfewed (e.g., SARS/MERS) [12]. In these cases, a relevant quantity for policymakers would be the total burden to the health systems, so modelers would find it helpful to include extra H or ICU compartments for severely ill individuals (distinguishing those merely diseases from those requiring intensive care), or economist would wonder

about the fraction of the population needed to be quarantined and the losses/disruptions that this would cause.

As the reader can already suspect, limitations in compartmental models are often solved by introducing more compartments. This strategy is relatively standard. For example, when diseases spread preferentially across given groups of society, it might be helpful to replicate the SIR-like structure for each required class. The complexity of the models, however, does not increase proportional to the number of compartments but to the square of it; in principle, we require cross-group infection probabilities and a proxy for the strength of interaction between groups. Interpreting the coupling strength between groups correctly is critical for not overestimating the epidemiological parameters lumped into it. Examples of situations solvable by employing multigroup models:

- Vaccine prioritization in diseases with age-dependent susceptibility and infection fatality risk. For example, diseases like COVID-19 require prioritizing the elderly, who are at higher risk of being severely ill if infected. In this case, models for the spreading dynamics of COVID-19 required knowing the contact structure of a given population to calculate the probability of susceptible individuals of group i meeting infectious individuals of group j . Examples are [54, 75, 76], and references in Wang et al. [1].
- Spatial heterogeneities and isolated communities within a population. Here, metapopulation models as, e.g., [77–79] can separate units where the spread is essentially homogeneous and link them through a connectivity matrix (e.g., proportional to mobility). This also includes models where each country is simulated independently and simultaneously.
- Implementing gradual loss of immunity through cascades of compartments [80].
- Conduct groups, where different behavioral traits might produce markedly different spread in the population. For example, groups agnostic to the disease would not adhere to interventions nor get vaccinated. A static approach to incorporate this is presented in [11], where a population group never accepts the vaccine. Including behavioral effects in simple models opens a wide variety of dynamical regimes [1, 21, 25, 55].

Mathematically, the SIR model is represented by the following ordinary differential equations:

$$S' = -\frac{\beta SI}{N}, \quad (3.1)$$

$$I' = \frac{\beta SI}{N} - \gamma I, \quad (3.2)$$

$$R' = \gamma I, \quad (3.3)$$

where β and γ are respectively the spreading and recovery rate of the disease. Although simple, the **SIR** model captures critical features of an infectious disease outbreak: i) the initial exponential growth and ii) the exponential slow-down of disease spread when large fractions of the population have been infected and recovered (also known as herd immunity effect). Once settled (i.e., stochastic effects aside), the initial stages of an outbreak are characterized by the following. First, there is no working cure or vaccine, and unless already infected and recovered, individuals are susceptible to being infected. Second, the outbreak has not reached most of the population, and thus (using the **SIR** formalism) we can approximate $\frac{S}{N} \approx 1$. The consequences of this assumption are overarching; in the **SIR** formalism, this means that the system can be reduced to a single differential equation. Replacing $\frac{S}{N} \approx 1$ in eq. (3.2) yields:

$$I' = \beta I - \gamma I, \quad (3.4)$$

The ODE above can be solved for I :

$$I' = I_0 \exp(\gamma(R_0 - 1)), \quad (3.5)$$

where $R_0 = \frac{\beta}{\gamma}$ is the basic reproduction number of the disease, i.e., the average number of secondary infections generated by each index case in a fully susceptible population. From this formula we can clearly see that $R_0 = 1$ marks a drastic change in the behavior of the solutions, i.e., a phase transition: for $R_0 > 1$, outbreaks grow exponentially, while for $R_0 < 1$ they die out exponentially fast. For the case $R_0 = 1$, the fixed point at $I = 0$ changes its stability. The rest of the equations are decoupled and only "count" infected and recovered cases, and thus all the dynamics of the system are captured by those of infection. This is a first-order dynamical system, and thus all possible solutions are a constant, or trajectories exponentially converging/escaping from it.

When larger fractions of the population have been infected, the approximation $\frac{S}{N} \approx 1$ does not hold anymore. In such a condition, it

becomes increasingly hard for the pathogen to find a contact to infect. Thus, the disease spreads at a rate given by the effective reproduction number $R_{\text{eff}} = R_0 \frac{S}{N}$, which quantifies the average number of secondary cases that each infectious individual generates in a population with partial immunity. Again, the spread will continue while $R_{\text{eff}} > 1$. The phase transition here marks the herd immunity threshold; when the susceptible pool has decreased enough so that $R_{\text{eff}} = 1$, outbreaks will on average die out due to the shielding effect of recovered individuals. We can estimate the herd immunity threshold as

$$R_0 \frac{S}{N} = 1 \Rightarrow HIT = N - \frac{N}{R_0} = N \left(1 - \frac{1}{R_0}\right) \quad (3.6)$$

In the following sections, we explore the effect of including different kinds of infectious individuals and **NPIs** find rich dynamics even in linear variations of the **SIR** model.

3.4 TEST-TRACE-AND-ISOLATE IN ODE COMPARTMENTAL MODELS

One of the first interventions enacted after an outbreak is **TTI**; individuals are tested (based on symptoms or following other screening plans), and the close contacts of those who tested positive are traced and tested too. Ultimately, all those who test positive are instructed to isolate, preventing them from further spreading the disease. The main idea behind this is to truncate infection chains, thereby slowing the spread ideally to the point where it is subcritical. However, there are certain limits to **TTI**. First, not all contacts can be followed due to the handling limit of manual contact tracers, the memory (and honesty) of individuals when reporting contacts, or the notification threshold for digital trace [81]. Second, there are good economic reasons not to quarantine the whole population simultaneously.

While **TTI** can efficiently break chains of contagion if appropriately done, its success depends on several factors. First, if the testing rate is low, the tracing inefficient, or the disease's base spreading rate too large, contact tracing delays can be critical, and containment through **TTI** impossible [30]. Second, the incidence of the disease can be too large to be handled by manual tracers and thus start missing fractions of the chains of contagions and the chains thereof. Third, **TTI** is imperfect. For example, tests have limited sensitivity, testing criteria can arbitrarily change depending on test availability, isolation mandates are not always

followed, and within-household transmission is harder to control. We aim to quantify these imperfections' impact on the overall effectiveness of **TTI** and describe the associated dynamical regimes and phase transitions. To that end, we proposed two models to study the dynamics of a COVID-19-like disease, i) a linear **SIR-TTI** model for the initial stages of an outbreak, and ii) a nonlinear Susceptible-Exposed-Infectious-Removed (**SEIR**)-**TTI** to study the mid-and long-term control of it, and a minimal nonlinear **SIR-TTI** model to study delay-induced bifurcations in diseases with longer spreading timescales than COVID-19.

3.4.1 Linear SIR-TTI model

Here, we introduce the **TTI** formalism in a linear version of an **SIR** model. However, for it to resemble a COVID-19-like disease, it must also incorporate the following possibilities:

- infections can be either symptomatic or asymptomatic,
- testing can be targeted to individuals with symptoms or applied randomly for population screening,
- the timescales of testing and contact tracing are that of disease spread (days), and
- an important fraction of the infections were acquired externally and imported into the country/system.

We also considered the behavioral implications of having a test result; individuals would adapt their behavior once tested, either voluntarily (social altruism) or compulsory (quarantine mandates by health authorities). Either way, it requires us to distinguish between two kinds of infections; those that are known and *traced*, and those that are unknown and *hidden*.

Our model considers two kinds of infectious individuals: hidden H and traced T (and their symptomatic and asymptomatic versions, denoted by a superscript). We schematize the situation following the metaphor of an iceberg (Fig. 3.1a). Hidden infections are the lower part of an iceberg, which can be surfaced through testing and contact tracing. The overall spread is slowed down by **TTI** as infectious individuals are moved from the hidden to the traced pools, where infections proliferate much slower. On the one hand, hidden infections spread when individuals are unaware of being infectious and thus behave normally and spread with a reproduction number R_t^H . This parameter captures both the base

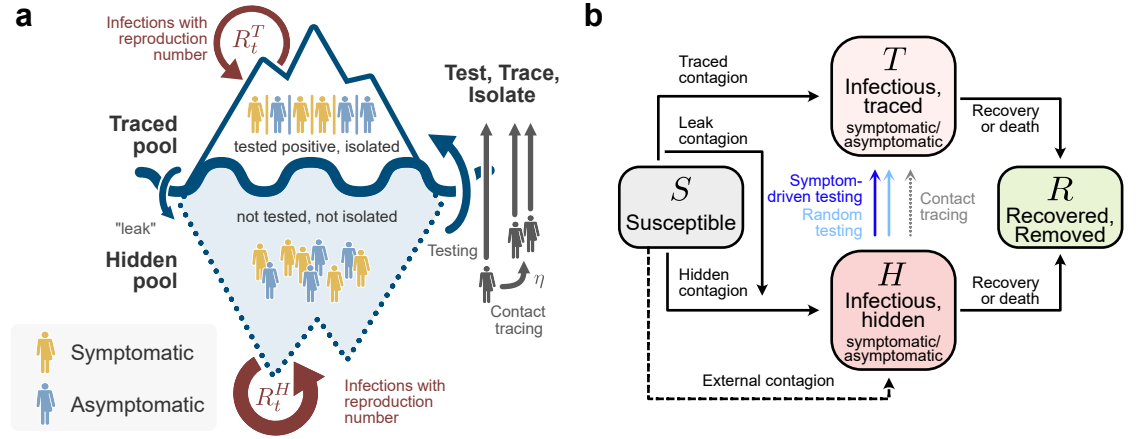


Figure 3.1: **Linear SIR model including test-trace-and-isolate.** **a:** Block diagram of our model, where solid blocks represent different SIR compartments. We distinguish between hidden H and traced T infections; the former are those infections where individuals are unaware of their state and thus spread the disease faster. Once testing positive, individuals become aware and are instructed to isolate. We represent these dynamics as an iceberg, where test-trace-and-isolate surface hidden infections (as schematized in **b**). Adapted from [28].

spreading potential of the disease and the behavior of the population so that we could also express it (like in Chapter 5) as the product between the basic reproduction number and the level of contagious contacts k_t of the population (i.e., the fraction of total contacts that bear the risk of contagion): $R_t^H = R_0 k_t$.

On the other hand, due to behavioral changes and isolation mandates, traced infections spread with a much smaller reproduction number R_t^T . This number captures both the in-household transmission of traced infection (at rate νR_t^H) and the "leak" of infections that are generated by non-reported (and unaware) contacts of traced cases (at rate ϵR_t^H). Besides, we assume a nonzero influx of externally acquired infections (Φ) that enter the system through the hidden pool.

Due to TTI, individuals from the hidden pool are tested (randomly or due to symptoms), and the contacts of positive cases, in principle, are followed and tested too. Random testing occurs at a rate λ_r . It acts over the whole population that is not currently isolated (i.e., only over the hidden pools). Symptom-based testing occurs at a rate λ_s , which captures both the active search for symptomatic patients and self-reporting. Contact tracing can handle a maximum of n_{\max} cases per day and with an efficiency η . Note that this absolute number differs from the number of observed cases at the day \hat{N}^{obs} , so that the maximum observed number of cases for which contact tracing breaks

down also depends on the spreading parameters. The whole dynamics is also represented as a block diagram (Fig. 3.1b). In the end, as we do not need to differentiate between symptomatic and asymptomatic infections in the traced pool, we have three state variables for infectious individuals, T , H^s , H^a . Altogether, the system of differential equations describing the dynamics is:

$$\frac{dT}{dt} = \underbrace{\Gamma (\nu R_t^H - 1) T}_{\text{spreading dynamics}} + \underbrace{\lambda_s H^s + \lambda_r H}_{\text{testing}} + \underbrace{f(H^s, H)}_{\text{tracing}}, \quad (3.7)$$

$$\begin{aligned} \frac{dH}{dt} = & \underbrace{\Gamma (R_t^H - 1) H}_{\text{spreading dynamics}} - \underbrace{(\lambda_s H^s + \lambda_r H)}_{\text{testing}} - \underbrace{f(H^s, H)}_{\text{tracing}} + \dots \\ & \dots \underbrace{\Gamma \epsilon R_t^H T}_{\text{missed contacts}} + \underbrace{\Phi}_{\text{external influx}}, \end{aligned} \quad (3.8)$$

$$\begin{aligned} \frac{dH^s}{dt} = & \underbrace{\Gamma (R_t^H s^{\text{ap}} H - H^s)}_{\text{spreading dynamics}} - \underbrace{(\lambda_s + \lambda_r) H^s}_{\text{testing}} - \underbrace{s^{\text{ap}} f(H^s, H)}_{\text{tracing}} + \dots \\ & \dots \underbrace{s^{\text{ap}} \Gamma \epsilon R_t^H T}_{\text{missed contacts}} + \underbrace{s^{\text{ap}} \Phi}_{\text{external influx}}, \end{aligned} \quad (3.9)$$

$$H^a = H - H^s, \quad (3.10)$$

$$f(H^s, H) = \min \left\{ n_{\max}, \eta R_t^H (\lambda_s H^s + \lambda_r H) \right\}. \quad (3.11)$$

Again, this model is an extension of the linear version of the SIR model discussed in the previous section (eq. 3.4), adding an external influx of infections (acting as constant bias in the set of differential equations). The dynamics for that simple system were described using R_0 as the control parameter, which separates controlled spread leading to the natural eradication of the disease when $R_0 < 1$ and exponential growth when $R_0 > 1$. This opens three questions for the linear SIR-TTI model: i) what are the possible dynamical regimes observable in the full model? ii) what is the effect of the slight non-linearity induced by the limited contact tracing (TTI) capacity? and iii) what is the stability of the equilibrium for both the cases when TTI is available or overwhelmed?

We hypothesize that the possible dynamics are a stable equilibrium set by the influx of infections, and two modes of exponential spread, depending on whether or not the TTI capacity has been reached. Furthermore, as spread happens in the hidden and traced pools, the system is as stable as the least stable of the infectious pools. Given the primarily linear nature of our model, we do not expect to find limit cycles.

However, to formally answer these questions, we use techniques of linear stability analysis and analyze the system for the two extreme cases mentioned above.

3.4.1.1 Linear stability analysis

We study the controllability of an outbreak in our model using linear stability analysis, i.e., studying the fixed points of the system of differential equations and whether perturbations around them will persist or decay. These techniques are particularly adequate for our case; our model's only source of non-linearity is the **TTI** capacity limit in eq. (3.11). However, for both extreme cases, i.e., assuming limitless **TTI** (i.e., $f(H^s, H) = \eta R_t^H (\lambda_s H^s + \lambda_r H)$) or overwhelmed **TTI** (i.e., $f(H^s, H) = n_{\max}$), the system is linear. Thus the system of equations (3.7)–(3.9) can be rewritten using a matrix formalism:

$$\frac{d}{dt} \begin{pmatrix} T \\ H \\ H^s \end{pmatrix} = A \begin{pmatrix} T \\ H \\ H^s \end{pmatrix} + \vec{b}, \quad (3.12)$$

where A and \vec{b} are fully determined by the model parameters. As we assume parameters such that the system is irreducible, the matrix A has full rank, and we can study the properties of the equilibrium defined as

$$(T_\infty, H_\infty, H_\infty^s)^T = -A^{-1}\vec{b} \quad (3.13)$$

by analyzing the largest eigenvalue of A . In particular, we define R_{crit}^H as the largest R_t^H such that the real part of μ_{\max} , the largest eigenvalue of matrix A , is strictly negative. We propose a formulation for the general case, which needs to be solved numerically, and study some particular cases that allow for analytical forms for the eigenvalues.

3.4.1.2 Equilibrium equations for case numbers below TTI capacity

Assuming no random testing (i.e., $\lambda_r = 0$), the pair A and \vec{b} defined above are given by:

$$A = \begin{pmatrix} \Gamma(\nu R_t^H - 1) & 0 & \lambda_s(1 + \eta R_t^H) \\ \Gamma \epsilon R_t^H & \Gamma(R_t^H - 1) & -\lambda_s(1 + \eta R_t^H) \\ s^{\text{ap}} \Gamma \epsilon R_t^H & s^{\text{ap}} R_t^H & -\eta s^{\text{ap}} R_t^H \lambda_s - (\lambda_s + \Gamma) \end{pmatrix} \quad (3.14)$$

and \vec{b} by

$$\vec{b} = \begin{pmatrix} 0 \\ \Phi \\ s^{\text{ap}}\Phi \end{pmatrix} \quad (3.15)$$

The equilibrium $-A^{-1}\vec{b}$ is defined as follows:

$$T_\infty = \frac{\lambda_s (1 + \eta R_t^H)}{\Gamma (1 - \nu R_t^H)} H_\infty^s \quad (3.16)$$

$$H_\infty = H_\infty^s \frac{\lambda_s}{\Gamma} \alpha \quad (3.17)$$

$$H_\infty^s = \frac{\Phi}{\lambda_s (1 + \eta R_t^H)} \left[\left(\frac{\epsilon R_t^H}{\nu R_t^H - 1} + R_t^H \right) - (R_t^H - 1) \frac{\eta R_t^H + \frac{1+\Gamma/\lambda_s}{1-\xi^{\text{ap}}}}{\eta R_t^H + 1} \right]^{-1} \quad (3.18)$$

$$N_\infty^{\text{obs}} = \Gamma \nu R_t^H T_\infty + \lambda_s H_\infty^s (1 + \eta R_t^H). \quad (3.19)$$

where α is defined as

$$\alpha = \frac{\xi^{\text{ap}} + \Gamma/\lambda_s}{1 - \xi^{\text{ap}}}, \quad (3.20)$$

and provides a link between the asymptomatic fraction of the population and the recovery-to-test ratio. To calculate N_∞^{obs} in terms of model parameters, we insert equations (3.16)–(3.18) into equation (3.19):

$$N_\infty^{\text{obs}} = \lambda_s H_\infty^s (1 + \eta R_t^H) \left(\frac{1}{1 - \nu R_t^H} + 1 \right), \quad (3.21)$$

$$= \lambda_s H_\infty^s \frac{1 + \eta R_t^H}{1 - \nu R_t^H}. \quad (3.22)$$

As we define R_{crit}^H as the value for the hidden reproduction number R_t^H such that the largest eigenvalue of the linear system becomes positive, this equilibrium is stable as soon as $R_t^H < R_{\text{crit}}^H$. We evaluate the value of H_∞^s in equation 3.22 using equation 3.18, and obtain:

$$N_\infty^{\text{obs}} = \frac{\Phi}{(1 - \nu R_t^H)} \left[\left(\frac{\epsilon R_t^H}{\nu R_t^H - 1} + R_t^H \right) - (R_t^H - 1) \frac{\eta R_t^H + \frac{1+\Gamma/\lambda_s}{1-\xi^{\text{ap}}}}{\eta R_t^H + 1} \right]^{-1}. \quad (3.23)$$

From the expression above, we can gain some analytical insights on the critical hidden reproduction number R_{crit}^H , as this might be related

to the values where N_∞^{obs} diverges. We then evaluate the denominator in equation 3.23 (assuming that $R_t^H \neq \frac{1}{\nu}$ – which signals the value for which the traced pool becomes unstable) and obtain

$$(R_t^H - 1)(\nu R_t^H - 1)(\eta R_t^H + 1 + \alpha) - (\epsilon R_t^H + R_t^H(\nu R_t^H - 1))(\eta R_t^H + 1) \neq 0, \quad (3.24)$$

As this is a cubic equation for R_t^H in principle, there is not much analytical insight that we can acquire. However, two interesting cases leading to a quadratic equation emerge: i) when the isolation within household is perfect (i.e., $\nu = 0$), and ii) when there is no leakage of infections (i.e., $\epsilon = 0$).

The first case leads to the following condition for R_{crit}^H :

$$(R_{\text{crit}}^H - 1)(\eta R_{\text{crit}}^H + 1 + \alpha) - R_{\text{crit}}^H(1 - \epsilon)(\eta R_{\text{crit}}^H + 1) = 0, \quad (3.25)$$

equivalently

$$\eta\epsilon \left(R_{\text{crit}}^H\right)^2 + (\alpha - \eta + \epsilon)R_{\text{crit}}^H - (1 + \alpha) = 0. \quad (3.26)$$

Given that the constant term in the quadratic equation above is negative, we know that the solutions will have different signs and be real numbers. R_{crit}^H is then given by

$$R_{\text{crit}}^H = \frac{1}{2\epsilon\eta} \left[\sqrt{(\alpha - \eta + \epsilon)^2 + 4\epsilon\eta(1 + \alpha)} - (\alpha - \eta + \epsilon) \right] \quad (3.27)$$

The second case ($\epsilon = 0$) is slightly more interesting, as we can also obtain a closed expression for the largest eigenvalue of A . Starting from equation (3.14) and replacing $\epsilon = \lambda_r = 0$, we evaluate the characteristic polynomial $p(\mu)$ of A :

$$p(\mu) = \begin{vmatrix} -\Gamma - \mu & 0 & \lambda_s (1 + \eta R_t^H) \\ 0 & \Gamma (R_t^H - 1) - \mu & -\lambda_s (1 + \eta R_t^H) \\ 0 & s^{\text{ap}} \Gamma R_t^H & -\eta s^{\text{ap}} R_t^H \lambda_s - (\lambda_s + \Gamma) - \mu \end{vmatrix}. \quad (3.28)$$

Factoring the trivial root $\mu = -\Gamma$, and writing the rest of the determinant as an arbitrary polynomial in μ , $\tilde{p}(\mu) = \mu^2 - \text{tr} \tilde{A} \mu + \det \tilde{A}$, where

$$\text{tr } \tilde{A} = R_t^H (\Gamma - \eta s^{\text{ap}} \lambda_s) - \lambda_s - 2\Gamma, \quad (3.29)$$

$$\det \tilde{A} = R_t^H (\lambda_s s^{\text{ap}} \Gamma (\eta + 1) - \Gamma (\lambda_s + \Gamma)) + \Gamma (\lambda_s + \Gamma) \quad (3.30)$$

We require both eigenvalues to be negative and one to become zero for the transition to an uncontrolled spread. This we can extract from the conditions above:

$$R_{\text{crit}}^H = \frac{\Gamma (\lambda_s + \Gamma)}{\Gamma (\lambda_s + \Gamma) - \Gamma s^{\text{ap}} \lambda_s (1 + \eta)} = \frac{1}{1 - s^{\text{ap}} \frac{1 + \eta}{1 + \Gamma / \lambda_s}} \quad (3.31)$$

The second condition required to guarantee that this is the value we search for comes from the trace (which is the second root and must be negative). Replacing in 3.29, we obtain

$$\frac{1}{1 - s^{\text{ap}} \frac{1 + \eta}{1 + \Gamma / \lambda_s}} (\Gamma - \eta s^{\text{ap}} \lambda_s) \leq \lambda_s + 2\Gamma, \quad (3.32)$$

further binding the two free parameters for **TTI** (i.e., λ_s and η).

$$\lambda_s \eta s^{\text{ap}} \Gamma (R_t^H)^2 + (s^{\text{ap}} \lambda_s \Gamma - \eta s^{\text{ap}} \lambda_s - \Gamma (\lambda_s + \Gamma)) R_t^H + \Gamma (\lambda_s + \Gamma). \quad (3.33)$$

Alternatively, we search for R_{crit}^H as the value for R_t^H for which the observed cases in equilibrium $\hat{N}_{\infty}^{\text{obs}}$ diverge. Replacing $\epsilon = 0$ in the equation for the denominator of $\hat{N}_{\infty}^{\text{obs}}$ (eq. (3.24)), we obtain

$$\left(\nu R_t^H - 1 \right) \left[R_t^H \left(\eta R_t^H + 1 \right) - \left(R_t^H - 1 \right) \left(\eta R_t^H + 1 + \alpha \right) \right] = 0 \quad (3.34)$$

Assuming that the trace pool is in an absorbing state (i.e., $R_t^H \leq \frac{1}{\nu}$), the above condition can be rewritten as:

$$R_{\text{crit}}^H = \frac{1 + \alpha}{\alpha - \eta} = \frac{1}{1 - s^{\text{ap}} \frac{1 + \eta}{1 + \Gamma / \lambda_s}} \quad (3.35)$$

which coincides with the condition found above for the largest eigenvalue. This condition provides important analytical insights into the determinants of the controllability of an outbreak. We can conclude the following

- No testing (i.e., $\lambda_s = 0$) retrieves the classical phase transition for epidemiological models $R_{\text{crit}}^H = 1$.

- The apparent symptomatic fraction of cases (s^{ap}) modulates the effect of (symptom-based) TTI; if it is zero (i.e., all cases would be asymptomatic), there is no way to increase the allowed R_{crit}^H .
- There can be combinations of s^{ap} and symptom-based TTI for which, theoretically, no other interventions would be ever required ($R_{\text{crit}}^H \rightarrow \infty$). Note that this requires the conditions for control in the traced pool to be also fulfilled, as we assumed $R_t^H \leq \frac{1}{\nu}$.

3.4.1.3 Equilibrium equations for case numbers above tracing capacity

Analyzing the case when the tracing capacity is exceeded ($\eta\lambda_s R_t^H H_\infty^s > n_{\text{max}}$) requires rewriting the equations for the equilibrium (i.e., it is not merely replacing $\eta = 0$). When TTI is overwhelmed, the number of cases that can be detected via contact tracing is constant $f(H^s, H) = n_{\text{max}}$. Then, the new versions of A and \vec{b} in eq. (3.12) (using again $\lambda_r = 0$) are:

$$A = \begin{pmatrix} \Gamma(\nu R_t^H - 1) & 0 & \lambda_s \\ \Gamma\epsilon R_t^H & \Gamma(R_t^H - 1) & -\lambda_s \\ s^{\text{ap}}\Gamma\epsilon R_t^H & s^{\text{ap}}\Gamma R_t^H & -(\lambda_s + \Gamma) \end{pmatrix} \quad (3.36)$$

and \vec{b} by

$$\vec{b} = \begin{pmatrix} n_{\text{max}} \\ \Phi - n_{\text{max}} \\ s^{\text{ap}}(\Phi - n_{\text{max}}) \end{pmatrix} \quad (3.37)$$

Again, as we assume parameters such that the system is irreducible, the matrix A has full rank and the equilibrium $(T_\infty, H_\infty, H_\infty^s)^T = -A^{-1}\vec{b}$ exists and is unique. The equilibrium pool sizes are:

$$T_\infty = \frac{\lambda_s H_\infty^s + n_{\text{max}}}{\Gamma(1 - \nu R_t^H)} \quad (3.38)$$

$$H_\infty = H_\infty^s \frac{\lambda_s}{\Gamma} \alpha \quad (3.39)$$

$$\lambda_s H_\infty^s = \frac{n_{\text{max}} \left(\frac{\epsilon R_t^H}{\nu R_t^H - 1} + 1 \right) - \Phi}{(R_t^H - 1) \alpha - \left(1 - \frac{\epsilon R_t^H}{1 - \nu R_t^H} \right)} \quad (3.40)$$

Similarly, we can derive an equation for $\hat{N}_\infty^{\text{obs}}$:

$$N_{\infty}^{\text{obs}} = \frac{(R_t^H - 1) \alpha n_{\max} - \Phi}{(R_t^H - 1) \alpha - \left(1 - \frac{\epsilon R_t^H}{1 - \nu R_t^H}\right)} \frac{1}{1 - \nu R_t^H}. \quad (3.41)$$

Following the same reasoning provided in the previous section, we search to identify the critical values R_{crit}^H for which the system changes its stability by analyzing the denominator of the equilibrium quantities. The condition for candidates for R_{crit}^H is:

$$(1 - \nu R_t^H) \left[(R_t^H - 1) (1 - \nu R_t^H) \alpha - (1 - (\nu + \epsilon) R_t^H) \right] = 0. \quad (3.42)$$

The equation above differs from the equation characterizing R_{crit}^H in the order of the polynomial in R_t^H ; we can find analytical solutions in all cases. Assuming that $R_t^H \leq \frac{1}{\nu}$, we obtain

$$\alpha \nu (R_{\text{crit}}^H)^2 - (\alpha(1 + \nu) + (\nu + \epsilon)) R_{\text{crit}}^H + \alpha + 1 = 0. \quad (3.43)$$

From here, we note two things: First, two roots have the same sign, and both have a positive real part. The condition for these to exist is given by imposing that

$$(\alpha(1 + \nu) + (\nu + \epsilon))^2 \geq 4(\alpha + 1)\nu\alpha.$$

Again, we evaluate the case $\epsilon = 0$, as we get a closed form for the eigenvalues of the Jacobian matrix of the system. Eq. (3.43) yields:

$$\alpha \nu (R_{\text{crit}}^H)^2 - (\alpha + \nu(1 + \alpha)) R_{\text{crit}}^H + \alpha + 1 = 0. \quad (3.44)$$

The roots of this equation are given by

$$\begin{aligned} R_{\text{crit}}^H &= \frac{1}{2\alpha\nu} \left(\alpha + \nu(1 + \alpha) \pm \sqrt{(\alpha + \nu(1 + \alpha))^2 - 4\nu\alpha(\alpha + 1)} \right), \\ &= \frac{1}{2\alpha\nu} \left(\alpha + \nu(1 + \alpha) \pm \sqrt{\alpha^2 - 2\nu\alpha(1 + \alpha) + (\nu(1 + \alpha))^2} \right), \\ &= \frac{1}{2\alpha\nu} (\alpha + \nu(1 + \alpha) \pm |\alpha - \nu(1 + \alpha)|), \end{aligned} \quad (3.45)$$

and thus

$$R_{\text{crit}}^H = \frac{1}{\nu} \quad \vee \quad R_{\text{crit}}^H = \frac{1 + \alpha}{\alpha} \quad (3.46)$$

To compare with the analytical result for the eigenvalues, we compute the characteristic polynomial.

$$p(\mu) = \left(\Gamma (\nu R_t^H - 1) - \mu \right) \begin{vmatrix} \Gamma (R_t^H - 1) - \mu & -\lambda_s (1 + \eta R_t^H) \\ s^{\text{ap}} \Gamma R_t^H & -(\lambda_s + \Gamma) - \mu \end{vmatrix}. \quad (3.47)$$

We again write the second part using the equivalent submatrix \tilde{A} , in a way that the associated polynomial $\tilde{p}(\mu) = \mu^2 - \text{tr } \tilde{A} \mu + \det \tilde{A}$, with:

$$\text{tr } \tilde{A} = \Gamma (R_t^H - 1) - (\lambda_s + \Gamma), \quad (3.48)$$

$$\det \tilde{A} = \Gamma (\lambda_s + \Gamma) (1 - R_t^H) + \lambda_s s^{\text{ap}} \Gamma R_t^H \quad (3.49)$$

We now impose a root to be equal to zero so that $\det \tilde{A} = 0$. The resulting candidate for R_{crit}^H is given by:

$$R_{\text{crit}}^H = \frac{1 + \Gamma/\lambda_s}{-s^{\text{ap}} + 1 + \Gamma/\lambda_s} = \frac{1 + \Gamma/\lambda_s}{\xi^{\text{ap}} + \Gamma/\lambda_s} = \frac{\alpha + 1}{\alpha}. \quad (3.50)$$

By imposing the second root in this situation ($\mu = \text{tr } \tilde{A}$) to be negative, we obtain a condition for the required testing rate λ_s .

3.4.1.4 Linear stability of the full model

Generally, our system will operate between the two extremes described in the previous sections. The fixed point of the system assuming limitless **TTI** will tell us the expected $\hat{N}_\infty^{\text{obs}}$ in situations where the current incidence is below the nominal **TTI** limit and $R_t^H < R_{\text{crit}}^H$, and the fixed point of the system assuming overwhelmed **TTI** will tell us what is the maximum number of cases attainable for the approximation of limitless **TTI** (and its stability) to be valid.

To analyze the full system, we first calculate R_{crit}^H when there is no contact tracing (i.e., $\eta = n_{\text{max}} = 0$). This value, hereafter $R_{\text{crit}}^{H,1}$, tells us the maximum hidden reproduction number R_t^H for which all outbreaks die out naturally (in a situation with testing at rates λ_s and λ_r). This case coincides with the situation where contact tracing has reached its maximum $n_{\text{max}} \neq 0$, and differs only on the fixed point, as discussed previously. Then, we calculate R_{crit}^H for situations with no contact tracing limit (i.e., $\eta \neq 0$ and $n_{\text{max}} \rightarrow \infty$). This value, hereafter $R_{\text{crit}}^{H,2}$, tells us the maximum hidden reproduction number R_t^H for which contact tracing can break contagion chains efficiently. Beyond this point, given current testing and spreading conditions, contact tracing

cannot break contagion chains on time; thus, the spread is supercritical. Altogether, these values define three regimes: stable ($R_t^H \leq R_{\text{crit}}^{H,1}$), *metastable* ($R_{\text{crit}}^{H,1} \leq R_t^H \leq R_{\text{crit}}^{H,2}$), and unstable ($R_t^H \geq R_{\text{crit}}^{H,2}$).

Table 3.1: Model parameters and values for simulations (linear SIR-TTI model).

Parameter	Meaning	Value	Units
Γ	Recovery rate	0.1	day ⁻¹
ξ^{ap}	Apparent asymptomatic ratio	0.32	–
s^{ap}	Apparent symptomatic ratio	0.68	–
λ_s	Symptom-driven testing and self-reporting rate	0.25	day ⁻¹
λ_r	Random testing rate	0	day ⁻¹
ϵ	Leak of infections	0.1	–
ν	Traced infection (secondary attack rate)	0.1	–
R_t^H	Hidden reproduction number	0.5–3.5	–
η	Contact tracing efficiency	0.66	–

For the parameter values described in Table 3.1, we plot the fixed points for both overwhelmed and limitless **TTI** and their critical R_t^H values R_{crit}^H (see Fig. 3.2). In the unconditionally stable zone ($R_t^H \leq R_{\text{crit}}^{H,1}$), only a stable fixed point exists; as this is the unconditionally stable regime, contact tracing always will asymptotically be within capacity.

In the second, *metastable* regime ($R_{\text{crit}}^{H,1} \leq R_t^H \leq R_{\text{crit}}^{H,2}$), things are more interesting. First, the solid blue curve represents the value for $\hat{N}_\infty^{\text{obs}}$ when **TTI** is available. The dashed red line represents the value for $\hat{N}_\infty^{\text{obs}}$ when **TTI** is overwhelmed. When these two curves meet, the interpretation of both is lost; no more equilibrium (see Fig. 3.2). Between the value at which they meet and $R_{\text{crit}}^{H,2}$, there is no fixed point, as this equilibrium also signals what the maximum incidence $N_{\text{max}}^{\text{test}}$ is, i.e., when the incidence reaches the **TTI** capacity, and we would have to change the system we analyze, we had already crossed the red line and are thus on the upper part of the graph, i.e., case numbers will grow from then on.

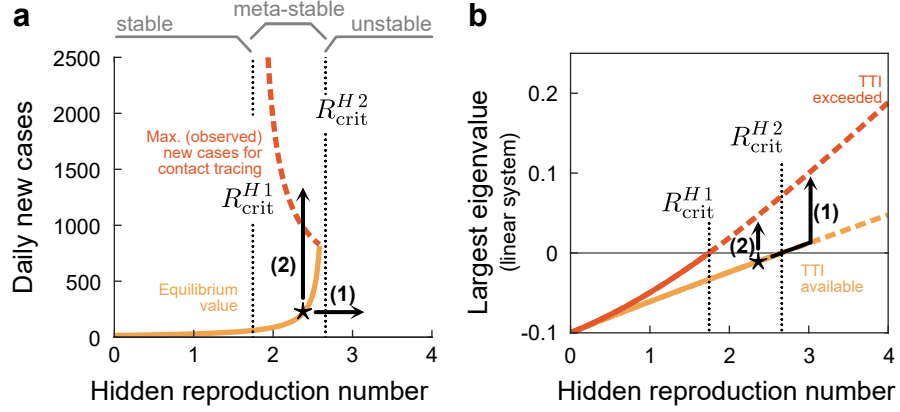


Figure 3.2: **Fixed points and linear stability of the SIR-TTI model.** **a:** Based on the critical values R_{crit}^H for a system without and with **TTI** (respectively, $R_{crit}^{H,1}$ and $R_{crit}^{H,2}$), we can define three zones of stability: an unconditionally stable regime for $R_t^H \leq R_{crit}^{H,1}$, an unconditionally unstable regime for $R_t^H \geq R_{crit}^{H,2}$, and a *metastable* regime when R_t^H ranges between these two values. In such a regime, two attractors exist: one (stable attractor) where case numbers stabilize (light orange, solid), and another (unstable attractor) that delimits the maximum incidence that health authorities can handle (dark orange, dashed). In this *metastable* regime, control can be lost through two pathways/tipping points, illustrated in a situation where we start from the point marked with a star: (1), the hidden reproduction number crossing the threshold $R_{crit}^{H,2}$ due to a permanent behavioral change, or (2) a sudden influx of cases driving current incidences to cross the unstable attractor. **b:** In terms of the system's eigenvalues, we change between two exponential modes, joined by a phase of self-acceleration featuring faster-than-exponential growth in case numbers.

3.4.1.5 A metastable regime at low case numbers

In the previous section, we determined the critical values of $R_t^H = R_{crit}^H$ such that the spread of the disease would be uncontrolled for different conditions of **TTI**. These values, which denote phase transitions from a physicist's point of view, can be understood as epidemiological "tipping points"; although reversible, the non-linear nature of disease spread makes it harder to return to controlled spread, and the system exhibits some sort of hysteresis. We can define two tipping points. The first tipping point is crossed when the hidden reproduction number becomes too large to be controlled by current **TTI** capabilities, no matter what the precise value of n_{max} is (cf. to the arrow marked with (1) in Fig. 3.2). The first tipping point is crossed when the current incidence surpasses the **TTI** capacity for contact tracing (cf. to the arrow marked with (2) in Fig. 3.2). In any case, as parts of the infection chains cannot be stopped on time, these start their own hidden chains, and the spread "self-

accelerates" until settling on a larger mode of exponential growth. This results from the slight non-linearity of our model, switching between two modes of exponential growth.

We will refer to the zone where $R_{\text{crit}}^{H,1} \leq R_t^H \leq R_{\text{crit}}^{H,2}$ as a *metastable* regime at *low case numbers*; here, spread is virtually stable (in the linear approximation of disease spread), if and only if the incidence at any time is below the **TTI** capacity limit. Moreover, while staying in this regime, the hidden reproduction number allowed for a controlled spread is larger than when the **TTI** capacity is overwhelmed (for having a controlled spread in that case, we would require $R_t^H \leq R_{\text{crit}}^{H,1}$). Therefore, the metastable regime at low case numbers offers a sweet spot for policy planning, which can be exploited to plan effective intermittent interventions.

3.4.2 A nonlinear SEIR-TTI model for intermittent interventions

After the initial stages of an outbreak, i.e., settlement and exponential spread, the approximation $S/N = 1$ no longer holds, and nonlinear effects kick in. Besides, incidence levels can also be high enough to merit action, such as curfews and lockdowns, to reduce the spreading rate of the disease and current incidence levels. Therefore, we need a more complex model. We modify the linear **SIR-TTI** model into a nonlinear **SEIR-TTI** model, including the population immunity effects on reducing the spreading rate (i.e., $\frac{S}{N}$) and a single delay for contact tracing. We use this model to study the effect of lockdowns and circuit breakers, i.e., recurrent lockdowns of short duration, aiming to profit from the metastable regime at low case numbers.

Including a compartment for those individuals exposed to the virus and are infected but not yet infectious (E), allows us to better represent the dynamics of COVID-19. Effectively, it slows down the nominal spread, as individuals do not become infectious immediately but after a period of latency (which ends at rate ρ). In this model, we also assume that once the contact tracing capacity is reached, the testing criteria are also impaired and become more specific, thus lowering the overall detection rate through testing. Furthermore, a fraction η of the contacts of positively tested individuals are traced with a delay of τ . Finally, we assume that testing and contact tracing have a limited capacity.

While this model helps study the effectiveness of intermittent interventions and calculate their magnitude so that the system can be brought to the metastable regime at low case numbers, it is too complex

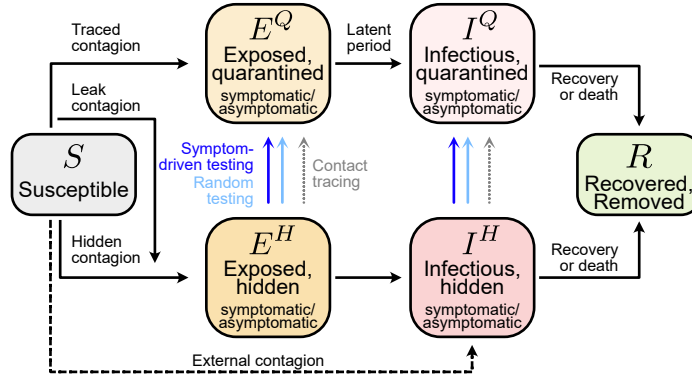


Figure 3.3: **Block diagram of the SEIR-TTI model in Chapter 5.** Solid blocks represent different SEIR compartments. We distinguish between hidden H and quarantined Q infections; the former are these infections where individuals are unaware of their state and thus spread the disease faster. Once testing positive, individuals become aware and are instructed to isolate.

to analyze the singular effects of delays and testing. We explore the dynamics and stability of the SEIR-TTI model in depth in Chapter 5. However, in the next section, we analyze the dynamics, stability, and bifurcations of a simpler version of it.

3.4.3 A nonlinear minimal SIR-TTI model with waning immunity and delayed contact tracing.

Here we describe a simplified version of the TTI model, with contact tracing delay and effective isolation of individuals. Susceptible individuals (S) become infectious upon contact with a hidden infectious one (I) at a rate proportional to R_t^H . Hidden infectious individuals can be tested or self-report at a rate λ and recover at a rate γ . A fraction η of the contacts of those individuals detected in $t - \tau$ that have not been tested nor recovered are detected by contact tracing. We assume that both tested and traced individuals are perfectly isolated and thus can be moved to the Recovered pool R .

Although intuitive, including delayed contact tracing complicates the algebra in the model. In particular, mechanistically, if the tracing of contacts and their testing is delayed, individuals might have already transitioned between compartments. In other words, a fraction of these new cases could have been tested or self-reported due to symptoms or even recovered by the time of tracing. In the following subsections, we explore the implications of these possibilities on the model equations.

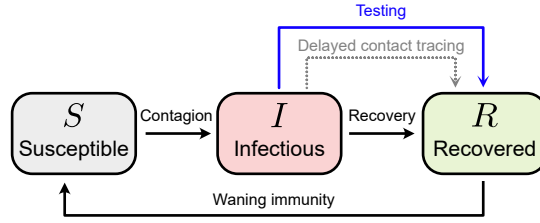


Figure 3.4: **Minimal non-linear SIR-TTI model with waning immunity and delayed contact tracing.** Solid blocks represent different SIR compartments. Compared to the model in Fig. 3.3, this model assumes i) perfect isolation of tested and traced individuals (i.e., $\nu = \epsilon = 0$), ii) no different classes for infectious individuals (i.e., no distinction between symptomatic and asymptomatic), iii) slow spreading dynamics and comparatively shorter latent period (i.e., E compartment is excluded), and iv) waning of natural immunity.

3.4.3.1 Individuals changing compartments by the time of tracing

As discussed above, TTI traces and tests the contacts of positively tested individuals. However, when contact tracing occurs with a delay, individuals might have already been detected by testing or stopped being infectious when contacted by health authorities. So, if we include a delay in our system of differential equations, we must correct for this possibility; contact tracing will detect (and remove from the infectious pool) only those contacts that remain there.

As our model moves individuals from one compartment to another at fixed transition rates (which produce exponential residence times), we can conceptualize the situation as the emptying of a compartment through first-order kinetics. Following the formalism in Contreras et al. [20], let $s \in I_\tau = [0, \tau]$ be the time elapsed from the moment of testing. The emptying of the normalized infectious compartment due to recovery and testing follows, as in the classical SIR model, a mass-action-inspired first-order kinetics:

$$\frac{dX}{ds} = -(\lambda + \gamma)X, \quad X(0) = 1 \tag{3.51}$$

The solution of (3.51) is given by $X(s) = \exp(-(\lambda + \gamma)s)$. Therefore, we define χ_τ as the fraction of the traced individuals remaining in the X compartment at $s = \tau$:

$$\chi_\tau = \exp(-(\lambda + \gamma)\tau). \tag{3.52}$$

3.4.3.2 *Modeling the number of traced individuals*

In the **TTI** framework, the contacts of those individuals who tested positive are followed after τ days and subsequently tested. However, the infectious period of the index case (and thus the number of offspring infections they generate) is truncated by testing; as they are removed before recovering, they produce, on average, fewer new cases than not-tested individuals. In the presence of symptom-based testing, the average residence time in the hidden infectious pool is $\frac{1}{\gamma+\lambda}$, while in natural conditions, it is $\frac{1}{\gamma}$.

Why does this matter? Let $N^{\text{test}}(t - \tau)$ be the total individuals tested τ days ago. If they spent their whole infectious period in the hidden pool, these would generate $R_t^H N^{\text{test}}(t - \tau)$ new cases. However, as these were detected by testing, they spent only a fraction of their time in the hidden pool. Thus, the amount of new cases they generate is reduced proportionally to the fraction of time they remain infectious, i.e., $\frac{\gamma}{\gamma+\lambda}$. Altogether, assuming that contact tracing at time t only detects a fraction η of the new cases generated, the number of cases detected via contact tracing is given by:

$$N^{\text{tracing}} = \eta \cdot \lambda \chi_\tau I(t - \tau) \cdot \frac{\gamma}{\gamma + \lambda} R_t^H. \quad (3.53)$$

The three contributions to N^{tracing} denote (from left to right), contact tracing efficiency, the number of individuals detected by testing τ days ago that remain infectious by the time of tracing, and their expected number of secondary infections.

3.4.3.3 *Model equations*

The model above is thus described by the following system of DDE:

$$\frac{dS}{dt} = - \underbrace{\gamma R_t^H SI}_{\text{contagion}} + \underbrace{\omega R}_{\text{waning imm.}}, \quad (3.54)$$

$$\frac{dI}{dt} = \underbrace{\gamma R_t^H SI}_{\text{contagion}} - \underbrace{\lambda I}_{\text{testing}} - \underbrace{N^{\text{tracing}}}_{\text{tracing}} - \underbrace{\gamma I}_{\text{recovery}}, \quad (3.55)$$

$$\frac{dR}{dt} = \underbrace{\gamma I}_{\text{recovery}} + \underbrace{\lambda I}_{\text{testing}} + \underbrace{N^{\text{tracing}}}_{\text{tracing}} - \underbrace{\omega R}_{\text{waning imm.}}, \quad (3.56)$$

$$(3.57)$$

Important: Here, S , I , and R denote fractions of the population. This induces a reinterpretation of the parameters and the "mass balance" condition, which now is $S + I + R = 1$. Note that the definition for N^{tracing} in eq. 3.53 facilitates the algebra at the cost of the assumption $S = 1$. Therefore, it overestimates the number of infections generated by each case detected by testing.

3.4.3.4 Fixed points and expected dynamics

Here we provide a linear stability analysis of the minimal non-linear SIR-TTI model with waning immunity and delayed contact tracing. First, the system can be reduced to two equations, as $R = 1 - S - I$. Then, we study the system's fixed points given by equations 3.54 and 3.55. We trivially find the disease-free equilibrium

$$\mathcal{E}_0 = (1, 0), \quad (3.58)$$

which is, in general, unstable (seen as a 2D system), or a saddle in the (S, I, R) plane; if starting with zero infections and a nonzero immune population, their immunity will wane until asymptotically approaching $(1, 0, 0)$. The nontrivial, *endemic equilibrium* $\mathcal{E}_* = (S^*, I^*)$ is given by:

$$S^* = \frac{1}{\gamma R_t^H} \left(\lambda + \gamma + \eta \lambda \chi_\tau \frac{\gamma R_t^H}{\gamma + \lambda} \right), \quad (3.59)$$

$$I^* = \frac{\omega (1 - S^*)}{\gamma R_t^H S^* + \omega}. \quad (3.60)$$

Note that R_t^H needs to be large enough for the equilibrium to be feasible (i.e., that $S^* \leq 1$). In this system, we expect two asymptotic behaviors. First, when $\tau = 0$, the model behaves as a SIRS model. Thus, the endemic equilibrium is globally asymptotically stable when the reproduction number is large enough [82]. Second, when $\tau \rightarrow \infty$, the term χ_τ becomes close to zero. Thus, the system's stability does not depend on the delay term and behaves as a SIRS model again, leading to a globally asymptotically stable endemic equilibrium (i.e., no periodic orbits [82]). However, could some values of τ lead to delay-induced sustained oscillations in this system? In the next section, we will look for the conditions for purely imaginary eigenvalues to emerge, i.e., whether τ can trigger a Hopf bifurcation.

3.4.3.5 *Linear stability and conditions for Hopf bifurcations*

In this section, we explore the conditions for Hopf bifurcations to occur using the time delay τ as a control parameter. To that end, we assume that R_t^H is large enough so that the endemic equilibrium \mathcal{E}_* exists. Then, as described in Section 2.3.1, we linearize the system of equations and rewrite it as:

$$x' = Ax(t) + Bx(t - \tau), \quad (3.61)$$

where $x = (S, I)$, and matrices A and B , evaluated in \mathcal{E}_* , are given by

$$A = \begin{pmatrix} a & c \\ b & d \end{pmatrix} = \begin{pmatrix} -\gamma R_t^H I^* - \omega & -\gamma R_t^H S^* - \omega \\ \gamma R_t^H I^* & \gamma R_t^H S^* - \lambda - \gamma \end{pmatrix}, \quad (3.62)$$

and

$$B = \begin{pmatrix} 0 & 0 \\ 0 & \varepsilon \end{pmatrix} = \begin{pmatrix} 0 & 0 \\ 0 & -\eta\gamma\lambda\chi_\tau \frac{R_t^H}{\gamma+\lambda} \end{pmatrix}, \quad (3.63)$$

The linear stability of the system is governed by the transcendental characteristic equation:

$$p(\mu) = \det(A - \mu I_{2 \times 2} + e^{-\mu\tau} B), \quad (3.64)$$

$$= \mu^2 - (a + d)\mu + \zeta + \varepsilon e^{-\mu\tau}(a - \mu) = 0, \quad (3.65)$$

where $\zeta = \det A$. We know that for the case $\tau = 0$, \mathcal{E}_* is globally asymptotically stable [82]. For the case $\tau \neq 0$, we then look for purely imaginary solutions, i.e., $\mu = i\phi$. We replace the ansatz $\mu = i\phi$ in eq. 3.65 and separate real and imaginary parts to obtain the system below:

$$\operatorname{Re}(p(i\phi)) = 0 \Leftrightarrow \varepsilon(a \cos(\phi\tau) - \phi \sin(\phi\tau)) = -\zeta + \phi^2, \quad (3.66)$$

$$\operatorname{Im}(p(i\phi)) = 0 \Leftrightarrow -\varepsilon(a \sin(\phi\tau) + \phi \cos(\phi\tau)) = (a + d)\phi. \quad (3.67)$$

To gain further analytical insights, we can add the square of equations 3.66 and 3.67, and use the substitution $z = \phi^2$ to obtain:

$$z^2 + \left((a + d)^2 - 2\zeta - \varepsilon^2\right)z + \zeta^2 - \varepsilon^2 a^2 = 0. \quad (3.68)$$

Although we can find an analytical solution for z in equation 3.68, this is of not much use, as parameters in eqs. 3.62 and 3.63 also depends on τ (which we aim to determine). Nonetheless, we can determine and narrow feasible intervals for other parameters from the conditions for the existence of roots. By numerically solving 3.66–3.67 for ϕ and τ , we calculate the stability diagram of the system in the (R_t^H, τ) plane. All other parameters are listed in Table 3.2. We use the MATLAB functions `fsolve` to find the roots and recursively build Fig. 3.5. However, finding these boundaries is not enough to determine whether a Hopf bifurcation is triggered, as we also need to know at what speed the real part of the eigenvalues crosses the imaginary axis. We can formally do this by analyzing the derivative of the real part of the eigenvalues on the line where $\mu = i\phi$.

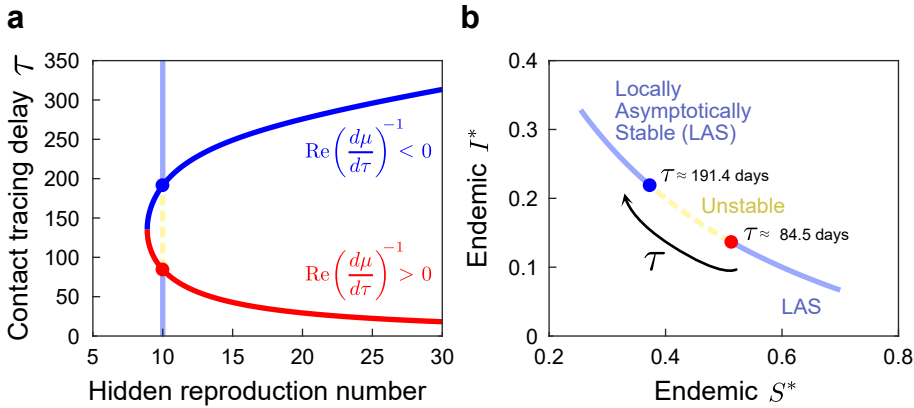


Figure 3.5: **Stability boundary and onset of Hopf bifurcation in the minimal SIR-TTI model.** **a:** Curves denote the stability boundary for the system, i.e., pairs (R_t^H, τ) for which the eigenvalues are purely imaginary and the sign of $\text{Re}\left(\frac{d\mu}{d\tau}\right)^{-1}$ when crossing the imaginary axis. We see the onset of two Hopf bifurcations for $R_t^H \geq 8.89$, joined in a cusp point of coordinates $(R_{\text{cusp}}, \tau_{\text{cusp}}) \approx (8.89, 135.48)$. The vertical line denotes the cut analyzed in panel **b**, analyzing the endemic equilibrium (S^*, I^*) of the system and its stability for $R_t^H = 10$.

Following the results in Section 2.3.1, to demonstrate that the eigenvalues cross the imaginary axis with a nonzero speed, we can calculate $\text{Re}\left(\frac{d\mu}{d\tau}\right)^{-1}$ instead. To do so, we differentiate $p(\mu)$ in equation 3.65 and obtain:

$$\begin{aligned} & \frac{d\mu}{d\tau} (2\mu - (a + d) - \varepsilon e^{-\mu\tau} (a\tau + 1 - \mu\tau)) \\ & - \mu \left(\frac{d(a + d)}{d\tau} + e^{-\mu\tau} \left(a\varepsilon + \frac{d\varepsilon}{d\tau} - \mu\varepsilon \right) \right) \end{aligned}$$

$$+\frac{d\zeta}{d\tau} + \frac{d(a\varepsilon)}{d\tau}e^{-\mu\tau} = 0. \quad (3.69)$$

We can rewrite equation 3.69 as:

$$\left(\frac{d\mu}{d\tau}\right)^{-1} = \frac{2\mu - (a + d) - \varepsilon e^{-\mu\tau} (a\tau + 1 - \mu\tau)}{\mu \left(\frac{d(a+d)}{d\tau} + e^{-\mu\tau} \left(a\varepsilon + \frac{d\varepsilon}{d\tau} - \mu\varepsilon\right)\right) - \left(\frac{d\zeta}{d\tau} + \frac{d(a\varepsilon)}{d\tau}e^{-\mu\tau}\right)}. \quad (3.70)$$

We evaluate it numerically along the critical lines, using the values in Table 3.2 again. We then confirm that what we have is a Hopf bifurcation and can delimit the stability boundaries in the $R_t^H - \tau$ plane, where the cusp point coordinates are $(R_{\text{cusp}}, \tau_{\text{cusp}}) \approx (8.89, 135.48)$ (Fig. 3.6a). We illustrate the dynamics in each regime by plotting some of the time series in Fig.3.6b. Time series were generated in MATLAB using the `dde23` solver with `RelTol = AbsTol = 10-12`, starting from $(S, I)\Big|_{t=0} = 0.9999(S^*, I^*)$. As the formulation for N^{tracing} in eq. 3.53 may overestimate the number of individuals to be removed from the I compartment, we stop the integration when the amplitude of the oscillations deviated more than a 20% from I^* . What would happen if we did not detect these events?

The overestimation of the fraction to be removed from the I compartment via contact tracing can lead to negative values for I , thereby violating the non-negativity constraint of our system of equations and rendering the model unphysical. To illustrate this, we proceed as follows. For a fixed value of R_t^H larger than R_{cusp} , we do a vertical cut on the parameter space and study the nature of the solutions for different values of τ in the different stability zones. For the experiment, we create an array of values for τ . We use as the initial condition (and constant his-

Table 3.2: Model parameters and values for simulations (minimal nonlinear SIR-TTI model).

Parameter	Meaning	Value	Units
γ	Recovery rate	1/360	day ⁻¹
τ	Contact tracing delay	0–350	day
λ	Testing and self-reporting rate	1/360	day ⁻¹
ω	waning immunity rate	2/360	day ⁻¹
R_t^H	Hidden reproduction number	5–30	–
η	Contact tracing efficiency	1	–

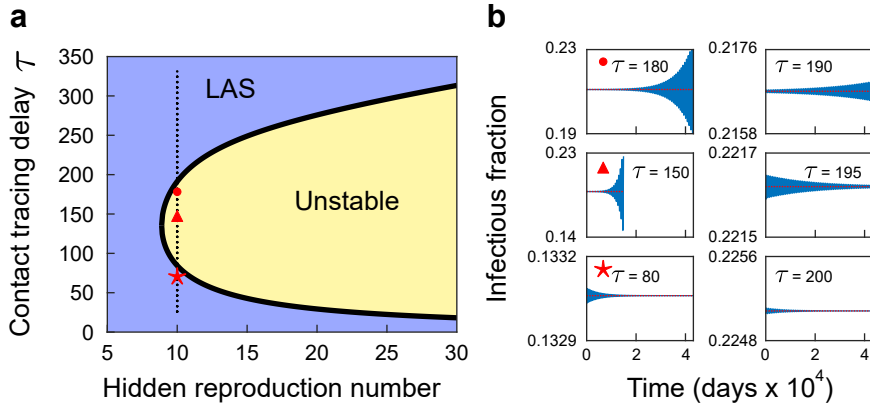


Figure 3.6: **Stability of the endemic equilibrium \mathcal{E}_* in the minimal SIR-TTI model.** **a:** Local stability boundary as a function of the contact tracing delay τ and the hidden reproduction number R_t^H . **b:** Time series for different values of τ when $R_t^H = 10$. We see that in the blue region in **a**, \mathcal{E}_* is Locally Asymptotically Stable (LAS), while it turns unstable inside of the yellow region. At $R_t^H = 10$, the boundary of the yellow region is given by $\tau_{\text{lower}} \approx 84.45$ and $\tau_{\text{upper}} \approx 191.38$.

tory function) for the i 'th simulation, the endemic equilibrium for τ_{i-1} . We let the system run for 500 years and detect when solutions become unphysical (e.g., negative or larger than one). Within the time frame analyzed, all solutions eventually yield unphysical solutions (Fig. 3.7). However, the results are the same if we start the swipe starting from the minimum or the maximum values of τ . While this suggests that hysteresis can be ruled out, it is not formal proof that the bifurcation is supercritical. To sum up, mathematical and physical conditions for a Hopf bifurcation are met, but the nature of this bifurcation cannot be ascertained as the model becomes unphysical before approaching the limit cycle.

If simple models as the minimal SIR-TTI model can feature such rich dynamics, what can we expect when adding the next layer of complexity, i.e., modeling human behavior?

3.5 SELF-REGULATION OF CONTAGIOUS CONTACTS AND VACCINATION WILLINGNESS

One of the major challenges of theoretical epidemiology is incorporating human behavior into disease spread models [4, 8, 9]. Why is this so important? As individuals become aware of the spread of the disease, e.g., by receiving information or being sick, they update their opinion, perception of risk, and behavior, readjusting contact patterns and

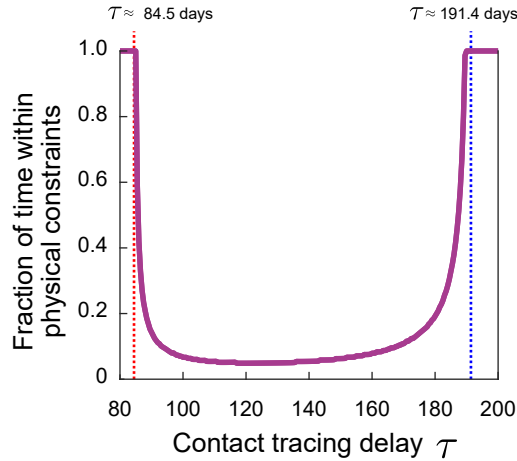


Figure 3.7: **Validity of the SIR-TTI model in the unstable regime.** After the Hopf bifurcation is triggered, oscillatory behavior renders our model unphysical in a finite time. We performed a vertical cut on the stability boundary described in Fig. 3.6a and determined the fraction of time (with respect to the total simulation time, 500 years) that a solution starting from a slightly perturbed endemic equilibrium would be physically feasible. We performed this swipe by recursively adapting the endemic equilibrium to $\mathcal{E}_*(\tau_{i-1})$ for the i 'th simulation. Results are robust and independent of the direction of the swipe, potentially hinting at a supercritical Hopf bifurcation.

compliance to interventions. Ultimately, this affects disease spread. The need to incorporate human behavior explicitly in disease models became apparent in the avian influenza and COVID-19 pandemics, where individuals drastically (and permanently) changed their behavior to cope with new threats.

However, incorporating human behavior in compartmental ODE models is not straightforward. We need to define *who* would react, to *what* they will react, and *how* they will react. First, we must capture potential heterogeneities in the population that can lead to different behavior. For example, in an age-stratified population leading to different beliefs or susceptibility to developing a severe course, or in a society with high inequality, do all social groups have the same resources to comply with official mandates or access trustworthy information? Second, we need to define a measure of risk or information index to which the population as a whole would react. For example, risk measures can be related to the current incidence or hospital occupancy from a "broadcast media" perspective or to the number of neighbors that are infected/hospitalized from a network/spatial perspective. Lastly, we need to define the effect of the behavior changes on the disease spread,

e.g., via a feedback loop between the perceived risk and their exposure to it.

Models dealing with any of the points above have been reported to feature rich dynamics. For example, populations with different susceptible classes feature synchronization in disease spread [83]. Resonance phenomena emerge from temporal contact patterns [84] or between interventions and the seasonal cycle of diseases [55]. People's opinion also forms clusters and even reshapes the contact network, thereby affecting disease spread [85]. Self-protective behavior, such as avoidance of the sick, can lead to changes in the social network and thereby decreases disease spread [86]. Seasonally forced models for disease spread in single and metapopulations show complex dynamics as phase locking and chaos (with realistically fewer infections) [87]. Chaos has also been reported in models incorporating behavior, and seasonality [21, 25].

Here, we illustrate the dynamics observable when including behavioral feedback loops for the self-regulation of contacts and vaccine willingness.

3.5.1 *Behavioral feedback loops*

One way to implement human behavior in mean-field compartmental models is through feedback loops. Particularly, using the probability of being infected and progressing to a severe course of the disease as risk measure, this feedback loop connects the current incidence (or hospital occupancy) with the force of infection or the perceived reward for being vaccinated. However, how this feedback loop should look like remains an open question.

Classical formulations (as, e.g., [25] and references therein) require three ingredients: i) how do people react to their perceived risk, ii) what people mind to build up their perceived risk or opinion, and iii) how do people learn this risk over time (or build their opinion). Model including these feature behavior-driven sustained oscillations (through a Hopf bifurcation induced by the delay kernel), and when coupled to seasonal forcing, even chaos and period doubling cascades to it [21, 22, 24]. In Chapter 7 we implement a data-inspired functional form for the behavioral feedback loop and use our model to assess different scenarios in the face of Winter 2022/2023.

3.5.2 *Long-term wave patterns and predictability*

A simple Susceptible-Infectious-Recovered-Susceptible (SIRS) model with mitigation feedback loop, as that in [21, 25], can have behavior-driven waves even in the absence of seasonality. These are triggered by a Hopf bifurcation which emerges when the reaction delay is sufficiently large. This induces a new way to understand disease spread as a "epidemiological oscillator", where the median mitigation delay τ of the memory kernel sets the natural frequency for oscillations.

However, when including seasonality, the epidemiological oscillator is subject to an external forcing, implying that we can study it as a driven oscillator (as, e.g., the van der Pol oscillator). This is thoroughly analyzed in Wagner [21].

3.5.3 *Short-term rebound waves*

In the context of disease spread, successful mitigation measures lead to a decrease in current incidence levels—not only in the targeted disease, but all diseases effected by the mitigation measures. However, when these measures are sustained for enough time, the levels of immunity among the population also decline (e.g., through waning immunity or demographic renewal). Therefore, when these measures are lifted, the population faces the disease with an *excess susceptibility*. As a result, the effective reproduction number of the disease is larger than expected and an atypical "rebound" wave emerges. How high these waves are depends on properties of the disease, the process and rates at which immunity is lost, and the particular mitigation measures.

Interventions that are active for a period comparable to the spreading rates of the disease can lead to resonance (or harvest it to be more effective). For example, if intermittent restrictions are acted and lifted such that the freedom days coincide with the onset of symptoms, then disease spread is accelerated (e.g., as discussed in Dehning et al. [88] regarding football matches in a championship). On the other end, lifting long-standing restrictions needs to take into account seasonality and other effects potentially leading to major surges in case numbers. The dependency with seasonality is not straightforward, and dominates over any other spreading parameters. This is thoroughly analyzed in Dönges [55].

Part II

COMPLEX DYNAMICS IN THE SPREAD OF
COVID-19

THE CHALLENGES OF CONTAINING
SARS-COV-2 VIA TEST-TRACE-AND-ISOLATE[†]







ABSTRACT

Without a cure, vaccine, or proven long-term immunity against SARS-CoV-2, test-trace-and-isolate (TTI) strategies present a promising tool to contain its spread. For any TTI strategy, however, mitigation is challenged by pre- and asymptomatic transmission, TTI-avoiders, and undetected spreaders, which strongly contribute to "hidden" infection chains. Here, we study a semi-analytical model and identify two tipping points between controlled and uncontrolled spread: (1) the behavior-driven reproduction number R_t^H of the hidden chains becomes too large to be compensated by the TTI capabilities, and (2) the number of new infections exceeds the tracing capacity. Both trigger a self-accelerating spread. We investigate how these tipping points depend on challenges like limited cooperation, missing contacts, and imperfect isolation. Our results suggest that TTI alone is insufficient to contain an otherwise unhindered spread of SARS-CoV-2, implying that complementary measures like social distancing and improved hygiene remain necessary.

Cite as: Contreras, S., Dehning, J., Loidolt, M., Zierenberg, J., Spitzner, F.P., Urrea-Quintero, J.H., Mohr, S.B., Wilczek, M., Wibral, M. and Priesemann, V., 2021. The challenges of containing SARS-CoV-2 via test-trace-and-isolate. Nature communications 12, 378 (2021). <https://doi.org/10.1038/s41467-020-20699-8>

[†] This chapter is identical to the publication [28]: *Contreras, S., Dehning, J., Loidolt, M., Zierenberg, J., Spitzner, F.P., Urrea-Quintero, J.H., Mohr, S.B., Wilczek, M., Wibral, M. and Priesemann, V.. The challenges of containing SARS-CoV-2 via test-trace-and-isolate. Nature communications 12, 378 (2021).* The article is published under the terms of a Creative Common License (<http://creativecommons.org/licenses/by/4.0/>). To this publication, I contributed equally with J. Dehning and M. Loidolt. Roles: Conceptualization, Methodology, Software, Validation, Formal analysis, Investigation, Writing – original draft, Writing – review & editing, Visualization (simulation-based figures).

The challenges of containing SARS-CoV-2 via test-trace-and-isolate

Sebastian Contreras ^{1,2,5}, Jonas Dehning^{1,5}, Matthias Loidolt ^{1,5}, Johannes Zierenberg ¹, F. Paul Spitzner¹, Jorge H. Urrea-Quintero¹, Sebastian B. Mohr ¹, Michael Wilczek ^{1,3}, Michael Wibral⁴ & Viola Priesemann ^{1,3}✉

Without a cure, vaccine, or proven long-term immunity against SARS-CoV-2, test-trace-and-isolate (TTI) strategies present a promising tool to contain its spread. For any TTI strategy, however, mitigation is challenged by pre- and asymptomatic transmission, TTI-avoiders, and undetected spreaders, which strongly contribute to "hidden" infection chains. Here, we study a semi-analytical model and identify two tipping points between controlled and uncontrolled spread: (1) the behavior-driven reproduction number R_t^H of the hidden chains becomes too large to be compensated by the TTI capabilities, and (2) the number of new infections exceeds the tracing capacity. Both trigger a self-accelerating spread. We investigate how these tipping points depend on challenges like limited cooperation, missing contacts, and imperfect isolation. Our results suggest that TTI alone is insufficient to contain an otherwise unhindered spread of SARS-CoV-2, implying that complementary measures like social distancing and improved hygiene remain necessary.

¹Max Planck Institute for Dynamics and Self-Organization, Am Faßberg 17, 37077 Göttingen, Germany. ²Centre for Biotechnology and Bioengineering, Universidad de Chile, Beauchef 851, 8370456 Santiago, Chile. ³Institute for the Dynamics of Complex Systems, University of Göttingen, Friedrich-Hund-Platz 1, 37077 Göttingen, Germany. ⁴Campus Institute for Dynamics of Biological Networks, University of Göttingen, Hermann-Rein-Straße 3, 37075 Göttingen, Germany. ⁵These authors contributed equally: Sebastian Contreras, Jonas Dehning, Matthias Loidolt. ✉email: viola.priesemann@ds.mpg.de

After SARS-CoV-2 started spreading rapidly around the globe in early 2020, many countries have successfully curbed the initial exponential rise in case numbers (“first wave”). Most of the successful countries employed a mix of measures combining hygiene regulations and mandatory physical distancing to reduce the reproduction number and the number of new infections^{1,2} together with testing, contact tracing, and isolation (TTI) of known cases^{3,4}. Among these measures, those aimed at distancing—like school closures and a ban of all unnecessary social contacts (“strict lockdown”)—were highly controversial, but have proven effective^{1,2}. Notwithstanding, distancing measures put an enormous burden on society and the economy. In countries that have controlled the initial outbreak, there is a strong motivation to relax distancing measures, albeit under the constraint to keep the spread of COVID-19 under control^{5,6}.

In principle, it seems possible that both goals can be reached when relying on the increased testing capacity for SARS-CoV-2 infections if complemented by contact tracing and quarantine measures (e.g., like TTI strategies⁴); South Korea and Singapore illustrate the success of such a strategy^{7–9}. In practice, resources for testing are still limited and costly, and health systems have capacity limits for the number of contacts that can be traced and isolated; these resources have to be allocated wisely to control disease spread¹⁰.

TTI strategies have to overcome several challenges to be effective. Infected individuals can become infectious before developing symptoms^{11,12}, and because the virus is quite infectious, it is crucial to minimize testing-and-tracing delays¹³. Furthermore, SARS-CoV-2 infections generally appear throughout the whole population (not only in regional clusters), which hinders an efficient and quick implementation of TTI strategies.

Hence, these challenges that impact and potentially limit the effectiveness of TTI need to be incorporated together into one model of COVID-19 control, namely (1) the existence of asymptomatic, yet infectious carriers^{14,15}—which are a challenge for symptom-driven but not for random-testing strategies; (2) the existence of a certain fraction of the population that is opposed to taking a test, even if symptomatic¹⁶; (3) the capacity limits of contact tracing and additional imperfections due to imperfect memory or non-cooperation of the infected. Last, enormous efforts are required to completely prevent the influx of COVID-19 cases into a given community, especially during the current global pandemic situation combined with relaxed travel restrictions^{5,17}. This influx makes virus eradication impossible; it only leaves a stable level of new infections or their uncontrolled growth as the two possible regimes of disease dynamics. Thus, policymakers at all levels, from nations to federal states, all the way down to small units like enterprises, universities, or schools, are faced with the question of how to relax physical distancing measures while confining COVID-19 progression with the available testing and contact-tracing capacity¹⁸.

Here, we employ a compartmental model of SARS-CoV-2 spreading dynamics that incorporates the challenges (1)–(3). We base the model parameters on literature or reports using the example of Germany. The aim is to determine the critical value for the reproduction number in the general (not quarantined) population (R_{crit}^H), for which disease spread can still be contained. We find that—even under optimal use of the available testing and contact tracing capacity—the “hidden” reproduction number R_t^H has to be maintained at sufficiently low levels, namely $R_t^H < R_{crit}^H \approx 2$ (95% CI: 1.42–2.70). Hence, hygiene and physical distancing measures are required in addition to TTI to keep the virus spread under control. To further assist the efficient use of resources, we investigate the relative merits of contact tracing, symptom-driven testing, and random testing. We demonstrate the danger of a

tipping point associated with the limited capacity of tracing contacts of infected people. Finally, we show how either testing scheme has to be increased to re-stabilize disease spread after an increase in the reproduction number.

Results

Model overview. We developed a SIR-type model^{19,20} with multiple compartments that incorporates the effects of test-trace-and-isolate (TTI) strategies (for a graphical representation of the model see Fig. 1 and Supplementary Fig. 1). We explore how TTI can contain the spread of SARS-CoV-2 for realistic scenarios based on the TTI system in Germany. A major difficulty in controlling the spread of SARS-CoV-2 are the cases that remain hidden and behave as the general population does, potentially having many contacts. We explicitly incorporate such a “hidden” pool H into our model and characterize the spread within by the reproduction number R_t^H , which reflects the population’s contact behavior. Cases remain hidden until they enter a “traced” pool through testing or by contact tracing of an individual that has already been tested positive (see Fig. 1). All individuals in the traced pool T isolate themselves (quarantine), reducing the reproduction number to R_t^T . Apart from a small leak, novel infections therein are then assumed to remain within the traced pool. We investigate both symptom-driven and random testing, which differ in the clinical characteristics of the cases they can reveal: random testing can, in principle, uncover even asymptomatic cases, while symptom-driven testing is limited to symptomatic cases willing to be tested. Parameters describing the spreading dynamics (Table 1) are based on the available literature on COVID-19^{15,16,21–23}, while parameters describing the TTI system are inspired by our example case of Germany wherever possible.

We provide the code of the different analyses at https://github.com/Priesemann-Group/covid19_tti (<https://doi.org/10.5281/zenodo.4290679>). An interactive platform to simulate scenarios different from those presented here is available on the same GitHub repository.

TTI strategies can in principle control SARS-CoV-2 spread. To demonstrate that TTI strategies can, in principle, control the disease spread, we simulated a new outbreak starting in the hidden pool (Fig. 2). We assume that the outbreak is unnoticed initially, and then evaluate the effects of two alternative testing and contact tracing strategies starting at day 0: Contact tracing is either efficient, i.e., 66% ($\eta = 0.66$) of the contacts of a positively tested person are traced and isolated without delay (“efficient tracing”), or contact tracing is assumed to be less efficient, identifying only 33% of the contacts (“inefficient tracing”). In both regimes, the default parameters are used (Table 1), which include symptom-driven testing with rate $\lambda_s = 0.1$, and isolation of all tested positively, which reduces their reproduction number by a factor of $\nu = 0.1$.

An efficient contact tracing rapidly depletes the hidden pool H and populates the traced pool T , and thus stabilizes the total number of infections $T + H$ (Fig. 2a). The system relaxes to its equilibrium, which is a function of TTI and epidemiological parameters (Supplementary Eqs. (3)–(5)). Consequently, the observed number of daily infections (\hat{N}^{obs}) approaches a constant value (Fig. 2b), while the observed reproduction number \hat{R}_t^{obs} approaches unity (Fig. 2c), further showing that effective TTI can be sufficient to stabilize the disease spread with $R_t^H = 1.8$.

In contrast, inefficient contact tracing cannot deplete the hidden pool sufficiently quickly to stabilize the total number of infections (Fig. 2d). Thus, the absolute and the observed daily

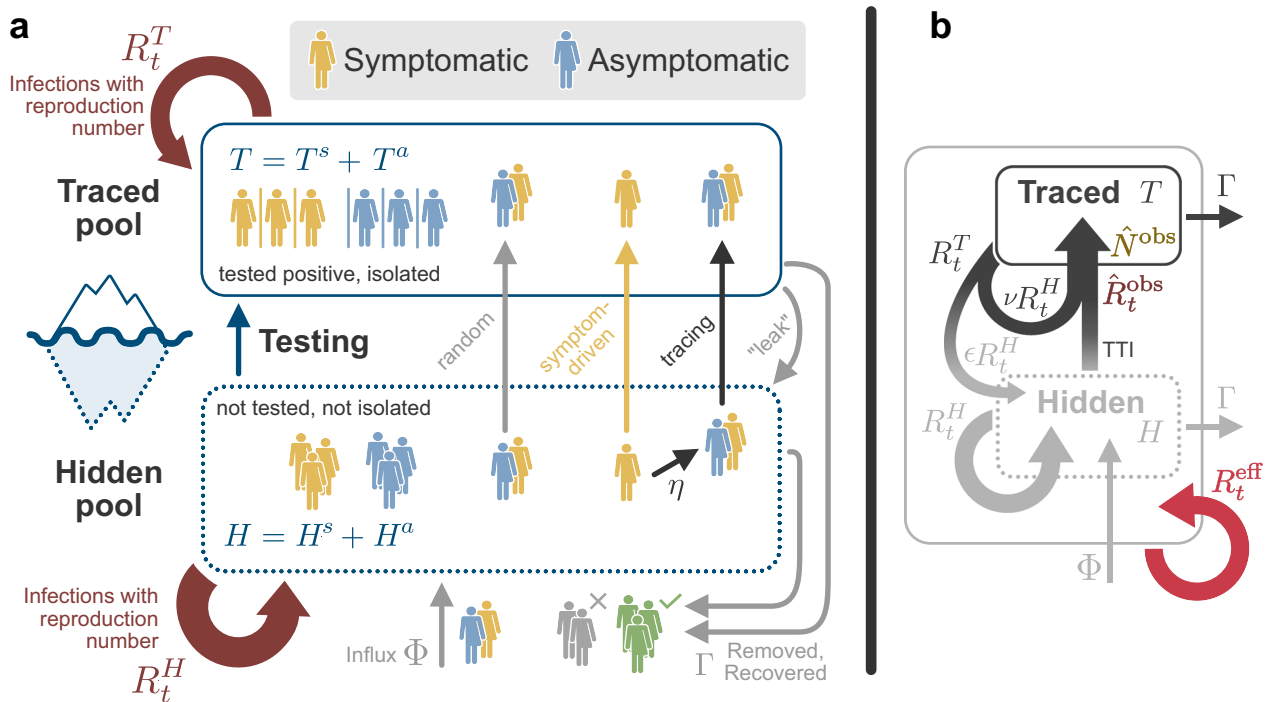


Fig. 1 Illustration of interactions between the hidden H and traced T pools in our model. **a** In our model, we distinguish two different infected population groups: the one that contains the infected individuals that remain undetected until tested (hidden pool H), and the one with infected individuals that we already follow and isolate (traced pool T). Super indexes s and a in both variables account for symptomatic and asymptomatic individuals. Until noticed, an outbreak will fully occur in the hidden pool, where case numbers increase according to this pool's reproduction number R_t^H . Testing and tracing of hidden infections transfers them to the traced pool and helps to empty the hidden pool; this prevents offspring infections and reduces the overall growth of the outbreak. Due to the self-isolation imposed in the traced pool, its reproduction number R_t^T is expected to be considerably smaller than R_t^H , and typically smaller than 1. Once an individual is tested positive, all the contacts since the infection are traced with some efficiency (η). Two external events further increase the number of infections in the hidden pool, namely, the new contagions occurring in the traced pool that leak to the hidden pool and an influx of externally acquired infections (Φ). In the absence of new infections, pool sizes are naturally reduced due to recovery (or removal), proportional to the recovery rate Γ . **b** Simplified depiction of the model showing the interactions of the two pools. New infections generated in the traced pool can remain there (ν) or leak to the hidden pool (ϵ). Note that the central epidemiological observables are highlighted in color: The \hat{N}^{obs} (brown) and \hat{R}_t^{obs} (dark red) can be inferred from the traced pool, but the effective reproduction number \hat{R}_t^{eff} (light red) that governs the stability of the whole system remains hidden.

Table 1 Model parameters.

Parameter	Meaning	Value (default)	Range	Units	Source
M	Population size	80,000,000		People	Assumed
R_t^H	Reproduction number (hidden)	1.80		-	2,67,68
Γ	Recovery rate	0.10	0.08–0.12	Day ⁻¹	58,69,70
ξ	Asymptomatic ratio	0.15	0.12–0.33	-	22,23
φ	Fraction skipping testing	0.20	0.10–0.40	-	16
ν	Isolation factor (traced)	0.10		-	Assumed
λ_r	random-testing rate	0	0–0.02	Day ⁻¹	Assumed
λ_s	symptom-driven testing rate	0.10	0–1	Day ⁻¹	Assumed
η	Tracing efficiency	0.66		-	Assumed
N_{max}	Maximal tracing capacity	≈ 718	200–6000	Cases day ⁻¹	Assumed ^a
ϵ	Missed contacts (traced)	0.10		-	Assumed
Φ	Influx rate (hidden)	15		Cases day ⁻¹	Assumed ^a
$\lambda_{r,\text{max}}$	Maximal test capacity per capita	0.002		Cases day ⁻¹	56,57
R_t^T	Reproduction number (traced)	0.36		-	$R_t^T = (\nu + \epsilon)R_t^H$
ξ^{aP}	Apparent asymptomatic ratio	0.32		-	$\xi^{\text{aP}} = \xi + (1 - \xi)\varphi$
R_{crit}^H	Critical reproduction number (hidden)	1.89		-	Numerically calculated from model parameters

^aChosen for a country with a population of $M = 80 \cdot 10^6$. See "Methods" for considerations.

number of infections N continue to grow approximately exponentially (Fig. 2e). In this case, the TTI strategy with ineffective contact tracing slows the spread but cannot control the outbreak.

TTI extends the stabilized regimes of spreading dynamics. Comparing the two TTI strategies from above demonstrates that two distinct regimes of spreading dynamics are attainable under the condition of a nonzero influx of externally acquired infections

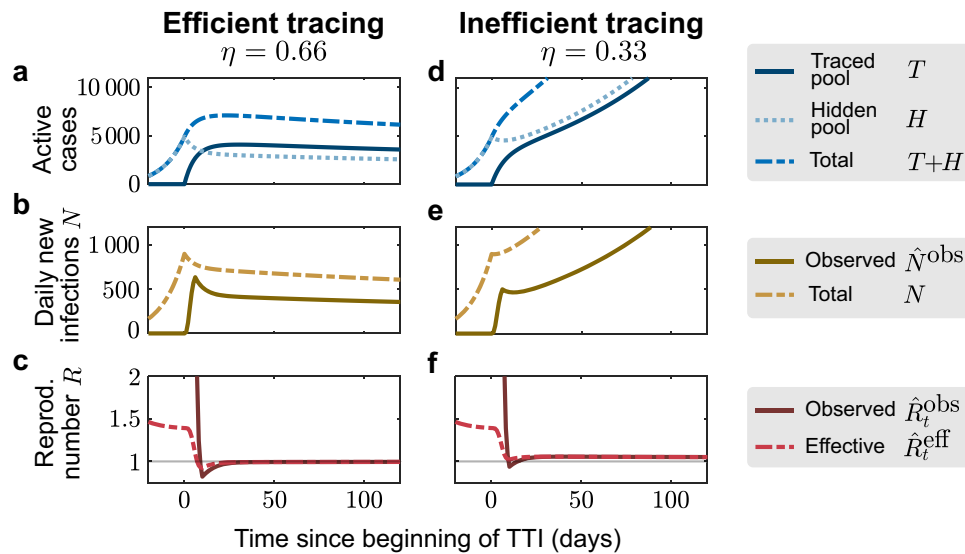


Fig. 2 Sufficient testing and contact tracing can control the disease spread, while insufficient TTI only slows it. We consider a test-trace-and-isolate (TTI) strategy with symptom-driven testing ($\lambda_s = 0.1$) and two tracing scenarios: For high tracing efficiency ($\eta = 0.66$, **a–c**), the outbreak can be controlled by TTI; for low tracing efficiency ($\eta = 0.33$, **d, e**) the outbreak cannot be controlled because tracing is not efficient enough. **a, d** The number of infections in the hidden pool grows until the outbreak is noticed on day 0, at which point symptom-driven testing ($\lambda_s = 0.1$) and contact tracing (η) starts. **b, e** The absolute number of daily infections (N) grows until the outbreak is noticed on day 0; the observed number of daily infections (\hat{N}^{obs}) shown here is simulated as being inferred from the traced pool and subject to a gamma-distributed reporting delay with a median of 4 days. **c, f** The observed reproduction number (\hat{R}_t^{obs}) is estimated from the observed new infections (\hat{N}^{obs}), while the effective reproduction number (\hat{R}_t^{eff}) is estimated from the total daily new infections (N). After an initial growth period, it settles to $\hat{R}_t^{\text{obs}} = 1$ if the outbreak is controlled (efficient tracing), or to $\hat{R}_t^{\text{obs}} > 1$ if the outbreak continues to spread (inefficient tracing). All the curves plotted are obtained from numerical integration of Eqs. (1)–(5).

Φ : The system either evolves towards some intermediate but stable number of new cases N (Fig. 2a–c), or it is unstable, showing a steep growth (Fig. 2d–f). These two dynamical regimes are characterized—after an initial transient—by different “observed” reproduction numbers \hat{R}_t^{obs} , inferred from the new cases of the traced pool \hat{N}^{obs} . If $\hat{R}_t^{\text{obs}} < 1$, the outbreak is under control (solid line in Fig. 2c), while for $\hat{R}_t^{\text{obs}} > 1$ the outbreak continues to spread (Fig. 2f). The former regime extends the “stable” regime of the simple SIR model beyond $R_t^H = 1$ and thus constitutes a novel “TTI-stabilized” regime of spreading dynamics (see below, and Supplementary Fig. 5 for the full phase diagram).

Limited TTI requires a safety margin to maintain stability. Having demonstrated that an effective TTI strategy can, in principle, control the disease spread, we now turn towards the problem of limited TTI capacity. So far, we assumed that the efficiency of the TTI strategy does not depend on the absolute number of cases. Yet, the amount of contacts that can reliably be traced by health authorities is limited due to the work to be performed by trained personnel: Contact persons have to be identified, informed, and ideally also counseled during the preventive quarantine. Exceeding this limit causes delays in the process, which will eventually become longer than the generation time of 4 days—rendering contact tracing ineffective. We model this tracing capacity as a hard cap N_{max} on the number of contacts that can be traced each day and explore its effects on stability.

As an example of how this limited tracing capacity can cause a new tipping point to instability, we simulate here a short but large influx of externally acquired infections (a total of 4000 hidden cases with 92% occurring in the 7 days around $t = 0$, normally distributed with $\sigma = 2$ days, see Fig. 3). This exemplary influx aims to resemble the large number of German holidaymakers returning from summer vacation. It is a rather conservative estimate given that there were 900 such cases observed in the first

two weeks of July at Bavarian highway test-centers alone²⁴. We set two different tracing-capacity limits, reached when the observed number of daily new cases \hat{N}^{obs} reaches $N_{\text{max}} = 718$ (or $N_{\text{max}} = 470$) observed cases per day (see “Methods”). In both scenarios, the sudden influx leads to a jump of infections in the hidden pool (Fig. 3a, d), followed by a rapid increase in new traced cases (Fig. 3b, e). With sufficiently high tracing capacity, the outbreak can then be contained, because during the initial shock \hat{N}^{obs} does not exceed the capacity limit N_{max} (Fig. 3b, brown vs gray lines). In contrast, with lower capacity, the outbreak accelerates as soon as the observed new cases \hat{N}^{obs} exceeds the capacity limit N_{max} . Not only the capacity limit but also the amplitude of the influx (Supplementary Fig. 3), its duration (Supplementary Fig. 4), or whether it occurs periodically (Fig. 4) can decide whether the observed new cases \hat{N}^{obs} exceed the capacity limit N_{max} and cause a tipping-over into instability. In particular, periodic influxes (e.g., holidays) may cause the tipping-over not necessarily because of a single event but due to their cumulative impact. These scenarios demonstrate that the limited tracing capacity renders the system metastable. If the capacity limit is exceeded due to some external perturbation, the tracing cannot compensate the perturbation, and the spread gets out of control.

Even without a large influx event, the tipping-over into instability can occur when a relaxation of contact restrictions causes slow growth in case numbers. This slow growth will accelerate dramatically once the tracing capacity limit is reached—constituting a transition from a slightly unstable to a strongly unstable regime (Fig. 5 and Supplementary Fig. 5d). To illustrate this, we simulated an increase of the hidden reproduction number R_t^H (of a system in stable equilibrium) at $t = 0$, from the subcritical default value of $R_t^H = 1.8$ to a supercritical value $R_t^H = 2$, which renders the system slightly unstable (Fig. 6). At $t = 0$, the case numbers start to grow slowly until the observed number of new cases exceeds the tracing capacity limit N_{max} .

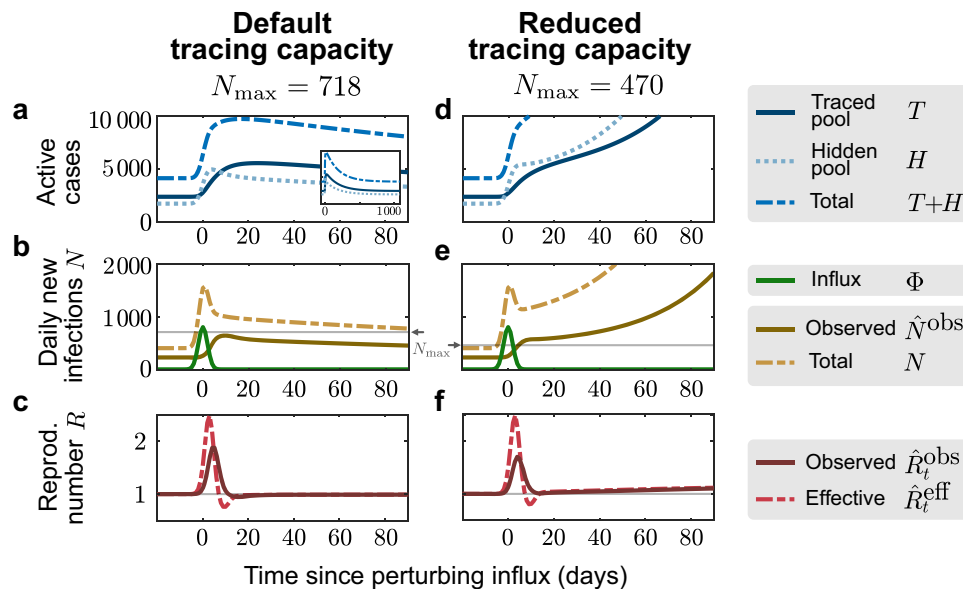


Fig. 3 Finite tracing capacity makes the system vulnerable to large influx events. A single large influx event (a total of 4000 hidden cases with 92% occurring in the 7 days around $t = 0$, normally distributed with standard deviation $\sigma = 2$ days) drives a metastable system with reduced tracing capacity (reached at $N_{\max} = 470$) to a new outbreak (**d-f**), whereas a metastable system with our default tracing capacity (reached at $N_{\max} = 718$) can compensate a sudden influx of this size (**a-c**). **a, d** The number of infections in the hidden pool (dotted) jump due to the influx event at $t = 0$, and return to stability for default capacity (**a**) or continue to grow in the system with reduced capacity (**d**). Correspondingly, the number of cases in the traced pool (solid line) either slowly increases after the event and absorbs most infections before returning to stability (inset in **a**, time axis prolonged to 1000 days), or proceeds to grow steeply (**d**). **b, e** The absolute number of new infections (dashed, yellow) jumps due to the large influx event (solid green line). The number of daily observed cases (solid brown line) slowly increases after the event, and relaxes back to baseline (**a**), or increases fast upon exceeding the maximum number of new observed cases N_{\max} (solid gray line) for which tracing is effective. **c, f** The effective (dashed red line) and observed (solid dark red line) reproduction numbers change transiently due to the influx event before returning to 1 for the default tracing capacity. In the case of a reduced tracing capacity and a new outbreak, they slowly begin to grow afterward (**f**). All the curves plotted are obtained from numerical integration of Eqs. (1)–(5).

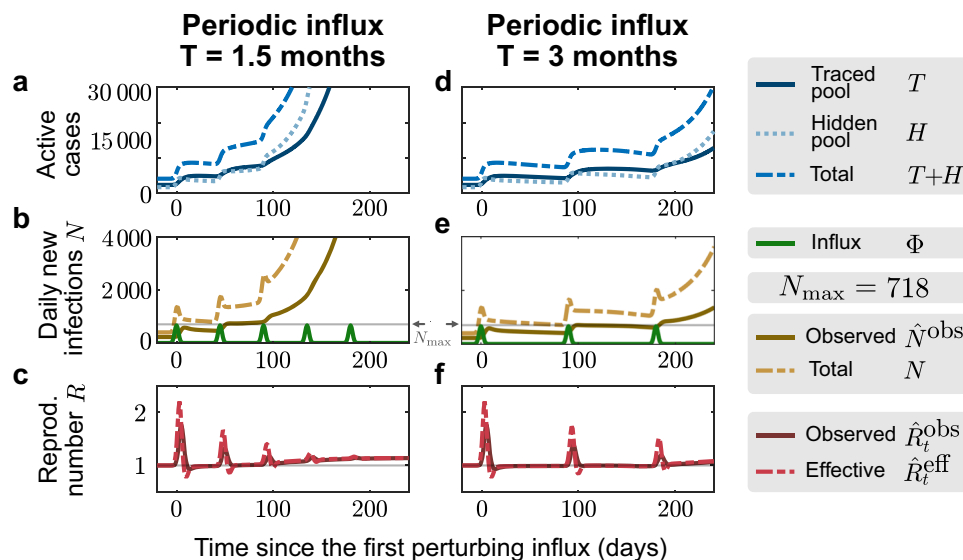


Fig. 4 Manageable influx events that recur periodically can overwhelm the tracing capacity. For the default capacity scenario, we explore whether periodic influx events can overwhelm the tracing capacity: A “manageable” influx that would not overwhelm the tracing capacity on its own (3331 externally acquired infections, 92% of which occur in 7 days) repeats every 1.5 months (**a-c**) or every 3 months (**d-f**). In the first case, the system is already unstable after the second event because case numbers remained high after the first influx (**b**). In the second case, the system remains stable after both the first and second event (**e**), but it becomes unstable after the third (**f**).

From thereon, the tracing system breaks down, and the growth self-accelerates. This is reflected in the steep rise of new cases after day 100—thus with a considerable delay after the change of R_t^H , i.e., the population’s behavior.

Both the initial change in the hidden reproduction number and the breakdown of the tracing system are reflected in the observed reproduction number \hat{R}_t^{obs} (Fig. 6c). It transits from stability ($\hat{R}_t^{\text{obs}} = 1$) to instability ($\hat{R}_t^{\text{obs}} > 1$). However, the absolute values

of \hat{R}_t^{obs} are not very indicative of the public's behavior (R_t^H), because already small changes in R_t^H can induce large transient changes in \hat{R}_t^{obs} . In our example, \hat{R}_t^{obs} shows a strong deflection after $t = 0$, although R_t^H changes only slightly; later, at $t \approx 100$ it starts to ramp to a new value, although R_t^H did not change. This ramping is due to the tracing capacity N_{max} being exceeded, which accelerates the spread. \hat{R}_t^{obs} finally approaches a new steady-state value, as sketched in Supplementary Fig. 5d. To summarize, deducing the stability of the spread from \hat{R}_t^{obs} is

challenging because \hat{R}_t^{obs} reacts very sensitively to many types of transients. R_t^H , in contrast, would be a reliable indicator of true spreading behavior but is not accessible easily.

Imperfect TTI would require further containment measures.

Above, we illustrated that a combination of symptom-driven testing and contact tracing could control the outbreak for a default reproduction number of $R_t^H = 1.8$. We now ask how efficient the TTI scheme and implementation must be to control the disease for a range of reproduction numbers—i.e., what TTI parameters are necessary to avoid the tipping over to $\hat{R}_t^{\text{eff}} > 1$. To this end, we perform linear stability analysis to calculate the critical reproduction number at which the tipping-over occurs (see Supplementary Eq. (1) in Supplementary Note 1). When assessing stability not only for a single scenario along the R_t^H -axis but for multiple parameter combinations, the tipping points turn into critical lines (or surfaces). Here, we examine how these critical lines depend on different combinations of symptom-driven testing, random testing, and contact tracing.

Random testing with tracing, but without symptom-driven testing ($\lambda_s = 0$), is not sufficient to contain an outbreak (under our default parameters and $R_t^H \leq 1.5$; Fig. 7a). This is because the rate of random testing λ_r would have to be unrealistically large. It exceeds the current capacity of testing ($\lambda_{r,\text{max}} \sim 0.002$, see “Methods” for details), even if ten tests are pooled ($\lambda_r \sim 10\lambda_{r,\text{max}}$ ²⁵). Thus, the contribution of symptom-driven testing is necessary to control any realistic new outbreak through TTI.

Contact tracing markedly contributes to outbreak mitigation (Fig. 7b). In its absence, i.e., when isolating only individuals that were positive in a symptom-driven or random test, the outbreak can be controlled for intermediate reproduction numbers ($R_t^H < 2.5$ in Fig. 7b) but not for higher ones if the limit of $\lambda_{r,\text{max}} < 0.02$ is respected.

The most effective combination appears to be symptom-driven testing together with contact tracing (Fig. 7c). This combination shows stability even for spreads close to the basic reproduction number $R_t^H = R_0 \approx 3.3$ ^{21,26,27}, when implemented extremely efficiently (e.g., with $\lambda_s = 0.66$ and $\eta = 0.66$). However, this

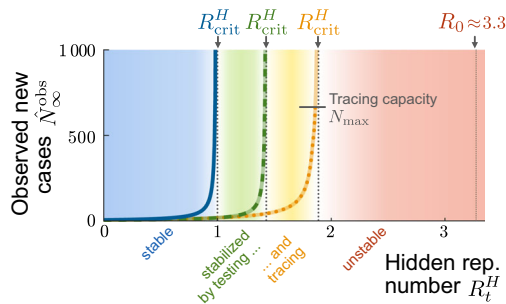


Fig. 5 Testing and tracing give rise to two TTI-stabilized regimes of spreading dynamics. In addition to the intrinsically stable regime of the simple SIR model (blue region), our model exhibits two TTI-stabilized regimes that arise from the isolation of formerly “hidden” infected individuals uncovered through symptom-based testing alone (green region) or additional contact tracing (amber region). Due to the external influx, the number of observed new cases reaches a nonzero equilibrium N_{∞}^{obs} that depends on the hidden reproductive number (colored lines). These equilibrium numbers of new cases diverge when approaching the respective critical hidden reproductive numbers (R_{crit}^H) calculated from linear stability analysis (dotted horizontal lines). Taking into account a finite tracing capacity N_{max} shrinks the testing-and-tracing stabilized regime and makes it metastable (dotted amber line). Note that, for our standard parameter set, the natural base reproduction number R_0 lies in the unstable regime. Please see Supplementary Fig. 5 for a full phase diagram and Supplementary Note 1 for the linear stability analysis.

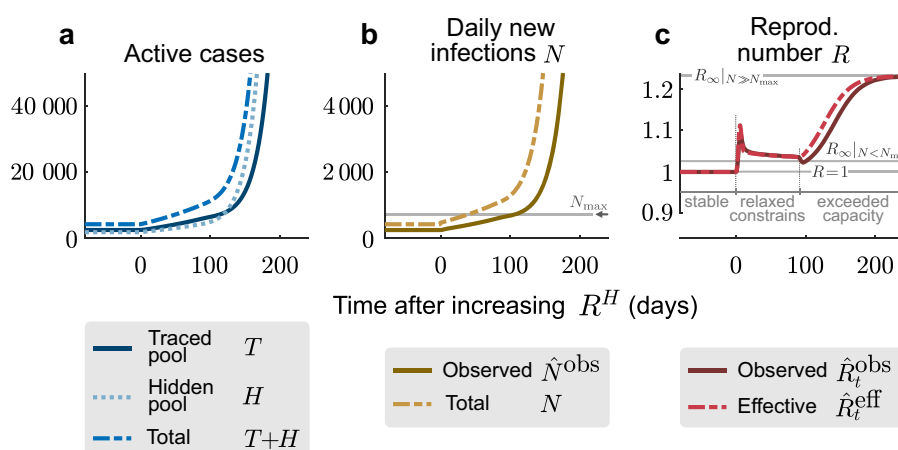


Fig. 6 A relaxation of restrictions can slowly overwhelm the finite tracing capacity and trigger a new outbreak. **a** At $t = 0$, the hidden reproduction number increases from $R_t^H = 1.8$ to $R_t^H = 2.0$ (i.e., slightly above its critical value). This leads to a slow increase in traced active cases (solid blue line). **b** When the number of observed new cases (solid brown line) exceeds the tracing capacity limit N_{max} (solid gray line), the tracing system breaks down, and the outbreak starts to accelerate. **c** After an initial transient at the onset of the change in R_t^H , the observed reproduction number (solid red line) faithfully reflects both the slight increase of the hidden reproduction number due to relaxation of contact constraints, and the strong increase after the tracing capacity (solid gray line) is exceeded at $t \approx 100$. In both cases, the observed reproduction number \hat{R}_t^{obs} approaches two different limit values R_{obs} , which are derived from a linear stability analysis (further details in Supplementary Fig. 5). All the curves plotted are obtained from numerical integration of Eqs. (1)–(5).

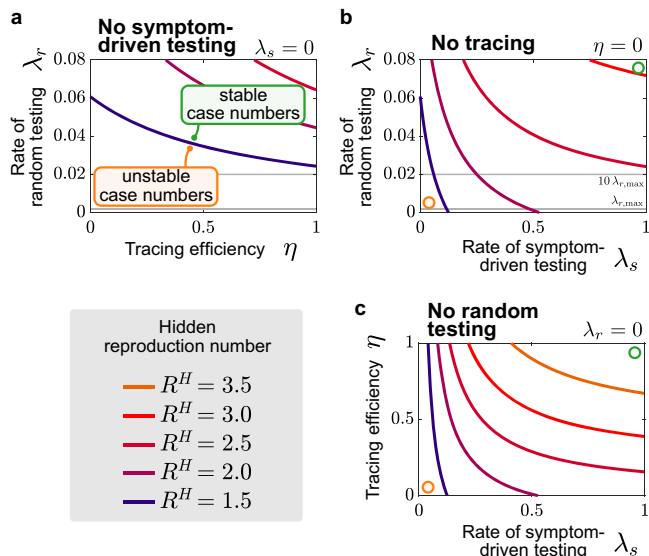


Fig. 7 Symptom-driven testing and contact tracing need to be combined to control the disease. Stability diagrams showing the boundaries (continuous curves) between the stable (controlled) and uncontrolled regimes for different testing strategies combining random testing (rate λ_r), symptom-driven testing (rate λ_s), and tracing (efficiency η). Gray lines in plots with λ_r -axes indicate capacity limits (for our example Germany) on random testing ($\lambda_{r,max}$) and when using pooling of ten samples, i.e., $10\lambda_{r,max}$. Colored lines depict the transitions between the stable and the unstable regime for a given reproduction number R_t^H (color-coded). The transition from ‘stable’ to ‘unstable’ case numbers is explicitly annotated for $R_t^H = 1.5$ in panel **a**. **a** Combining tracing and random testing without symptom-driven testing is in all cases not sufficient to control outbreaks, as the necessary random tests exceed even the pooled testing capacity ($10\lambda_{r,max}$). **b** Combining random and symptom-driven testing strategies without any contract tracing requires unrealistically high levels of random testing to control outbreaks with large reproduction numbers in the hidden pool ($R_t^H > 2.0$). The required random tests to significantly change the stability boundaries exceed the available capacity in Germany $\lambda_{r,max}$. Even considering the possibility of pooling tests ($10\lambda_{r,max}$) often does not suffice to control outbreaks. **c** Combining symptom-driven testing and tracing suffices to control outbreaks with realistic testing rates λ_s and tracing efficiencies η for moderate values of reproduction numbers in the hidden pool, R_t^H , but fails to control the outbreak for large R_t^H . The curves showing the critical reproduction number are obtained from the linear stability analysis (Supplementary Eq. (1)).

implementation would require that all symptomatic persons get tested within 1–2 days after getting infectious, thus potentially already in their pre-symptomatic phase, which may be difficult to realize. (Note that the asymptomatic cases are already accounted for in the model and do not pose an additional problem). Considering these difficulties, the combination of symptom-driven testing and contact tracing appears to be sufficient to contain outbreaks with intermediate reproduction numbers ($R_t^H \sim 2$ can be controlled with e.g., $\lambda_s \leq 0.5$ and $\eta = 0.66$, Fig. 7c).

Overall, our model suggests that the combination of timely symptom-driven testing within very few days, together with isolation of positive cases and efficient contact tracing, can be sufficient to control the spread of SARS-CoV-2 given the reproduction number in the hidden pool is $R_t^H \approx 2$ or lower. For random testing at the population level to be effective, one would require much higher test rates than currently available in Germany. Nevertheless, random testing can be useful to control highly localized outbreaks and is paramount for screening frontline workers in healthcare, eldercare, and education.

How can TTI allow the relaxation of contact constraints? There are currently strong incentives to loosen restrictive measures and return to a more pre-COVID-19 lifestyle^{28,29}. However, any such loosening can lead to a higher reproduction number R_t^H , which could potentially exceed the critical value R_{crit}^H , for which current TTI strategies ensure stability. To retain stability despite increasing R_t^H , this increase has to be compensated by stronger mitigation efforts, such as further improvement of TTI. Thereby the critical value R_{crit}^H is effectively increased. In the following, we compare the capacity of the different TTI and model parameter changes to compensate for increases in the reproduction number R_t^H . In detail, we start from the highest reproduction number that can be controlled by the default parameters, $R_{crit}^H = 1.89$, and calculate how each model parameter would have to be changed to achieve the desired increase in R_{crit}^H . For all default parameters, see Table 1.

First, we explore how well an increase of random and symptom-driven test rates can compensate for an increase in R_t^H (Fig. 8a). We find that population-wide random testing would need to increase extensively to compensate for increases in R_t^H , i.e., λ_r quickly exceeds realistic values (gray lines in Fig. 8a). Thus, random testing at a whole population level is not the most efficient tool to compensate for increases of the hidden reproduction rate, but that does not diminish its usefulness in controlling localized outbreaks or protecting frontline workers and highly vulnerable populations.

In contrast, scaling up symptom-driven testing can in principle compensate an increase of R_t^H up to about 3 (Fig. 8a). Beyond $R_t^H = 3$ and $\lambda_s \approx 0.4$, λ_s increases more steeply, making this compensation increasingly costly (Fig. 8a). Furthermore, levels of $\lambda_s > 0.5$ seem hard to realize as they would require testing within < 2 days of becoming infectious, i.e., while many infected are still pre-symptomatic. Realistically, only moderate increases in R_t^H can be compensated by decreasing the average delay of symptom-driven testing alone.

Tracing the contacts of an infected person and asking them to quarantine preventively is a vital contribution to contain the spread of SARS-CoV-2 if done without delay^{3,13}. As a default value, we assumed that a fraction $\eta = 0.66$ of contacts are traced and isolated within a day. This fraction can, in principle, be increased further to compensate for an increase in R_t^H and still guarantee stability (Fig. 8a). However, because η is already high in the first place, its range is quite limited, and even perfect contact tracing cannot compensate for an R_t^H of 2.5. More elaborate contact tracing strategies, like backward-forward tracing, might further improve its practical efficacy.

As an alternative to improved TTI rates and efficiencies, improved compliance may compensate for an increase in R_t^H : One might aim to reduce the number of contacts missed in the traced pool ϵ , improve the isolation factor ν , or reduce the fraction of people avoiding tests despite showing symptoms ϕ (Fig. 8c). These improvements might be more challenging to achieve from a policymaker perspective but could be targeted by educational and awareness-raising campaigns. However, since we assumed already in the default scenario that the behavioral factors (ϵ, ν, ϕ) are not too large, the potential improvement is limited.

The amount of reduction achievable by each method is limited, which calls to leverage all these strategies together. Furthermore, as can be seen from the curvature of the lines in Fig. 7, the beneficial effects are synergistic, i.e., they are larger when combining several strategies instead of spending twice the efforts on a unique one. This synergy of improved TTI measures and awareness campaigning could relax contact constraints while keeping outbreaks under control. Nonetheless, our model still

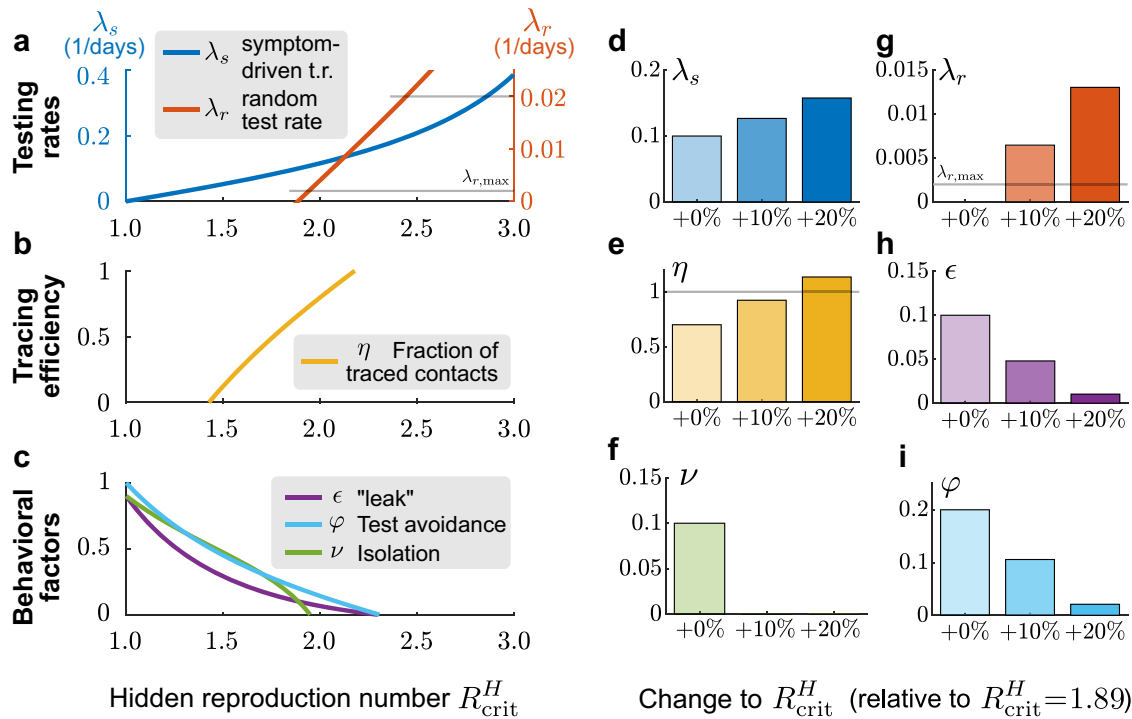


Fig. 8 Adapting testing strategies allows the relaxation of contact constraints to some degree. The relaxation of contact constraints increases the reproduction number of the hidden pool R_t^H , and thus needs to be compensated by adjusting model parameters to keep the system stable. **a–c** Value of a single parameter required to keep the system stable despite a change in the hidden reproduction number, while keeping all other parameters at default values. **a** Increasing the rate of symptom-driven testing (λ_s , blue) can in principle compensate for hidden reproduction numbers close to R_0 . However, this is optimistic as it requires that anyone with symptoms compatible with COVID-19 gets tested and isolated on average within 2.5 days—requiring extensive resources and efficient organization. Increasing the random-testing rate (λ_r , red) to the capacity limit (for the example Germany, gray line $\lambda_{r,max}$) would have almost no effect, pooling tests to achieve $10\lambda_{r,max}$ can compensate partly for larger increases in R_t^H . **b** Increasing the tracing efficiency (η) can compensate only small increases in R_t^H . **c** Decreasing the fraction of symptomatic individuals who avoid testing (φ), the leak from the traced pool (ϵ) or the escape rate from isolation (ν) can in principle compensate for small increases in R_t^H . **d–i** To compensate a 10% or 20% increase of R_t^H , while still keeping the system stable, symptom-driven testing (λ_s) could be increased (**d**), or ϵ or φ could be decreased (**h,i**). In contrast, only changing λ_r , η , or ν would not be sufficient to compensate a 10% or 20% increase in R_t^H , because the respective limits are reached (**e, f, g**). All parameter changes are computed through stability analysis (Supplementary Eq. (1)).

indicates that compensating the basic reproduction number $R_t^H = R_0 \approx 3.3^{21,26,27}$ might be very costly, and hence some degree of physical distancing might be required.

Robustness against parameter changes and model limitations.

Above, we showed that changing the implementation of the TTI strategy can accommodate higher reproduction numbers R_{crit}^H — but how robust are these implementations against parameter uncertainties? To explore the robustness of the resulting hidden reproduction number R_{crit}^H against simultaneous variation of multiple TTI parameters, we draw these parameters from beta distributions (because all parameters are bounded by 0 and 1) centered on the default values, and perform an error propagation analysis (Supplementary Table 1). We found that a hidden reproduction number of $R_t^H \leq 1.4$ (95% CI, 1.23–1.69) can be compensated by testing alone, whereas additional contact tracing allows a hidden reproduction number of $R_t^H \leq 1.9$ (95% CI, 1.42–2.70, Supplementary Fig. 2 and Supplementary Table 1). This shows that the exact implementation of the TTI strategy strongly impacts the public behavior that can be controlled. However, none of them allows for a complete lifting of the contact restrictions ($R_0 = 3.3$).

However, not only the robustness against variation of parameters is an important aspect but also underlying

assumptions in the model structure. Our model also comes with some inevitable simplifications, but these do not compromise the conclusions drawn here. Specifically, our model is simple enough to allow for a mechanistic understanding of its dynamics and analytical treatment of the control and stability problems. This remains true even when extending the model to incorporate more biological realism, e.g., the different transmissibility of asymptomatic and symptomatic cases (Supplementary Fig. 6). Owing to its simplicity it has certain limitations: In contrast to agent-based simulations^{30,31}, we do not include realistic contact structures^{4,5,32}—the infection probability is uniform across the whole population. This limitation will become relevant mostly when trying to devise even more efficient testing-and-tracing strategies or stabilizing a system very close to its tipping point. Compared to other mean-field based studies, which included a more realistic temporal evolution of infectiousness^{33,34}, we implicitly assume that infectiousness decays exponentially. This assumption has the disadvantage of making the interpretation of rate parameters more difficult, but should not affect the stability analyses presented here.

Discussion

Using a compartmental SIR-type model with realistic parameters based on our example case in Germany, we find that test-trace-and-isolate can, in principle, contain the spread of SARS-CoV-2 if

some physical distancing measures are continued. We analytically derived the existence of a novel metastable regime of spreading dynamics governed by the limited capacity of contact tracing and show how transient perturbations can tip a seemingly stable system into the unstable regime. Furthermore, we explored the boundaries of this regime for different TTI strategies and efficiencies of the TTI implementation.

Our results agree with other simulation and modeling studies investigating how efficient TTI strategies are in curbing the spread of the SARS-CoV-2. Both agent-based studies with realistic contact structures⁴ and studies using mean-field spreading dynamics with tractable equations^{33–37} agree that TTI measures are an important contribution to control the pandemic. Fast isolation is arguably the most crucial factor, which is included in our model in the testing rate λ_s . Yet, TTI is generally not perfect and the app-based solutions that have been proposed at present still lack the necessary large adoption that was initially foreseen, and that is necessary for these solutions to work³⁴. Our work, as well as others^{4,34,38,39}, shows that realistic TTI can compensate reproduction numbers of around 1.5–2.5, which is however lower than the basic reproduction number of around 3.3^{21,26,27}. This calls for continued contact reduction on the order of 25–55%, and it does highlight not only the importance of TTI but also the need for other mitigation measures.

Our work extends previous studies by combining the explicit modeling of a hidden pool (including test avoiders) to explore various ways of allocating testing-and-tracing resources. This allows us to investigate the effectiveness of multiple approaches to stabilize disease dynamics in the face of relaxation of physical distancing. This yields important insights for policymakers into how to allocate resources. We also include a capacity limit of tracing, which is typically not included in other studies. However, it is crucial to understand the metastable regime of a TTI-stabilized system and understand the importance of keeping a safety-distance to the critical reproduction number of a given TTI strategy. Last, we highlight the essential differences between the observed reproduction numbers—as they are reported in the media—and the more important, but hard to access, reproduction number in the hidden pool. Specifically, we show how the transient behavior of the observed reproduction number may be easily misinterpreted.

Limited TTI capacity implies a metastable regime with the risk of sudden explosive growth. Both testing and tracing contribute to containing the spread of SARS-CoV-2. However, if the number of new infections exceeds their capacity limit, an otherwise controlled spread becomes uncontrolled. This is particularly troubling because the spread is self-accelerating: the more the capacity limit is exceeded, the less testing and tracing can contribute to containment. The reproduction number has to stay below its critical value to avoid this situation and the number of new infections below TTI capacity. Therefore, it is advisable to maintain a safety margin to these limits. Otherwise, a small increase of the reproduction number, a super-spreading event⁴⁰, or a sudden influx of externally acquired infections e.g., after holidays, leads to uncontrolled spread. Re-establishing stability is then quite difficult.

As the number of available tests is limited, the relative efficiencies of random, symptom-driven and tracing-based testing should determine the allocation of resources¹⁰. The efficiency of test strategies in terms of the positivity rate is a primary metric to determine the allocation of tests⁴¹. Contact-tracing-based testing will generally be the most efficient use of tests (positivity rate on the order of $R_t^H / \{\text{number of contacts}\}$), especially in the regime of low contact numbers^{37,42}. The efficiency of symptoms-driven testing depends on the set of symptoms used for admission: Highly specific symptom sets will allow for a high yield, but miss a number of cases

(for instance, 33% of cases do not show a loss of smell/taste⁴³). In contrast, unspecific symptom sets will require a high number of tests, especially in seasons where other respiratory conditions are prominent (currently, the fraction of SARS-CoV-2 cases among all influenza-like cases is less than 4%⁴⁴). Random testing on a population level has the lowest positive rate in the regime of low prevalence that we focus on^{41,45}, but could be used in a targeted manner, e.g., screening of healthcare workers, highly vulnerable populations^{10,46} or those living in the vicinity of localized outbreaks. We conclude that contact-tracing-based testing and highly specific symptoms-based testing should receive the highest priority, with the remaining test capacity used on less specific symptoms-based testing and random screening in particular settings.

The cooperation of the general population in maintaining a low reproduction number is essential even with efficient TTI strategies in place. Our results illustrate that the reproduction number in the hidden pool R_t^H —which reflects the public's behavior—is still central to disease control. Specifically, we found that $R_t^H \leq 1.4$ (95% CI, 1.23–1.69) can very likely be compensated by testing and isolating alone, whereas additional contact tracing shifts this boundary to $R_t^H \leq 1.9$ (95% CI, 1.42–2.70, Supplementary Fig. 2 and Supplementary Table 1). Both of these values are substantially lower than the basic reproduction number of SARS-CoV-2, $R_0 \approx 3.3$ ^{21,26,27}. Thus, if the goal is to contain the spread of SARS-CoV-2 with the available TTI-related resources, the reproduction number in the hidden pool will have to be reduced effectively by roughly 25–55% compared to the beginning of the pandemic. This effective reduction may be achieved by a suitable combination of hygiene measures, such as mask-wearing, filtering or exchanging contaminated air, and physical distancing. Useful accompanying measures voluntarily include: immediately and strictly self-isolating upon any symptoms compatible with COVID-19, avoiding travel to any region with a higher infection rate, keeping a personal contact diary, using the digital tracing app, selecting only those contacts that are essential for one's well being, and avoiding contacts inside closed rooms if possible. Most of these measures and also an efficient tracing cannot be achieved without the widespread cooperation of the population. This cooperation might be increased by a ramping up of coordinated educational efforts around explaining mechanisms and dynamics of disease spreading to a broad audience—instead of just providing behavioral advice.

The parameters of the model have been chosen to suit the situation in Germany. We expect our general conclusions to hold for other countries, but of course, parameters would have to be adapted to local circumstances. For instance, some Asia-Pacific countries can keep the spread under control, employing mainly test-trace-and-isolate measures⁴⁷. Factors that contribute to this are (1) significantly larger investment in tracing capacity, (2) a smaller influx of externally acquired infections (especially in the case of New Zealand), and (3) the broader acceptance of mask-wearing and compliance with physical distancing measures. These countries illustrate that even once "control is lost" in the sense of our model, it can in principle be regained through political measures. A currently discussed mechanism to regain control is the "circuit breaker", a relatively strict lockdown to interrupt infection chains and bring case number down⁴⁸. Such a circuit breaker or reset is particularly effective if it brings the system below the tipping point and thereby enables controlling the spread by TTI again. Therefore, it should be designed to keep a delicate balance between duration, stringency, and timeliness⁴⁹.

To conclude, based on a simulation of disease dynamics influenced by realistic TTI strategies with parameters taken from the example of Germany, we show that the spreading dynamics of SARS-CoV-2 can only be stabilized if effective TTI strategies are combined with hygiene and physical distancing measures that

Table 2 Model variables.

Variable	Meaning	Units	Explanation
H^a	Hidden asymptomatic pool	People	Non-traced, non-isolated people who are asymptomatic or avoid being tested
H^s	Hidden symptomatic pool	People	Non-traced, non-isolated people who are symptomatic
T^a	Traced asymptomatic pool	People	Known infected and isolated people who are asymptomatic
T^s	Traced symptomatic pool	People	Known infected and isolated people who are symptomatic
H	Hidden pool	People	Total non-traced people: $H = H^a + H^s$
T	Traced pool	People	Total traced people: $T = T^a + T^s$
N	New infections (traced and hidden)	Cases day ⁻¹	Given by: $N = \Gamma(\nu + \epsilon)\hat{R}_t^H T + \Gamma R_t^H H + \Phi$
\hat{N}^{obs}	Observed new infections (influx to traced pool)	Cases day ⁻¹	Only cases of the traced pool; delayed on average by 4 days because of reporting
\hat{R}_t^{eff}	Estimated effective reproduction number	-	Estimated from the cases of all pools: $\hat{R}_t^{\text{eff}} = N(t)/N(t-4)$
\hat{R}_t^{obs}	Observed reproduction number	-	The reproduction number that can be estimated only from the observed cases: $\hat{R}_t^{\text{obs}} = \hat{N}^{\text{obs}}(t)/\hat{N}^{\text{obs}}(t-4)$

keep the reproduction number in the general population below a value of approximately $R_t^H \leq 1.9$ (95% CI, 1.42–2.70). As a system stabilized by TTI with a finite capacity is only in a metastable state and can be tipped into instability by one-time effects, it would be desirable to keep a safety-distance even to these values, if possible. The above bounds on the reproduction number in the hidden pool can be easily recomputed for other countries with different TTI capacities and reproduction numbers.

Methods

Model overview. We model the spreading dynamics of SARS-CoV-2 as the sum of contributions from two pools, i.e., traced T and hidden H infections (see the sketch in Fig. 1, and a complete list of parameters and variables, respectively in Tables 1 and 2). The first pool (T) contains traced cases revealed through testing or by contact tracing of an individual that has already been tested positive; all individuals in the traced pool are assumed to isolate themselves (quarantine), avoiding further contacts as well as possible. In contrast, in the second pool, infections spread silently and only become detected when individuals develop symptoms and get tested, or via random testing in the population. This second pool (H) is therefore called the hidden pool H ; individuals in this pool are assumed to exhibit the behavior of the general population, thus of everyone who is not aware of being infected. We model the mean-field interactions between the hidden and the traced pool by transition rates, determining the timescales of the model dynamics. These transition rates can implicitly incorporate both the time course of the disease and the delays inherent to the TTI process, but we do not explicitly model delays between compartments. We distinguish between symptomatic and asymptomatic carriers—this is central when exploring different testing strategies (as detailed below). We also include effects of non-compliance and imperfect contact tracing, as well as a nonzero influx Φ of new cases that acquired the virus from outside. As this influx makes the eradication of SARS-CoV-2 impossible, only an exponential growth of cases or a stable rate of new infections is possible modeling outcomes. Given the two possible behaviors of the system, indefinite growth, or stable cases, we frame our investigation as a stability problem. The aim is to implement test-trace-and-isolate strategies to allow the system to remain stable.

Spreading dynamics. Concretely, we use a modified SIR-type model, where infections I are either symptomatic (I^s) or asymptomatic (I^a), and they belong to the hidden (H) or a traced (T) pool of infections (Fig. 1), thus creating in total four compartments of infections (H^s , H^a , T^s , T^a). New infections are asymptomatic with a ratio ξ^{ap} ; the others are symptomatic. In all compartments, individuals are removed with a rate Γ because of recovery or death (see Table 1 for all parameters). In the hidden pool, the disease spreads according to the reproduction number R_t^H . This reproduction number reflects the disease spread in the general population, without testing induced isolation of individuals. In addition, the hidden pool receives a mobility-induced influx Φ of new infections. Cases are removed from the hidden pool (i) when detected by TTI, and put into the traced pool, or (ii) due to recovery or death.

The traced pool T contains those infected individuals who have been tested positive as well as their positively tested contacts. As these individuals are (imperfectly) isolated, they cause infections with a rate $\nu\Gamma R_t^H$, which are subsequently isolated and therefore stay in the traced pools and additional infections with a rate $\epsilon\Gamma R_t^H$, which are missed and act as an influx to the hidden pools. ν is the isolation factor, and ϵ is the leak factor. The overall reproduction number of the traced pool is therefore $R_t^T = (\nu + \epsilon)R_t^H$.

In the scope of our model, it is important to differentiate exchanges from pool to pool that are based either on the "reassignment" of individuals or on infections. To the former category belongs the testing and tracing, which transfer cases from the hidden pool to the traced pool. These transfers involve a subtraction and addition of case numbers in the respective pools. To the latter category belongs the recurrent infections ΓR_t^H or $\nu\Gamma R_t^H$ and the 'leak' infections $\epsilon\Gamma R_t^H$. Exchanges of this category involve only the addition of case numbers in the respective pool.

Within our model, we concentrate on the case of low incidence and a low fraction of immune people, as in the early phase of any new outbreak. Our model can also reflect innate or acquired immunity; one must rescale the population or the reproduction number. The qualitative behavior of the dynamics is not expected to change.

Parameter choices and scenarios. For any testing strategy, the fraction of infections that do not develop any symptoms across the whole infection timeline is an important parameter, and this also holds for testing strategies applied to the case of SARS-CoV-2. In our model, this parameter is called ξ^{ap} and includes, besides the real asymptomatic infections ξ , the fraction of individuals that avoid testing φ .

The exact value of the fraction of asymptomatic infections ξ , however, is still fraught with uncertainty, and it also depends on age^{15,50,51}. While early estimates were as high as 50% (for example ranging from 26 to 63%⁵²), these early estimates suffered from reporting bias, small sample sizes and sometimes included pre-symptomatic cases as well^{22,53}. Recent bias-corrected estimates from large sample sizes range between 12%²² and 33%²³. We decided to use 15% for the pure asymptomatic ratio ξ .

In addition, we include a fraction φ of individuals avoiding testing. This can occur because individuals do not want to be in contact with governmental authorities or because they deem risking a spread of SARS-CoV-2 less important than having to quarantine¹⁶. As this part of the population may act in the same manner as asymptomatic persons, we include it in the asymptomatic compartment of the hidden pool, assuming a value of 0.2. We thus arrive at an effective ratio of asymptomatic infections $\xi^{\text{ap}} = \xi + (1 - \xi)\varphi = 0.32$. We assume that both symptomatic and asymptomatic persons have the same reproduction number.

In general, infected individuals move from the hidden to the traced pool after being tested; yet, a small number of infections will leak from the traced to the hidden pool with rate $\epsilon\Gamma R_t^H$, with $\epsilon = 0.1$. A source of the leak would be a contact that has been infected, traced, and tested positive but still ignores quarantine instructions. For the model, this individual has the same effect on disease dynamics as someone from the hidden pool.

Another crucial parameter for any TTI strategy is the reproduction number in the hidden pool R_t^H . This parameter that typically represents the main driver of the spreading dynamics is, by definition, impossible to measure. It depends mainly on the contact behavior of the population and ranges from R_0 in the absence of contact restrictions to values below 1 during strict lockdown². For the default parameters of our model, we used a value of $R_t^H = 1.8$. This parameter was chosen after all others, aiming to mirror the epidemic situation in Germany during the early summer months, when infections remained approximately constant. It is just below the critical value $R_{\text{crit}}^H = 1.98$ for the default scenario, hence $\hat{R}_t^{\text{eff}} = 1$. This value of $R_t^H = 1.8$ is ~54% lower than the basic reproduction number $R_0 \approx 3.3$. Hence, we assume that some non-pharmacological interventions (physical distancing or hygiene measures) are in place, as was the case in Germany during the early summer months^{1,2}. For additional scenarios, we explored the impact of both higher and lower values of R_t^H on our TTI strategy (see Figs. 7, 8 and Supplementary Fig. 2).

Testing-and-tracing strategies. We consider three different testing-and-tracing strategies: random testing, symptom-driven testing, and specific testing of traced

contacts. Despite the naming—chosen to be consistent with existing literature^{4,36,42,54,55}—isolation of the cases tested positive is part of all of these strategies. The main differences lie in whom the tests are applied to and whether past contacts of an infected person are traced and told to isolate. Our model simulates the parallel application of all three strategies—as it is typical for real-world settings, and yields the effects of the ‘pure’ application of these strategies as corner cases realized via specific parameter settings.

Random testing is defined here as applying tests to individuals irrespective of their symptom status or whether they belonged to the contact-chain of other infected individuals. In our model, random testing transfers infected individuals from the hidden to the traced pool with a fixed rate λ_r , irrespective of them showing symptoms or not. In reality, random testing is often implemented as situation-based testing for a sub-group of the population, e.g., at a hot-spot, for groups at risk, or for people returning from travel. Such situation-based strategies would be more efficient than the random testing assumed in this model. Nonetheless, because random testing can detect symptomatic and asymptomatic persons alike, we decided to evaluate its potential contribution to containing the spread.

The number of random tests that can be performed is limited by the available laboratory and sample collection capacity. For orientation, we included therefore a maximal testing capacity of $\lambda_{r,max} = 0.002$ test per person and day, which reflects the laboratory capacity in Germany (1.2 Mio. per week)^{56,57}. Potentially, the testing capacity can be increased by pooling PCR tests, without strongly reducing the sensitivity²⁵. We acknowledge this possibility by taking into account a ten times larger testing capacity, $10 \cdot \lambda_{r,max} = 0.02$. This would correspond to every person being tested on average every 50 days (7 weeks)—summing to about 12 Mio. tests per week in Germany.

Symptom-driven testing is defined as applying tests to individuals presenting symptoms of COVID-19. In this context, it is important to note that non-infected individuals can have symptoms similar to those of COVID-19, as many symptoms are rather unspecific. Although symptom-driven testing suffers less from imperfect specificity, it can only uncover symptomatic cases that are willing to be tested (see below). Here, ‘symptomatic infected individuals’ are transferred from the hidden to the traced pool at rate λ_s .

We define λ_s as the daily rate at which symptomatic individuals get tested, among the subset who are willing to get tested. As the default value, we use $\lambda_s = 0.1$, which means that one in ten people that show symptoms gets tested each day and are subsequently isolated. Testing and isolation happen immediately in this model, but their report into the observed new daily cases \hat{N}^{obs} is delayed. Further real-world delays can effectively be modeled by a lower effective λ_s . In theory, this rate could be increased to one per day. However, this parameter range is on purpose, not simulated here. For SARS-CoV-2, such a fast detection is unrealistic because typically infected people show a delay of 1–2 days between the beginning of infectiousness and showing symptoms⁵⁸. Hence, $\lambda_s \approx 0.5$ is an upper limit to the symptom-driven testing rate.

Tracing contacts of positively tested individuals presents a very specific test strategy and is expected to be effective in breaking the infection chains if contacts self-isolate sufficiently quickly^{4,42,59}. However, as every implementation of a TTI strategy is bound to be imperfect, we assume that only a fraction $\eta < 1$ of all contacts can be traced. These contacts, if tested positive, are then transferred from the hidden to the traced pool. No delay is assumed here. The parameter η effectively represents the fraction of secondary and tertiary infections found through contact tracing. As this fraction decreases when the delay between testing and contact tracing increases, we assumed a default value of $\eta = 0.66$, i.e., on average, only two-thirds of subsequent infections are prevented.

Contact tracing is mainly done by the health authorities in Germany, and this clearly limits the maximum number N_{max} of observed new cases \hat{N}^{obs} , for which contact tracing is still functional. In the first part of the manuscript, we assume for simplicity that \hat{N}^{obs} is sufficiently small to not exceed the tracing capacity; in the second part, we explicitly explore the role of this limit.

In principle, the tracing capacity limit can be expressed in two ways, either as the number of observed cases \hat{N}^{obs} , at which tracing starts to break down (denoted by N_{max}), or as number of positive contacts that can maximally be detected and handled on average by the health departments (n_{max}). Both values depend strongly on the personnel capacity of the health departments and the population’s contact behavior. From the system’s equilibrium equations, we derive a linear relation between the two, with the proportionality being a function of the epidemiological and TTI parameters (Supplementary Eq. (14)). For simplicity, we only use N_{max} in the main text and refer the interested reader to the derivation in Supplementary Note 2.

As a default value, we assume $n_{max} = 300$ positive contacts that can be handled per day. This corresponds to $N_{max} = 718$ observed cases per day, from which the above-mentioned 300 cases were found through contact tracing. Thus, the remaining 418 either originate within the traced pool (e.g., infected family members) or were found through symptom-based testing and are therefore considered to be detected with much less effort. This limit of $n_{max} = 300$ is currently well within reach of the 400 health departments in Germany. At first sight, this limit may appear low (about one case per working day per health department). However, identifying, contacting, and counseling all contact persons

(thus many more persons than 300), and finally testing them and controlling their quarantine requires considerable effort.

Any testing can, in principle, produce both false-positive (quarantined individuals who were not infected) and false-negative (non-quarantined infected individuals) cases. In theory, false-positive rates should be meager (0.2% or less for RT-PCR tests). However, testing and handling of the probes can induce false-positive results^{60,61}. Under the low prevalence of SARS-CoV-2, false-positive could therefore outweigh true-positive, especially for the random-testing strategy, where the number of tests required to detect new infections would be very high^{62,63}. This should be carefully considered when choosing an appropriate testing strategy but has not been explicitly modeled here, as it does not contribute strongly to whether or not the outbreak could be controlled.

Model equations. The contributions of the spreading dynamics and the TTI strategies are summarized in the equations below. They govern the spreading dynamics of case numbers in and between the hidden and the traced pool, H and T . We assume a regime of low prevalence and low immunity, i.e., the majority of the population is susceptible. Thus, the dynamics are completely determined by spread (represented by the reproduction numbers R_i), recovery (characterized by the recovery rate Γ), external influx Φ and the impact of the TTI strategies:

$$\frac{dT}{dt} = \underbrace{\Gamma(\nu R_i^H - 1)T}_{\text{spreading dynamics}} + \underbrace{\lambda_s H^S + \lambda_r H}_{\text{testing}} + \underbrace{f(H^S, H)}_{\text{tracing}}, \tag{1}$$

$$\frac{dH}{dt} = \underbrace{\Gamma(R_i^H - 1)H}_{\text{spreading dynamics}} - \underbrace{(\lambda_s H^S + \lambda_r H)}_{\text{testing}} - \underbrace{f(H^S, H)}_{\text{tracing}} + \underbrace{\Gamma \epsilon R_i^H T}_{\text{missed contacts}} + \underbrace{\Phi}_{\text{external influx}}, \tag{2}$$

$$\frac{1}{1 - \xi^{ap}} \frac{dH^S}{dt} = \underbrace{\Gamma \left(R_i^H H - \frac{H^S}{1 - \xi^{ap}} \right)}_{\text{spreading dynamics}} - \underbrace{\frac{(\lambda_s + \lambda_r) H^S}{1 - \xi^{ap}}}_{\text{testing}} - \underbrace{f(H^S, H)}_{\text{tracing}} + \underbrace{\Gamma \epsilon R_i^H T}_{\text{missed contacts}} + \underbrace{\Phi}_{\text{external influx}}, \tag{3}$$

$$H^a = H - H^S, \tag{4}$$

with

$$f(H^S, H) = \min \{ n_{max}, \eta R_i^H (\lambda_s H^S + \lambda_r H) \}. \tag{5}$$

Equations (1) and (2) describe the dynamical evolution of both the traced and hidden pools. However, they are not sufficient to completely describe the underlying dynamics of the system in the hidden pool, as the symptomatic and asymptomatic sub-pools behave slightly differently: only from the symptomatic hidden pool (H^S) cases can be removed because of symptom-driven testing. Thus the specific dynamics of H^S is defined by equation (3). The dynamics of the asymptomatic hidden pool (H^a) can be inferred from Eq. (4). In the traced compartment, the asymptomatic and symptomatic pools do not need to be distinguished, as their behavior is assumed to be identical. Equation (5) reflects a potential limit n_{max} of the tracing capacity of the health authorities. It is expressed as the total number of positive cases that can be detected from tracing the contacts of people detected via symptom-driven testing (from H^S) or via random testing (from H).

Central epidemiological parameters that can be observed. In the real world, the disease spread can only be observed by the traced pool. While the ‘true’ number of daily infections N is a sum of all new infections in the hidden and traced pools, the ‘observed’ number of daily infections \hat{N}^{obs} is the number of new infections in the traced pool delayed by a variable reporting delay α . This includes internal contributions and contributions from testing and tracing:

$$N(t) = \underbrace{\Gamma(\nu + \epsilon) R_i^H T(t)}_{\text{traced pool}} + \underbrace{\Gamma R_i^H H(t)}_{\text{hidden pool}} + \underbrace{\Phi}_{\text{external influx}} \tag{6}$$

$$\hat{N}^{obs}(t) = \left[\underbrace{\Gamma \nu R_i^H T(t)}_{\text{traced pool}} + \underbrace{\lambda_s H^S(t) + \lambda_r H(t)}_{\text{testing}} + \underbrace{f(H^S(t), H(t))}_{\text{tracing}} \right] \mathcal{G}[\alpha = 4, \beta = 1](t), \tag{7}$$

where $f(H^S, H)$ is defined in (5), \otimes denotes a convolution and \mathcal{G} a Gamma distribution that models a variable reporting delay. The spreading dynamics are usually characterized by the observed reproduction number R_i^{obs} , which is calculated from the observed number of new cases $\hat{N}^{obs}(t)$. We here use the definition underlying the estimates that are published by Robert-Koch-Institute, the official body responsible for epidemiological control in Germany⁶⁴: the reproduction number is the relative change of daily new cases N separated by 4 days (the

assumed serial interval of COVID-19⁶⁵):

$$\hat{R}_t^{\text{obs}} = \frac{\hat{N}^{\text{obs}}(t)}{\hat{N}^{\text{obs}}(t-4)} \quad (8)$$

$$\hat{R}_t^{\text{eff}} = \frac{N(t)}{N(t-4)} \quad (9)$$

While only \hat{R}_t^{obs} is accessible from the observed new cases, in the model, one can also define an effective reproduction number \hat{R}_t^{eff} from the total number of daily new infections.

In contrast to the original definition of \hat{R}_t^{obs} ⁶⁴, we do not need to remove real-world noise effects by smoothing this ratio.

Numerical calculation of solutions and critical values. The numerical solution of the differential equations governing our model was obtained using a versatile solver based on an explicit Runge–Kutta (4,5) formula, `@ode45`, implemented in MATLAB (version 2020a), with default settings. This algorithm allows the solution of non-stiff systems of differential equations in the shape $y' = f(t, y)$, given a user-defined time-step (for us, 0.1 days). Suitability and details on the algorithm are further discussed in ref. ⁶⁶.

To derive the tipping point between controlled and uncontrolled outbreaks (e.g., critical values of R_t^H), and to plot the stability diagrams, we used the `@fzero` MATLAB function. This function uses a combination of bisection, secant, and inverse quadratic interpolation methods to find the roots of a function. For instance, following the discussion of Supplementary Note 1, R_{crit}^H was determined by finding the roots of the function returning the real part of the linear system's largest eigenvalue.

Reporting summary. Further information on research design is available in the Nature Research Reporting Summary linked to this article.

Data availability

Data used in this study was obtained through numerical simulation. It is available together with the code for solving our model's equations for default and user-customized parameters at https://github.com/Priesemann-Group/covid19_tti (<https://doi.org/10.5281/zenodo.4290679>). Alternatively, an interactive platform for simulating scenarios different from the herein presented is available on <http://covid19-tti.ds.mpg.de>, and users may download the data generated.

Code availability

We provide the code for generating graphics and all the different analyses included in both this manuscript and its Supplementary Information at https://github.com/Priesemann-Group/covid19_tti (<https://doi.org/10.5281/zenodo.4290679>). An interactive platform for simulating scenarios different from the herein presented is available on <http://covid19-tti.ds.mpg.de>.

Received: 4 September 2020; Accepted: 10 December 2020;
Published online: 15 January 2021

References

- Brauner, J. M. et al. Inferring the effectiveness of government interventions against COVID-19. *Science* <https://doi.org/10.1126/science.abd9338> (2020).
- Dehning, J. et al. Inferring change points in the spread of COVID-19 reveals the effectiveness of interventions. *Science* **369**, 1–10 (2020).
- Salathé, M. et al. COVID-19 epidemic in Switzerland: on the importance of testing, contact tracing and isolation. *Swiss Med. Weekly* **150**, w20225 (2020).
- Kucharski, A. J. et al. Effectiveness of isolation, testing, contact tracing, and physical distancing on reducing transmission of SARS-CoV-2 in different settings: a mathematical modelling study. *Lancet Infect. Dis.* [https://www.thelancet.com/journals/laninf/article/PIIS1473-3099\(20\)30457-6/abstract](https://www.thelancet.com/journals/laninf/article/PIIS1473-3099(20)30457-6/abstract) (2020).
- Ruktanonchai, N. W. et al. Assessing the impact of coordinated COVID-19 exit strategies across Europe. *Science* **369**, 1465–1470 (2020).
- Alwan, N. A. et al. Scientific consensus on the COVID-19 pandemic: we need to act now. *Lancet* **6736**, 19–20 (2020).
- Lee, V. J., Chiew, C. J. & Khong, W. X. Interrupting transmission of COVID-19: lessons from containment efforts in Singapore. *J. Travel Med.* **27**, taaa039 (2020).
- Pung, R. et al. Investigation of three clusters of COVID-19 in Singapore: implications for surveillance and response measures. *Lancet* **395**, 1039–1046 (2020).
- Kang, J. et al. South Korea's responses to stop the COVID-19 pandemic. *Am. J. Infect. Control* **48**, 1080–1086 (2020).
- Emanuel, E. J. et al. Fair allocation of scarce medical resources in the time of COVID-19. *New England J. Medicine* **382**, 2049–2055 (2020).
- Li, G., Li, W., He, X. & Cao, Y. Asymptomatic and presymptomatic infections: hidden sources of COVID-19 disease. *Clin. Infect. Dis.* **71**, 2018–2018 (2020).
- Ye, F. et al. Delivery of infection from asymptomatic carriers of COVID-19 in a familial cluster. *Int. J. Infect. Dis.* **94**, 133–138 (2020).
- Kretzschmar, M., Rozhnova, G. & van Boven, M. Effectiveness of isolation and contact tracing for containment and slowing down a COVID-19 epidemic: a modelling study. *SSRN 3551343* (2020).
- Rothe, C. et al. Transmission of 2019-nCoV infection from an asymptomatic contact in Germany. *N. Engl. J. Med.* **382**, 970–971 (2020).
- Lai, C.-C. et al. Asymptomatic carrier state, acute respiratory disease, and pneumonia due to severe acute respiratory syndrome coronavirus 2 (SARS-CoV-2): facts and myths. *J. Microbiol. Immunol. Infect.* **53**, 404–412 (2020).
- McDermott, J. H. & Newman, W. G. Refusal of viral testing during the SARS-CoV-2 pandemic. *Clin. Med.* **20**, e163 (2020).
- Linka, K., Rahman, P., Goriely, A. & Kuhl, E. Is it safe to lift COVID-19 travel bans? The Newfoundland story. *Comput. Mech.* **66**, 1081–1092 (2020).
- Panovska-Griffiths, J. et al. Determining the optimal strategy for reopening schools, the impact of test and trace interventions, and the risk of occurrence of a second COVID-19 epidemic wave in the UK: a modelling study. *The Lancet Child & Adolescent Health.* **4**, 817–827 (2020).
- Kermack, W. O. & McKendrick, A. G. A contribution to the mathematical theory of epidemics. *Proc. Royal Soc. Lond. Ser. A* **115**, 700–721 (1927).
- Hethcote, H. W. An immunization model for a heterogeneous population. *Theor. Popul. Biol.* **14**, 338–349 (1978).
- Liu, Y., Gayle, A. A., Wilder-Smith, A. & Rocklöv, J. The reproductive number of COVID-19 is higher compared to SARS coronavirus. *J. Travel Med.* **27**, taaa021 (2020).
- Byambasuren, O. et al. Estimating the extent of true asymptomatic COVID-19 and its potential for community transmission: systematic review and meta-analysis. *Official Journal of the Association of Medical Microbiology and Infectious Disease Canada* **5**, 223–234 (2020).
- Pollán, M. et al. Prevalence of SARS-CoV-2 in Spain (ENE-COVID): a nationwide, population-based seroepidemiological study. *Lancet* **396**, 535–544 (2020).
- Rising, D. Coronavirus positive? Thousands in Germany left wondering. https://www.washingtonpost.com/world/europe/german-coronavirus-tests-backlog-900-positive-not-yet-told/2020/08/13/c62382e2-dd41-11ea-b4f1-25b762cddbfb4_story.html (2020).
- Lohse, S. et al. Pooling of samples for testing for SARS-CoV-2 in asymptomatic people. *Lancet Infect. Dis.* (2020). [https://www.thelancet.com/journals/laninf/article/PIIS1473-3099\(20\)30362-5/abstract](https://www.thelancet.com/journals/laninf/article/PIIS1473-3099(20)30362-5/abstract) (2020).
- Alimohamadi, Y. et al. Estimate of the basic reproduction number for COVID-19: a systematic review and meta-analysis. *J. Prev. Med. Public Health* **53**, 151–157 (2020).
- Barber, A. et al. The basic reproduction number of SARS-CoV-2: a scoping review of available evidence. Preprint at <https://www.medrxiv.org/content/10.1101/2020.07.28.20163535v1> (2020).
- Bonaccorsi, G. et al. Economic and social consequences of human mobility restrictions under COVID-19. *Proc. Natl Acad. Sci. USA* **117**, 15530–15535 (2020).
- Rowthorn, R. & Maciejowski, J. A cost-benefit analysis of the COVID-19 disease. *Oxford Rev. Econ. Policy* **36** (Suppl 1), S38–S55 (2020).
- Kerr, C. C. et al. Covasim: an agent-based model of COVID-19 dynamics and interventions. Preprint at <https://www.medrxiv.org/content/10.1101/2020.05.10.20097469v1> (2020).
- Jalayer, M., Orsenigo, C. & Vercellis, C. CoV-ABM: a stochastic discrete-event agent-based framework to simulate spatiotemporal dynamics of COVID-19. Preprint at <https://arxiv.org/abs/2007.13231> (2020).
- Meloni, S. et al. Modeling human mobility responses to the large-scale spreading of infectious diseases. *Sci. Rep.* **1**, 62 (2011).
- Fraser, C., Riley, S., Anderson, R. M. & Ferguson, N. M. Factors that make an infectious disease outbreak controllable. *Proc. Natl Acad. Sci. USA* **101**, 6146–6151 (2004).
- Ferretti, L. et al. Quantifying SARS-CoV-2 transmission suggests epidemic control with digital contact tracing. *Science* **368** <https://doi.org/10.1126/science.abb6936> (2020).
- Lunz, D., Batt, G. & Ruess, J. To quarantine, or not to quarantine: A theoretical framework for disease control via contact tracing. *Epidemics* <https://doi.org/10.1016/j.epidem.2020.100428> (2020).
- Sturniolo, S., Waites, W., Colbourn, T., Manheim, D. & Panovska-Griffiths, J. Testing, tracing and isolation in compartmental models. Preprint at <https://www.medrxiv.org/content/10.1101/2020.05.14.20101808v3> (2020).

37. Colbourn, T. et al. Modelling the health and economic impacts of population-wide testing, contact tracing and isolation (PTTI) strategies for COVID-19 in the UK. SSRN <https://doi.org/10.2139/ssrn.3627273> (2020).
38. Hellewell, J. et al. Feasibility of controlling COVID-19 outbreaks by isolation of cases and contacts. *Lancet Global Health* **8**, e488–e496 (2020).
39. Davis, E. L. et al. An imperfect tool: COVID-19 'test & trace' success relies on minimising the impact of false negatives and continuation of physical distancing. Preprint at <https://www.medrxiv.org/content/10.1101/2020.06.09.20124008v3> (2020).
40. Althouse, B. M. et al. Stochasticity and heterogeneity in the transmission dynamics of SARS-CoV-2. Preprint at <https://arxiv.org/abs/2005.13689> (2020).
41. Kasy, M. & Teytelboym, A. Adaptive targeted infectious disease testing. *Oxford Rev. Econ. Policy* **36**, S77–S93 (2020).
42. Firth, J. A. et al. Combining fine-scale social contact data with epidemic modelling reveals interactions between contact tracing, quarantine, testing and physical distancing for controlling COVID-19. Preprint at <https://www.medrxiv.org/content/10.1101/2020.05.26.20113720v2> (2020).
43. Chen, A. et al. Are gastrointestinal symptoms specific for coronavirus 2019 infection? A prospective case-control study from the United States. *Gastroenterology* [https://www.gastrojournal.org/article/S0016-5085\(20\)30664-8/abstract](https://www.gastrojournal.org/article/S0016-5085(20)30664-8/abstract) (2020).
44. Influenza, A. Influenza-Monatsbericht. https://influenza.rki.de/Wochenberichte/2019_2020/2020-32.pdf (2020).
45. Cleavelly, M., Susskind, D., Vines, D., Vines, L. & Wills, S. A workable strategy for COVID-19 testing: stratified periodic testing rather than universal random testing. *Oxford Rev. Econ. Policy* **36**, S14–S37 (2020).
46. Rivett, L. et al. Screening of healthcare workers for SARS-CoV-2 highlights the role of asymptomatic carriage in COVID-19 transmission. *eLife* **9**, 1–20 (2020).
47. Han, E. et al. Lessons learnt from easing COVID-19 restrictions: an analysis of countries and regions in Asia Pacific and Europe. *Lancet* **6736**, 1–10 (2020).
48. Keeling, M. J. et al. Precautionary breaks planned limited duration circuit breaks to control the prevalence of COVID-19. Preprint at <https://medrxiv.org/cgi/content/short/2020.10.13.20211813> (2020).
49. Contreras, S., Dehning, J., Mohr, S. B., Spitzner, F. P. & Priesemann, V. Low case numbers enable long-term stable pandemic control without lockdowns. *medRxiv* <https://doi.org/10.1101/2020.12.10.20247023> (2020).
50. Kronbichler, A. et al. Asymptomatic patients as a source of COVID-19 infections: a systematic review and meta-analysis. *Int. J. Infect. Dis.* **98**, 180–186 (2020).
51. Huang, L. et al. Rapid asymptomatic transmission of COVID-19 during the incubation period demonstrating strong infectivity in a cluster of youngsters aged 16–23 years outside Wuhan and characteristics of young patients with COVID-19: a prospective contact-tracing study. *J. Infect.* **80**, e1–e13 (2020).
52. Lavezzo, E. et al. Suppression of a SARS-CoV-2 outbreak in the Italian municipality of Vo'. *Nature* **584**, 425–429 (2020).
53. Chau, N. V. V. et al. The natural history and transmission potential of asymptomatic SARS-CoV-2 infection. *Clin. Infect. Dis.* **71**, 2679–2687 (2020).
54. Aleta, A. et al. Modeling the impact of social distancing, testing, contact tracing and household quarantine on second-wave scenarios of the COVID-19 epidemic. Preprint at <https://www.medrxiv.org/content/10.1101/2020.05.06.20092841v1> (2020).
55. Chung, S.-C. et al. A rapid systematic review and case study on test, contact tracing, testing, and isolation policies for COVID-19 prevention and control. Preprint at <https://www.medrxiv.org/content/10.1101/2020.06.04.20122614v2> (2020).
56. Institut, R. K. Epidemiologisches Bulletin 32/33 2020. https://www.rki.de/DE/Content/Infekt/EpidBull/Archiv/2020/Ausgaben/32-33_20.pdf (2020).
57. Eddy, M. Welcome back to Germany. Now take your free virus test. The New York Times. <https://www.nytimes.com/2020/08/05/world/europe/germany-coronavirus-test-travelers.html> (2020).
58. He, X. et al. Temporal dynamics in viral shedding and transmissibility of COVID-19. *Nat. Med.* **26**, 672–675 (2020).
59. Kojaku, S., Hébert-Dufresne, L. & Ahn, Y.-Y. The effectiveness of contact tracing in heterogeneous networks. Preprint at <https://arxiv.org/abs/2005.02362> (2020).
60. Smyrliaki, I. et al. Massive and rapid COVID-19 testing is feasible by extraction-free SARS-CoV-2 RT-qPCR. *Nat Commun* **11**, 4812 (2020).
61. Cohen, A. N. & Kessel, B. False positives in reverse transcription PCR testing for SARS-CoV-2. Preprint at <https://www.medrxiv.org/content/10.1101/2020.04.26.20080911v1.full.pdf> (2020).
62. Cencetti, G. et al. Using real-world contact networks to quantify the effectiveness of digital contact tracing and isolation strategies for COVID-19 pandemic. Preprint at <https://www.medrxiv.org/content/10.1101/2020.05.29.20115915v1.full.pdf> (2020).
63. Kirkcaldy, R. D., King, B. A. & Brooks, J. T. COVID-19 and postinfection immunity: limited evidence, many remaining questions. *J. Am. Med. Assoc.* **323**, 2245–2246 (2020).
64. an der Heiden, M. & Hamouda, O. Schätzung der aktuellen Entwicklung der SARS-CoV-2-Epidemie in Deutschland – Nowcasting. *Epidemiologisches Bull.* **2020**, 10–15 (2020).
65. Lauer, S. A. et al. The incubation period of coronavirus disease 2019 (COVID-19) from publicly reported confirmed cases: estimation and application. *Ann. Int. Med.* **172**, 577–582 (2020).
66. Shampine, L. F. & Reichelt, M. W. The MATLAB ode suite. *SIAM J. Sci. Comput.* **18**, 1–22 (1997).
67. Contreras, S. et al. Statistically-based methodology for revealing real contagion trends and correcting delay-induced errors in the assessment of COVID-19 pandemic. *Chaos, Solitons Fractals* **139**, 110087 (2020).
68. Pan, A. et al. Association of public health interventions with the epidemiology of the COVID-19 outbreak in Wuhan, China. *J. Am. Med. Assoc.* **323**, 1915–1923 (2020).
69. Pan, F. et al. Time course of lung changes on chest CT during recovery from 2019 novel coronavirus (COVID-19) pneumonia. *Radiology* **295**, 715–721 (2020).
70. Ling, Y. et al. Persistence and clearance of viral RNA in 2019 novel coronavirus disease rehabilitation patients. *Chinese Med. J.* **133**, 1039–1043 (2020).

Acknowledgements

We thank the Priesemann group for exciting discussions and their valuable comments. We also thank helpful comments and suggestions from Jakob Ruess (Inria), Ralf Meyer (Göttingen Uni), Álvaro Olivera-Nappa (Universidad de Chile). Open Access funding enabled and organized by Projekt DEAL. All authors received support from the Max-Planck-Society. S.C. acknowledges funding from the Centre for Biotechnology and Bioengineering - CeBiB (PIA project FB0001, Conicyt, Chile). M.L., J.D., and P.S. acknowledge funding by SMARTSTART, the joint training program in computational neuroscience by the VolkswagenStiftung and the Bernstein Network. JZ received financial support from the Joachim Herz Stiftung. M. Wibral is employed at the Campus Institute for Dynamics of Biological Networks funded by the VolkswagenStiftung.

Author contributions

S.C., J.D., J.Z., and V.P. designed research. S.C. conducted research. S.C., J.D., J.Z., M.L., M. Wibral, M. Wilczek, and V.P. analyzed the data. S.C., P.S., M.L., J.U., and S.B.M. created figures. All authors wrote the paper.

Funding

Open Access funding enabled and organized by Projekt DEAL.

Competing interests

The authors declare no competing interests.

Additional information


Supplementary information is available for this paper at <https://doi.org/10.1038/s41467-020-20699-8>.

Correspondence and requests for materials should be addressed to V.P.

Peer review information *Nature Communications* thanks Seth Blumberg and the other, anonymous reviewer(s) for their contribution to the peer review of this work. Peer review reports are available.

Reprints and permission information is available at <http://www.nature.com/reprints>

Publisher's note Springer Nature remains neutral with regard to jurisdictional claims in published maps and institutional affiliations.

 **Open Access** This article is licensed under a Creative Commons Attribution 4.0 International License, which permits use, sharing, adaptation, distribution and reproduction in any medium or format, as long as you give appropriate credit to the original author(s) and the source, provide a link to the Creative Commons license, and indicate if changes were made. The images or other third party material in this article are included in the article's Creative Commons license, unless indicated otherwise in a credit line to the material. If material is not included in the article's Creative Commons license and your intended use is not permitted by statutory regulation or exceeds the permitted use, you will need to obtain permission directly from the copyright holder. To view a copy of this license, visit <http://creativecommons.org/licenses/by/4.0/>.

© The Author(s) 2021

LOW CASE NUMBERS ENABLE LONG-TERM
STABLE PANDEMIC CONTROL WITHOUT
LOCKDOWNS[†]

ABSTRACT

The traditional long-term solutions for epidemic control involve eradication or population immunity. Here, we analytically derive the existence of a third viable solution: a stable equilibrium at low case numbers, where test-trace-and-isolate policies partially compensate for local spreading events and only moderate restrictions remain necessary. In this equilibrium, daily cases stabilize around ten or fewer new infections per million people. However, stability is endangered if restrictions are relaxed or case numbers grow too high. The latter destabilization marks a tipping point beyond which the spread self-accelerates. We show that a lockdown can reestablish control and that recurring lockdowns are not necessary given sustained, moderate contact reduction. We illustrate how this strategy profits from vaccination and helps mitigate variants of concern. This strategy reduces cumulative cases (and fatalities) four times more than strategies that only avoid hospital collapse. In the long term, immunization, large-scale testing, and international coordination will further facilitate control.

Cite as: Contreras, S., Dehning, J., Mohr, S. B., Bauer, S., Spitzner, F. P., and Priesemann, V. (2021). Low case numbers enable long-term stable pandemic control without lockdowns. Science advances, 7(41), eabg2243. <https://doi.org/10.1126/sciadv.abg2243>

[†] This chapter is identical to the publication [20]: Contreras, S., Dehning, J., Mohr, S. B., Bauer, S., Spitzner, F. P., and Priesemann, V. (2021). Low case numbers enable long-term stable pandemic control without lockdowns. *Science advances*, 7(41), eabg2243. The article is published under the terms of a Creative Commons License (<http://creativecommons.org/licenses/by/4.0/>). To this publication, all coauthors contributed equally. Roles: Conceptualization, Methodology, Software, Validation, Formal analysis, Investigation, Writing – original draft, Writing – review & editing, Visualization (simulation-based figures).

EPIDEMIOLOGY

Low case numbers enable long-term stable pandemic control without lockdowns

Sebastian Contreras^{1,2†}, Jonas Dehning^{1†}, Sebastian B. Mohr^{1†}, Simon Bauer^{1†}, F. Paul Spitzner^{1†}, Viola Priesemann^{1,3,*†}

The traditional long-term solutions for epidemic control involve eradication or population immunity. Here, we analytically derive the existence of a third viable solution: a stable equilibrium at low case numbers, where test-trace-and-isolate policies partially compensate for local spreading events and only moderate restrictions remain necessary. In this equilibrium, daily cases stabilize around ten or fewer new infections per million people. However, stability is endangered if restrictions are relaxed or case numbers grow too high. The latter destabilization marks a tipping point beyond which the spread self-accelerates. We show that a lockdown can reestablish control and that recurring lockdowns are not necessary given sustained, moderate contact reduction. We illustrate how this strategy profits from vaccination and helps mitigate variants of concern. This strategy reduces cumulative cases (and fatalities) four times more than strategies that only avoid hospital collapse. In the long term, immunization, large-scale testing, and international coordination will further facilitate control.

INTRODUCTION

As severe acute respiratory syndrome coronavirus 2 (SARS-CoV-2) is becoming endemic and knowledge about its spreading is accumulated, it becomes clear that neither global eradication nor population immunity will be achieved soon. Eradication is hindered by the worldwide prevalence and by asymptomatic spreading. Reaching population immunity without an effective vaccine or medication would take several years and cost countless deaths, especially among the elderly (1, 2). Moreover, evidence for long-term effects (“long COVID”) is surfacing (3–6), advising against strategies aiming to progressively exposing people to the disease so that they acquire natural immunity. Hence, we need long-term, sustainable strategies to contain the spread of SARS-CoV-2. The common goal, especially in countries with an aging population, should be to minimize the number of infections and, thereby, allow reliable planning for individuals and the economy, while not constraining individuals’ number of contacts too much (7). Intuitively, a regime with low case numbers not only would benefit public health and psychological well-being but also would profit the economy (8, 9).

However, control of SARS-CoV-2 is challenging. Many infections originate from asymptomatic or presymptomatic cases (10) or indirectly through aerosols (11), rendering mitigation measures difficult. Within test-trace-and-isolate (TTI) strategies, the contribution of purely symptom-driven testing is limited, but together with contact tracing, it can uncover asymptomatic chains of infections. The rising availability of effective vaccines against SARS-CoV-2 promises to relieve the social burden caused by nonpharmaceutical interventions (NPIs). However, it is unclear how fast the restrictions can be lifted without risking another wave (12–14) and how well vaccines will protect against more contagious or immune response-escaping variants. Additional challenges are the potential influx of SARS-CoV-2 infections (brought in by travelers or

commuting workers from abroad), imperfect quarantine, limited compliance, and TTI and case-reporting delays. Last, any country’s capacity to perform TTI is limited, so spreading dynamics change depending on the level of case numbers. Understanding these dynamics is crucial for informed policy decisions.

RESULTS

Analytical framework: Overview

We analytically show the existence of a stable regime at low case numbers, where control of SARS-CoV-2 is much easier to achieve and sustain. In addition, we investigate mitigation strategies and long-term control for corona virus disease 2019 (COVID-19), where we build on our past work to understand the effectiveness of NPIs, particularly TTI strategies (15–17). The strategy that we propose does not rely on the availability of a cure or vaccine, and it is applicable not only to further waves of COVID-19 but also to other emerging diseases with pandemic potential. Nonetheless, we also show how vaccination campaigns will further facilitate the success of the proposed strategy, assuming a vaccination rate as planned for countries in the European Union (13).

For quantitative assessments, we adapt a susceptible-exposed-infectious-recovered (SEIR)-type compartmental model (18) to explicitly include a realistic TTI system that considers the challenges above. In our framework, individuals can be tested (and subsequently quarantined if tested positive) by three different mechanisms. First, symptomatic infections with COVID-19-specific symptoms would self-report or be diligently identified by surveillance and get a preferential test. Second, random asymptomatic screening would be homogeneously deployed in the general population disregarding symptoms so that every individual could be tested alike. Third, all the close contacts of those individuals recently tested positive by the two mechanisms mentioned above would also be tested. Understandably, limited resources pose a complex challenge for resource allocation, where efficient TTI would only be possible at low case numbers. We also built an interactive platform where enthusiastic readers can simulate scenarios different from those presented here in <http://covid19-metastability.ds.mpg.de/>.

¹Max Planck Institute for Dynamics and Self-Organization, Am Faßberg 17, 37077 Göttingen, Germany. ²Centre for Biotechnology and Bioengineering, Universidad de Chile, Beauchef 851, 8370456 Santiago, Chile. ³Department of Physics, University of Göttingen, Friedrich-Hund-Platz 1, 37077 Göttingen, Germany.

*Corresponding author. Email: viola.priesemann@ds.mpg.de

†All authors contributed equally to this work.

A central parameter for our analysis is the level of contagious contacts k_t (relative to pre-COVID-19). More precisely, k_t refers to the fraction of infection risk-bearing encounters compared to pre-COVID-19 contact levels. We can then interpret k_t in terms of the hidden reproduction number R_t^H , which accounts for the number of offspring infections generated by individuals unaware of being infectious, i.e., hidden infections in a naive and fully susceptible population (15). Thus, in terms of R_t^H , k_t can be understood as the ratio between the offspring infections a hidden individual would generate in the presence and in the absence of NPIs, in other words, $R_t^H = k_t R_0$. Apart from direct contact reduction, contributions that allow increasing k_t without compromising the stability of the system also come from improved hygiene, mandatory face mask policies, frequent ventilation of closed spaces, and avoiding indoor gatherings, among other precautionary measures. As the latter measures are relatively fixed, direct contact reduction remains the central free variable, which is also the one tuned during lockdowns. All other parameters (and their references) are listed in Table 1.

Equilibrium at low case numbers

We find a regime where the spread reaches an equilibrium at low daily case numbers between the scenarios of eradication of the disease or uncontrolled spreading. The main control parameter that

determines whether the system can reach an equilibrium is the level of contagious contacts k_t .

If the reduction in the contact level k_t is mild, then case numbers grow exponentially, as measures could not counterbalance the basic reproduction number [$R_0 \approx 3.3$ for SARS-CoV-2 (19, 20)] (Fig. 1B). In contrast, if the reduction in k_t is strong and (together with hygiene and TTI) outweighs the drive by the basic reproduction number, then case numbers decrease to a low equilibrium value (Fig. 1D).

If the reduction in k_t is moderate (and just about balances the drive by the basic reproduction number), we find a metastable regime: The spread is stabilized if and only if the overall case numbers are sufficiently low to enable fast and efficient TTI (Fig. 1C). However, this control is lost if the limited TTI capacity is overwhelmed. Beyond that tipping point, the number of cases starts to grow exponentially as increasingly more infectious individuals remain undetected (15).

The capacity of TTI determines the minimal required contact reduction for controlling case numbers around an equilibrium. If case numbers are sufficiently below the TTI capacity limit, then the maximum allowed level of contacts to enable the (meta-)stable regime in our default scenario (cf. Table 1, with $R_0 = 3.3$) is $k_t^{crit} = 61\%$ [95% confidence interval (CI): [47, 76]]. When the level of contacts k_t is below the threshold, case numbers asymptotically

Table 1. Model parameters.

Parameter	Meaning	Value (default)	Range	Units	Source
M	Population size	1,000,000		People	–
R_0	Basic reproduction number	3.3	2.2–4.4	–	(19, 20)
ν	Registered contacts (quarantined)	0.075		–	Assumed
ϵ	Lost contacts (quarantined)	0.05		–	Assumed
γ	Recovery/removal rate	0.10	0.08–0.12	Day ⁻¹	(64, 65)
ξ	Asymptomatic ratio	0.32	0.15–0.43	–	(51, 52, 54)
λ_s	Symptom-driven testing rate	0.25	0–1	Day ⁻¹	Assumed
λ'_s	Symptom-driven testing rate (reduced capacity)	0.1		Day ⁻¹	Assumed
λ_r	Random testing rate	0.0	0.0–0.1	Day ⁻¹	Assumed
η	Tracing efficiency	0.66		–	Assumed
τ	Contact tracing delay	2		Days	Assumed
N_{max}^{test}	Maximal tracing capacity	50	10–75	Cases day ⁻¹	Assumed
Φ_t	External influx	1		Cases day ⁻¹	Assumed
ρ	Exposed-to-infectious rate	0.25		Day ⁻¹	(10, 66)
D_L	Lockdown duration	4	0–8	Weeks	(27)
D_{ramp}	Phase-transition duration (lockdown)	1		Weeks	(27)
χ_τ	Fraction of contacts traced before becoming infectious	0.61		–	Eq. 17
$\chi_{s,r}$	Fraction of contacts traced after becoming infectious, before being tested (symptomatic and random)	0.30		–	Eq. 20
χ_r	Fraction of contacts traced after becoming infectious, before being tested (random)	0.39		–	Eq. 18

Table 2. Model variables.

Variable	Meaning	Units	Explanation
S	Susceptible pool	People	Noninfected people that may acquire the virus
E^Q	Exposed pool (quarantined)	People	Total quarantined exposed people
E^H	Exposed pool (hidden)	People	Total nontraced, nonquarantined exposed people
$I^{H,s}$	Infectious pool (hidden, symptomatic)	People	Nontraced, nonquarantined people who are symptomatic
I^H	Infectious pool (hidden)	People	Total nontraced, nonquarantined infectious people
I^Q	Infectious pool (quarantined)	People	Total quarantined infectious people
N	New infections (total)	Cases day ⁻¹	Given by: $N = \gamma k_t R_0 I^H + \gamma(v + \epsilon) R_0 I^Q + \frac{S}{M} \Phi_t$.
k_t	Contact reduction	%	Reduction of infectious contacts, related to pre-COVID-19 times
\hat{N}^{obs}	Observed new infections (influx to traced pool)	Cases day ⁻¹	Daily new cases, observed from the quarantined pool; delayed because of imperfect reporting and realistic contact tracing
\hat{R}_t^{obs}	Observed reproduction number		The reproduction number that can be estimated only from the observed cases: $\hat{R}_t^{\text{obs}} = \hat{N}^{\text{obs}}(t) / \hat{N}^{\text{obs}}(t - 4)$
N^{test}	Number of cases found through testing	People	Cases can be found either through symptomatic or random testing $N^{\text{test}} = N_t^{\text{test}} + N_s^{\text{test}}$
N^{traced}	Number of uncovered infections through tracing	People	This number is limited (depending on the reproduction number) by the maximal tracing capacity $N_{\text{max}}^{\text{test}}$

approach to an equilibrium that shows the following features: (i) When the level of contacts k_t is close to its critical value k_t^{crit} , small changes in k_t generate large modifications of the equilibrium level (Fig. 1E). (ii) Larger influxes lead to larger equilibrium values, however not modifying the maximum allowed level of contacts (Fig. 1F). (iii) Behavioral changes and policies leading to a reduction in the transmission probability will also lower the equilibrium value because the maximum allowed level of contacts k_t^{crit} would be larger (Fig. 1G). However, if case numbers exceed the TTI capacity limit, then a considerably stronger reduction in contacts is required to reach the stable regime, so that $k_t^{\text{crit}} = 42\%$ (95% CI: [38, 47]) (Fig. 2B, fig. S2B, and table S1).

Equilibrium depends on influx and contact reduction

If an equilibrium is reached, the precise value of daily new cases $\hat{N}_\infty^{\text{obs}}$ at which the system stabilizes depends on both the contact level (k_t) and the external influx of new cases (Φ_t) (Fig. 2A). In general, for realistic low values of influx Φ_t , the equilibrium level $\hat{N}_\infty^{\text{obs}}$ is low. However, $\hat{N}_\infty^{\text{obs}}$ increases steeply (diverges) when the contact level k_t approaches the tipping point to unstable dynamics (Fig. 2, A and B). Such a divergence near a critical point k_t^{crit} is a general feature of continuous transitions between stable and unstable dynamics (21, 22). As a rule of thumb, in an analytical mean-field approximation (22), $\hat{N}_\infty^{\text{obs}}$ would be proportional to Φ_t and diverge when k_t approaches its critical value k_t^{crit} from below

$$\hat{N}_\infty^{\text{obs}} \propto \frac{\Phi_t}{k_t^{\text{crit}} - k_t} \tag{1}$$

Robust control of the pandemic requires maintaining a sufficient safety margin from the tipping point (and the subsequent transition to instability) for two reasons. First, small fluctuations in k_t and Φ_t (or other model variables) could easily destabilize the system. Second, near the critical value k_t^{crit} , reductions in k_t are especially

effective: Already, small further reductions below k_t^{crit} lead to substantially lower stable case numbers (Fig. 2A). Already, with moderate reductions in k_t (50 % < k_t < 60%), the spread can be stabilized to a regime of case numbers clearly below 10 per million (fig. S1B, lower right region).

Limited TTI and self-acceleration

If mitigation measures are insufficient, then case numbers rise and eventually surpass the TTI capacity limit. Beyond it, health authorities cannot efficiently trace contacts and uncover infection chains. Thus, the control of the spread becomes more difficult. We start our scenario with a slight increase in the case numbers over a few months, as seen in many European countries throughout summer 2020 (figs. S4 and S5). A tipping point is then visible in the following observables (Fig. 2, C to F)

First, when case numbers surpass the TTI capacity, the increase in daily new observed cases \hat{N}^{obs} becomes steeper, growing even faster than the previous exponential growth (Fig. 2C, full versus faint line). The spread self-accelerates because increasingly more contacts are missed, which, in turn, infect more people. In this scenario, the accelerated spread arises solely because of exceeding the TTI limit, without any underlying behavior change among the population.

Second, after case numbers surpass the TTI limit, the observed reproduction number \hat{R}_t^{obs} , which had been only slightly above the critical value of unity, increases substantially by about 20% (Fig. 2D). This reflects a gradual loss of control over the spread and explains the faster-than-exponential growth of case numbers. The initial dip in \hat{R}_t^{obs} is a side effect of the limited testing: As increasingly many cases are missed, the observed reproduction number reduces transiently.

Third, compared to the infectious individuals who are quarantined I^Q , the number of infectious individuals who are hidden I^H (i.e., those who are not isolated or in quarantine) increases disproportionately (Fig. 2E), which is measured by the “underreporting

Downloaded from https://www.science.org on October 11, 2021

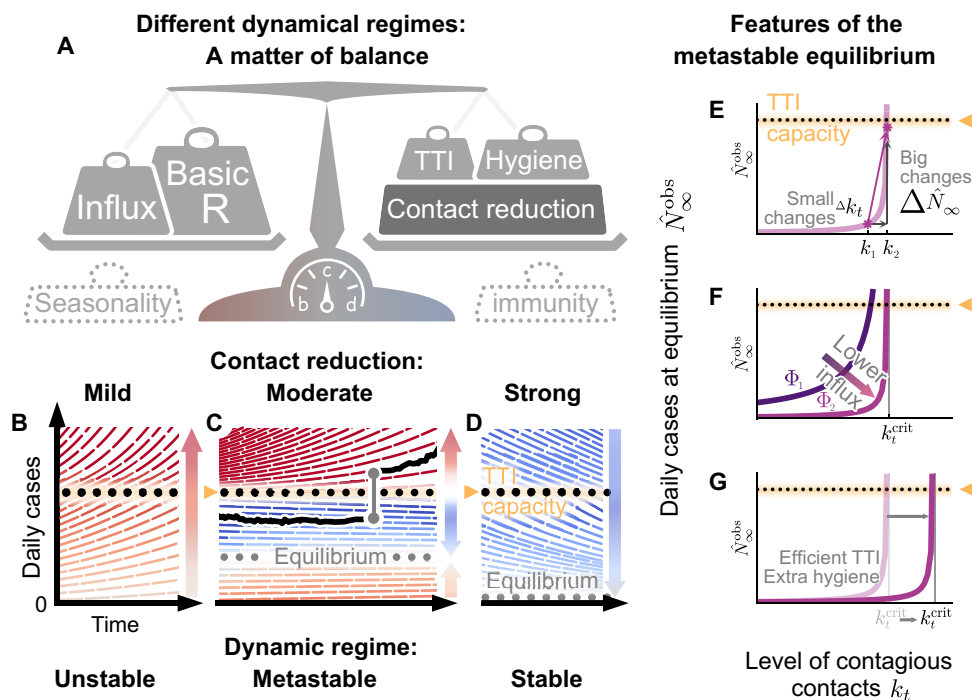


Fig. 1. Spreading dynamics depend on the balance between destabilizing and stabilizing contributions and on the level of case numbers. (A) Among the factors that destabilize the spread, we find the basic reproduction number R_0 and the external influx of infections (and, possibly, seasonality). On the other hand, increased hygiene, TTI strategies, contact reduction, and immunity contribute to stability. We specifically investigated how reductions in the contact level k_t and limited TTI capacity determine the stabilization of case numbers. (B) At mild contact reduction ($k_t = 80\%$ compared to pre-COVID-19 times), TTI is not sufficient; case numbers would grow even when TTI capacity is available. (C) At moderate contact reduction ($k_t = 60\%$), a metastable equilibrium emerges (gray dots) to which case numbers converge, if they were below the TTI capacity. However, destabilizing events (e.g., a sudden influx of infections) can push a previously stable system above the TTI capacity and lead to an uncontrolled spread (black line as an example). (D) Assuming strong contact reduction ($k_t = 40\%$), case numbers decrease even if the TTI capacity is exceeded. (E) Near to the critical level of contacts k_t^{crit} , small changes in the contact level will lead to a considerable increase in observed cases in equilibrium \hat{N}_∞^{obs} . (F) Reducing the influx of infections Φ_i (by closing borders or deploying extensive testing at arrival) reduces the number of infections. (G) Increasing the efficiency of manual contact tracing and additional measures such as increased hygiene and compulsory use of face masks will increase the maximum allowed level of contacts k_t^{crit} .

factor” (I^H/I^Q) (Fig. 2F). The hidden infectious individuals are the silent drivers of the spread, as they, unaware of being infectious, inadvertently transmit the virus. This implies a considerable risk, especially for vulnerable people. The TTI system can compensate for the hidden spread at low case numbers because it uncovers hidden cases through contact tracing. However, at high case numbers, the TTI becomes inefficient: If the TTI measures are “slower than the viral spread,” many contacts cannot be quarantined before they become spreaders.

Reestablishing control with lockdowns

Once the number of new infections has overwhelmed the TTI system, reestablishing control can be challenging. A recent suggestion is the application of a circuit breaker (23–25), a short lockdown to substantially lower the number of daily new infections. Already, during the so-called first wave of COVID-19 in Europe (i.e., the time frame between March and June 2020), lockdowns have proven capable of lowering case numbers by a factor of 2 or more every week (corresponding to an observed reproduction number of $\hat{R}_t^{obs} \approx 0.7$) (17, 26). With the knowledge that we now have acquired about the spreading of SARS-CoV-2, more targeted restrictions may yield a similarly strong effect.

Inspired by the lockdowns installed in many countries (27), we assume a default lockdown of 4 weeks, starting 4 weeks after case numbers exceed the TTI capacity limit, and a strong reduction of

contagious contacts during a lockdown, leading to $k_t = 25\%$ (which corresponds to an $\hat{R}_t^{obs} \approx 0.85$; see table S2). We further assume that during lockdown, the external influx of infections Φ_i is reduced by a factor of 10 and that after the lockdown, a moderate contact reduction (allowing $k_{nLD} = 60\%$) is maintained. By varying the parameters of this default lockdown, we show in the following that the lockdown strength, duration, and starting time determine whether the lockdown succeeds or fails to reach equilibrium.

In our scenario, a lockdown duration of 4 weeks is sufficient to reach the stable regime (Fig. 3A). However, if lifted too early (before completing 4 weeks), case numbers will rise again shortly afterward. The shorter an insufficient lockdown, the faster case numbers will rise again. In addition, it is advantageous to remain in lockdown for a short time even after case numbers have fallen below the TTI limit, to establish a safety margin, as shown above. Overall, the major challenge is not to ease the lockdown too early; otherwise, the earlier success is soon squandered.

During a lockdown, it is necessary to severely reduce contagious contacts to decrease case numbers below the TTI capacity limit (Fig. 3B). In our scenario, the contact level has to be reduced to at least $k_{LD} = 25\%$ to bring the system back to equilibrium. Otherwise, a lockdown that is slightly weaker would fail to reverse the increasing trend in cases. Furthermore, increasing the lockdown strength decreases both the required lockdown duration (Fig. 3, G and H)

Downloaded from https://www.science.org on October 11, 2021

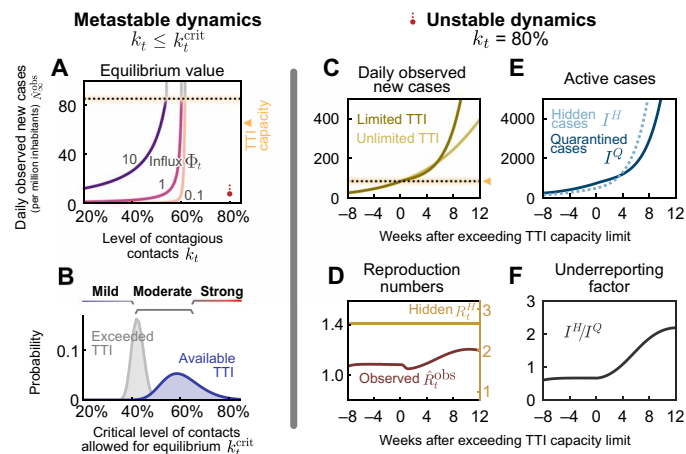


Fig. 2. When the TTI capacity is fixed, the contact level determines the dynamical regime. (A and B) In the stable and metastable regimes, daily new cases approach an equilibrium value \hat{N}_{∞}^{obs} that depends on contact level k_t and the external influx of new cases Φ_t . (A) The equilibrium value \hat{N}_{∞}^{obs} increases with increased contact level k_t or higher influx Φ_t . No equilibrium is reached if either k_t or Φ_t is above the respective (critical) threshold values. (B) The critical value k_t^{crit} represents the maximal contact level that is allowed to reach equilibrium and stabilize case numbers. If case numbers are below the TTI capacity limit, then higher values of k_t^{crit} are permitted for stabilization (blue) than if cases exceed TTI (gray). CIs originate from error propagation of the underlying model parameters. (C to F) In the unstable dynamic regime ($k_t = 80\%$), a tipping point is visible when exceeding TTI capacity. We observe a self-accelerating increase of case numbers after crossing the TTI limit (C) and a subsequent increase of the reproduction number (D). Furthermore, the absolute number (E) and the fraction (F) of cases that remain unnoticed increase over time.

and the total number of cases accumulated over 3 months (Fig. 3E). This shows that stricter lockdowns imply shorter-lasting social and economic restrictions.

The earlier a lockdown begins after exceeding the TTI capacity limit, the faster control can be reestablished, and constraints can be loosened again (Fig. 3C). If started right after crossing the threshold, in principle, then only a few days of lockdown are necessary to bring back case numbers below the TTI capacity limit. On the other hand, if the lockdown is started weeks later, then its duration needs to increase (Fig. 3, C and D) and the total number of cases will be substantially larger (Fig. 3F). The parameter regime between these two options is relatively narrow; it is not likely that equilibrium can eventually be reached as a lockdown exceeds many weeks (cf. Fig. 3H). For practical policies, this means that if a lockdown does not start to show apparent effects after 2 or 3 weeks, then the strategy should be revised (this assessment time is necessary because of the delay of 1 to 2 weeks between contagion and case report).

Maintaining control without lockdowns

We show that repeated lockdowns are not required to maintain control over the COVID-19 spread if moderate contact reduction is maintained once case numbers are below the TTI capacity limit (an initial lockdown might still be necessary to establish control). A natural goal would be to keep case numbers below the hospital capacity. However, our model suggests that lowering them below TTI capacity requires fewer contact restrictions (in the long term), involves a shorter total lockdown duration, and costs fewer lives. In the following, we compare the long-term perspective of these two goals and their dependence on the necessary contact reduction.

In our scenario (Fig. 4), we start from the unstable regime, where the initial contact level ($k_t = 80\%$ of the pre-COVID-19 level) is not sufficient to control the spread. We start a 2-week lockdown when crossing either the TTI or the hospital capacity. During the lockdown, contacts are reduced to $k_t = 25\%$. After the first and all subsequent lockdowns, contacts k_t are reduced to 80, 60, or 40% relative to pre-COVID-19 levels, thus representing a mild, moderate, or strong reduction. When assuming mild contact reduction after lockdowns, case numbers rise after lifting the lockdown, independent of the chosen threshold (TTI or hospital capacity; Fig. 4A). Thus, repeated lockdowns are necessary.

However, maintaining a moderate contact reduction while not in lockdown (i.e., a contact level of $k_t = 60\%$) is sufficient to stay within the metastable regime, if lockdowns are enacted such that case numbers remain below the TTI capacity (Fig. 4B, yellow line). This is a promising perspective for a long-term control strategy that avoids recurrent lockdowns. Otherwise, if case numbers are above TTI capacity but below hospital capacity, then control of the pandemic requires repeated lockdowns (Fig. 4B, red line). Alternatively, lasting strong contact reductions even after the lockdown can be sufficient to drive down case numbers (Fig. 4C).

The advantage of the strategy to stay below the TTI capacity limit becomes very clear when considering the total cost of the required lockdowns: Independent of the degree of contact reduction, (i) the total number of cases (and consequently deaths and long COVID risk) is lower (Fig. 4D), (ii) the total duration spent in lockdown is shorter (Fig. 4E), and (iii) the frequency at which lockdowns have to reoccur—should the after-lockdown contact reduction not be enough to grant metastability—is lower (Fig. 4A). As case numbers and lockdown duration indicate economic costs, a strategy that respects the TTI limit offers a low economic toll, enables mid-term planning, and provides trust to people and society.

The scalability of random testing (screening) (28–30) and immunization programs play a critical role in long-term strategies; both will increase the maximum level of contacts allowed (k_t^{crit}) to maintain control (Fig. 4, F and G). Early effects of immunity can be seen in our scenario of the system stabilized at hospital capacity: The need for lockdowns becomes less frequent over time (Fig. 4, A and B, red lines). However, acquiring natural immunity comes at the cost of a prolonged high level of case numbers, subsequent long COVID cases (4–6), and deceased people. Whereas the duration of the immunity is yet unknown (31), this phenomenon still shows that immunity effects play an increasing role as model predictions extend further into the future.

Vaccination greatly facilitates containment in the effective TTI regime

In the following, we show how growing immunity granted by vaccination programs further facilitates both reaching low case numbers below TTI capacity and the stable control thereof. For quantitative assessments, we studied the effect of COVID-19 vaccination programs and how they affect the two control strategies discussed in the previous section.

Investigating explicit vaccination scenarios, we assume that 80% of people getting offered vaccination accept this offer. Since, as of now, none of the available vaccines has been approved for people younger than 16 years, this corresponds to a vaccine uptake of roughly 70% of the overall population (for European demographics). We model the delivery and administration of all doses to be

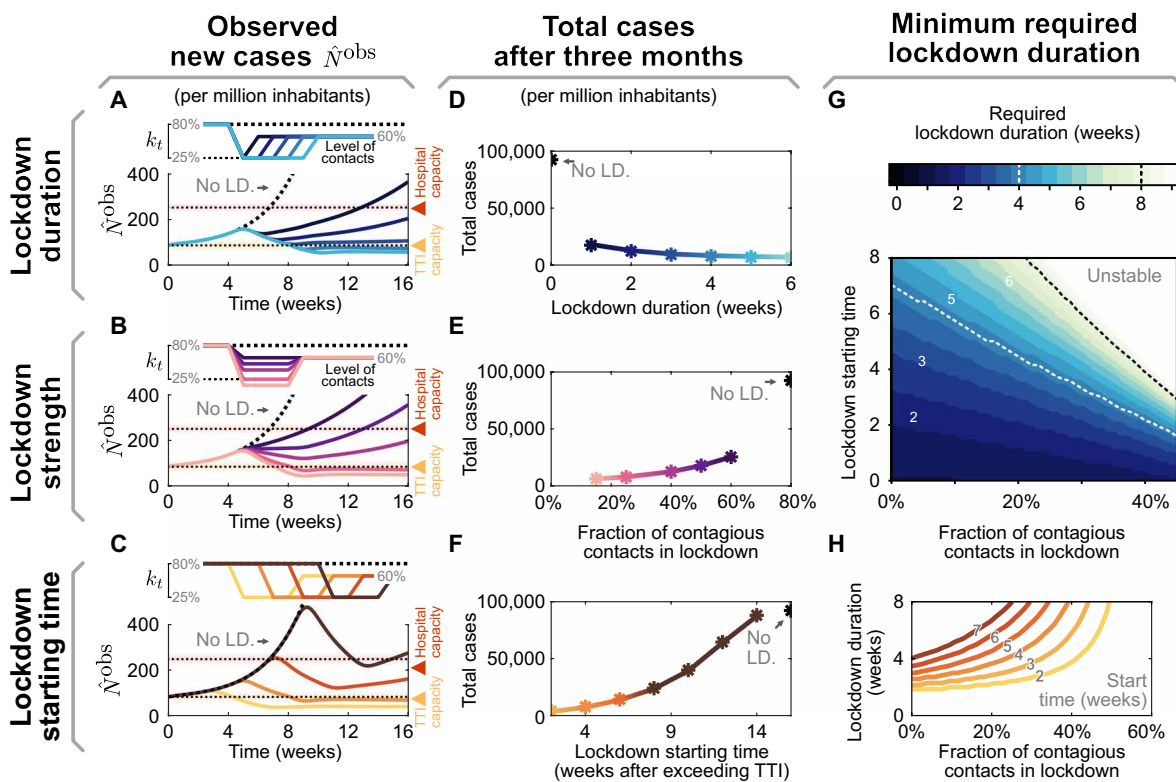


Fig. 3. The effectiveness of a lockdown depends on three primary parameters: its duration, stringency (strength), and starting time. (A to C) Observed daily new cases for a lockdown (LD.), enacted after exceeding the TTI capacity. Reference parameters are a lockdown duration of 4 weeks, reducing contact level to $k_t = 25\%$, and a start time at 4 weeks after exceeding TTI capacity. We vary lockdown duration from 1 to 5 weeks (A), lockdown strength (B), and lockdown starting time (C) to investigate whether stable case numbers can be reached. (D to F) Total cases after 3 months, if the lockdown is parameterized as described in (A) to (C), respectively. (G and H) The minimal required duration of lockdown to reach equilibrium depends both on strength and start time. (G) Heavy contact reduction (leading to lower values of k_t) and timely lockdown enacting can create effective short lockdowns (≤ 2 weeks, lower left, dark region). Whereas with mild contact reduction and very late start times, lockdowns become ineffective even when they last indefinitely (upper right, bright area). (H) Horizontal slices through the color map (G). Here, colors match (C) and (F) and correspond to the lockdown start time.

completed within 32 weeks (13), which is comparable to the increasing vaccination rate in the European Union. We investigate two scenarios: that the average vaccine efficacy against transmission is 80%, in line with reported values for current vaccines against the wild type and the widely dominant B.1.1.7 variant (32–34), or 40%, a possible scenario for partially immune-escaping variants.

Comparing the two different control strategies introduced in the preceding section, i.e., either aiming to keep case numbers below the TTI or below the hospital capacity limit, the progressing vaccination Fig. 5, A and B) will eventually lead to declining case numbers Fig. 5, C and D). However, this point will be reached several weeks earlier if case numbers are kept below TTI capacity. Until then, repeated lockdowns will remain necessary if contact reductions outside of lockdown are insufficient (see discussion in the preceding section). A decreasing number of infections will even be reached months earlier if TTI capacity is available than if it is overwhelmed.

Low case numbers are greatly beneficial even in light of progressing vaccination programs. In the high–case number regime, only in the most optimistic scenario can the spread of SARS-CoV-2 be controlled without contact reductions after the vaccination program is finished (Fig. 5E, the full gray line reaches 100%). In all other scenarios, because of the dominance of more contagious (dotted lines) or immune escape variants lowering vaccine efficacy (lower

row), an efficiently functioning TTI program is necessary to allow for a high level of contacts (Fig. 5, E and F, blue lines). Therefore, reaching low case numbers is complementary to the vaccination efforts and necessary to maximize the population’s freedom.

DISCUSSION

We demonstrated that between the two extremes of eradication and uncontrolled spread, a metastable regime of SARS-CoV-2 spreading exists. In such a regime, every person only has to reduce their contacts moderately. Simultaneously, case numbers can still be maintained robustly at low levels because the TTI system can operate efficiently. If this regime is within reach, then keeping case numbers below TTI capacity is a suitable strategy for the long-term control of COVID-19 (or other infectious diseases) that features low fatalities and a small societal burden. In addition, it maximizes the effect of large-scale pharmaceutical interventions (as vaccination programs).

Among countries worldwide, variability in governmental policies and the chosen strategy to face COVID-19 substantially affect the levels of observed COVID-19 case numbers (see also Fig. 6 and note S1.1). Sustained high levels of more than 100 daily new cases per million have been observed in several (but not exclusively)

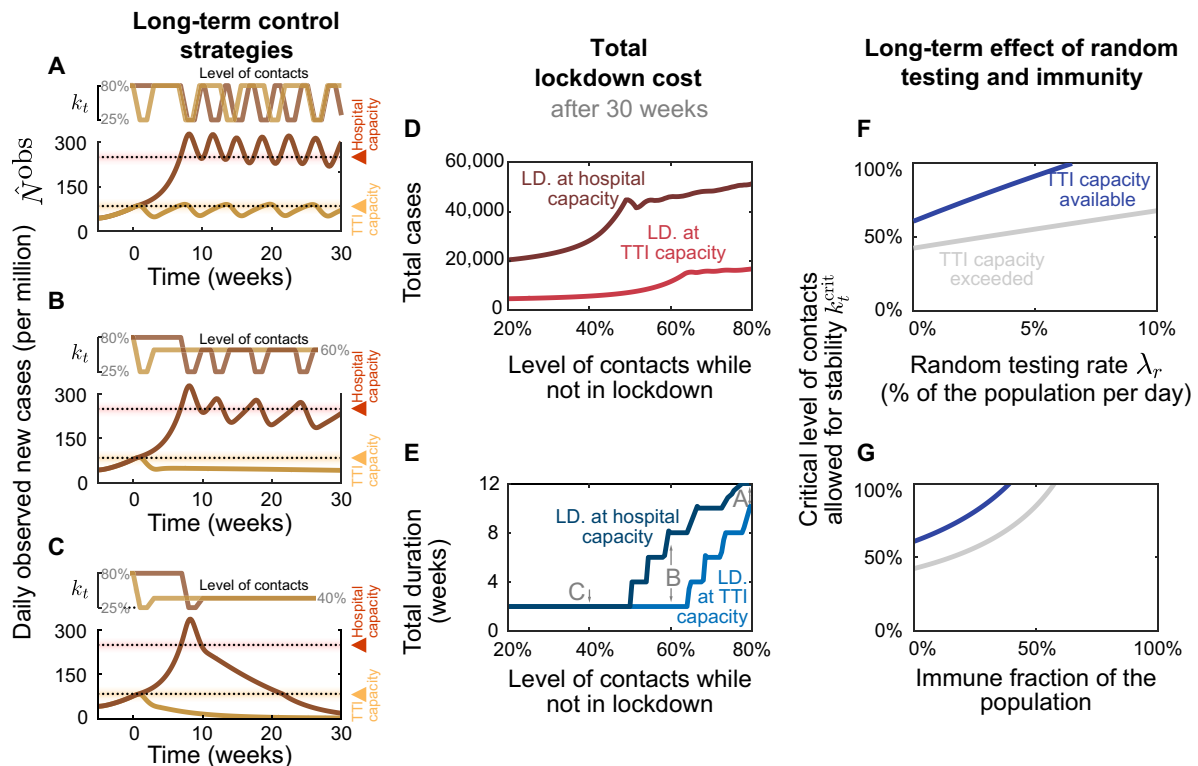


Fig. 4. From a long-term perspective, recurrent lockdowns are not required if the subsequent contact levels k_t are sufficiently low to reach equilibrium. A 2-week lockdown of default strength (reducing contact level to $k_t = 25\%$ relative to pre-COVID-19 levels) is either enacted when the TTI (yellow lines) or the hospital (red lines) capacity limits are crossed. **(A)** Given only a mild contact reduction while not in lockdown (to $k_t = 80\%$), the imposed lockdowns need to reoccur with a high frequency. Moreover, the frequency at which they reoccur is higher at high case numbers (aiming at hospital capacity) than when aiming at the TTI capacity limit because of the self-accelerating effect described previously. **(B)** If the contact reduction remains moderate (to $k_t = 60\%$), lockdowns only need to reoccur if they fail to bring case numbers below TTI capacity. **(C)** Only lasting strong contact reduction (to $k_t = 40\%$) is sufficient to continue to bring down case numbers after the lockdown. **(D and E)** The total cost (in terms of cumulative cases and total lockdown duration) depends on the level of contact reduction and the lockdown policy: The cost is low if lockdowns are initiated at the TTI capacity limit and if the contact level k_t after the lockdown is low. **(F and G)** Large-scale random testing (F) or immunization of the population [either after infection or through vaccination (G)] increases the maximal contact level allowed for stability k_t^{crit} .

American countries (Fig. 6A). This shows that high levels of daily new infections can be maintained. However, the stringency of interventions is similar to other countries (35), without signs of reaching population immunity. On the other hand, very low case numbers and even local eradication have been achieved by several South and East Asian countries, Australia, and New Zealand. At the time of writing, these countries profit from the absorbing state at zero SARS-CoV-2 infections, but maintaining this state requires substantial international travel restrictions (Fig. 6C). An intermediate level of case numbers could predominantly be observed over summer 2020 in Europe. Case numbers for many countries were typically around 10 daily new cases per million (Fig. 6B), although contacts were only mildly restricted. These stable numbers demonstrate that also, in practice, a regime below TTI capacity limits is maintainable. Nonetheless, in September, the spread substantially accelerated in several European countries, when case numbers began to exceed 20 to 50 daily new cases per million (fig. S5). Beyond these levels of case numbers, the TTI systems began to be overwhelmed, making control difficult, in line with our model's results.

To focus our model on the general spreading dynamics, we made simplifying assumptions: We assumed that spreading happens homogeneously in the population, with neither regional nor

age-related differences. In reality, heterogeneous spreading can lead to regionally differing case numbers, which illustrates the need for regional monitoring of the remaining TTI capacity to allow for early and targeted control measures. In our scenarios, we further assumed that the population's behavior and subsequent contact reduction are constant over time (except during lockdown). Real situations are more dynamic, necessitating frequent reevaluations of the current restrictions and mitigation measures. We also assumed constant TTI effectiveness if below the capacity limit. However, if case numbers are very low, then all the available test and trace efforts could be concentrated on the remaining infection chains. This would further facilitate control at low case numbers. Overall, our analytical results describe the general behavior across countries well and identify the relevant factors for controlling the pandemic.

Quantitatively, our assumptions regarding the efficiency of TTI are in agreement with those of other modeling studies. Agent-based models with detailed contact structures (36, 37) and mean-field models (38–41) both agree that TTI measures are an essential contribution for the control of the pandemic but typically do not suffice alone. Their success strongly depends on their implementation: Fast testing, rigorous isolation, and a large proportion of traced contacts are essential. Given our informed assumptions about these parameters, our model shows that TTI can only compensate a basic

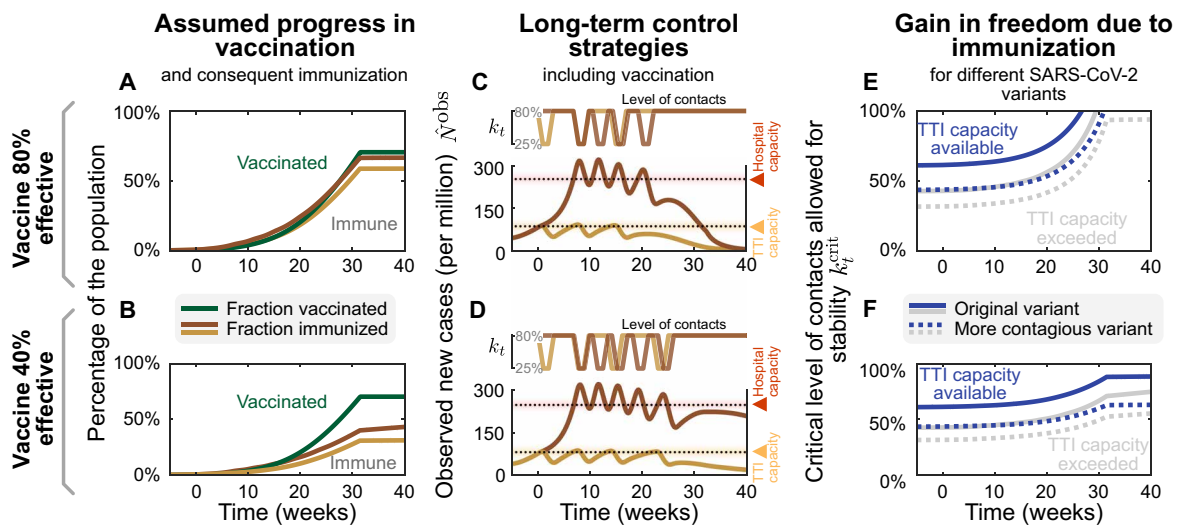


Fig. 5. Growing immunity due to mass vaccination will lead to declining case numbers and enable increasing contact levels for 80% (top row) and 40% (bottom row) vaccine efficacy against transmission; we explore the effect of mass vaccination. (A and B) Vaccine rollout is assumed to accelerate over 32 weeks, ending when 70% of the population has been vaccinated. (C and D) As in Fig. 4A, a 2-week lockdown of default strength (allowing only a $k_t = 25\%$ of pre-COVID-19 contacts) is either enacted when the TTI (yellow lines) or the hospital (red lines) capacity limits are reached. While not in lockdown, people maintain a level of contacts of $k_t = 80\%$. Without a major change in these policies, repeated lockdowns will eventually cease to be necessary because of the growing immunity, and case numbers will decline in all scenarios. However, this decline would occur weeks earlier if case numbers are below TTI capacity and vaccine efficacy is high. (E and F) Growing immunity among the population will considerably increase the maximal, critical, level of contacts allowed for stabilization of case numbers for both strategies but more substantially if not exceeding TTI capacity limit. More contagious variants such as B.1.1.7 (with an assumed base reproduction number of 4.3) will require a lower level of contacts (dotted lines).

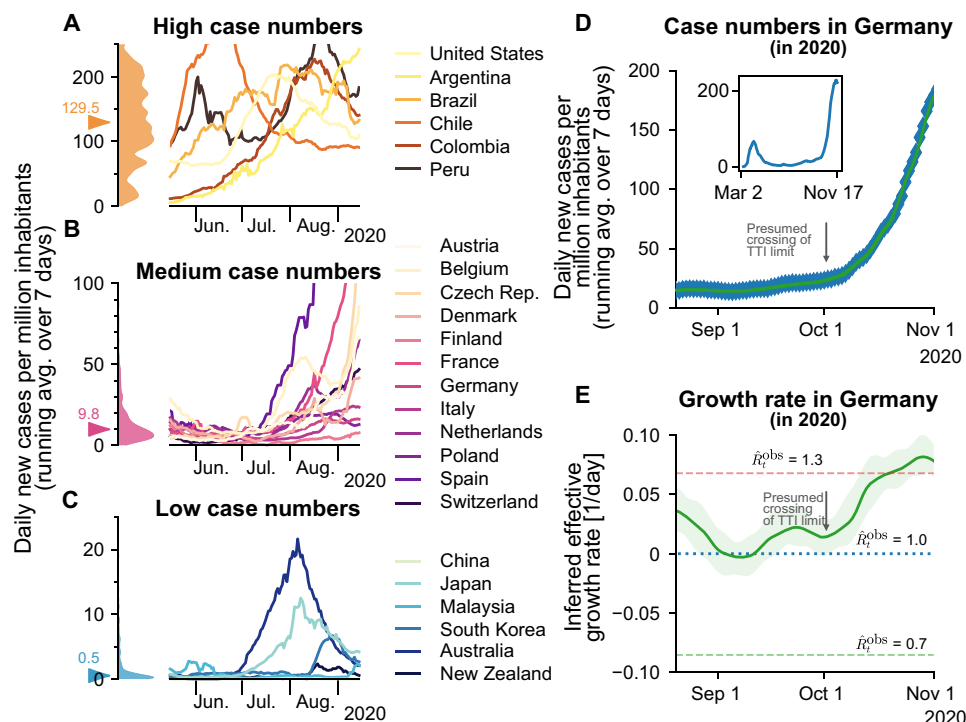


Fig. 6. Strategies of countries to fight SARS-CoV-2 differ widely and are reflected in case numbers. (A) Strategies that involve little NPIs rely on the population to hinder the spread in a self-regulated manner and are often accompanied by high case numbers. (B) Strategies that aim to keep case numbers low through extensive TTI, combined with temporary lockdowns, can lead to medium case numbers. As TTI measures' effectiveness depends on daily infections, case numbers can seemingly explode when the (hard-to-estimate) TTI capacity limit is exceeded. Many European countries managed to stabilize case numbers over summer 2020. However, stability was short lived, and they quickly saw case numbers rising faster than exponentially. (C) When the external influx is low or strategies used to reduce contacts are very effective, the stable regime can be reached. In this case, average case numbers are very low, and local outbreaks can be controlled well through local interventions. Raw data and preliminary visualizations were obtained from (62). (D and E) A substantial increase in Germany's effective growth rate occurred during October, suggesting that regional TTI capacity limits were exceeded. (D) Observed case numbers were below 20 daily new cases per million until, presumably, a transition into the unstable regime took place over ~4 weeks in October. The inset compares the extents of the so-called first and second waves. (E) Before October, the reproduction number was slightly above one (corresponding to a daily growth rate slightly above zero). More details are in fig. S4.

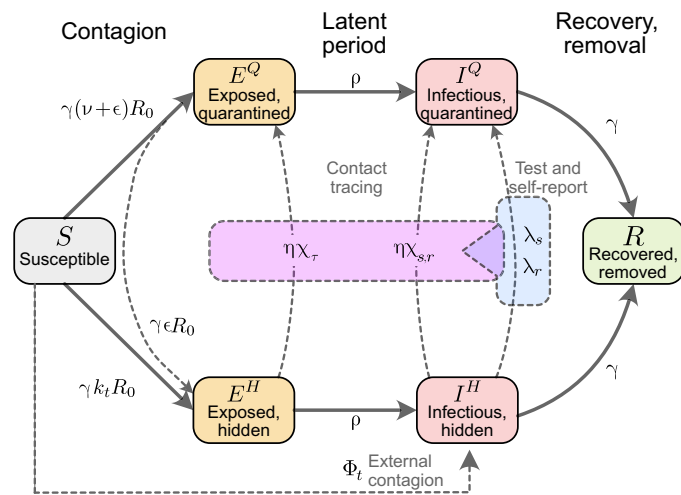


Fig. 7. Flowchart of the complete model. The solid blocks in the diagram represent different SEIR compartments for both hidden and quarantined individuals. Hidden compartments account for both symptomatic and asymptomatic carriers (as described in Methods). Solid lines represent the natural progression of the infection (contagion, latent period, and recovery). On the other hand, dashed lines account for imperfect quarantine and limited compliance, external factors, and TTI policies.

reproduction number R_0 of 3.3, if contagious contacts are also reduced to at most 61% (95% CI: [47, 76]) compared to pre-COVID-19. This is in agreement with the results of other studies (36, 37, 39, 42, 43).

The capacity limit of TTI plays a central role in the control of the spread but depends strongly on the local environment. The precise limit of TTI depends on several factors, including the number of available tests, personnel at the tracing units, potentially a tracing app (39), and the number of relevant contacts a person has on average. Already, the latter can easily differ by a factor of 10, depending on contact restrictions and cultural factors (44). We assumed that the capacity is reached at about 85 daily new cases per million for our scenarios, which is comparably high. Independent of the exact value, when this limit is approached, the risk of tipping over to uncontrolled spread strongly increases, and countermeasures should be taken without delay.

Given the large deviations of the capacity limit of TTI across regions, policy-makers should monitor local health authorities' and tracing agencies' capacity instead of relying on fixed limits. Health authorities can also assess whether a local outbreak is controlled or whether infection chains cannot be traced anymore, allowing an early and adaptive warning system. However, one can safely state that daily case numbers larger than 85 per million (corresponding to our modeled limit) are above the capacity limit of TTI programs in Europe, therefore requiring, in any case, further restrictions to reach controllable levels.

Even given the ongoing vaccination campaigns, a low level of case numbers below TTI capacity limits remains essential. We find that during and after the campaigns, TTI still greatly facilitates the containment of COVID-19. The vaccinations' exact effect depends on several hard-to-model factors. It can change with newly emerging variants of the virus, which can be more contagious, more severe, or escape the immune response. In our analysis of the effect of vaccination, we also neglected age and high-risk-group distributions and contact networks in the population, the exact design of national

vaccination plans, or the differential efficacy of vaccines against infection and severe disease. Some of these factors were taken into account in other publications (12–14). However, the long-term success of vaccinations alone remains hard to predict. Thus, it is sensible to accompany mass vaccinations to achieve low case numbers in the vaccine rollout and the time beyond.

Our results show that a stable equilibrium at low case numbers can be maintained with a moderate contact reduction of about 40% less contagious contacts compared to pre-COVID-19. In terms of our parameters, this translates to a maximum, critical, level of contacts k_t^{crit} of 61% (95% CI: [47, 76]). This level of contacts can be achieved with preventive mitigation measures, as shown by studies analyzing the effectiveness of NPIs during the first wave (17, 26, 27, 45, 46). Restrictions on the maximum size of gatherings already lead to an effective reduction in the range of 10 to 40% (17, 26, 27, 46). Improved hygiene, frequent ventilation of rooms, and the compulsory use of masks can further reduce the number of infectious contacts [by a factor that is more difficult to estimate (47, 48)]. Overall, until mass vaccination plans have been deployed worldwide and available vaccines have been shown to be successful against emerging variants, the regime of low case numbers is very promising for a mid- and long-term management of the pandemic, as it poses the least burden on economy and society.

On the other hand, stabilizing the spread at higher levels of case numbers (e.g., at the hospital capacity limit) requires more stringent and more frequent NPIs because the TTI system cannot operate efficiently. Examples of more stringent measures are the closure of schools and public businesses, stay-at-home orders, and contact ban policies (17, 26, 45).

In conclusion, this paper recommends reaching and maintaining low case numbers that allow efficient TTI measures complementary to pharmaceutical interventions. To this end, it is mandatory to counteract local super-spreading events (or an acute influx of infections) as early as possible and to sustain a sufficient level of mitigation measures. If low case numbers are reached and maintained throughout Europe, it will be possible to lift restrictions moderately in the medium term, and we will be better prepared for the emergence of future variants of concerns.

METHODS

Model overview

We model the spreading dynamics of SARS-CoV-2 as the sum of contributions from two pools of infectious individuals, i.e., quarantined-isolated I^Q and hidden nonisolated I^H individuals, while also modeling the infectivity timeline through the incorporation of compartments for individuals exposed to the virus (E^Q , E^H), following an SEIR-like formalism. The quarantined infectious pool (I^Q) contains cases revealed through testing or by contact tracing and subsequently sent to quarantine/isolation to avoid further contacts as much as possible. In contrast, in the hidden infectious pool (I^H), infections spread silently and only become detectable when individuals develop symptoms and get tested, via random testing in the population or as part of the chain of contacts of recently identified individuals. This second pool (I^H) is called the hidden pool; individuals in this pool are assumed to exhibit the general population's behavior, thus of everyone who is not aware of being infected. Healthy individuals that can be infected belong to the susceptible pool S . At the same time, we assume that, after they recover and for the relatively short

time frame here studied, they remain immunized in the R compartment (for a graphical representation of the model, see Fig. 7). We model the mean-field interactions between compartments by transition rates, determining the time scales involved. These transition rates can implicitly incorporate both the disease's time course and the delays inherent to the TTI process. Individuals exposed to the virus become infectious after the latent period, modeled by the transition rate ρ . We distinguish between symptomatic and asymptomatic carriers; this is central when exploring different testing strategies (as detailed below). We also include the effects of non-compliance to TTI measures, modeled as a higher asymptomatic ratio, and imperfect contact tracing, including an explicit delay between testing and contact tracing of contacts. In the different scenarios analyzed, we include a nonzero influx Φ_i of new cases that acquired the virus from outside. Although this influx makes a complete eradication of SARS-CoV-2 impossible, different outcomes in the spreading dynamics might arise depending on both contact intensity (contact level k_i) and TTI. We then investigate the system's stability and dynamics, aiming to control the spread with a low total number of cases without necessitating a too large reduction of infectious contacts.

Spreading dynamics

Concretely, we use a modified SEIR-type model, where infected individuals can be either symptomatic or asymptomatic. They belong to hidden (E^H, I^H) or a quarantined (E^Q, I^Q) pools of infections, thus creating, in total, one compartment of susceptible (S), two compartments of exposed individuals (E^H and E^Q), four compartments of infectious individuals ($I^{H,s}, I^{H,a}, I^{Q,s}$, and $I^{Q,a}$), and one compartment for recovered/removed individuals (R).

New infections are asymptomatic with a ratio ξ ; the others are symptomatic. In all compartments, individuals are removed with a rate γ because of recovery or death (see Table 1 for all parameters and Table 2 for all variables of the model).

In the hidden pools, the disease spreads according to the population's contact patterns, which can be expressed as a level k_i of the intensity they had before COVID-19-related contact restrictions. Defining R_0 as the base reproduction number without contact restrictions, the reproduction number of the hidden pool I^H is given by $k_i R_0$. This reproduction number reflects the disease spread in the general population without testing-induced isolation of individuals. In addition, the hidden pool receives a mobility-induced influx Φ_i of new infections. Cases are removed from the hidden pool (i) when detected by TTI and put into the quarantined pool I^Q or (ii) due to recovery or death.

The quarantined exposed and infectious pools (E^Q, I^Q) contain those infected individuals who have been tested positive and their positively tested contacts. Infectious individuals in I^Q are (imperfectly) isolated; we assume that their contacts have been reduced to a fraction $(\nu + \epsilon)$ of the ones they had in pre-COVID-19 times, of which only ν are captured by the tracing efforts of the health authorities. The subsequent infections remain quarantined, thus entering the E^Q pool and, afterward, the I^Q pool. The remaining fraction of produced infections, ϵ , are missed and act as an influx to the hidden pools (E^H). Therefore, the overall reproduction number in the I^Q pool is $(\nu + \epsilon)R_0$.

As our model is an expanded SEIR model, it assumes postinfection immunity, which is a realistic assumption given the limited time frame considered in our analysis. Our model can also reflect innate

immunity; one has to rescale the population or the reproduction number. The qualitative behavior of the dynamics is not expected to change.

Parameter choices and scenarios

For any testing strategy, the fraction of infections that do not develop any symptoms across the whole infection timeline is an important parameter, and this also holds for testing strategies applied to the case of SARS-CoV-2. In our model, this parameter is called ξ^{ap} and includes, beside true asymptomatic infections ξ , also the effect of individuals that avoid testing (49). The exact value of the fraction of asymptomatic infections ξ , however, is still fraught with uncertainty, and it also depends on age (50). While early estimates were as high as 50% [for example, ranging from 26 to 63% (51)], these early estimates suffered from reporting bias and small sample sizes and sometimes included presymptomatic cases as well (52). Recent studies estimate the asymptomatic transmission to be more minor (53), estimates of the fraction of asymptomatic carriers range between 12% (52) and 33% (54).

Another crucial parameter for any TTI strategy is the reproduction number of the hidden infections. This parameter is, by definition, impossible to measure, but it is typically the main driver of the spreading dynamics. It depends mainly on the contact behavior of the population and ranges from R_0 in the absence of contact restrictions to values below 1 during strict lockdown (17). Here, we decided to include instead contact level compared to the pre-COVID-19 baseline k_i to represent the reproduction number of hidden infections $R_i^H = k_i R_0$. For the default parameters of our model, we evaluated different contact levels k_i .

Testing and tracing strategies

We consider a testing and tracing strategy: symptom-driven testing and specific testing of traced contacts, with subsequent isolation (quarantine) of those who tested positive. Our model can also include random testing, but this case is only explored in Fig. 4 of this paper.

Symptom-driven testing is defined as applying tests to individuals presenting symptoms of COVID-19. In this context, note that noninfected individuals can have symptoms similar to those of COVID-19, as many symptoms are rather unspecific. Although symptom-driven testing suffers less from imperfect specificity, it can only uncover symptomatic cases that are willing to be tested (see below). Here, symptomatic, infectious individuals are transferred from the hidden to the traced pool at rate λ_s .

We define λ_s as the daily rate at which symptomatic individuals get tested among the subset who are willing to get tested because of surveillance programs or self-report. As default value, we use $\lambda_s = 0.25$, which means that, on average, an individual willing to get tested that develops COVID-19-specific symptoms would get a test within 4 days from the end of the latency period. Testing and isolation happen immediately in this model, but their report into the observed new daily cases \hat{N}^{obs} is delayed and so is the tracing of their contacts.

Tracing contacts of positively tested infectious individuals presents a very specific test strategy and is expected to be effective in breaking the infection chains if contacts self-isolate sufficiently quickly (36, 55, 56). However, as every implementation of a TTI strategy is bound to be imperfect, we assume that only a fraction $\eta < 1$ of all contacts can be traced. These contacts, if tested positive, are then transferred from the hidden to the quarantined infectious

pools ($I^H \rightarrow I^Q$) with an average delay of $\tau = 2$ days. The parameter η effectively represents the fraction of secondary and tertiary infections that are found through contact tracing. As this fraction decreases when the delay between testing and contact tracing increases, we assumed a default value of $\eta = 0.66$, i.e., on average, only two-thirds of subsequent offspring infections are prevented. Contact tracing is mainly done manually by the health authorities in Germany. This limits the maximum number N_{\max}^{test} of new cases observed through testing N^{test} , for which contact tracing is still functional.

Random testing is defined here as applying tests to individuals irrespective of their symptom status or whether they belonged to the contact chain of other infected individuals. In our model, random testing transfers infected individuals from the hidden to the quarantined infectious pools with a fixed rate λ_r , irrespective of whether they are showing symptoms or not. In reality, random testing is often implemented as situation-based testing for a subgroup of the population, e.g., at a hotspot, for groups at risk, or for people returning from travel. These situation-based strategies would be more efficient than the random testing assumed in this model, which may be unfeasible at a country level because of testing limitations (15).

Lockdown modeling

To assess the effectiveness of lockdowns in the broad spectrum of contact-ban governmental interventions, we model how the reduction of contacts and the duration of such restrictive regimes help lower case numbers. We model contact reductions as reductions in the reproduction number of the hidden population, which, for these matters, is presented as percentages of the basic reproduction number R_0 , which sets the pre-COVID-19 baseline for the number of close contacts.

For the sake of simplicity, we assume that the lockdown scenarios have three stages: (i) an uncontrolled regime, where the TTI capacity is overwhelmed because of high case numbers and unsustainable contact levels, reflected by a high value of k_t and a high influx of infections Φ_t . (ii) Lockdown is enacted, imposing a strong reduction of contacts, leading to lower values of k_t , and borders closing, leading to a lower influx of Φ_t . (iii) Measures are relaxed, allowing higher levels of contacts k_t and restoring international transit. All the changes between the different regimes $i \rightarrow ii \rightarrow iii$ are modeled as linear ramps for both parameters, which take $D_{\text{ramp}} = 7$ days to reach their set point. The duration of the lockdown, namely, the time frame between the start of the restrictive measures and the beginning of their relaxation, is measured in weeks. Its default length, for analysis purposes, is $D_L = 4$ weeks. These values have been chosen following the results of (27), where the first effects of an NPI were seen after 7 days and the maximum effect was seen after 4 weeks.

Model equations

The contributions of the spreading dynamics and the TTI strategies are summarized in the equations below. They govern the dynamics of case numbers between the different SEIR pools, both hidden (nonisolated) and quarantined. We assume a regime where most of the population is susceptible, and the time frame analyzed is short enough to assume postinfection immunity. Thus, the dynamics are completely determined by the spread [characterized by the reproduction numbers $k_t R_0$ and $(v + \epsilon)R_0$], the transition from exposed to

infectious (at rate ρ), recovery (characterized by the recovery rate γ), external influx Φ_t , and the impact of the TTI strategies

$$\frac{dS}{dt} = - \underbrace{\gamma k_t R_0 \frac{S}{M} I^H}_{\text{hidden contagion}} - \underbrace{\gamma(v + \epsilon) R_0 \frac{S}{M} I^Q}_{\text{traced contagion}} - \underbrace{\frac{S}{M} \Phi_t}_{\text{ext. influx}} \quad (2)$$

$$\frac{dE^Q}{dt} = \underbrace{\gamma v R_0 \frac{S}{M} I^Q}_{\text{traced contagion}} + \underbrace{\chi_\tau N^{\text{traced}}}_{\text{contact tracing}} - \underbrace{\rho E^Q}_{\text{end of latency}} \quad (3)$$

$$\frac{dE^H}{dt} = \underbrace{\gamma \frac{S}{M} (k_t R_0 I^H + \epsilon R_0 I^Q)}_{\text{hidden contagion}} - \underbrace{\chi_\tau N^{\text{traced}}}_{\text{contact tracing}} - \underbrace{\rho E^H}_{\text{end of latency}} \quad (4)$$

$$\frac{dI^Q}{dt} = \underbrace{\rho E^Q - \gamma I^Q}_{\text{spreading dynamics}} + \underbrace{N^{\text{test}}}_{\text{testing}} + \underbrace{(\chi_{s,r}(1 - \xi) + \chi_r \xi) N^{\text{traced}}}_{\text{contact tracing}} \quad (5)$$

$$\frac{dI^H}{dt} = \underbrace{\rho E^H - \gamma I^H}_{\text{spreading dynamics}} - \underbrace{N^{\text{test}}}_{\text{testing}} - \underbrace{(\chi_{s,r}(1 - \xi) + \chi_r \xi) N^{\text{traced}}}_{\text{contact tracing}} + \underbrace{\frac{S}{M} \Phi_t}_{\text{ext.influx}} \quad (6)$$

$$\frac{dI^{H,s}}{dt} = \underbrace{(1 - \xi) \rho E^H - \gamma I^{H,s}}_{\text{spreading dynamics}} - \underbrace{N_s^{\text{test}}}_{\text{testing}} - (1 - \xi) \left(\underbrace{\chi_{s,r} N^{\text{traced}}}_{\text{contact tracing}} + \underbrace{\frac{S}{M} \Phi_t}_{\text{ext.influx}} \right) \quad (7)$$

$$I^{H,a} = I^H - I^{H,s} \quad (8)$$

$$\frac{dR}{dt} = \underbrace{\gamma(I^Q + I^H)}_{\text{recovered/removed individuals}} \quad (9)$$

Initial conditions

Let x be the vector collecting the variables of all different pools

$$x = [S, E^Q, E^H, I^Q, I^H, I^{H,s}, R] \quad (10)$$

We assume a population size of $M = 10^6$ individuals, so that $\sum_{i \neq 6} x_i = M$, and a prevalence of $I_0 = 200$ infections per million, so that $I^Q(0) = I_0$. Assuming that the hidden amount of infections is in the same order of magnitude I_0 , we would have $I^H(0) = I_0$, $I^{H,s}(0) = (1 - \xi)I_0$. We would expect the exposed individuals to scale with $k_t R_0 I_0$, but we rather assume them to have the same size of the corresponding infectious pool. To calculate the initially susceptible individuals, we use $S(0) = 1 - \sum_{i \neq \{1,6\}} x_i$.

Effect of delays and capacity limit on the effectiveness of TTI strategies

In this section, we discuss further details on the derivation of the different parameters and variables involved in Eqs. 2 to 9. First, as we assume contact tracing to be effective after a delay of τ days, some of the individuals who acquired the infection from those recently tested might have also become infectious by the time of tracing. Moreover, a fraction of those who became infectious might also have been tested by the tracing time, should they have developed symptoms.

Furthermore, we give explicit forms for N^{test} and N^{traced} the number of cases identified by testing and contact tracing, respectively. When surpassing TTI capacity, we assume that both testing and contact tracing change their dynamics simultaneously. This happens when the daily amount of cases identified by testing N^{test} overpasses the TTI threshold N_{\max}^{test} . After being overwhelmed, the overhead testing would change its rate $\lambda_s \rightarrow \lambda_s'$, as only patients with

a more specific set of symptoms would be tested. Nonetheless, the contact tracing efforts can only follow the contacts of those N_{\max}^{test} observed cases, identifying a fraction η of the offspring infections that they produced in their infectious period spent in unawareness of their state. The possibility of random testing is analyzed in note S1.6.

Limited testing capacity leading to lower testing rates

In the first stages of an outbreak, individuals with any symptoms from the broad spectrum of COVID-19-related symptoms would be tested, disregarding how specific those symptoms are. At this stage, we assume that the rate at which symptomatic individuals are tested is λ_s , such that the number of individuals identified through testing (which, for simplicity, is assumed to be solely symptom-driven, i.e., $\lambda_r = 0$) is given by

$$N^{\text{test}} = N_s^{\text{test}} = \lambda_s I^{H,s} \tag{11}$$

If, in addition, some random testing, independent of symptomatic status, is performed ($\lambda_r \neq 0$), then $N^{\text{test}} \neq N_s^{\text{test}}$. For this case see note S1.6.

When reaching the daily number N_{\max}^{test} of positive tests, the testing capacity is reached. We then assume that further tests are only carried out for a more specific set of symptoms, leading to a smaller fraction of the tested population. We, therefore, implement the testing capacity as a soft threshold. Assuming that after reaching N_{\max}^{test} , the testing rate for further cases would decrease to λ'_s , the testing term N^{test} would be given by

$$N^{\text{test}} = \lambda_s \min(I^{H,s}, I_{\max}^{H,s}) + \lambda'_s \max(0, I^{H,s} - I_{\max}^{H,s}) \tag{12}$$

where $I_{\max}^{H,s}$ represent the size of the infectious-symptomatic, hidden pool, i.e., $I_{\max}^{H,s} = \frac{N_{\max}^{\text{test}}}{\lambda_s}$.

Modeling the number of traced individuals

To calculate the number of traced individuals, we assume that a fraction η of the newly tested individuals' contacts, and therefore their offspring infections, will be traced and subsequently quarantined. However, in the presence of TTI, individuals stay, on average, a shorter amount of time in the infectious pool because they are quarantined before recovering. Therefore, the number of offspring infections has to be corrected by a factor, the average residence time in the infectious pool. For the case $\lambda_r = 0$, the average residence time is $\frac{1}{\gamma + \lambda_s}$, as $I^{H,s}$ is emptied by $-\gamma I^{H,s} - N_s^{\text{test}} = -(\gamma + \lambda_s) I^{H,s}$, i.e., with a rate $\gamma + \lambda_s$. The average residence time in the absence of TTI (natural progression of the disease) is $\frac{1}{\gamma}$. Dividing these two times gives us the wanted correction factor. Thus, the number of traced persons N^{traced} at time t is a fraction η from the offspring infections generated during the residence time, per each individual

$$N^{\text{traced}}(t) = \eta R_{t-\tau} \frac{\gamma}{\gamma + \lambda_s} N^{\text{test}}(t - \tau) \tag{13}$$

where $R_{t-\tau}$ represents the effective reproduction number

$$R_{t-\tau} = k_{t-\tau} R_0 \frac{S}{M} \tag{14}$$

In other words, the number of infectious individuals found by contact tracing at time t are a fraction η of the number of offspring infections generated by individual while they were untested $R_{t-\tau} \frac{\gamma}{\gamma + \lambda_s}$,

times the number of individuals tested τ days ago $N^{\text{test}}(t - \tau)$. However, when the TTI capacity is overwhelmed, we assume that the number of traced individuals is limited, that only the contacts of N_{\max}^{test} individuals (already introduced in the previous section) can be traced

$$N^{\text{traced}}(t) = \eta R_{t-\tau} \frac{\gamma}{\gamma + \lambda_s} N_{\max}^{\text{test}} \tag{15}$$

Individuals becoming infectious or being tested by the time of tracing

The traced individuals are removed from either the exposed hidden pool E^H or from the infectious hidden pool I^H after a delay of τ days after testing. As we assume a tracing delay τ of only 2 days, a fraction of the traced individuals would still be in exposed compartments by the time of contact tracing. However, some might already become infectious by that time. To calculate the exact fraction of individuals remaining in the hidden exposed pool by the time of tracing, we proceed as follows. Let $s \in I_t = [0, \tau]$ be the time elapsed from the moment of testing. The emptying of the normalized exposed compartment (denoted E^H) due to progression to the infectious stage follows first-order kinetics

$$\frac{dE^H}{ds} = -\rho E^H, E^H(0) = 1 \tag{16}$$

The solution of Eq. 16 is given by $E^H(s) = \exp(-\rho s)$. Therefore, we define χ_τ as the fraction of the traced individuals remaining in the E^H compartment at $s = \tau$

$$\chi_\tau = \exp(-\rho\tau) \tag{17}$$

The remaining individuals are removed from the infectious compartment, which are then simply described by the fraction

$$\chi_r = 1 - \chi_\tau \tag{18}$$

This, however, only holds for the asymptomatic hidden infectious pool. For the symptomatic hidden pool $I^{H,s}$, we do not want to remove the individuals who have already been tested, as they would be removed twice. For modeling the fraction of nontested individuals remaining in the normalized symptomatic infectious compartment (denoted $I^{H,s}$), we couple two first-order kinetics

$$\frac{dI^{H,s}}{ds} = -\lambda_s I^{H,s} + \rho E^H, I^{H,s}(0) = 0 \tag{19}$$

The solution of Eq. 19 depends on whether $\lambda_s = \rho$ or not. The solution at $s = \tau$, which is the fraction of traced individuals removed from $I^{H,s}$, is given by

$$\chi_{s,r} = \begin{cases} \rho\tau \exp(-\rho\tau) & \text{if } \lambda_s \approx \rho, \\ \frac{\rho}{\lambda_s - \rho} (\exp(-\rho\tau) - \exp(-\lambda_s\tau)) & \text{else} \end{cases} \tag{20}$$

For the case $\lambda_r \neq 0$, the reader is referred to note S1.6.

Including the effects of ongoing vaccination campaigns

To incorporate the effects of COVID-19 vaccination programs in our model, we made some simplifying assumptions. First, we assume

that vaccinated individuals have a probability κ of not being infected even if they have a contact with somebody infectious and then not contributing to the spreading dynamics. We define this parameter as the “vaccine efficacy against infection,” which has been reported to be around 50 to 90% for available vaccines (32–34). Thus, they can be assumed to have developed perfect immunity and therefore can be removed from the susceptible (S) and put into the removed compartment (R). The assumption above also implies that these individuals would not take part in the TTI scheme, which would resemble the growing trend of “vaccination passports.” Second, we assume a logarithmically increasing daily vaccination rate $\nu(t)$ consistent with the projections in the European Union and assume that 70% of the total population gets vaccinated (see Fig. 5, B and E). This would, e.g., in Germany, amount to roughly 80% of the adult population (16+ years old) accepting the offer of vaccination, since as of now, none of the available vaccines is approved for children. We find that efficient TTI can substantially enhance the effect of the growing immunity.

To include gradually growing immunity due to an ongoing vaccination campaign, we modify Eq. 2 with an additional term $-\kappa \cdot \nu(t)$, as well as Eq. 9 with a $+\kappa \cdot \nu(t)$, with a daily vaccination rate

$$\nu(t) = \frac{9.3 \times 10^3}{1 + \exp(-0.025(t - 150))} \text{ doses per million per day} \quad (21)$$

centered at $t = 0$, which denotes the start of the vaccinations. This logistic increase in vaccination rates and parameters involved was adapted from (13) and roughly mirrors the projected vaccinations in the European Union (projections dated to the beginning of February 2021). The factor 9.3×10^3 is determined assuming that after $t_{\text{ref}} = 220$ days, 70% of the population would be vaccinated. Using as reference the age distribution of Germany, the above would amount to roughly 80% of the adult population (16+ years old) accepting the offer of vaccination. After that time, for simplicity, we assume that the vaccination stops [and therefore $\nu(t) = 0$, for $t > 220$].

This treatment of the vaccination is simplistic. In reality, most currently available vaccines imply receiving two doses in the span of a few weeks, where the first only gives partial protection. Furthermore, vaccinated individuals need some time to develop a proper immune response after receiving the vaccine (57), in which they can still get infected. We also do not incorporate the efficacy of vaccines against a severe course of the disease or death. Since vaccinated but yet infected individuals would have a lower chance of being admitted to the hospital, this would falsify our assumption that hospital capacity can be adequately measured by case numbers alone. As more and more of the daily new infections correspond to individuals already vaccinated, hospitals would only fill up at higher case numbers. To include this effect, the distribution of high-risk groups in the population and the prioritized vaccination programs would have to be taken into account. Including all this is beyond the scope of this work. We addressed those in a separate work, building on the results presented herein (13). However, this simplified implementation is sufficient for our qualitative assessments.

Central epidemiological parameters that can be observed

In the real world, the disease spread can only be observed through testing and contact tracing. While the true number of daily infections N is a sum of all new infections in the hidden and traced pools, the observed number of daily infections \hat{N}^{obs} is the number of new

infections discovered by testing, tracing, and surveillance of the contacts of those individuals in the quarantined infectious pool I^Q , delayed by a variable reporting time. This includes internal contributions and contributions from testing and tracing

$$N = \underbrace{\gamma k_t R_0 \frac{S}{M} I^H}_{\text{hidden contagion}} + \underbrace{\gamma(\nu + \epsilon) R_0 \frac{S}{M} I^Q}_{\text{traced contagion}} + \underbrace{\frac{S}{M} \Phi_t}_{\text{ext. influx}} \quad (22)$$

$$\hat{N}^{\text{obs}} = \left[\underbrace{\rho E^Q}_{\text{traced contagion}} + \underbrace{N^{\text{test}} + (\chi_{s,r}(1 - \xi) + \chi_r \xi) N^{\text{traced}}}_{\text{TTI}} \right] \otimes \mathcal{K} \quad (23)$$

where \otimes denotes a convolution and \mathcal{K} is an empirical probability mass function that models a variable reporting delay, inferred from German data (as the Robert Koch Institute reports the date the test is performed, the delay until the appearance in the database can be inferred): The total delay between testing and reporting a test corresponds to 1 day more than the expected time the laboratory takes for obtaining results, which is defined as follows: from testing, 50% of the samples would be reported the next day, 30% would be reported the second day, 10% would be reported the third day, and further delays complete the remaining 10%, which, for simplicity, we will truncate at day 4. Considering the extra day needed for reporting, the probability mass function for days 0 to 5 would be given by $\mathcal{K} = [0, 0, 0.5, 0.3, 0.1, 0.1]$. The spreading dynamics are usually characterized by the observed reproduction number \hat{R}_t^{obs} , which is calculated from the observed number of new cases $\hat{N}^{\text{obs}}(t)$. We here use the definition underlying the estimates that Robert Koch Institute publishes, the official body responsible for epidemiological control in Germany (58): The reproduction number is the relative change of daily new cases N separated by 4 days (the assumed serial interval of COVID-19)

$$\hat{R}_t^{\text{obs}} = \frac{\hat{N}^{\text{obs}}(t)}{\hat{N}^{\text{obs}}(t - 4)} \quad (24)$$

In contrast to the original definition of \hat{R}_t^{obs} (58), we do not need to remove real-world noise effects by smoothing this ratio.

Numerical calculation of solutions and critical values

The numerical solution of the delay differential equations (DDEs) governing our model were obtained using a versatile solver that tracks discontinuities and integrates with the explicit Runge-Kutta (2,3) pair, @dde23 implemented in MATLAB (version 2020a), with default settings. This algorithm allows the solution of nonstiff systems of differential equations in the shape $y'(t) = f(t, y(t), y(t - \tau_1), \dots, y(t - \tau_k))$, for a set of discrete lags $\{\tau_i\}_{i=1}^k$. Suitability and details on the algorithm are further discussed in (59).

To derive the tipping point between controlled and uncontrolled outbreaks (e.g., critical, minimal required contact reduction k_t^{crit} for both stability and metastability) and to plot the stability diagrams, we used the @fzero MATLAB function, and the linear approximation of the system of DDE (3)–(7) for the $\frac{S}{M} \approx 1$ limit. This function uses a combination of bisection, secant, and inverse quadratic interpolation methods to find the roots of a function. For instance, following the discussion of note S1.2, the different critical values for the contact reduction k_t^{crit} were determined by systematically solving the nonlinear eigenvalues problem for stability (60), where the solution operation was approximated with a Chebyshev differentiation matrix (61).

We also study the effect of dividing the exposed compartment into three subcompartments, thereby reducing the variability of the latent period distribution (understood as the distribution of waiting times from being infected until becoming infectious). We explored this extended system's linear stability in note S1.8 and confirmed that using a single compartment efficiently characterizes the tipping points.

SUPPLEMENTARY MATERIALS

Supplementary material for this article is available at <https://science.org/doi/10.1126/sciadv.abg2243>

REFERENCES AND NOTES

- H. E. Randolph, L. B. Barreiro, Herd immunity: Understanding COVID-19. *Immunity* **52**, 737–741 (2020).
- A. T. Levin, W. P. Hanage, N. Owusu-Boaitey, K. B. Cochran, S. P. Walsh, G. Meyerowitz-Katz, Assessing the age specificity of infection fatality rates for COVID-19: Systematic review, meta-analysis, and public policy implications. *Eur. J. Epidemiol.* **35**, 1123–1138 (2020).
- N. A. Alwan, R. A. Burgess, S. Ashworth, R. Beale, N. Bhadelia, D. Bogaert, J. Dowd, I. Eckerle, L. R. Goldman, T. Greenhalgh, D. Gurdasani, A. Hamdy, W. P. Hanage, E. B. Hodcroft, Z. Hyde, P. Kellam, M. Kelly-Irving, F. Krammer, M. Lipsitch, A. McNally, M. McKee, A. Nouri, D. Pimenta, V. Priesemann, H. Rutter, J. Silver, D. Sridhar, C. Swanton, R. P. Walensky, G. Yamey, H. Ziauddeen, Scientific consensus on the COVID-19 pandemic: We need to act now. *Lancet* **396**, e71–e72 (2020).
- E. Fraser, Long term respiratory complications of COVID-19. *BMJ* **370**, m3001 (2020).
- T. Greenhalgh, M. Knight, C. A. Court, M. Buxton, L. Husain, Management of post-acute COVID-19 in primary care. *BMJ* **370**, m3026 (2020).
- E. J. Topol, COVID-19 can affect the heart. *Science* **370**, 408–409 (2020).
- V. Priesemann, M. M. Brinkmann, S. Ciesek, S. Cuschieri, T. Czyzionka, G. Giordano, D. Gurdasani, C. Hanson, N. Hens, E. Iftekhar, M. Kelly-Irving, P. Klimek, M. Kretzschmar, A. Peichl, M. Perc, F. Sannino, E. Schernhammer, A. Schmidt, A. Staines, E. Szcurek, Calling for pan-European commitment for rapid and sustained reduction in SARS-CoV-2 infections. *Lancet* **397**, 92–93 (2021).
- A. Scherbina, Determining the optimal duration of the COVID-19 suppression policy: A cost-benefit analysis (2019); <https://ssrn.com/abstract=3562053>.
- J. Xiong, O. Lipsitz, F. Nasri, L. M. Lui, H. Gill, L. Phan, D. Chen-Li, M. Iacobucci, R. Ho, A. Majeed, R. S. McIntyre, Impact of COVID-19 pandemic on mental health in the general population: A systematic review. *J. Affect. Disord.* **277**, 55–64 (2020).
- R. Li, S. Pei, B. Chen, Y. Song, T. Zhang, W. Yang, J. Shaman, Substantial undocumented infection facilitates the rapid dissemination of novel coronavirus (SARS-CoV-2). *Science* **368**, 489–493 (2020).
- N. Van Doremalen, T. Bushmaker, D. H. Morris, M. G. Holbrook, A. Gamble, B. N. Williamson, A. Tamin, J. L. Harcourt, N. J. Thornburg, S. I. Gerber, J. O. Lloyd-Smith, E. de Wit, V. J. Munster, Aerosol and surface stability of SARS-CoV-2 as compared with SARS-CoV-1. *N. Engl. J. Med.* **382**, 1564–1567 (2020).
- S. Moore, E. M. Hill, M. J. Tildesley, L. Dyson, M. J. Keeling, Vaccination and non-pharmaceutical interventions for COVID-19: A mathematical modelling study. *Lancet Infect. Dis.* **21**, 793–802 (2021).
- S. Bauer, S. Contreras, J. Dehning, M. Linden, E. Iftekhar, S. B. Mohr, Á. Olivera-Nappa, V. Priesemann, Relaxing restrictions at the pace of vaccination increases freedom and guards against further COVID-19 waves in Europe. [arXiv:2103.06228 \[q-bio.PE\]](https://arxiv.org/abs/2103.06228) (2021).
- S. Contreras, V. Priesemann, Risking further COVID-19 waves despite vaccination. *Lancet Infect. Dis.* **21**, 745–746 (2021).
- S. Contreras, J. Dehning, M. Loidolt, J. Zierenberg, F. P. Spitzner, J. H. Urrea-Quintero, S. B. Mohr, M. Wilczek, M. Wibrál, V. Priesemann, The challenges of containing SARS-CoV-2 via test-trace-and-isolate. *Nat. Commun.* **12**, 378 (2021).
- M. Linden, S. B. Mohr, J. Dehning, J. Mohring, M. Meyer-Hermann, I. Pigeot, A. Schöbel, V. Priesemann, Case numbers beyond contact tracing capacity are endangering the containment of COVID-19. *Dtsch. Arztebl. Int.* **117**, 790–791 (2020).
- J. Dehning, J. Zierenberg, F. P. Spitzner, M. Wibrál, J. P. Neto, M. Wilczek, V. Priesemann, Inferring change points in the spread of COVID-19 reveals the effectiveness of interventions. *Science* **369**, eabb9789 (2020).
- H. W. Hethcote, The mathematics of infectious diseases. *SIAM Rev.* **42**, 599–653 (2000).
- S. Zhao, Q. Lin, J. Ran, S. S. Musa, G. Yang, W. Wang, Y. Lou, D. Gao, L. Yang, D. He, M. H. Wang, Preliminary estimation of the basic reproduction number of novel coronavirus (2019-nCoV) in China, from 2019 to 2020: A data-driven analysis in the early phase of the outbreak. *Int. J. Infect. Dis.* **92**, 214–217 (2020).
- Y. Alimohamadi, M. Taghdir, M. Sepandi, Estimate of the basic reproduction number for COVID-19: A systematic review and meta-analysis. *J. Prev. Med. Public Health* **53**, 151–157 (2020).
- J. P. La Salle, *The Stability of Dynamical Systems* (SIAM, 1976).
- J. Wilting, V. Priesemann, Inferring collective dynamical states from widely unobserved systems. *Nat. Commun.* **9**, 2325 (2018).
- M. J. Keeling, G. Guyver-Fletcher, A. Holmes, L. Dyson, M. J. Tildesley, E. M. Hill, G. F. Medley, Precautionary breaks: Planned, limited duration circuit breaks to control the prevalence of COVID-19. *medRxiv*, 2020.10.13.20211813 (2020).
- E. Mahase, COVID-19: Experts recommend two week circuit break to reduce transmission in the UK. *BMJ* **371**, m4038 (2020).
- Z. Kmietowicz, Covid-19: "There is no alternative," says Johnson, announcing new restrictions for England. *BMJ* **371**, m4247 (2020).
- J. M. Brauner, S. Mindermann, M. Sharma, D. Johnston, J. Salvatier, T. Gavenčič, A. B. Stephenson, G. Leech, G. Altman, V. Mikulík, A. J. Norman, J. T. Monrad, T. Besiroglu, H. Ge, M. A. Hartwick, Y. W. Teh, L. Chindelevitch, Y. Gal, J. Kulveit, Inferring the effectiveness of government interventions against covid-19. *Science* **371**, eabd9338 (2021).
- Y. Li, H. Campbell, D. Kulkarni, A. Harpur, M. Nundy, X. Wang, H. Nair, The temporal association of introducing and lifting non-pharmaceutical interventions with the time-varying reproduction number (R) of SARS-CoV-2: A modelling study across 131 countries. *Lancet Infect. Dis.* **21**, 193–202 (2020).
- E. Holt, Slovakia to test all adults for SARS-CoV-2. *Lancet* **396**, 1386–1387 (2020).
- M. J. Mina, R. Parker, D. B. Larremore, Rethinking Covid-19 test sensitivity—A strategy for containment. *N. Engl. J. Med.* **383**, e120 (2020).
- D. B. Larremore, B. Wilder, E. Lester, S. Shehata, J. M. Burke, J. A. Hay, M. Tambe, M. J. Mina, R. Parker, Test sensitivity is secondary to frequency and turnaround time for COVID-19 screening. *Sci. Adv.* **7**, eabd5393 (2021).
- R. D. Kirkcaldy, B. A. King, J. T. Brooks, COVID-19 and postinfection immunity: Limited evidence, many remaining questions. *JAMA* **323**, 2245–2246 (2020).
- M. Thompson, J. Burgess, A. Naleway, H. L. Tyner, S. K. Yoon, J. Meece, L. E. W. Olsho, A. J. Caban-Martinez, A. Fowlkes, K. Lutrick, J. L. Kuntz, K. Dunnigan, M. J. Odean, K. T. Hegmann, E. Stefanski, L. J. Edwards, N. Schaefer-Solle, L. Grant, K. Ellingson, H. C. Groom, T. Zunie, M. S. Thiese, L. Ivacic, M. G. Wesley, J. M. Lamberte, X. Sun, M. E. Smith, A. L. Phillips, K. D. Groover, Y. M. Yoo, J. Gerald, R. T. Brown, M. K. Herring, G. Joseph, S. Beitel, T. C. Morrill, J. Mak, P. Rivers, K. M. Harris, D. R. Hunt, M. L. Arvay, P. Kutty, A. M. Fry, M. Gagliani, Interim estimates of vaccine effectiveness of BNT162b2 and mRNA-1273 COVID-19 vaccines in preventing SARS-CoV-2 infection among health care personnel, first responders, and other essential and frontline workers—Eight U.S. locations, December 2020–March 2021. *MMWR Morb. Mortal. Wkly. Rep.* **70**, 495–500 (2021).
- N. Dagan, N. Barda, E. Kepten, O. Miron, S. Perchik, M. A. Katz, M. A. Hernán, M. Lipsitch, B. Reis, R. D. Balicer, BNT162b2 mRNA Covid-19 vaccine in a nationwide mass vaccination setting. *N. Engl. J. Med.* **384**, 1412–1423 (2021).
- M. Voysey, S. A. C. Clemens, S. A. Madhi, L. Y. Weckx, P. M. Folegatti, P. K. Aley, B. Angus, V. L. Baillie, S. L. Barnabas, Q. E. Bhorat, S. Bibi, C. Briner, P. Cicconi, A. M. Collins, R. Coljin-Jones, C. L. Cutland, T. C. Darton, K. Dheda, C. J. A. Duncan, K. R. W. Emary, K. J. Ewer, L. Fairlie, S. N. Faust, S. Feng, D. M. Ferreira, A. Finn, A. L. Goodman, C. M. Green, C. A. Green, P. T. Heath, C. Hill, H. Hill, I. Hirsch, S. H. C. Hodgson, A. Izu, S. Jackson, D. Jenkin, C. C. D. Joe, S. Kerridge, A. Koen, G. Kwatra, R. Lazarus, A. M. Lawrie, A. Lelliott, V. Libri, P. J. Lillie, R. Mallory, A. V. A. Mendes, E. P. Milan, A. M. Minassian, A. M. Gregor, H. Morrison, Y. F. Mujajidi, A. Nana, P. J. O'Reilly, S. D. Padayachee, A. Pittella, E. Plested, K. M. Pollock, M. N. Ramasamy, S. Rhead, A. V. Schwarzbold, N. Singh, A. Smith, R. Song, M. D. Snape, E. Sprinz, R. K. Sutherland, R. Tarrant, E. C. Thomson, M. E. Török, M. Toshner, D. P. J. Turner, J. Vekemans, T. L. Villafana, M. E. O. Watson, C. J. Williams, A. D. Douglas, A. V. S. Hill, T. Lambe, S. C. Gilbert, A. J. Pollard, Oxford COVID Vaccine Trial Group, Safety and efficacy of the ChAdOx1 nCoV-19 vaccine (AZD1222) against SARS-CoV-2: An interim analysis of four randomised controlled trials in Brazil, South Africa, and the UK. *Lancet* **397**, 99–111 (2021).
- T. Hale, S. Webster, A. Petherick, T. Phillips, B. Kira, Oxford COVID-19 Government Response Tracker, Blavatnik School of Government (2020); www.fda.gov/media/136472/download.
- A. J. Kucharski, P. Klepac, A. J. K. Conlan, S. M. Kissler, M. L. Tang, H. Fry, J. R. Gog, W. J. Edmunds; CMMID COVID-19 working group, Effectiveness of isolation, testing, contact tracing, and physical distancing on reducing transmission of SARS-CoV-2 in different settings: A mathematical modelling study. *Lancet Infect. Dis.* **20**, 1151–1160 (2020).
- C. C. Kerr, D. Mistry, R. M. Stuart, K. Rosenfeld, G. R. Hart, R. C. Núñez, J. A. Cohen, P. Selvaraj, R. G. Abeyuriya, M. Jastrzebski, L. George, B. Hagedorn, J. Panovska-Griffiths, M. Fagalde, J. Duchin, M. Famulare, D. J. Klein, Controlling COVID-19 via test-trace-quarantine. *Nat. Commun.* **12**, 2993 (2021).
- C. Fraser, S. Riley, R. M. Anderson, N. M. Ferguson, Factors that make an infectious disease outbreak controllable. *Proc. Natl. Acad. Sci. U.S.A.* **101**, 6146–6151 (2004).
- L. Ferretti, C. Wymant, M. Kendall, L. Zhao, A. Nurtay, L. Abeler-Dörner, M. Parker, D. Bonsall, C. Fraser, Quantifying SARS-CoV-2 transmission suggests epidemic control with digital contact tracing. *Science* **368**, eabb6936 (2020).

40. D. Lunz, G. Batt, J. Ruess, To quarantine, or not to quarantine: A theoretical framework for disease control via contact tracing. *Epidemics* **34**, 100428 (2021).
41. S. Sturniolo, W. Waites, T. Colbourn, D. Manheim, J. Panovska-Griffiths, Testing, tracing and isolation in compartmental models. *PLOS Comput. Biol.* **17**, e1008633 (2021).
42. J. Hellewell, S. Abbott, A. Gimma, N. I. Bosse, C. I. Jarvis, T. W. Russell, J. D. Munday, A. J. Kucharski, W. J. Edmunds, F. Sun, Feasibility of controlling COVID-19 outbreaks by isolation of cases and contacts. *Lancet Glob. Health* **8**, e488–e496 (2020).
43. E. L. Davis, T. C. D. Lucas, A. Borlase, T. M. Pollington, S. Abbott, D. Ayabina, T. Crellen, J. Hellewell, L. Pi; CMMID COVID-19 working group, G. F. Medley, T. D. Hollingsworth, P. Klepac, An imperfect tool: COVID-19 'test & trace' success relies on minimising the impact of false negatives and continuation of physical distancing. *medRxiv*, 2020.06.09.20124008 (2020).
44. J. J. Van Bavel, K. Baicker, P. S. Boggio, V. Capraro, A. Cichocka, M. Cikara, M. J. Crockett, A. J. Crum, K. M. Douglas, J. N. Druckman, J. Drury, O. Dube, N. Ellemers, E. J. Finkel, J. H. Fowler, M. Gelfand, S. Han, S. A. Haslam, J. Jetten, S. Kitayama, D. Mobbs, L. E. Napper, D. J. Packer, G. Pennycook, E. Peters, R. E. Petty, D. G. Rand, S. D. Reicher, S. Schnall, A. Shariff, L. J. Skitka, S. S. Smith, C. R. Sunstein, N. Tabri, J. A. Tucker, S. van der Linden, P. van Lange, K. A. Weeden, M. J. A. Wohl, J. Zaki, S. R. Zion, R. Willer, Using social and behavioural science to support COVID-19 pandemic response. *Nat. Hum. Behav.* **4**, 460–471 (2020).
45. S. Hsiang, D. Allen, S. Annan-Phan, K. Bell, I. Bolliger, T. Chong, H. Druckenmiller, L. Y. Huang, A. Hultgren, E. Krasovich, P. Lau, J. Lee, E. Rolf, J. Tseng, T. Wu, The effect of large-scale anti-contagion policies on the COVID-19 pandemic. *Nature* **584**, 262–267 (2020).
46. M. Sharma, S. Mindermann, C. Rogers-Smith, G. Leech, B. Snodin, J. Ahuja, J. B. Sandbrink, J. T. Monrad, G. Altman, G. Dhaliwal, L. Finnveden, A. J. Norman, S. B. Oehm, J. F. Sandkühler, T. Mellan, J. Kulveit, L. Chindelevitch, S. Flaxman, Y. Gal, S. Mishra, J. M. Brauner, S. Bhatt, Understanding the effectiveness of government interventions in Europe's second wave of COVID-19. *medRxiv*, 2021.03.25.21254330 (2021).
47. D. K. Chu, E. A. Akl, S. Duda, K. Solo, S. Yaacoub, H. J. Schünemann; COVID-19 Systematic Urgent Review Group Effort (SURGE) study authors, Physical distancing, face masks, and eye protection to prevent person-to-person transmission of SARS-CoV-2 and COVID-19: A systematic review and meta-analysis. *Lancet* **395**, 1973–1987 (2020).
48. J. Howard, A. Huang, Z. Li, Z. Tufekci, V. Zdimal, H.-M. van der Westhuizen, A. von Delft, A. Price, L. Fridman, L.-H. Tang, V. Tang, G. L. Watson, C. E. Bax, R. Shaikh, F. Questier, D. Hernandez, L. F. Chu, C. M. Ramirez, A. W. Rimoin, An evidence review of face masks against COVID-19. *Proc. Natl. Acad. Sci. U.S.A.* **118**, e2014564118 (2021).
49. J. H. McDermott, W. G. Newman, Refusal of viral testing during the SARS-CoV-2 pandemic. *Clin. Med.* **20**, e163–e164 (2020).
50. C.-C. Lai, Y. H. Liu, C.-Y. Wang, Y.-H. Wang, S.-C. Hsueh, M.-Y. Yen, W.-C. Ko, P.-R. Hsueh, Asymptomatic carrier state, acute respiratory disease, and pneumonia due to severe acute respiratory syndrome coronavirus 2 (SARS-CoV-2): Facts and myths. *J. Microbiol. Immunol. Infect.* **53**, 404–412 (2020).
51. E. Lavezzo, E. Franchin, C. Ciavarella, G. Cuomo-Dannenburg, L. Barzon, C. Del Vecchio, L. Rossi, R. Manganelli, A. Lorigian, N. Navarin, D. Abate, M. Sciro, S. Merigliano, E. De Canale, M. C. Vanuzzo, V. Besutti, F. Saluzzo, F. Onelia, M. Pacenti, S. G. Parisi, G. Arretta, D. Donato, L. Flor, S. Cocchio, M. Masi, A. Sperduti, L. Cattarino, R. Salvador, M. Nicoletti, F. Caldart, G. Castelli, E. Nieddu, B. Labella, L. Fava, M. Drigo, K. A. M. Gaythorpe; Imperial College COVID-Response Team, A. R. Brazzale, S. Toppo, M. Trevisan, V. Baldo, C. A. Donnelly, N. M. Ferguson, I. Dorigatti, A. Crisanti, Suppression of COVID-19 outbreak in the municipality of Vo, Italy. *Nature* **584**, 425–429 (2020).
52. O. Byambasuren, M. Cardona, K. Bell, J. Clark, M.-L. McLaws, P. Glasziou, Estimating the extent of asymptomatic COVID-19 and its potential for community transmission: Systematic review and meta-analysis. *J. Assoc. Med. Microbiol. Infect. Dis. Canada* **5**, 223–234 (2020).
53. M. Cevik, K. Kuppalli, J. Kindrachuk, M. Peiris, Virology, transmission, and pathogenesis of SARS-CoV-2. *BMJ* **371**, m3862 (2020).
54. M. Pollán, B. Pérez-Gómez, R. Pastor-Barriuso, J. Oteo, M. A. Hernán, M. Pérez-Olmeda, J. L. Sanmartín, A. Fernández-García, I. Cruz, N. F. de Larrea, M. Molina, F. Rodríguez-Cabrera, M. Martín, P. Merino-Amador, J. L. Paniagua, J. F. Muñoz-Montalvo, F. Blanco, R. Yotti; ENE-COVID Study Group, Prevalence of sars-cov-2 in spain (ene-covid): A nationwide, population-based seroepidemiological study. *Lancet* **396**, 535–544 (2020).
55. J. A. Firth, J. Hellewell, P. Klepac, S. M. Kissler, A. J. Kucharski, L. G. Spurgin, Combining fine-scale social contact data with epidemic modelling reveals interactions between contact tracing, quarantine, testing and physical distancing for controlling COVID-19. *medRxiv* 10.1101/2020.05.26.20113720 (2020).
56. S. Kojaku, L. Hébert-Dufresne, E. Mones, S. Lehmann, Y.-Y. Ahn, The effectiveness of backward contact tracing in networks. *Nat. Phys.* **17**, 652–658 (2021).
57. F. P. Polack, S. J. Thomas, N. Kitchin, J. Absalon, A. Gurtman, S. Lockhart, J. L. Perez, G. Pérez Marc, E. D. Moreira, C. Zerbini, R. Bailey, K. A. Swanson, S. Roychoudhury, K. Koury, P. Li, W. V. Kalina, D. Cooper, R. W. Frenck Jr., L. L. Hammitt, Ö. Türeci, H. Nell, A. Schaefer, S. Ünal, D. B. Tresnan, S. Mather, P. R. Dormitzer, U. Şahin, K. U. Jansen, W. C. Gruber; C4591001 Clinical Trial Group, Safety and efficacy of the bnt162b2 mrna covid-19 vaccine. *N. Engl. J. Med.* **383**, 2603–2615 (2020).
58. M. an der Heiden, O. Hamouda, Schätzung der aktuellen Entwicklung der SARS-CoV-2-Epidemie in Deutschland – Nowcasting. *Epidemiologisches Bull.* **2020**, 10–15 (2020).
59. L. F. Shampine, S. Thompson, Solving ddes in matlab. *Appl. Numer. Math.* **37**, 441–458 (2001).
60. E. Jarlebring, Some numerical methods to compute the eigenvalues of a time-delay system using MATLAB. *E-Delay System Letter* **2**, 155 (2008).
61. L. N. Trefethen, *Spectral Methods in MATLAB* (SIAM, 2000).
62. H. Ritchie, E. Mathieu, L. Rodés-Guirao, C. Appel, C. Giattino, E. Ortiz-Ospina, J. Hasell, B. Macdonald, D. Beltekian, M. Roser, Coronavirus pandemic (COVID-19), *Our World in Data* (2020); <https://ourworldindata.org/coronavirus>.
63. J. Dehning, Priesemann-Group/covid19_metastability. Zenodo (2021); <https://doi.org/10.5281/zenodo.5220793>.
64. X. He, E. H. Y. Lau, P. Wu, X. Deng, J. Wang, X. Hao, Y. C. Lau, J. Y. Wong, Y. Guan, X. Tan, X. Mo, Y. Chen, B. Liao, W. Chen, F. Hu, Q. Zhang, M. Zhong, Y. Wu, L. Zhao, F. Zhang, B. J. Cowling, F. Li, G. M. Leung, Temporal dynamics in viral shedding and transmissibility of COVID-19. *Nat. Med.*, 1491–1493 (2020).
65. F. Pan, T. Ye, P. Sun, S. Gui, B. Liang, L. Li, D. Zheng, J. Wang, R. L. Hesketh, L. Yang, C. Zheng, Time course of lung changes on chest CT during recovery from 2019 novel coronavirus (COVID-19) pneumonia. *Radiology* **295**, 200370 (2020).
66. Y. M. Bar-On, A. Flamholz, R. Phillips, R. Milo, SARS-CoV-2 (COVID-19) by the numbers. *eLife* **9**, e57309 (2020).
67. A. F. Siegenfeld, Y. Bar-Yam, The impact of travel and timing in eliminating COVID-19. *Commun. Phys.* **3**, 204 (2020).
68. P. Bittihn, R. Golestanian, Containment strategy for an epidemic based on fluctuations in the SIR model. *arXiv:2003.08784 [q-bio.PE]* (2020).
69. J. Salvatier, T. V. Wiecki, C. Fonnesbeck, Probabilistic programming in Python using PyMC3. *PeerJ Comput. Sci.* **2**, e55 (2016).

Acknowledgments: We thank M. Brinkmann and Á. Olivera-Nappa for helpful comments and encouraging feedback. We thank M. Loidolt, M. Wibrál, J. Zierenberg, J. Wagner, and A. Sanchez for carefully reading, commenting, and improving the manuscript. We thank the Priesemann group for exciting discussions and valuable input. **Funding:** All authors received support from the Max Planck Society (Max-Planck-Gesellschaft MPRG-Priesemann). S.C. acknowledges funding by the Centre for Biotechnology and Bioengineering (CeBiB; PIA project FB0001, ANID, Chile). J.D. and F.P.S. acknowledge funding by SMARTSTART, the joint training program in computational neuroscience by the VolkswagenStiftung and the Bernstein Network. S.B.M. and S.B. were financially supported by the German Federal Ministry of Education and Research (BMBF) as part of the Network University Medicine (NUM), project egePan (funding code: 01KX2021). **Author contributions:** Conceptualization: S.C., J.D., and V.P. Methodology: S.C., J.D., and V.P. Software: S.C. and S.B.M. Validation: S.C., J.D., S.B.M., S.B., and V.P. Formal analysis: S.C., J.D., S.B.M., F.P.S., S.B., and V.P. Investigation: S.C., J.D., S.B.M., F.P.S., and S.B. Writing (original draft): S.C., J.D., S.B.M., F.P.S., and V.P. Writing (review and editing): S.C., J.D., S.B.M., F.P.S., S.B., and V.P. Visualization: S.C., F.P.S., and S.B.M. Supervision: V.P. **Competing interests:** V.P. is currently active in various groups to advise the government. The authors declare that they have no other competing interests. **Data and materials availability:** All data needed to evaluate the conclusions in the paper are present in the paper and/or the Supplementary Materials. Raw data and preliminary visualizations of Fig. 6 and figs. S4 and S5 were obtained from (62). Analysis code is available in https://github.com/Priesemann-Group/covid19_metastability and permanently stored in <https://doi.org/10.5281/zenodo.5220793> (63). In addition, an interactive platform to simulate scenarios different from those presented here is available at <http://covid19-metastability.ds.mpg.de/>.

Submitted 21 December 2020

Accepted 19 August 2021

Published 8 October 2021

10.1126/sciadv.abg2243

Citation: S. Contreras, J. Dehning, S. B. Mohr, S. Bauer, F. P. Spitzner, V. Priesemann, Low case numbers enable long-term stable pandemic control without lockdowns. *Sci. Adv.* **7**, eabg2243 (2021).

Low case numbers enable long-term stable pandemic control without lockdowns

Sebastian ContrerasJonas DehningSebastian B. MohrSimon BauerF. Paul SpitznerViola Priesemann

Sci. Adv., 7 (41), eabg2243.

View the article online

<https://www.science.org/doi/10.1126/sciadv.abg2243>

Permissions

<https://www.science.org/help/reprints-and-permissions>

Use of this article is subject to the [Terms of service](#)

Science Advances (ISSN) is published by the American Association for the Advancement of Science, 1200 New York Avenue NW, Washington, DC 20005. The title *Science Advances* is a registered trademark of AAAS. Copyright © 2021 The Authors, some rights reserved; exclusive licensee American Association for the Advancement of Science. No claim to original U.S. Government Works. Distributed under a Creative Commons Attribution License 4.0 (CC BY).

RELAXING RESTRICTIONS AT THE PACE OF
VACCINATION INCREASES FREEDOM AND
GUARDS AGAINST FURTHER COVID-19 WAVES[†]

ABSTRACT

Mass vaccination offers a promising exit strategy for the COVID-19 pandemic. However, as vaccination progresses, demands to lift restrictions increase, despite most of the population remaining susceptible. Using our age-stratified SEIRD-ICU compartmental model and curated epidemiological and vaccination data, we quantified the rate (relative to vaccination progress) at which countries can lift non-pharmaceutical interventions without overwhelming their healthcare systems. We analyzed scenarios ranging from immediately lifting restrictions (accepting high mortality and morbidity) to reducing case numbers to a level where test-trace-and-isolate (TTI) programs efficiently compensate for local spreading events. In general, the age-dependent vaccination roll-out implies a transient decrease of more than ten years in the average age of ICU patients and deceased. The pace of vaccination determines the speed of lifting restrictions; Taking the European Union (EU) as an example case, all considered scenarios allow for steadily increasing contacts starting in May 2021 and relaxing most restrictions by autumn 2021. Throughout summer 2021, only mild contact restrictions will remain necessary. However, only high vaccine uptake can prevent further severe waves. Across EU countries, seroprevalence impacts the long-term success of vaccination campaigns more strongly than age demographics. In addition, we highlight the need for preventive measures to reduce contagion in school settings throughout the year 2021, where children might be drivers of contagion because of them remaining susceptible. Strategies that maintain low case numbers, instead of high ones, reduce infections and deaths by factors of eleven and five, respectively. In general, policies with low case numbers significantly benefit from vaccination, as the overall reduction in susceptibility will further diminish viral spread. Keeping case numbers low is the safest long-term strategy because it considerably reduces mortality and morbidity and offers better preparedness against emerging escape or more contagious virus variants while still allowing for higher contact numbers (freedom) with progressing vaccinations.

Cite as: Bauer, S., Contreras, S., Dehning, J., Linden, M., Iftekhar, E., Mohr, S.B., Olivera-Nappa, A. and Priesemann, V., 2021. Relaxing restrictions at the pace of vaccination increases freedom and guards against further COVID-19 waves. PLoS computational biology, 17(9), p.e1009288.
https://doi.org/10.1371/journal.pcbi.1009288

† This chapter is identical to the publication [28]: Bauer, S.* , Contreras, S.* , Dehning, J., Linden, M., Iftekhar, E., Mohr, S.B., Olivera-Nappa, A. and Priesemann, V., 2021. Relaxing restrictions at the pace of vaccination increases freedom and guards against further COVID-19 waves. PLoS computational biology, 17(9), p.e1009288. The article is published under the terms of a Creative Common License (<http://creativecommons.org/licenses/by/4.0/>). To this publication, I contributed equally with S. Bauer. Roles: Conceptualization, Formal analysis, Investigation, Methodology, Validation, Visualization, Writing – original draft, Writing – review & editing.

RESEARCH ARTICLE

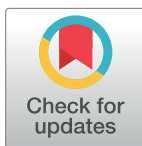
Relaxing restrictions at the pace of vaccination increases freedom and guards against further COVID-19 waves

Simon Bauer¹ , Sebastian Contreras^{1,2} , Jonas Dehning¹ , Matthias Linden^{1,3} , Emil Iftekhar¹ , Sebastian B. Mohr¹ , Alvaro Olivera-Nappa² , Viola Priesemann^{1,4*} 

1 Max Planck Institute for Dynamics and Self-Organization, Göttingen, Germany, 2 Centre for Biotechnology and Bioengineering, Universidad de Chile, Santiago, Chile, 3 Institute for Theoretical Physics, Leibniz University, Hannover, Germany, 4 Institute for the Dynamics of Complex Systems, University of Göttingen, Göttingen, Germany

 These authors contributed equally to this work.

* viola.priesemann@ds.mpg.de



Abstract

Mass vaccination offers a promising exit strategy for the COVID-19 pandemic. However, as vaccination progresses, demands to lift restrictions increase, despite most of the population remaining susceptible. Using our age-stratified SEIRD-ICU compartmental model and curated epidemiological and vaccination data, we quantified the rate (relative to vaccination progress) at which countries can lift non-pharmaceutical interventions without overwhelming their healthcare systems. We analyzed scenarios ranging from immediately lifting restrictions (accepting high mortality and morbidity) to reducing case numbers to a level where test-trace-and-isolate (TTI) programs efficiently compensate for local spreading events. In general, the age-dependent vaccination roll-out implies a transient decrease of more than ten years in the average age of ICU patients and deceased. The pace of vaccination determines the speed of lifting restrictions; Taking the European Union (EU) as an example case, all considered scenarios allow for steadily increasing contacts starting in May 2021 and relaxing most restrictions by autumn 2021. Throughout summer 2021, only mild contact restrictions will remain necessary. However, only high vaccine uptake can prevent further severe waves. Across EU countries, seroprevalence impacts the long-term success of vaccination campaigns more strongly than age demographics. In addition, we highlight the need for preventive measures to reduce contagion in school settings throughout the year 2021, where children might be drivers of contagion because of them remaining susceptible. Strategies that maintain low case numbers, instead of high ones, reduce infections and deaths by factors of eleven and five, respectively. In general, policies with low case numbers significantly benefit from vaccination, as the overall reduction in susceptibility will further diminish viral spread. Keeping case numbers low is the safest long-term strategy because it considerably reduces mortality and morbidity and offers better preparedness against emerging escape or more contagious virus variants while still allowing for higher contact numbers (freedom) with progressing vaccinations.

 OPEN ACCESS

Citation: Bauer S, Contreras S, Dehning J, Linden M, Iftekhar E, Mohr SB, et al. (2021) Relaxing restrictions at the pace of vaccination increases freedom and guards against further COVID-19 waves. *PLoS Comput Biol* 17(9): e1009288. <https://doi.org/10.1371/journal.pcbi.1009288>

Editor: Claudio José Struchiner, Fundação Getúlio Vargas: Fundacao Getulio Vargas, BRAZIL

Received: March 31, 2021

Accepted: July 19, 2021

Published: September 2, 2021

Peer Review History: PLOS recognizes the benefits of transparency in the peer review process; therefore, we enable the publication of all of the content of peer review and author responses alongside final, published articles. The editorial history of this article is available here: <https://doi.org/10.1371/journal.pcbi.1009288>

Copyright: © 2021 Bauer et al. This is an open access article distributed under the terms of the [Creative Commons Attribution License](https://creativecommons.org/licenses/by/4.0/), which permits unrestricted use, distribution, and reproduction in any medium, provided the original author and source are credited.

Data Availability Statement: The source code for data generation and analysis is available online on GitHub https://github.com/Priesemann-Group/covid19_vaccination. All other relevant data are

within the manuscript and its [Supporting information files](#).

Funding: SB, SC, JD, ML, EI, SM, and VP received support from the Max-Planck-Gesellschaft (MPRG Priesemann), <https://www.mpg.de/de>. SC and AO-N received support from the Comisión Nacional de Investigación Científica y Tecnológica PIA project FB0001, ANID, Chile. ML, JD, SM acknowledge funding from the “Netzwerk Universitätsmedizin” (NUM) project egePan (01KX2021). The funders had no role in study design, data collection and analysis, decision to publish, or preparation of the manuscript.

Competing interests: The authors have declared that no competing interests exist.

Author summary

In this work, we quantify the rate at which non-pharmaceutical interventions can be lifted as COVID-19 vaccination campaigns progress. With the constraint of not exceeding ICU capacity, there exists only a relatively narrow range of plausible scenarios. We selected different scenarios ranging from the immediate release of restrictions to more conservative approaches aiming at low case numbers. In all considered scenarios, the increasing overall immunity (due to vaccination or post-infection) will allow for a steady increase in contacts. However, deaths and total cases (potentially leading to *long covid*) are only minimized when aiming for low case numbers, and restrictions are lifted at the pace of vaccination. These qualitative results are general. Taking EU countries as quantitative examples, we observe larger differences only in the long-term perspectives, mainly due to varying seroprevalence and vaccine uptake. Thus, the recommendation is to keep case numbers as low as possible to facilitate test-trace-and-isolate programs, reduce mortality and morbidity, and offer better preparedness against emerging variants, potentially escaping immune responses. Keeping moderate preventive measures in place (such as improved hygiene, use of face masks, and moderate contact reduction) is highly recommended will further facilitate control.

Introduction

The rising availability of effective vaccines against SARS-CoV-2 promises the lifting of restrictions, thereby relieving the social and economic burden caused by the COVID-19 pandemic. However, it is unclear how fast the restrictions can be lifted without risking another wave of infections; we need a promising long-term vaccination strategy [1]. Nevertheless, a successful approach has to take into account several challenges; vaccination logistics and vaccine allocation requires a couple of months [2–4], vaccine eligibility depends on age and eventually serostatus [5], vaccine acceptance may vary across populations [6], and more contagious [7] and escape variants of SARS-CoV-2 that can evade existing immunity [8, 9] may emerge, thus posing a persistent risk. Last but not least, disease mitigation is determined by how well vaccines block infection, and thus prevent the propagation of SARS-CoV-2 [3, 4], the time to develop effective antibody titers after vaccination, and their efficacy against severe symptoms. All these parameters will greatly determine the design of an optimal strategy for the transition from epidemicity to endemicity [10].

To bridge the time until a significant fraction of the population is vaccinated, a sustainable public health strategy has to combine vaccination with non-pharmaceutical interventions (NPIs). Otherwise it risks further waves and, consequently, high morbidity and excess mortality. However, the overall compliance with NPIs worldwide has on average decreased due to a “pandemic-policy fatigue” [11]. Therefore, the second wave has been more challenging to tame [12] although NPIs, in principle, can be highly effective, as seen in the first wave [13, 14]. After vaccinating the most vulnerable age groups, the urge and social pressure to lift restrictions will increase. However, given the wide distribution of fatalities over age groups and the putative incomplete protection of vaccines against severe symptoms and against transmission, NPIs cannot be lifted entirely or immediately. With our study, we want to outline at which pace restrictions can be lifted as the vaccine roll-out progresses.

Public-health policies in a pandemic have to find a delicate ethical balance between reducing the viral spread and restricting individual freedom and economic activities. However, the interest of health on the one hand and society and economy on the other hand are not always

contradictory. For the COVID-19 pandemic, all these aspects clearly profit from low case numbers [15–17], i.e., an incidence where test-trace-and-isolate (TTI) programs can efficiently compensate for local spreading events. The challenge is to reach low case numbers and maintain them [18, 19]. Especially with the progress of vaccination, restrictions should be lifted when the threat to public health is reduced. However, the apparent trade-off between public health interest and freedom is not always linear and straightforward. Taking into account that low case numbers facilitate TTI strategies (i.e., health authorities can concentrate on remaining infection chains and stop them quickly) [18–20], an optimal strategy with a low public health burden *and* large freedom may exist and be complementary to vaccination.

Here, we quantitatively study how the planned vaccine roll-out in the European Union (EU), together with the cumulative post-infection immunity (seroprevalence), progressively allows for lifting restrictions. In particular, we study how precisely the number of contacts can be increased without rendering disease spread uncontrolled over the year 2021. Our study builds on carefully curated epidemiological and contact network data from Germany, France, the UK, and other European countries. Thereby, our work can serve as a blueprint for an opening strategy.

Analytical framework

Our analytical framework builds on our deterministic, age-stratified, SEIRD-ICU compartmental model, modified to incorporate vaccination through delay differential equations. It includes compartments for a 2-dose staged vaccine roll-out, immunization delays, intensive care unit (ICU)-hospitalized, and deceased individuals. A central parameter for our model is the gross reproduction number R_t . It is essentially the time-varying effective reproduction number without considering the effects of immunity nor of TTI. That number depends (among several factors) on i) the absolute number of contacts per individual, and ii) the probability of being infected given a contact. In other words, R_t is defined as the average number of contacts an infected individual has that would lead to an offspring infection in a fully susceptible population. Therefore, an increase in R_t implies an increase in contact frequency or the probability of transmission per contact, e.g., due to less mask-wearing. The core idea is that increasing immunity levels among the population (post-infection or due to vaccination) allows for a higher average number of potentially contagious contacts and, thus, freedom (quantified by R_t), given the same level of new infections or ICU occupancy. Hence, with immunization progress reducing the susceptible fraction of the population, R_t can be dynamically increased while maintaining control over the pandemic, i.e., while keeping the effective reproduction number below one (Fig 1A).

To adapt the gross reproduction number R_t such that a specific strategy is followed (e.g. staying below TTI or ICU capacity), we include an automatic, proportional-derivative (PD) control system [21]. This control system allows for steady growth in R_t as long as it does not lead to overflowing ICUs (or surpassing the TTI capacity). However, when risking surpassing the ICU capacity, restrictions might be tightened again. In that way, we approximate the feedback-loop between political decisions, people's behavior, reported case numbers, and ICU occupancy.

The basic reproduction number is set to $R_0 = 4.5$, reflecting the dominance of the B.1.1.7 variant [3, 7]. We further assume that the reproduction number can be decreased to about 3.5 by hygiene measures, face masks, and mild social distancing. This number is informed by the estimates of Sharma et al. [22], who estimate the combined effectiveness of mask wearing, limiting gatherings to at most 10 people and closing night clubs to a reduction of about 20–40%, thus leading to a reproduction number between 2.7 and 3.6. We use a conservative estimate, as

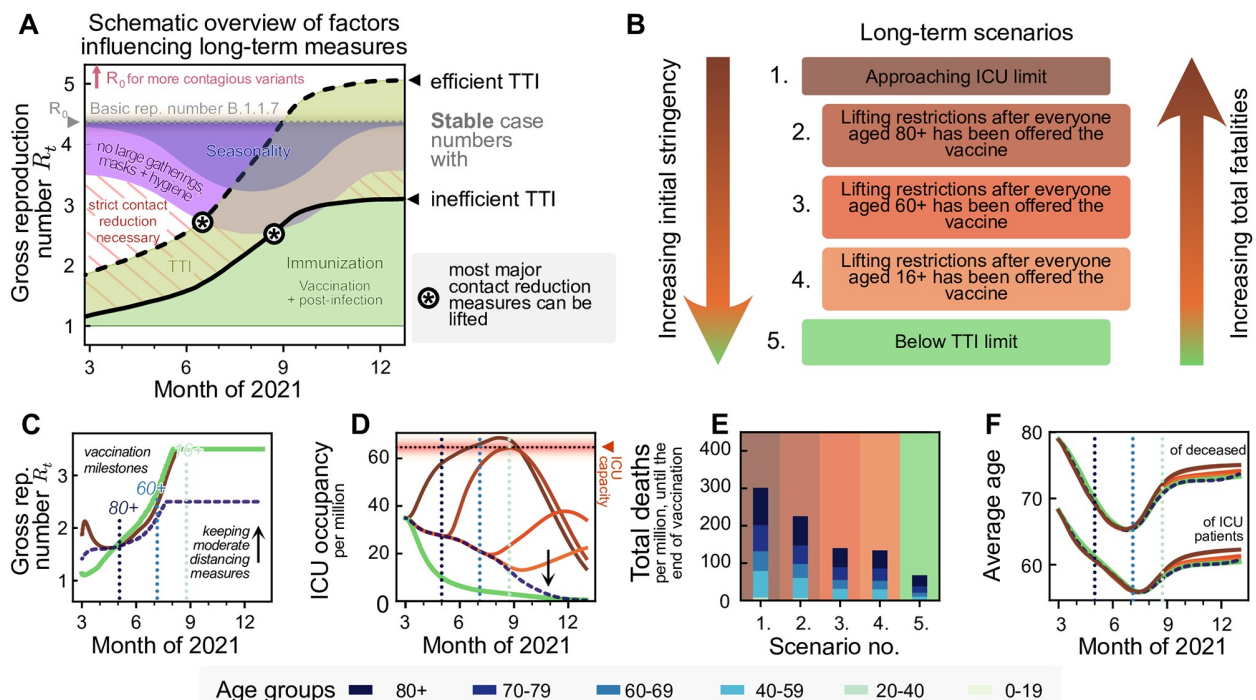


Fig 1. With progressing vaccination in the European Union, a slow but steady increase in freedom will be possible. However, premature lifting of NPIs considerably increases the total fatalities without a major reduction in restrictions in the middle term. A: A schematic outlook into the effect of vaccination on societal freedom. Freedom is quantified by the maximum time-varying gross reproduction number (R_t) allowed to sustain stable case numbers. As R_t does not consider the immunized population, gross reproduction numbers above one are possible without rendering the system unstable. A complete return to pre-pandemic behavior would be achieved when R_t reaches the value of the basic reproduction number R_0 (or possibly at a lower value due to seasonality effects during summer, purple-blue shaded area). The thick full and dashed lines indicate the gross reproduction number R_t allowed to sustain stable case numbers if test-trace-isolate (TTI) programs are inefficient and efficient, respectively, which depends on the case numbers level. Increased population immunity (green) is expected to allow for lifting the most strict contact reduction measures while only keeping mild NPIs (purple) during summer 2021 in the northern hemisphere. Note that seasonality is not explicitly modeled in this work. See S4 Fig for an extended version including the year 2020. B: We explore five different scenarios for lifting restrictions in the EU, in light of the EU-wide vaccination programs. We sort them according to the initial stringency that they require and the total fatalities that they may cause. One extreme (Scenario 1) offers immediate (but still comparably little) freedom by approaching ICU-capacity limits quickly. The other extreme (Scenario 5) uses a strong initial reduction in contacts to allow long-term control at low case numbers. Finally, the intermediate scenarios initially maintain moderate case numbers and lift restrictions at different points in the vaccination program. C: All extreme strategies allow for a steady noticeable increase in contacts in the coming months (cf. panel A), but vary greatly in the (D) ICU-occupancy profiles and (E) total fatalities. F: Independent on the strategy, we expect a transient but pronounced decrease in the average age of ICU patients and deceased over the summer.

<https://doi.org/10.1371/journal.pcbi.1009288.g001>

this is only a exemplary set of restrictions. Therefore, we restrict R_t in general not to exceed 3.5 (Fig 1C).

Efficient TTI contributes to reducing the effective reproduction number. Hence, it increases the average number of contacts (i.e., R_t) that people may have under the condition that case numbers remain stable (Fig 1A) [18]. This effect is particularly strong at low case numbers, where the health authorities can concentrate on tracing every case efficiently [19]. Here, we approximate the effect of TTI on R_t semi-analytically to achieve an efficient implementation (see Methods).

For vaccination, we use as default parameters an average vaccine efficacy of 90% protection against severe illness [23] and of 75% protection against infection [24]. We further assume that vaccinated individuals with a breakthrough infection carry a lower viral load and thus are 50% less infectious [25] than unvaccinated infected individuals. We assume a total average vaccine uptake of 80% [26] that increases with age from 73% in the 0–19 to 89% in the 80+ age group, and an age-prioritized vaccine delivery as described in the Methods section. In detail, most of

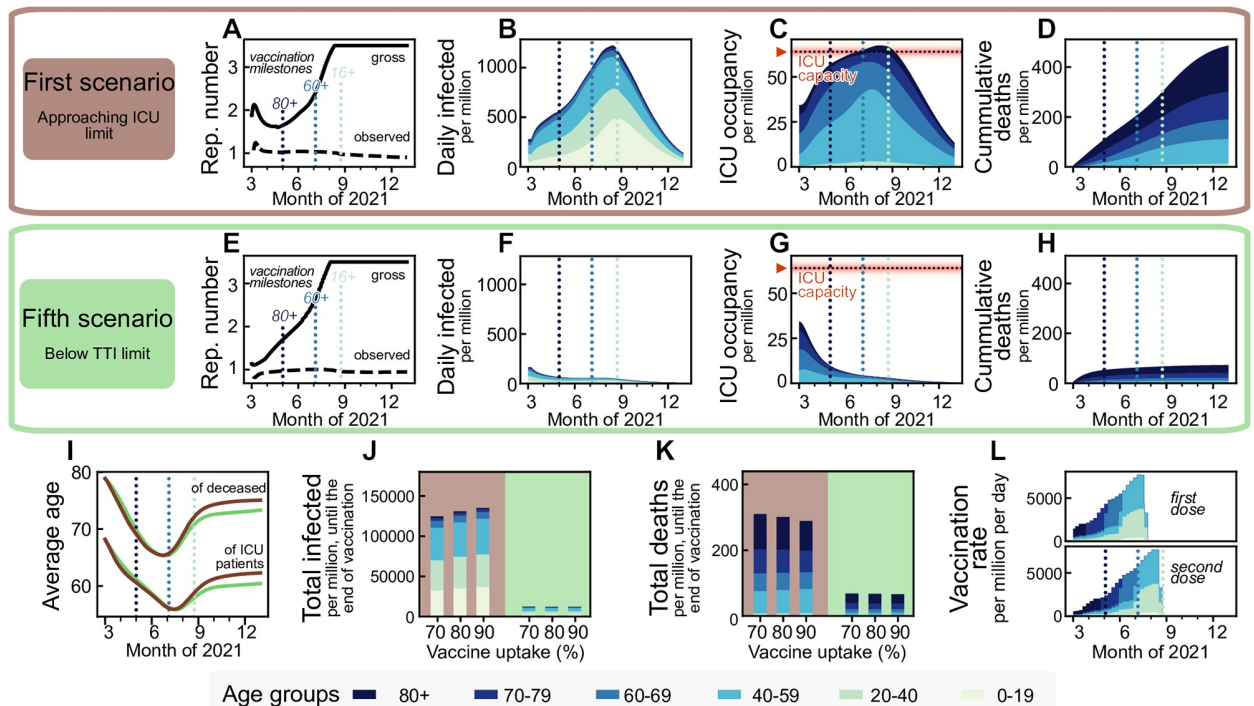


Fig 2. Maintaining low case numbers during vaccine roll-out reduces the number of ICU patients and deaths by about a factor five compared to quickly approaching the ICU limit while hardly requiring stronger restrictions. Aiming to maximize ICU occupancy (A–D) allows for a slight increase of the allowed gross reproduction number R_t early on, whereas lowering case numbers below the TTI capacity limit (E–H) requires comparatively stronger initial restrictions. Afterwards, the vaccination progress allows for a similar increase in freedom (quantified by increments in R_t) for both strategies, starting approximately in May 2021. B–D, F–H: These two strategies lead to a completely different evolution of case numbers, ICU occupancy, and cumulative deaths, but differ only marginally in the evolution of the average age of deceased and ICU patients (I), as the latter is rather an effect of the age-prioritized vaccination than of a particular strategy. J, K: The total number of cases until the end of the vaccination period (of the 80% uptake scenario, i.e., end of August, the rightmost dotted light blue line in sub-panels A–H) differ by a factor of eleven between the two strategies, and the total deaths by a factor of five. Vaccine uptake (i.e., the fraction of the eligible, 16+, population that gets vaccinated) has a minor impact on these numbers until the end of the vaccine roll-out but determines whether a wave would follow afterward (see below). L: Assumed vaccination rate as projected for Germany, which is expected to be similar across the European Union. For a full display of the time-evolution of the compartments for different uptakes see S6–S8 Figs.

<https://doi.org/10.1371/journal.pcbi.1009288.g002>

the vaccines are distributed first to the age group 80+, then 70+, 60+, and then to anyone of age 16+. A small fraction of the weekly available vaccines is distributed randomly (e.g. because of profession). After everyone got a vaccine offer roughly by the end of August, we assume no further vaccination (see Fig 2L). The daily amount of vaccine doses per million is derived from German government projections, but is expected to be similar across the EU. For the course of the disease, the age-dependent fraction of non-vaccinated, infected individuals requiring intensive care is estimated from German hospitalization data, using the infection-fatality-ratio (IFR) reported in [27] (see Table 1 and Methods).

In our default scenario we use a contact structure between age groups as measured during pre-pandemic times [28]. However, we halve the infection probability in the 0–19 year age group to account for reduced in-person classes and better ventilation and systematic random screening in school settings using rapid COVID-19 tests. Under these assumptions, the infection probability among the 0–19 age group is similar to the one among the 20–39 and 40–69 age groups. We start our simulations at the beginning of March 2021, with an incidence of 200 daily infections per million, two daily deaths per million, an ICU occupancy of 30 patients per million, a seroprevalence of 10%, and about 4% of the population already vaccinated. This is

Table 1. Age-dependent infection-fatality-ratio (IFR), probability of requiring intensive care due to the infection (ICU probability) and ICU fatality ratio (ICU-FR). The IFR is defined as the probability of an infected individual dying, whereas the ICU-FR is defined as the probability of an infected individual dying while receiving intensive care.

Age	IFR [27]	ICU probability	ICU-FR	Avg. ICU time (days)
0–19	0.00002	0.00014	0.0278	5
20–39	0.00022	0.00203	0.0389	5
40–59	0.00194	0.01217	0.0678	11
60–69	0.00739	0.04031	0.1046	11
70–79	0.02388	0.05435	0.1778	9
>80	0.08292	0.07163	0.4946	6
Average	0.00957	0.02067	0.0969	9

<https://doi.org/10.1371/journal.pcbi.1009288.t001>

comparable to German data (assuming a case under-reporting factor of 2, which had been measured during the first wave in Germany [29]) and typical for EU countries at the beginning of March 2021 (further details in the [Methods](#) section). We furthermore explore the impact of important differences between EU countries, namely the seroprevalance by the start of the vaccination program, demographics, and vaccine uptake exemplary for Finland, Italy and the Czech Republic in addition to the default German parameters.

Results

Aiming for low case numbers has the best long-term outcome

We first present the two extreme scenarios: case numbers quickly rise so that the ICU capacity limit is approached (Scenario 1), or case numbers quickly decline below the TTI capacity limit (Scenario 5; [Fig 2](#)). We set the ICU capacity limit at 65 patients/million, reflecting the maximal occupancy and improved treatments during the second wave in Germany [30] and use German demographics. The incidence (daily new cases) limit up to which TTI is fully efficient is set to 20 daily infections per million [15], but depends strongly on the gross reproduction number, as described in [Methods](#).

The first scenario ('approaching ICU limit', [Fig 2A–2D](#)) maximizes the initial freedom individuals might have (quantified as the allowed gross reproduction number R_t). However, the gained freedom is only transient as, once ICUs approach their capacity limit, restrictions need to be tightened ([Fig 2J and 2K](#)). Additionally, stabilization at high case numbers leads to many preventable fatalities, especially in light of likely temporary overflows of the ICU capacity due to the hard-to-control nature of high case numbers.

The fifth scenario ('below TTI limit', [Fig 2E and 2F](#)) requires maintaining stronger restrictions for about two months to lower case numbers below the TTI capacity. Afterward, the progress of the vaccination allows for a steady increase in R_t while keeping case numbers low, enabling TTI to contribute to the containment effectively. From May 2021 on, this fifth scenario would allow for slightly more freedom, i.e., a higher R_t , than the first scenario ([Fig 1C](#)). Furthermore, this scenario reduces morbidity and mortality: Deaths until the of the vaccination period (end of August) are reduced by a factor of five, total infections even by a factor of eleven. Due to the prioritization of the elderly in vaccination, the average age of ICU patients and fatalities drops by roughly 12 and 15 years, respectively, independently of the choice of scenarios ([Fig 2I](#)). Overall, the low-case-number scenario thus allows for a very similar increase in freedom over the whole time frame (quantified as the increase in R_t) and implies about five times fewer deaths by the end of the vaccination program compared to the first scenario with high case numbers ([Fig 2K](#)).

The vaccine uptake has little influence on the number of deaths and total cases during the vaccination period (Fig 2J and 2K), mainly because restrictions are quickly enacted when reaching the ICU capacity. However, uptake becomes a crucial parameter; It controls the pandemic progression after completing the vaccine roll-out as it determines the residual susceptibility of the population (cf. below). With insufficient vaccination uptake, a novel wave will follow as soon as restrictions are lifted [3].

Maintaining low case numbers at least until vulnerable groups (60+) are vaccinated is necessary to prevent a severe further wave

Between the two extreme scenarios 1 and 5, which respectively allow maximal or minimal initial freedom, we explore three alternative scenarios, where the vaccination progress and the slow restriction lifting roughly balance out (Figs 3 and 1B). These scenarios assume approximately constant case numbers and then a swift lifting of most of the remaining restrictions within a month after three different vaccination milestones: when the age group 80+ has been vaccinated (Scenario 2, Fig 3A–3D), when the age groups 60+ has been vaccinated (Scenario 3, Fig 3E–3H) and when the entire adult population (16+) has been vaccinated (Scenario 4, Fig 3I–3L).

The relative freedom gained by lifting restrictions early in the vaccination timeline (Scenario 2) hardly differs from the freedom gained from the other two scenarios (Fig 3M), as since new contact restrictions need to take place once reaching the ICU capacity limit, and the initial freedom is partly lost. Significantly, lifting restrictions later reduces the number of infections and deaths by more than 50% and 35% respectively if case numbers have been kept at a moderate level (250 daily infections per million) and by more than 85% and 65%, respectively if case numbers have been kept at a low level (50 per million) beforehand (Fig 3N and 3O). Lifting restrictions entirely after either offering vaccination to everyone aged 60+ or everyone aged 16+ only changes the total fatalities by a small amount, mainly because the vaccination pace is planned to be quite fast by then, and the 60+ age brackets make up the bulk of the highest-risk groups. Hence, a potential subsequent wave only unfolds after the end of the planned vaccination campaign (Fig 3F and 3H). Thus, with the current vaccination plan, it is recommended to keep case numbers at moderate or low levels, at least until the population at risk and people of age 60+ have been vaccinated.

If maintaining low or intermediate case numbers in the initial phase, vaccination starts to decrease the ICU occupancy considerably in May 2021 (Fig 3G and 3K). However, This decrease in ICU occupancy must not be mistaken for a generally stable situation. As soon as restrictions are relaxed too quickly, ICU occupancy surges again (Fig 3C, 3G and 3H), without any relevant gain in freedom for the total population. Nonetheless, the progress in vaccination will, in any case, allow lifting restrictions gradually.

The long-term success of the vaccination campaign strongly depends on vaccine uptake and vaccine efficacy

The vaccination campaign's long-term success will depend on both people's vaccine uptake and the efficacy of the vaccine against those variants of SARS-CoV-2 prevalent at the time of writing of this paper. A vaccine's efficacy has two contributions: first, vaccinated individuals become less likely to develop severe symptoms and require intensive care [31–33] (vaccine efficacy, κ). Second, a fraction η of vaccinated individuals gains sterilizing immunity, i.e., is completely protected against infections and does not contribute to viral spread at all [24, 34]. We also assume that breakthrough infections among vaccinated individuals would bear lower viral loads, thus exhibit reduced transmissibility [25] (reduced viral load, σ). However, the

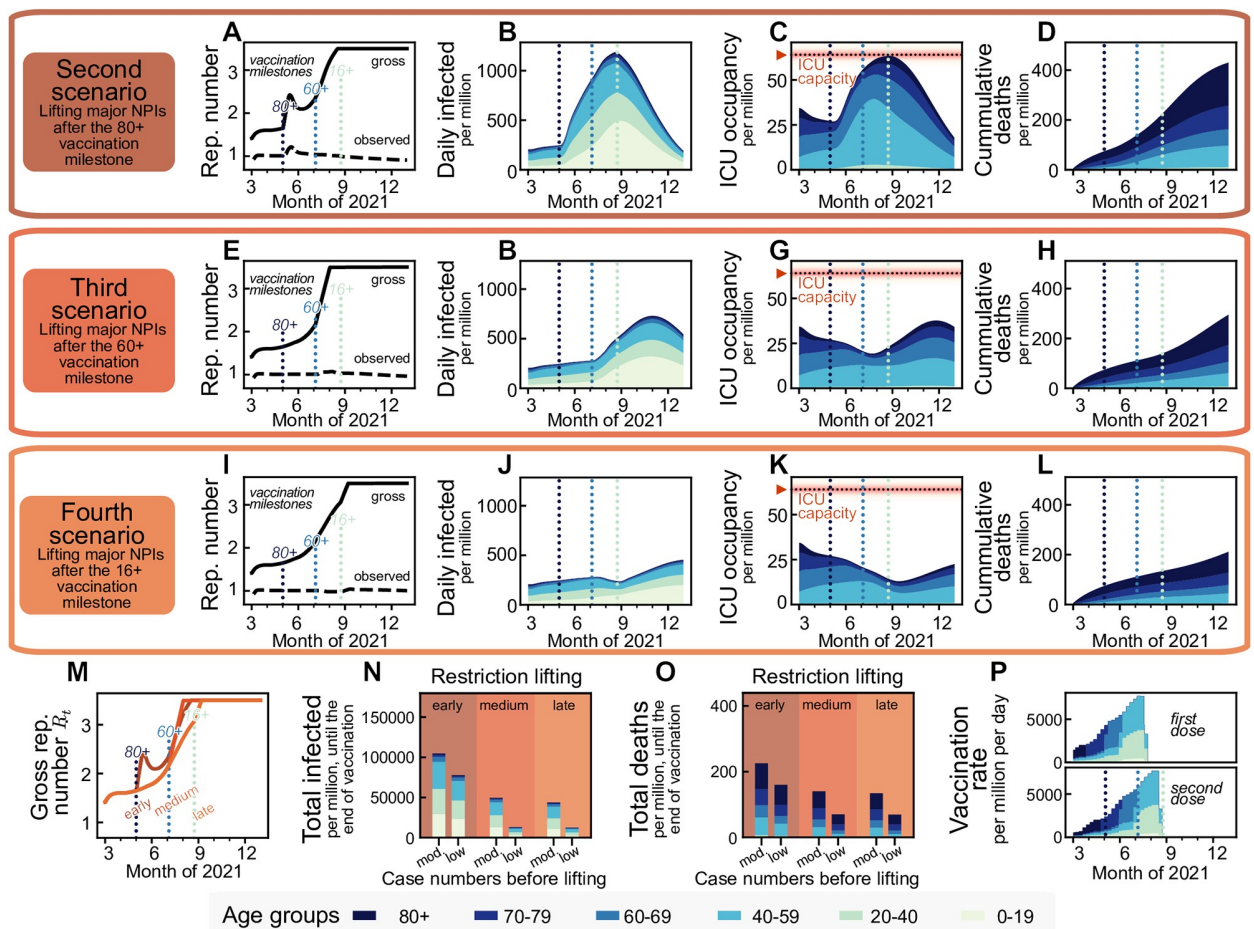


Fig 3. Vaccination offers a steady return to normality until the end of summer 2021 in the northern hemisphere, no matter whether a transient easing of restrictions is allowed earlier or later (second and fourth scenario, respectively). However, lifting restrictions later reduces fatalities by more than 35%. We assume that the vaccine immunization progress is balanced out by a slow lifting of restrictions, keeping case numbers at a moderate level (≤ 250 daily new cases per million people). We simulated lifting all restrictions within a month starting from different time points: when (A–D) the 80+ age group, (E–H) the 60+ age group or (I–L) everyone 16+ has been offered vaccination. Restriction lifting leads to a new surge of cases in all scenarios. New restrictions are put in place if ICUs would otherwise collapse. M: Lifting all restrictions too early increases the individual freedom only temporarily before new restrictions have to be put in place to avoid overwhelming ICUs. Overall, trying to lift restrictions earlier has a small influence on the additional increase in the allowed gross reproduction number R_t . N, O: Relaxing major restrictions only medium-late or late reduces fatalities by more than 35% and infections by more than 50%. Fatalities and infections can be cut by an additional factor of more than two when aiming for a low (50 per million) instead of moderate (250 per million) level of daily infections before major relaxations. P: Assumed daily vaccination rates, same as in Fig 2.

<https://doi.org/10.1371/journal.pcbi.1009288.g003>

possibly reduced effectiveness of vaccines against current variants of concern (VOCs), e.g., B.1.351 and P.1 [32, 35, 36], and potential future VOCs render long-term scenarios about the success of vaccination uncertain.

Therefore, we explore different parameters of vaccine uptake and effectiveness. We quantify the success, or rather the lack of success of the vaccination campaign by the duration of the period where ICUs function near capacity limit, until population immunity is reached. Two different scenarios are considered upon finishing the vaccination campaign: in the first scenario, most restrictions are lifted, like in the previous scenarios (Fig 4B). In the second, restrictions are only lifted partially, to a one third lower gross reproduction number ($R_t = 2.5$) (Fig 4C). This second scenario presents the long-term maintenance of moderate social distancing

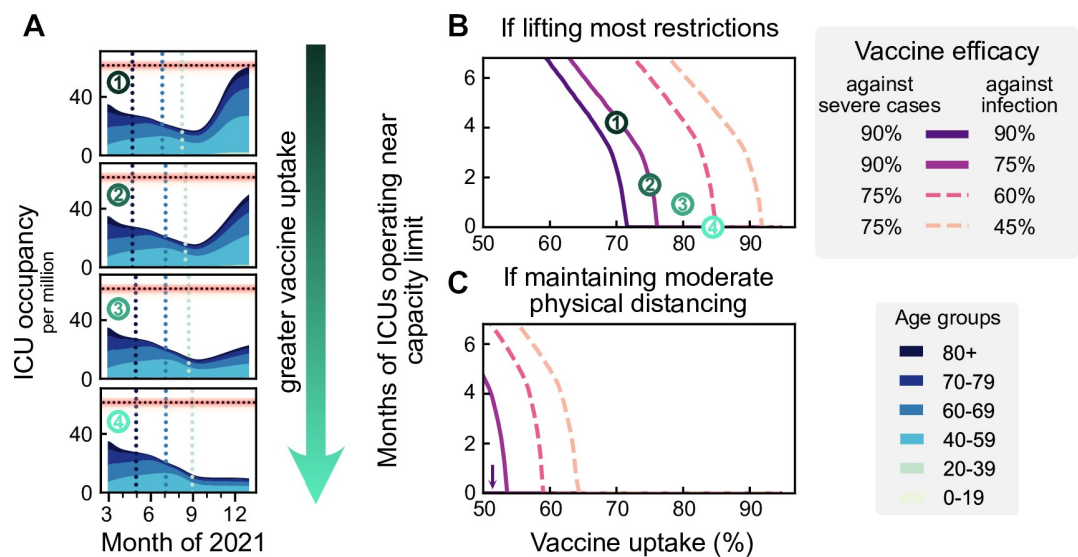


Fig 4. A high vaccine uptake (> 90% or higher among the eligible population) is crucial to prevent a wave when lifting restrictions after completing vaccination campaigns. A: We assume that infections are kept stable at 250 daily infections until all age groups have been vaccinated. Then restrictions are lifted, leading to a wave if the vaccine uptake has not been high enough (top three plots). B: The duration of the wave (measured by the total time that ICUs function close to their capacity limit) depends on vaccine uptake and vaccine efficacy. We explore the dependency on the efficacy both for preventing severe cases (full versus dashed lines) and preventing infection (shades of purple). The dashed lines might correspond to vaccine efficacy in the event of the emergence of escape variants of SARS-CoV-2. C: If some NPIs remain in place (such that the gross reproduction number stays at $R_t = 2.5$), ICUs will not overflow even if the protection against infection is only around 60%. See S2 Fig for all possible combinations of vaccine efficacies, also in the event of different contact structures.

<https://doi.org/10.1371/journal.pcbi.1009288.g004>

measures, including the restriction of large gatherings to smaller than 100 people, encouraging home-office, enabling effective test-trace-and-isolate (TTI) programs at very low case numbers, and supporting hygiene measures and face mask usage. Fig 4B and 4C indicates how long ICUs are expected to be full in both scenarios, and for different parameters of vaccine efficacy (which may account for the emergence of vaccine escape variants).

The primary determinant for the success of vaccination programs after lifting most restrictions is the vaccine uptake among the population aged 20+; only with a high vaccine uptake (> 90%) we can avoid a novel wave of full ICUs (default parameters as in scenario 3; Fig 4B, $\kappa = 90\%$, $\eta = 75\%$). However, if vaccine uptake was lower or vaccines prove to be less effective against prevalent or new variants, lifting most restrictions would imply that ICUs will work at the capacity limit for months.

In contrast, maintaining moderate social distancing measures (Fig 4C) may prevent a wave after completing the vaccine roll-out. This strategy can also compensate for a low vaccine uptake, requiring only about 55% uptake to avoid surpassing ICU capacity for our default parameters. Nonetheless, any increase in vaccine uptake lowers intensive care numbers, increases freedom, and most importantly, provides better protection in case of the emergence of escape variants, as this would involve an effective reduction of vaccine efficacy (dashed lines). A full exploration of vaccine efficacy parameter combinations and different contact structures is presented in S2 Fig.

Heterogeneity among countries on an EU-wide level will affect the probability and strength of a new wave after completing vaccination campaigns. We chose some exemplary European countries to investigate how our results depend on age demographics, contact structure, and the degree of initial post-infection immunization (seroprevalence). We obtained the

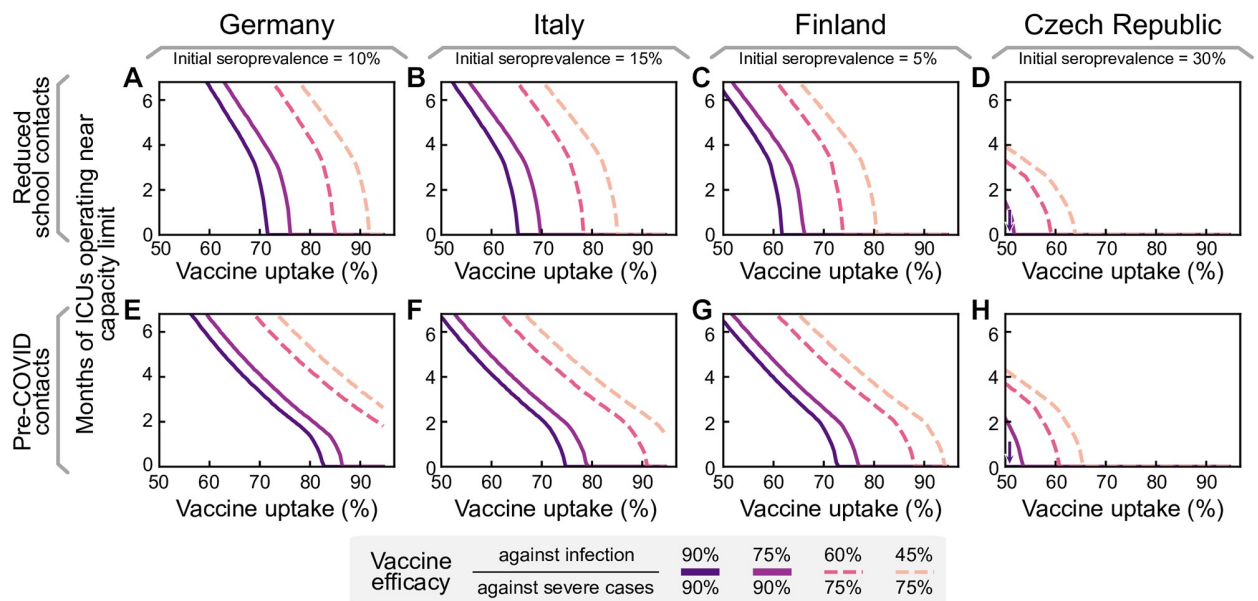


Fig 5. Seroprevalence and different demographics across EU countries determine the vaccine uptake required for population immunity. As in Fig 4B, we assume that case numbers are stable at 250 daily infections per million per day until the end of vaccination, when most restrictions are lifted (such that the gross reproduction number goes up to 3.5). We vary the initial seroprevalence and age demographics and contact structures to represent German, Italian, Finnish, and Czech data. A–D: Projected ICU occupancy in a subsequent wave depending on vaccine uptake, assuming reduced transmission risk in schools but otherwise default pre-pandemic contact structures. E–H: Projected ICU occupancy depending on vaccine uptake, assuming default pre-pandemic contact structures everywhere (including schools). See S3 Fig for a more comprehensive exploration of combinations of vaccine efficacies.

<https://doi.org/10.1371/journal.pcbi.1009288.g005>

seroprevalence in the different countries by scaling the German 10% seroprevalence with the relative differences in cumulative reported case numbers between Germany and the other countries, i.e., we assume the under-reporting factor to be roughly the same across the chosen countries. All other parameters are left unchanged. Specifically, we leave the capacities of the health systems at the estimated values for Germany, as lacking TTI data and varying definitions of ICU treatment make any comparison difficult. We repeated the analysis presented above (Fig 4) for Finland, Italy and the Czech Republic (see Fig 5A–5D). Germany, Finland, and Italy would need a similarly high vaccine uptake in the population to prevent another severe wave. In the Czech Republic, a much smaller uptake is sufficient. The largest deviations in the necessary vaccine uptake are due to the initial seroprevalence, which we estimate to range from 5% in Finland to 30% in the Czech Republic. In contrast, the differences in age demographics and contact structures only have a minor effect on the dynamics (see also S1 Fig).

If no further measures remain in place to reduce the potential contagious contacts in school settings, the young age group (0–19 years) will drive infections after completing the vaccination program as they remain mostly unvaccinated. The combination of intense contacts and high susceptibility among school-aged children considerably increase the vaccine uptake required in the adult population to restrain a further wave (Fig 5E–5H). High seroprevalence, also in this age group, reduces the severity of this effect for the Czech Republic (Fig 5H).

Discussion

Our results demonstrate that the pace of vaccination first and foremost determines the expected gain in freedom (i.e., lifting of restrictions) during and after completion of the

COVID-19 vaccination programs. Any premature lifting of restrictions risks another wave with high COVID-19 incidence and full ICUs. Moreover, the increase in freedom gained by these premature strategies is only transient because once ICU capacity is reached again, restrictions would have to be reinstated. Simultaneously, these early relaxations significantly increase morbidity and mortality rates, as a fraction of the population has not yet been vaccinated and thus remains susceptible. In contrast, maintaining low case numbers avoids another wave, and *still* allows to lift restrictions steadily and at a similar pace as with high case numbers. Despite this qualitative behavior being general, the precise quantitative results depend on several parameters and assumptions, which we discuss in the following.

The specific time evolution of the lifting of restrictions is dependent on the progress of the vaccination program. Therefore, a steady lifting of restrictions may start in May 2021, when the vaccination rate in the European Union gains speed. However, if the vaccination roll-out stalls more than we assume, the lifting of restrictions has to be delayed proportionally. In such a slowdown, the total number of cases and deaths until the end of the vaccination period increases accordingly. Thus, cautious lifting of restrictions and a fast vaccination delivery is essential to reduce death tolls and promptly increase freedom.

The spreading dynamics after concluding vaccination campaigns (Fig 4B and 4C) will be mainly determined by i) final vaccine uptake, ii) the contact network structure, iii) vaccine effectiveness, and iv) initial seroprevalence. Regarding vaccine uptake, we assumed that after the vaccination of every willing person, no further people would get vaccinated. This assumption enables us to study the effects of each parameter separately. However, vaccination willingness might change over time: it will probably be higher if reported case numbers and deaths are high, and vice versa. This poses a fundamental challenge: If low case numbers are maintained during the vaccine roll-out, the overall uptake might be comparably low, thus leading to a more severe wave once everyone has received a vaccination offer and restrictions are fully lifted. In contrast, a severe wave during vaccine roll-out might either increase vaccine uptake, because of individuals looking to protect themselves, or reduce it, because of damaged credibility on vaccine efficacy among vaccine hesitant groups. Thus, to avoid any further wave, policymakers have to maintain low case numbers *and* foster high vaccine uptake.

Besides vaccine uptake, the population's contact network also determines whether population immunity will be reached. We studied different real-world and theoretical possibilities for the contact matrices in Germany and other EU countries and evaluated how our results depend on the connectivity among age groups. For the long-term success of the vaccination programs, there must be exceptionally sensible planning of measures to prevent contagion among school-aged children. Otherwise, they could become the drivers of a novel wave because they might remain mostly unvaccinated. Provided adequate vaccine uptake among the adult population, our results suggest that reducing either the intensity of contacts or the infectiousness in that age group by half would be sufficient for preventing a rebound wave. This reduction is attainable by implementing soft-distancing measures, plus systematic, preventive random screening with regular COVID-19 rapid tests in school settings or via vaccination [22]. Although at the time of writing some vaccines have been provisionally approved for use in children aged 12–15 years old, vaccine uptake among children remains highly uncertain because of their very low risk for severe illness from COVID-19. We therefore did not include their vaccination in our model.

One of the largest uncertainties regarding the dynamics after vaccine roll-out arises from the efficacies of the vaccines. First, the sterilizing immunity effect (i.e., blocking the transmission of the virus), is still not well quantified and understood [24]. Second, the emergence of new viral variants that at least partially escape immune response is continuously under

investigation [35, 37, 38]. Furthermore, there is no certainty about whether escape variants might produce a more severe course of COVID-19 or whether reinfections with novel variants of SARS-CoV-2 would be milder. Therefore, we cannot conclusively quantify the level of contact reductions necessary in the long term to avoid a further wave of infections or whether such wave would overwhelm ICUs. However, for our default parameters, moderate contact reductions and hygiene measures would be sufficient to prevent further waves.

Although most examples are presented for countries from the European Union, our results can also be generalized to other countries. Differences across countries come from i) demographics, ii) varying seroprevalence—which originated from large differences in the severity of past waves—, iii) vaccines (types, availability, delivery scheme, and uptake), as well as iv) capacities of the health systems, including hospitals and TTI capabilities. For the EU, we find that during the mass vaccination phase, all these differences have only a minor effect on the pace at which restrictions can be lifted (cf. [S1 Fig](#)). However, differences become evident in the long term when most restrictions are lifted by the end of the vaccination campaigns. Demographics and contact patterns are qualitatively very similar across EU countries and thus do not strongly change the expected outcome. On the contrary, we found the initial seroprevalence to significantly determine the minimum vaccine uptake required to guard against further waves after the vaccine roll-out (cf. [Fig 5](#)). Naturally acquired immunity, like vaccinations, contributes to reducing the overall susceptibility of the population and thus impedes viral spread. Notably, naturally acquired immunity can compensate for drops in vaccine uptake in specific age groups unwilling to vaccinate or that cannot access the vaccine, e.g. in children. Furthermore, expected vaccine uptake considerably varies across EU countries (e.g., Serbia 38%, Croatia 41%, France 44%, Italy 70%, Finland 81% [6], Czech Republic 40% [39], Germany 80% [26]). The risk of rebound waves after the mass vaccinations might thus be highly heterogeneous across the EU.

Since we neither know what kind of escape variants might still surface nor their potential impact on vaccine efficacies or viral spread, maintaining low case numbers is the safest strategy for long-term planning. This strategy i) prevents avoidable deaths during vaccine roll-out, ii) offers better preparedness should escape variants emerge, and iii) lowers the risk of further waves because local outbreaks are easier to contain with efficient TTI. Hence, low case numbers only have advantages for health, society, and the economy. Furthermore, a low case number strategy would greatly profit from an EU-wide commitment, and coordination [15]. Otherwise, strict border controls with testing and quarantine policies need to be installed as drastically different case numbers between neighboring countries or regions promote destabilization; infections could (and will) propagate between countries triggering a “ping-pong” effect, especially if restrictions are not jointly planned. Therefore, promoting a high vaccine uptake and low case numbers strategy should not only be a priority for each country but also for the whole European community.

In practice, there are several ways to lower case numbers to the capacity limit of TTI programs without the need to enact stringent NPIs immediately. For example, if restrictions are lifted gradually but marginally slower than the rate vaccination pace would allow, case numbers will still decline. Alternatively, restrictions could be relaxed initially to an intermediate level where case numbers do not grow exponentially while giving people some freedom. In such circumstances one can take advantage of the reduced susceptibility to drive case numbers down without the need of stringent NPIs ([S5\(E\)–S5\(H\) Fig](#)).

To conclude, the opportunity granted by the progressing vaccination should not only be used to lift restrictions carefully but also to bring case numbers down. This will significantly reduce fatalities, allow to lift all major restrictions gradually moving into summer 2021, and guard against newly-emerging variants or potential further waves in the EU.

Methods

Model overview

We model the spreading dynamics of SARS-CoV-2 following a SEIRD-ICU deterministic formalism through a system of delay differential equations. Our model incorporates age-stratified dynamics, ICU stays, and the roll-out of a 2-dose vaccine. For a graphical representation of the infection and core dynamics, see Fig 6. The contagion dynamics include the effect of externally

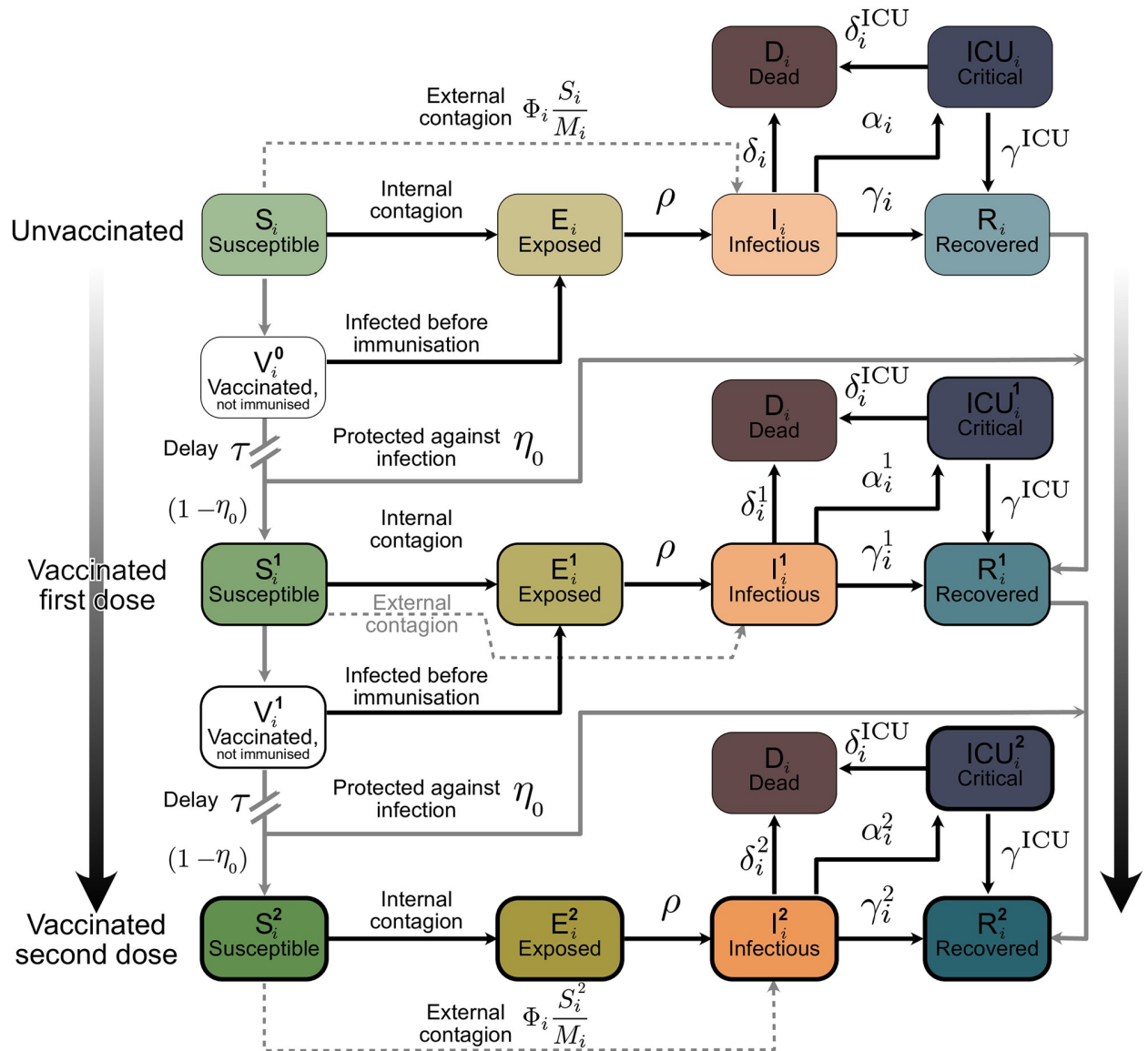


Fig 6. Scheme of our age-stratified SEIRD-ICU+vaccination model. The solid blocks in the diagram represent different SEIRD compartments. Solid black lines represent transition rates of the natural progression of the infection (contagion, latent period, and recovery). On the other hand, dashed lines account for external factors and vaccination. Solid gray lines represent non-linear transfers of individuals between compartments, e.g. through scheduled vaccination. From top to bottom, we describe the progression from unvaccinated to vaccinated, with stronger color and thicker edges indicating more protection from the virus. Subscripts i indicate the age groups, while superscripts represent the number of vaccine doses that have successfully strengthened immune response in individuals receiving them. Contagion can occur internally, where an individual from age group i can get infected from an infected person from any age group, or externally, e.g., abroad on vacation. If the contagion happens externally, we assume that the latent period is already over when the infected returns and, hence, they are immediately put into the infectious compartments I_i^j .

<https://doi.org/10.1371/journal.pcbi.1009288.g006>

acquired infections as a non-zero influx Φ_i based on the formalism previously developed by our group [18, 19]: susceptible individuals of a given age group i (S_i) can acquire the virus from infected individuals from any other age group j and subsequently progress to the exposed ($S_i \rightarrow E_i$) and infectious ($E_i \rightarrow I_i$) compartments. They can also acquire the virus externally. However, in this case, they progress directly to the infectious compartment ($S_i \rightarrow I_i$), i.e., they get infected abroad, and by the time they return, the latent period is already over. Individuals exposed to the virus (E_i) become infectious after the latent period and thus progress from the exposed to the infectious compartments (I_i) at a rate ρ ($E_i \rightarrow I_i$). The infectious compartment has three different possible transitions: i) direct recovery ($I_i \rightarrow R_i$), ii) progression to ICU ($I_i \rightarrow ICU_i$) or iii) direct death ($I_i \rightarrow D_i$). Individuals receiving ICU treatment can either recover ($ICU_i \rightarrow R_i$) or decrease ($ICU_i \rightarrow D_i$).

A contact matrix weights the infection probability between age groups. We investigated three different settings for the contact structure to assess its impact on the spreading dynamics of COVID-19: i) Interactions between age groups are proportional to the group size, i.e., the whole population is mixed perfectly homogeneously, ii) interactions are proportional to pre-COVID contact patterns in the EU population [28], and iii) interactions are proportional to “almost” pre-COVID contact patterns [28], i.e., the contact intensity in the youngest age group (0–19 years) is halved. This accounts for some preventive measures kept in place in schools, e.g., regular rapid testing or smaller class sizes. Scenario iii) is the default scenario unless explicitly stated. However, figures for Scenarios i) and ii) are provided in S9–S14 Figs. We scale all the contact structures by a linear factor, which increases or decreases the stringency of NPIs so that the settings are comparable. However, the scaling above does not account for heterogeneous NPIs acting only on contacts between specific age groups, such as workplace or school restrictions.

Our model includes the effect of vaccination, where vaccines are administered with an age-stratified two-dosage delivery scheme. The scheme does not discriminate on serological status, i.e., recovered individuals with natural antibodies may also access the vaccine when offered to them. Immunization, understood as the development of proper antibodies against SARS-CoV-2, does not occur immediately after receiving the vaccination dose. Thus, newly vaccinated individuals get temporarily put into extra compartments (V_i^0 and V_i^1 for the first and second dose respectively) where, if infected, they would progress through the disease stages as if they would not have received that dose. For modeling purposes, we assume that a sufficient immune response is build up τ days after being vaccinated ($V_i^0 \rightarrow S_i^1$ and $V_i^1 \rightarrow S_i^2$), and that a fraction $p_i(t)$ of those individuals that received the dose acquire the infection before being immunized. Furthermore, there is some evidence that the vaccines partially prevent the infection with and transmission of the disease [40, 41]. Our model incorporates the effectiveness against infection following an ‘all-or-nothing’ scheme, removing a fraction of those vaccinated individuals to the recovered compartments ($V_i^0 \rightarrow R_i^1$ and $V_i^1 \rightarrow R_i^2$), thus assuming that they would not participate in the spreading dynamics. However, we consider those vaccinated individuals with a breakthrough infection have a lower probability of going to ICU or to die than unvaccinated individuals, i.e., effectiveness against severe disease follows a ‘leaky’ scheme. Furthermore, we assume those individuals carry a lower viral load and thus are less infectious by a factor of two [25]. All parameters and values are listed in Table 2.

We model the mean-field interactions between compartments by transition rates, determining the timescales involved. These transition rates can implicitly incorporate both the time course of the disease and the delays inherent to the case-reporting process. In the different scenarios analyzed, we include a non-zero influx Φ_i , i.e., new cases that acquired the virus from outside. Even though this influx makes a complete eradication of SARS-CoV-2 impossible,

Table 2. Model parameters. The range column either describes the range of values used in the various scenarios, or if values depend on the age group (indexed by i), the lowest and highest value across age-groups.

Parameter	Meaning	Value (default)	Range	Units	Source
R_t	Reproduction number (gross)	1.00	0–3.5	—	Assumed
η	Vaccine protection against transmission	0.75	0.5–0.85	—	[24, 40, 41]
κ	Vaccine efficacy (against severe disease)	0.9	0.7–0.95	—	[23, 57]
σ^v	Relative virulence of unvaccinated and vaccinated individuals	[1.0, 0.5, 0.5]	0.5–1	—	[25]
τ	Immunization delay	7	—	days	[24, 31]
v_r	Random vaccination fraction	0.35	—	—	[64, 65]
M_i	Population group size	Table 4	—	people	[43]
u_i	Vaccine uptake	Table 4	—	—	[6]
ρ	Transition rate $E \rightarrow I$	0.25	—	day ⁻¹	[66, 67]
γ_i^v	Recovery rate from I_i^v	Table 5	0.088–0.1	day ⁻¹	[54–56]
γ_i^{ICU}	Recovery rate from ICU ^v	Table 5	0.08–0.2	day ⁻¹	[50, 52, 68]
δ_i^v	Death rate from I_i^v	Table 5	10 ⁻⁶ –0.005	day ⁻¹	[50, 52, 68]
δ_i^{ICU}	Death rate from ICU ^v	Table 5	0.0055–0.083	day ⁻¹	[50, 52, 68]
α_i^v	Transition rate $I \rightarrow \text{ICU}$	Table 5	10 ⁻⁵ –0.007	day ⁻¹	[50, 52, 68]
Φ_i	Infections from external sources	1	—	cases day ⁻¹ per million	Assumed
$p_i(t)$	Fraction of individuals getting infected before acquiring antibodies	—	—	—	Eq (34)
$\bar{\gamma}$	Effective removal rate from infectious compartment	—	—	day ⁻¹	($\gamma_i^v + \alpha_i^v + \delta_i^v$)
$f_i^1(t), f_i^2(t)$	Administered 1 st and 2 nd vaccine doses	—	—	doses/day	Eqs (19) and (20)

<https://doi.org/10.1371/journal.pcbi.1009288.t002>

different outcomes in the spreading dynamics might arise depending on both contact intensity and TTI [18]. Additionally, we include the effects of non-compliance and unwillingness to be vaccinated as well as the effects of the TTI capacities from health authorities, building on [19]. Throughout the manuscript, we do not make explicit differences between symptomatic and asymptomatic infections. However, we implicitly consider asymptomatic infections by accounting for their effect on modifying the reproduction number R_t and all other epidemiological parameters. To assess the lifting of restrictions in light of progressing vaccinations, we use a Proportional-Derivative (PD) control approach to adapt the internal reproduction number R_t targeting controlled case numbers or ICU occupancy.

Model equations

The contributions of the spreading dynamics and the age-stratified vaccination strategies are summarized in the equations below. They govern the infection dynamics between the different age groups, each of which is represented by their susceptible-exposed-infectious-recovered-dead-ICU (SEIRD+ICU) compartments for all three vaccination statuses. We assume a regime that best resembles the situation in Germany at the beginning of March 2021, and we estimate the initial conditions for the different compartments of each age group accordingly. Furthermore, we assume that neither post-infection immunity [42] nor the immunization obtained through the different dosages of the vaccine vanish significantly in the considered time frames. The spreading parameters completely determine the resulting dynamics (characterized by the different age- and dose-dependent parameters, together with the gross reproduction number R_t) and the vaccination logistics.

All of the following parameters and compartments are shortly described in Tables 2 and 3. Some of these are elaborated in more detail in the following sections. Subscripts i in the equations denote the different age groups, while superscripts denote the vaccination status:

Table 3. Model variables. Subscripts i denote the i th age group, superscripts the vaccination status (unvaccinated, immunized by one dose, by two doses).

Variable	Meaning	Units	Explanation
S_i, S_i^1, S_i^2	Susceptible pools	people	Non-infected people that may acquire the virus.
V_i^0, V_i^1	Vaccinated pools	people	Non-infected people that have been vaccinated but have not developed antibodies yet, thus may acquire the virus.
E_i, E_i^1, E_i^2	Exposed pools	people	Infected people in latent period. Cannot spread the virus.
I_i, I_i^1, I_i^2	Infectious pools	people	Currently infectious people.
ICU_i, ICU_i^1, ICU_i^2	ICU pools	people	Infected people receiving ICU treatment, isolated.
D_i, D_i^1, D_i^2	Dead pools	people	Dead people.
R_i, R_i^1, R_i^2	Recovered pools	people	Recovered/immune people that have acquired post-infection or sterilizing vaccination immunity.
\hat{N}^{obs}	Observed new infections	people day ⁻¹	Daily new infections, including reporting delays. Eq (42)
\hat{R}_i^{obs}	Observed reproduction number	-	The reproduction number that can be estimated only from the observed cases: $\hat{R}_i^{obs} = \hat{N}^{obs}(t) / \hat{N}^{obs}(t - 4)$.

<https://doi.org/10.1371/journal.pcbi.1009288.t003>

unvaccinated (⁰ or none), immunized by one dose (¹), or by two doses (²).

$$\frac{dS_i}{dt} = \underbrace{-\bar{\gamma}R_t S_i \sum_{j,v} C_{ji} \frac{\sigma^v I_j^v}{M_j}}_{\text{internal contagion}} - \underbrace{f_i^1(t) \frac{S_i}{S_i + R_i}}_{\text{administering first dose}} - \underbrace{\frac{S_i}{M_i} \Phi_i}_{\text{external contagion}} \tag{1}$$

$$\begin{aligned} \frac{dV_i^0}{dt} = & \underbrace{-\bar{\gamma}R_t V_i^0 \sum_{j,v} C_{ji} \frac{\sigma^v I_j^v}{M_j}}_{\text{internal contagion}} + \underbrace{f_i^1(t) \frac{S_i}{S_i + R_i}}_{\text{administering first dose}} \dots \\ & \dots - \underbrace{f_i^1(t - \tau) \frac{S_i}{S_i + R_i} \Big|_{t-\tau} (1 - p_i(t))}_{\text{first dose showing effect}} - \underbrace{\frac{V_i^0}{M_i} \Phi_i}_{\text{external contagion}} \end{aligned} \tag{2}$$

$$\begin{aligned} \frac{dS_i^1}{dt} = & \underbrace{-\bar{\gamma}R_t S_i^1 \sum_{j,v} C_{ji} \frac{\sigma^v I_j^v}{M_j}}_{\text{internal contagion}} - \underbrace{f_i^2(t) \frac{S_i^1}{S_i^1 + R_i^1}}_{\text{administering second dose}} \dots \\ & \dots + \underbrace{(1 - \eta_0) f_i^1(t - \tau) \frac{S_i}{S_i + R_i} \Big|_{t-\tau} (1 - p_i(t))}_{\text{first dose (not immune)}} - \underbrace{\frac{S_i^1}{M_i} \Phi_i}_{\text{external contagion}} \end{aligned} \tag{3}$$

$$\begin{aligned} \frac{dV_i^1}{dt} = & \underbrace{-\bar{\gamma}R_t V_i^1 \sum_{j,v} C_{ji} \frac{\sigma^v I_j^v}{M_j}}_{\text{internal contagion}} + \underbrace{f_i^2(t) \frac{S_i^1}{S_i^1 + R_i^1}}_{\text{administering second dose}} \dots \\ & \dots - \underbrace{f_i^2(t - \tau) \frac{S_i^1}{S_i^1 + R_i^1} \Big|_{t-\tau} (1 - p_i(t))}_{\text{second dose showing effect}} - \underbrace{\frac{V_i^1}{M_i} \Phi_i}_{\text{external contagion}} \end{aligned} \tag{4}$$

$$\frac{dS_i^2}{dt} = \underbrace{-\bar{\gamma}R_t S_i^2 \sum_{j,v} C_{ji} \frac{\sigma^v I_j^v}{M_j}}_{\text{internal contagion}} + \underbrace{(1 - \eta_0) f_i^2(t - \tau) \frac{S_i^1}{S_i^1 + R_i^1} \Big|_{t-\tau}}_{\text{second dose (not immune)}} (1 - p_i(t)) \cdots \underbrace{\cdots - \frac{S_i^2}{M_i} \Phi_i}_{\text{external contagion}} \tag{5}$$

$$\frac{dE_i}{dt} = \underbrace{\bar{\gamma}R_t (S_i + V_i^0) \sum_{j,v} C_{ji} \frac{\sigma^v I_j^v}{M_j}}_{\text{internal contagion}} - \underbrace{\rho E_i}_{\text{end of latency}} \tag{6}$$

$$\frac{dE_i^1}{dt} = \underbrace{\bar{\gamma}R_t (S_i^1 + V_i^1) \sum_{j,v} C_{ji} \frac{\sigma^v I_j^v}{M_j}}_{\text{internal contagion}} - \underbrace{\rho E_i^1}_{\text{end of latency}} \tag{7}$$

$$\frac{dE_i^2}{dt} = \underbrace{\bar{\gamma}R_t S_i^2 \sum_{j,v} C_{ji} \frac{\sigma^v I_j^v}{M_j}}_{\text{internal contagion}} - \underbrace{\rho E_i^2}_{\text{end of latency}} \tag{8}$$

$$\frac{dI_i}{dt} = \underbrace{\rho E_i}_{\text{end of latency}} - \underbrace{\bar{\gamma}I_i}_{\text{recovery, ICU admission, or death}} + \underbrace{\frac{S_i + V_i^0}{M_i} \Phi_i}_{\text{external contagion}} \tag{9}$$

$$\frac{dI_i^1}{dt} = \underbrace{\rho E_i^1}_{\text{end of latency}} - \underbrace{\bar{\gamma}I_i^1}_{\text{recovery, ICU admission, or death}} + \underbrace{\frac{S_i^1 + V_i^1}{M_i} \Phi_i}_{\text{external contagion}} \tag{10}$$

$$\frac{dI_i^2}{dt} = \underbrace{\rho E_i^2}_{\text{end of latency}} - \underbrace{\bar{\gamma}I_i^2}_{\text{recovery, ICU admission, or death}} + \underbrace{\frac{S_i^2}{M_i} \Phi_i}_{\text{external contagion}} \tag{11}$$

$$\frac{dICU_i^v}{dt} = \underbrace{-(\delta_i^{ICU} + \gamma_i^{ICU})ICU_i^v}_{\text{recovery or death}} + \underbrace{\alpha_i^v I_i^v}_{\text{ICU admission}} \tag{12}$$

$$\frac{dD_i}{dt} = \underbrace{\sum_v (\delta_i^{ICU} ICU_i^v + \delta_i^v I_i^v)}_{\text{total deaths}} \tag{13}$$

$$\frac{dR_i}{dt} = \underbrace{\gamma_i^{ICU} ICU_i + \gamma_i I_i}_{\text{recovery}} - \underbrace{f_i^1(t) \frac{R_i}{S_i + R_i}}_{\text{first dose}} \tag{14}$$

$$\begin{aligned} \frac{dR_i^1}{dt} = & \underbrace{\gamma_i^{\text{ICU}} \text{ICU}_i^1 + \gamma_i^1 I_i^1}_{\text{recovery}} + \underbrace{f_i^1(t) \frac{R_i}{S_i + R_i}}_{\text{first dose after recovery}} - \underbrace{f_i^2(t) \frac{R_i^1}{S_i^1 + R_i^1}}_{\text{second dose}} \dots \\ & \dots + \underbrace{\eta_0 f_i^1(t - \tau) \frac{S_i}{S_i + R_i} \Big|_{t-\tau}}_{\text{first dose (sterilizing immunity)}} (1 - p_i(t)) \end{aligned} \tag{15}$$

$$\begin{aligned} \frac{dR_i^2}{dt} = & \underbrace{\gamma_i^{\text{ICU}} \text{ICU}_i^2 + \gamma_i^2 I_i^2}_{\text{recovery}} + \underbrace{f_i^2(t) \frac{R_i^1}{S_i^1 + R_i^1}}_{\text{second dose after recovery}} \dots \\ & \dots + \underbrace{\eta_0 f_i^2(t - \tau) \frac{S_i^1}{S_i^1 + R_i^1} \Big|_{t-\tau}}_{\text{second dose (sterilizing immunity)}} (1 - p_i(t)) \end{aligned} \tag{16}$$

Contact structure and the effect of NPIs on the contact levels

We model the probability of a susceptible individual from age group i to get infected from an individual from age group j to be proportional to the –effective– incidence in that group ($\sum_v I_j^v \sigma^v$) and the contact intensity between the two groups, given by the entries $(C)_{ij}$ of a contact matrix C scaled with the gross reproduction number R_t . The contact matrices are normalized to force their largest eigenvalue (i.e., their spectral radius) to be 1, so that, when multiplied with R_t , their spectral radius equals R_t . The total contact levels for different levels of NPIs are then just linearly scaled with R_t . We thus neglect any inhomogeneities in the NPIs that might affect contact between specific age groups more than others.

As described previously, we study three different configurations for the contact matrix C : i) a perfectly homogeneously mixed population, ii) pre-COVID structure in the EU population [28], and iii) “almost” pre-COVID contact structure [28], but with reduced potentially-contagious contacts in the youngest age group (0–19 years) accounting for some preventive measures kept in place in schools. If not explicitly stated otherwise, the default contact matrix we use in the main text is always the intermediate “almost” pre-COVID contact structure matrix. For the three scenarios, we analyze the demographics and contact structures in Germany, Finland, the Czech Republic, and Italy as a sample for varying demographics across the EU.

First scenario: Homogeneous contact structure. In this scenario, we consider that everyone has the same probability of meeting anyone from any other age group. The probability of meeting somebody from a given age group is thus proportional to the fraction of this age group within the whole population. Let f be the column vector collecting these fractions, $f_i = \frac{M_i}{M}$, the contact matrix for the n age-groups herein considered $C \in \mathbb{R}^{n \times n}$ is thus given by

$$(C)_{ij} = f_j, \forall j \tag{17}$$

and can be seen in Fig 7A, 7D, 7G and 7J, for the chosen demographics. Note that by this construction the largest eigenvalue of this C (i.e., its spectral radius) is automatically 1 for any demographics, i.e., for any f that fulfills $\sum_j f_j = 1$ (proof in S1 Supplementary Note).

Second scenario: Pre-COVID contact intensity, real-world contact structure. Here, we use the whole contact matrices from before the pandemic reported with one-year age resolution in [28], converted into the age brackets that we chose. We normalize them by their

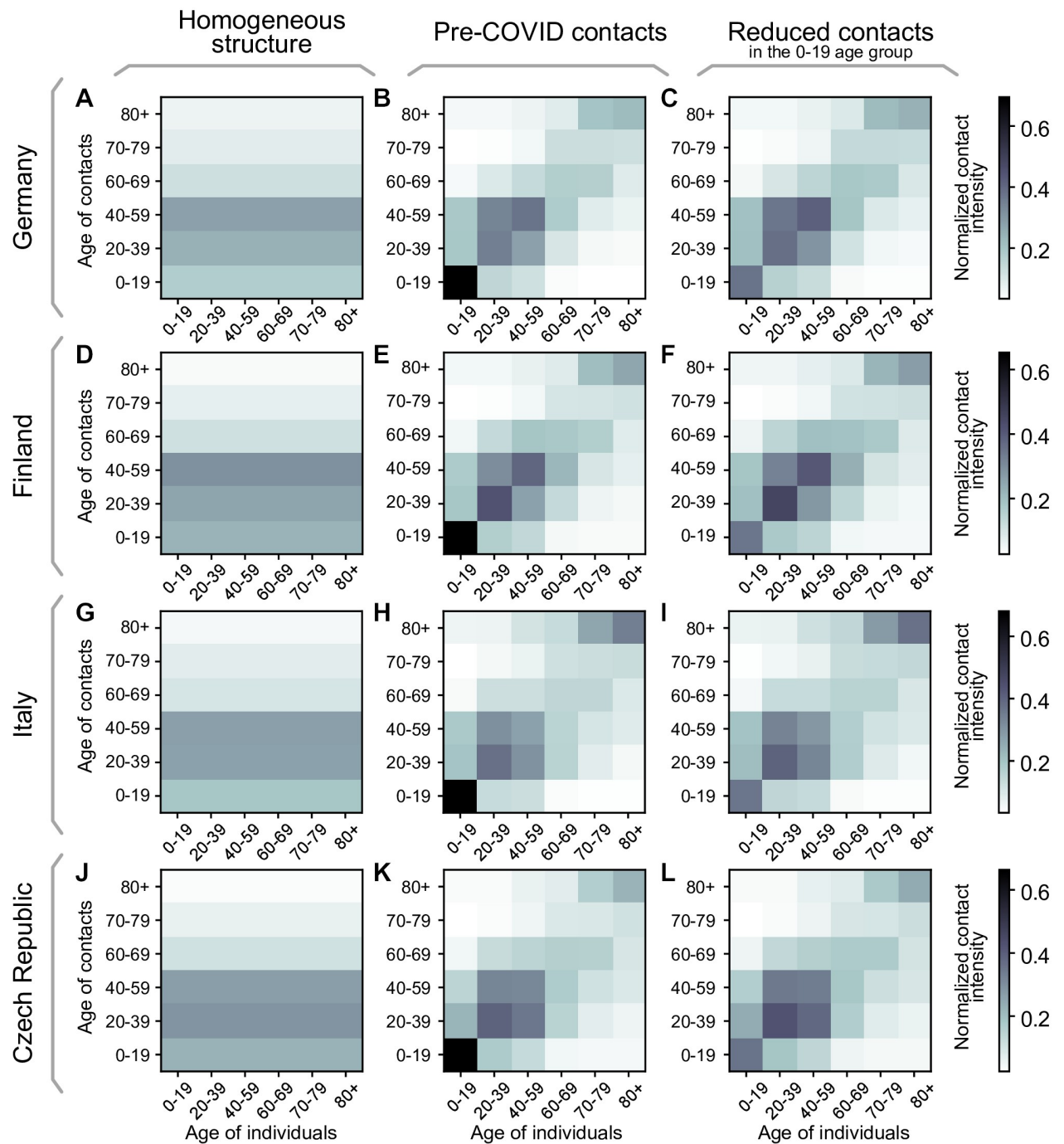


Fig 7. Contact structures for different EU countries in the three scenarios. The chosen contact matrices for i) homogeneous contact structure, ii) pre-COVID contact structure, and iii) “almost” pre-COVID structure with reduced potentially-contagious contacts in schools for Germany (A-C), Finland (D-F), Italy (G-I) and the Czech Republic (J-L). Entries of the matrices show the contact intensity between age groups normalized to give each matrix a spectral radius of 1.

<https://doi.org/10.1371/journal.pcbi.1009288.g007>

spectral radius, leaving their internal contact structure intact. This scenario thus resembles completely homogeneous NPIs that affect every possible contact equally. The matrices are given in Fig Fig 7B, 7E, 7H and 7K for the chosen countries.

Third scenario: “Almost” pre-COVID contact intensity, real-world contact structure.

Finally, we again use the contact matrices from before the pandemic reported in [28] but adapt them to reduce the intensity of contacts of the youngest age group by half, accounting for those measures that remain in place to prevent contagion and mitigate outbreaks in school settings. Specifically, we halve the matrix element connecting the 0–19 age group with itself and normalize the obtained contact matrix C by its spectral radius. As can be seen in the resulting matrices, given in Fig 7C, 7F, 7I and 7L, this affects that the main contributions in the contacts are more evenly spread in the 0–59 year age groups. This serves as a first approximation to the contact structure with inhomogeneous NPIs targeting different age groups differently both in a complete lockdown, as well as some continued measures in schools.

Vaccination dynamics and logistics

In real-world settings, not every person accepts the vaccine when offered. Additionally, vaccine uptake is bounded because some vulnerable groups cannot be vaccinated because of health-related reasons. A systematic survey [26] estimates the vaccine uptake to be approximately 80% across the adult population in Germany, which we choose as our baseline. Due to a higher perception of the risk caused by an infection, we expect that the uptake is higher for elderly population. Thus, we set the uptake u_i to be age-group dependent. Besides the default 80%, we choose two more sets of uptakes averaging to a total of 70% and 90%, respectively. We suppose that an increase in the uptake is possible by education and information measures. They are listed in Table 4. We linearly interpolate between the three values to model arbitrary total vaccine uptakes.

Using official data of the German vaccine stock and stock projections [44, 45] we build up an estimated delivery function w_T that models the weekly number of doses delivered as a function of time. We assume it takes a logistic form, as we assume the number of daily doses increases strongly at the beginning until it reaches a stable level. Adapting the logistic function to the German stock projection (see Fig 8) yields:

$$w_T(\text{week}) = \frac{11 \times 10^6 \text{ doses}}{1 + \exp(-0.17(\text{week} - 21))}, \quad (18)$$

where the parameters were chosen to roughly match past and projected deliveries, taking into account that some delays in the projections might appear because of logistic or manufacturing issues. Since the vaccine deliveries and distributions are done collectively and uniformly in the

Table 4. Parameters for the three main different vaccine uptake scenarios for Germany. The averages are to be understood across the vaccinable (16+) population. Slightly rescaled uptakes for Finnish, Italian and Czech age-demographics can be found in S1, S2 and S3 Tables.

Group ID	age group	eligible fraction	minimal uptake u_i	mid uptake u_i (default)	maximal uptake u_i	population fraction [43] M_i/M
1	0–19	0.2 (16+)	0.58	0.73	0.88	0.18
2	20–39	1.0	0.64	0.76	0.89	0.25
3	40–59	1.0	0.69	0.79	0.90	0.28
4	60–69	1.0	0.74	0.82	0.91	0.13
5	70–79	1.0	0.79	0.86	0.92	0.09
6	>80	1.0	0.85	0.89	0.93	0.07
average	—	—	0.70	0.80	0.90	—

<https://doi.org/10.1371/journal.pcbi.1009288.t004>

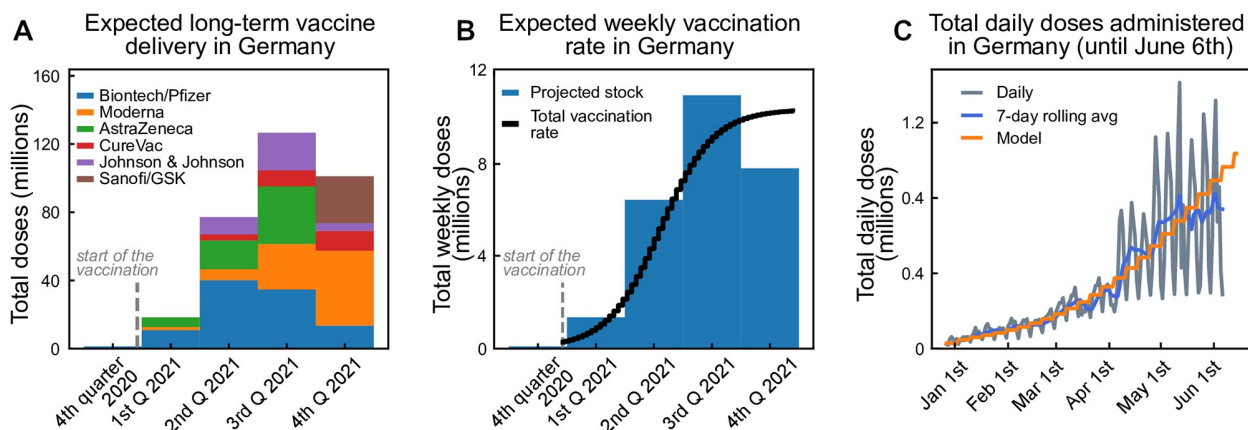


Fig 8. Estimated vaccination rates for Germany. From the announced vaccination stock, we estimate the vaccination delivery function. **A:** Total aggregated doses of different vaccine producers in Germany. **B:** Equivalent amount of 2-dose vaccines available per week in Germany, parameterized using a logistic function. **C:** Comparison between expected and observed vaccination progress in Germany.

<https://doi.org/10.1371/journal.pcbi.1009288.g008>

EU, we scale this German projection by the respective population sizes for the other countries studied herein (Finland, Italy, Czech Republic). We further assume that because of logistic delays, the vaccination of the delivered doses occurs with some delay, which we model as a convolution with an empirical delay kernel given by $K = [0.6, 0.3, 0.1]$ (fraction of vaccines administered in the same, second and third week following delivery). With that, we get the total vaccination rates per week.

These doses are distributed among the age groups, taking into account that each individual requires two doses, spaced by at least four weeks, aware of the potential benefits of further delaying the two doses [46].

The vaccine prioritization order is the following:

1. First, to meet the demand of second doses, τ_{vac} weeks after the first dose.
2. Second, to distribute a fraction ν_r of the remaining doses uniformly among age groups, to model the earlier vaccination of exposed occupations (health sector, first responders, among others).
3. Last, to plan the rest of the doses for the oldest age group that has not been fully vaccinated yet.

Exceptions to rule 3 are the low-risk groups 16–19, 20–39, and 40–59 that get vaccinated simultaneously. For each age group, only a fraction u_i is vaccinated because of limited willingness to get vaccinated (Table 4). In addition, the total number of vaccinations in the youngest age group 0–19 is further reduced since we consider only a fraction of around 20% (fraction of 16–19 year-old individuals in the group) to be *eligible* for vaccination (see Table 4). The uptake u_i in this age group is thus understood only among the eligible individuals.

This procedure results in the number of first $w_i^1(\text{week})$ and second doses $w_i^2(\text{week})$ vaccinated to the age group i as a function of the week. Dividing by 7 we obtain the daily administered first and second doses for age group i

$$f_i^1(t) = w_i^1(\lfloor t/7 \rfloor)/7 \quad \text{and} \quad (19)$$

$$f_i^2(t) = w_i^2(\lfloor t/7 \rfloor)/7. \quad (20)$$

Table 5. Age-dependent parameters.

Age group	ICU admission rate α_i (days ⁻¹)	Death rate in I δ_i (days ⁻¹)	Natural recovery rate γ_i (days ⁻¹)	Death rate in ICU δ_i^{ICU} (days ⁻¹)	ICU recovery rate γ_i^{ICU} (days ⁻¹)	Avg. duration in ICU $T_{\text{res}}^{\text{ICU}}$ (days)
0–19	0.000014	0.000002	0.09998	0.005560	0.194440	5
20–39	0.000204	0.000014	0.09978	0.007780	0.192220	5
40–59	0.001217	0.000111	0.09867	0.006164	0.084745	11
60–69	0.004031	0.000317	0.09565	0.009508	0.081401	11
70–79	0.005435	0.001422	0.09314	0.019756	0.091355	9
>80	0.007163	0.004749	0.08809	0.082433	0.084233	6

<https://doi.org/10.1371/journal.pcbi.1009288.t005>

Age-stratified transition rates

Here, we will introduce the transition rates used in the model equations; details about their estimation are presented in the later sections.

The recovery rate γ_i of a given age group describes the recovery without the need for critical care. It is estimated from the literature. We expect this parameter to vary across age groups, mainly because of the strong correlation between the severity of symptoms and age. Age-resolved recovery rates estimated from data of the non-vaccinated population in Germany are listed in Table 5.

The ICU recovery rate γ_i^{ICU} is the rate of a given age group for leaving ICU care. This parameter varies across age groups, mainly because of the strong correlation between the severity of symptoms, age, and duration of ICU stay. Age-resolved ICU recovery rates estimated from data of the non-vaccinated population in Germany are listed in Table 5.

The ICU admission rate α_i of a given age group describes the transition from the infected compartment to the ICU compartment. It accounts for those cases developing symptoms where intensive care is required and is estimated from the literature. We expect this parameter to vary across age groups, mainly because of the strong correlation between the severity of symptoms and age. Age-resolved ICU-transition rates estimated from data of the non-vaccinated population in Germany are listed in Table 5. Further, we assume that anyone requiring intensive care would have access to ICU beds and care.

The death rate δ_i also varies across age groups, mainly because of the strong correlation between the severity of symptoms and age. This parameter accounts for those individuals dying because of COVID-19, but without being treated in the ICU. In that way, it is expected to be even smaller than the infection fatality ratio (IFR). Age-resolved death rates (outside ICU) estimated from data of the non-vaccinated population in Germany are listed in Table 5.

The death rate in ICU δ_i^{ICU} also varies across age groups, mainly because of the strong correlation between the severity of symptoms and age. In addition, this parameter accounts for those individuals dying because of COVID-19 when being treated in the ICU. In that way, it is expected to be even larger than the case fatality ratio CFR. Age-resolved ICU death rates estimated from data of the non-vaccinated population in Germany are listed in Table 5.

We estimate these age-dependent rates by combining hospitalization data with published IFR data. A comparison of ICU transition rates α_i^v across the EU is difficult as the definition of stationary treatment differs with regard to *hospitalization*, *ICU low* and *high-care*. In order to obtain sensible estimates for these rates, we need to consider the size of the unobserved pool in each age group. Our analysis of ICU transition rates is based on 14043 hospitalization reports collected in Germany between early 2020 and Oct. 26, 2020, as part of the official reporting data [47]. Those reports contain 20-year wide age strata but only represent a small sub-sample of all ICU-admissions ($n = 723$). A complete count of ICU-admissions is maintained by the

Deutsche Interdisziplinäre Vereinigung für Intensiv- und Notfallmedizin [48], without additional patient-data, like age. 19250 ICU admissions were reported throughout the same time frame. We estimated the number of ICU admissions in each 20-year wide age group by combining both sources, matching well with German studies on the first wave [49].

Throughout the first and second wave, the per age-group case-fatality rates (CFRs) in Germany are more than two times larger than the age-specific infection fatality rates (IFRs) estimated by [27, 50]. This difference indicates unobserved infections. Seroprevalence studies from Q3 2020 [51] confirm the existence of unobserved pools. The total number of infections in each age group is inferred from observed deaths assuming the age-specific IFR from [27]. α_i^v (*low-* and *high-care*) is calculated by dividing estimated ICU-admissions in each age group by the estimated total infections in each of those groups. A similar method is applied for the ICU-death-rate δ_i^{ICU} by taking hospitalization-deaths from [47] as a proxy for the age distribution.

The ICU-rates from the 10-year wide age-groups [52] based on French data (*high-care* only) were used to subdivide the 20-year wide age-group 60–79, replicating the French rate-ratio between 60–69 and 70–79 for the German ICU-ratios, while maintaining the German age-agnostic ICU-rate. Noteworthy, there is great variability between the reported ICU rates among different countries, and it seems to be more a problem of reporting criteria rather than differences in virus and host response [53]. Furthermore, as treatments become more effective compared to the first wave, the residence times have decreased in the second wave [30], thus modifying the transition rates.

We also considered the influence of our decision to use the IFR of O’Driscoll et al. [27] instead of Levin et al. [50]. The IFR from Levin et al. is about 50% larger and would lead to a lower level of infections overall in our scenarios, therefore reducing the fraction of natural immunity acquired at the end of the scenarios.

Estimation of general transition rates

After listing all transition rates that we consider in our work, we will now explain how we estimate them. Since we have to start somewhere, let us look at the ICU_i compartment first (see Fig 6 top right). The differential equation, without influx and including the initial condition ICU_0 , is given by

$$\text{ICU}_i' = -\underbrace{\delta_i^{\text{ICU}} \text{ICU}_i}_{\text{to } D_i} - \underbrace{\gamma_i^{\text{ICU}} \text{ICU}_i}_{\text{to } R_i}, \quad \text{ICU}_i(0) = \text{ICU}_0. \quad (21)$$

The solution of this ODE is known to be

$$\text{ICU}_i = \text{ICU}_0 \exp(-(\delta_i^{\text{ICU}} + \gamma_i^{\text{ICU}})t). \quad (22)$$

If we know the average ICU_i residence time $T_{\text{res}}^{\text{ICU}}$, we can obtain an expression for $(\delta_i^{\text{ICU}} + \gamma_i^{\text{ICU}})$:

$$\delta_i^{\text{ICU}} + \gamma_i^{\text{ICU}} = \frac{1}{T_{\text{res}}^{\text{ICU}}}. \quad (23)$$

Further, assuming that a fraction f_δ of those individuals being admitted to ICUs would die, we obtain an expression linking all rates:

$$f_\delta = \frac{\# \text{ people dead by } t = \infty}{\text{people entering ICU}_i \text{ at } t = 0} = \frac{\delta_i^{\text{ICU}} \text{ICU}_0 \int_0^\infty \exp\left(-\frac{t}{T_{\text{res}}^{\text{ICU}}}\right) dt}{\text{ICU}_0} = \delta_i^{\text{ICU}} T_{\text{res}}^{\text{ICU}}. \tag{24}$$

Therefore, the transition rates are given by:

$$\delta_i^{\text{ICU}} = \frac{f_\delta}{T_{\text{res}}^{\text{ICU}}} \quad \text{and} \quad \gamma_i^{\text{ICU}} = \frac{(1-f_\delta)}{T_{\text{res}}^{\text{ICU}}}. \tag{25}$$

Using this modeling approach, we implicitly assume the time scales at which people leave the ICU through recovery or death to be the same, i. e., the average ICU stay duration is independent of the outcome of the course of the disease.

Similarly, we can estimate the infected-to-death rate (δ_i), the infected-to-ICU transition rate (ICU admission rate α_i) and the infected-to-recovered rate (γ_i) based on these fractions and average times. If we assume that all the relevant median times are the same, we obtain the following expressions for the rates:

$$\delta_i = \frac{f_{I \rightarrow D_i}}{T_{\text{res}}^I}, \quad \alpha_i = \frac{f_{\text{ICU}}}{T_{\text{res}}^I}, \quad \gamma_i = \frac{(1 - (f_{I \rightarrow D_i} + f_{\text{ICU}}))}{T_{\text{res}}^I}. \tag{26}$$

As the average residence time in the I compartment is dominated by recoveries we assume $T_{\text{res}}^I = 10$ days [54–56].

Modeling vaccine efficacies

We assume the main effect of vaccinations on the individual to be twofold. A fraction η that has received both vaccine doses will develop total immunity and not contribute to the spreading dynamics. The rest may, in principle, be infected with the virus but still have some protection against a severe course of the illness, resulting in a lower probability of dying or going to ICU. Both effects combined give the total protection against severe infections seen in vaccine studies, which we will denote with κ . For current COVID-19 vaccines, efficacies against severe disease κ ranging from 70–99% [23, 31–33, 57–59] and infection blocking potentials η of 60–90% [24, 41, 60, 61] are reported. The roughly uniform distribution of vaccine types in the European Union (see also Fig 8), consists to a larger part of mRNA-type vaccines for which comparatively high values κ of 97–99% [33, 59] and η of 80–90% are reported. We thus chose the rather conservative 90% for κ and 75% for η as our default values. The explicit κ and η do not explicitly appear in our equations, but as parameters η_0 and κ_0 , which we derive from the reported numbers as follows.

Due to the lack of solid evidence on the effects of the first dose, we assume that the fraction of individuals developing total immunity already after the first dose is given by η_0 . We further assume that of the $(1 - \eta_0)$ people that do not develop the immunity after the first dose, the same fraction η_0 acquires it after the second dose, i. e. the total vaccination path of the people that do not develop total immunity after both doses is given by $S_i \xrightarrow{1-\eta_0} S_i \xrightarrow{1-\eta_0} S_i^2$. η_0 can thus be

related to η by the formula

$$\begin{aligned}\eta &= 1 - \frac{\text{not fully protected}}{\text{total vaccinated}} \\ &= 1 - (1 - \eta_0)^2 = \eta_0(2 - \eta_0).\end{aligned}\quad (27)$$

For individuals vaccinated with both doses without total immunity, i. e., from S_i^2 , we reduce the probabilities to die or go to ICU after infection to account for the reduced risk of severe symptoms due to the vaccine. Of the total number of people who get vaccinated the risk of going to ICU or dying is thus reduced by a factor

$$1 - \kappa = (1 - \eta) \cdot (1 - \kappa_0), \quad (28)$$

from which we can deduce the value of κ_0 .

Again, due to lack of solid data on the first doses we assume the risk of severe COVID-19 is reduced to a factor $\sqrt{1 - \kappa}$ when only a single dose has been received. From these assumptions we arrive at

$$\delta_i^v = (\sqrt{1 - \kappa_0})^v \delta_i, \quad (29)$$

$$\alpha_i^v = (\sqrt{1 - \kappa_0})^v \alpha_i, \quad (30)$$

$$\gamma_i^v + \delta_i^v + \alpha_i^v = \bar{\gamma}, \quad (31)$$

where $v = \{1, 2\}$ represents the dose of the vaccine for which an individual has successfully developed antibodies. Note that v is used as a super-index on the left-hand side of the equation but as an exponent on the right-hand side. Eq 31 enforces vaccination not to alter the total average timescale of the disease course.

The transition rates from ICU to death, δ_i^{ICU} , and from ICU to recovered, γ_i^{ICU} , are assumed to remain equal across doses. The reasons for this assumption are i) a lack of solid evidence for significant differences, and ii) once in ICU, it is reasonable to assume that the vaccine failed to work for this individual.

In addition to the effects of complete sterilizing immunity (η) and protection against severe disease (κ), we include a third effect of vaccines: Individuals that happen to have a breakthrough infection despite being vaccinated carry a lower viral load and are consequently less infectious than unvaccinated infected individuals. This has been shown already after the first dose [25, 60]. We include this effect by a factor σ in the contagion term (cf. (1)).

Individuals becoming infectious while developing antibodies

One special case that one has to consider is when individuals acquire the virus in the time frame between being vaccinated and developing an adequate antibody level. We assume that individuals share behavioral characteristics with the members of the corresponding susceptible compartment, so contagion follows the same dynamics. Let $X_i(s)$ be the fraction of susceptible individuals of a given age group vaccinated at time $s_0 < s$ and are not infected until time s . Assuming they can only leave the compartment by getting infected, the differential equation

governing their dynamics is:

$$\frac{dX_i}{ds} = -R_t X_i \sum_{j,v} C_{ji} \frac{\sigma^v I_j^v}{M_j} - \frac{X_i}{M_i} \Phi_i, \quad \text{with } X_i(s_0) = 1. \tag{32}$$

The solution of (32) is given by

$X_i(s) = \exp\left(-\int_{s_0}^s \sum_{j,v} R_{s'} C_{ji} \frac{\sigma^v I_j^v(s')}{M_j} ds'\right) \exp\left(-\frac{\Phi_i(s-s_0)}{M_i}\right)$. Following the same formalism for every batch of vaccinated individuals produced at time $t - \tau$, the ones that remain susceptible by time t are given by:

$$X_i(t) = \exp\left(-\int_{t-\tau}^t \sum_{j,v} R_{t'} C_{ji} \frac{\sigma^v I_j^v(t')}{M_j} dt'\right) \exp\left(-\frac{\Phi_i \tau}{M_i}\right). \tag{33}$$

Therefore, we define the fraction of susceptible individuals acquiring the virus in the time-frame of antibodies development as

$$p_i(t) = 1 - \exp\left(-\int_{t-\tau}^t \sum_{j,v} R_{t'} C_{ji} \frac{\sigma^v I_j^v(t')}{M_j} dt'\right) \exp\left(-\frac{\Phi_i \tau}{M_i}\right). \tag{34}$$

This fraction is then subtracted in the transitions $V_i^v \rightarrow S_i^{v+1}$ from the vaccinated to the immunized pools in the differential equations.

Effect of test-trace-and-isolate

At low case numbers and moderate contact reduction, the spreading dynamics can be mitigated through test-trace-and-isolate (TTI) policies [18, 19]. In such a regime, individuals can have slightly more contacts because the overall low amount of cases enables a diligent system to trace offspring infections and stop the contagion chains. In other words, efficient TTI would allow for having a larger gross reproduction number R_t without rendering the system unstable. The precise allowed increase in R_t is determined by i) the rate at which symptomatic individuals are tested, ii) the probability of being randomly screened, and iii) the maximum capacity and fraction of contacts that health authorities can manually trace. When the different components of this meta-stable regime break down, we observe a self-accelerating growth in case numbers.

In our age-stratified model, we do not explicitly include TTI, given all the uncertainties that arise from the age-related modifying factors. However, we use our previous results to estimate the gross reproduction number R_t that would produce the same observed reproduction number in the different regimes of i) no test or contact tracing, ii) strict testing criteria, iii) self-reporting, and iv) full TTI. Doing so, we build an empirical relation to evaluating the contextual stringency of the different strategies herein compared (namely, long-term stabilization at high or low case numbers).

In the phase diagram of Fig 9 we illustrate the conversion methodology. Two different R_t might produce the same observed reproduction number \hat{R}_t^{obs} , depending on the regime in which they operate. Fitting all curves to an exponential function, and assuming that the largest eigenvalue of the system (for all possibilities of testing and tracing) can be represented as a

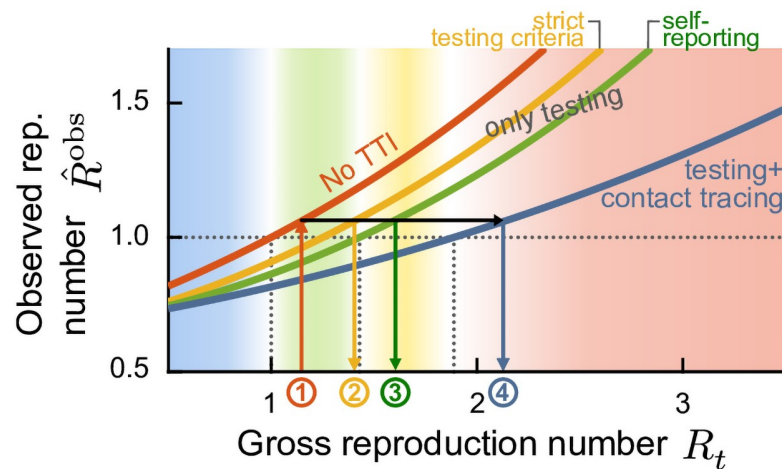


Fig 9. Test-trace-and-isolate (TTI) policies allow for greater freedom (quantified by the gross reproduction number R_t) while observing the same reproduction number \hat{R}_t^{obs} . Systematic efforts to slow down the spread of the disease, such as mass testing (random screening) and contact tracing, allow decreasing the observed reproduction number of the disease. For observing the same outcome in \hat{R}_t^{obs} , the gross reproduction number R_t would increase, or, in other words, individuals would be allowed to increase their potentially contagious contacts. Therefore, we extrapolate the R_t allowed in a full TTI setting at low case numbers and determine the equivalent R_t trends required to reach the same \hat{R}_t^{obs} in different regimes, starting from the raw value considering no TTI (red curve). Assuming that the relationship between R_t and \hat{R}_t^{obs} is exponential (Eq (35)), we can obtain the expected R_t trends in the low-case numbers TTI regime. Starting from the raw R_t curve (red, 1), we can obtain R_t in all the other possible regimes: under strict testing criteria (yellow, 2), self-reporting (green, 3), or full TTI (blue, 4). Adapted from [18].

<https://doi.org/10.1371/journal.pcbi.1009288.g009>

function of the gross reproduction number R_t , we obtain

$$\hat{R}_t^{obs} = a \exp(bR_t). \tag{35}$$

We then want to evaluate how to translate the values we get from our control problem (which has no testing nor tracing) to the equivalent in other regimes. Assuming that all strategies have the same \hat{R}_t^{obs} (as schematized in Fig 9), we can relate their gross reproduction numbers in each regime through a simple equation:

$$R_t^i = \frac{1}{b_i} \left(\ln\left(\frac{a_0}{a_i}\right) + b_0 R_t \right), \tag{36}$$

which corresponds to a line, and where the subscript 0 represents the base scenario (with no testing or contact tracing) and the subscript i represents the other strategies. The exponential fit to the curves shown in Fig 9 gives to the following line equations:

$$R_t^{test(ineff)} = 1.0211R_t + 0.2229, \tag{37}$$

$$R_t^{test(eff)} = 1.0756R_t + 0.3272, \tag{38}$$

$$R_t^{TTI} = 1.6842R_t + 0.1805. \tag{39}$$

Assuming smooth transitions for these conversions in R_t , which are related to certain values of the new daily cases N ($N_{TTI} < N_{test(eff)} < N_{test(ineff)} < N_{no\ test}$ respectively), we can define a

general conversion $R_t(N)$:

$$R_t(N) = \begin{cases} R_t^{\text{TPI}}, & \text{if } N < N_{\text{TPI}} \\ R_t^{\text{test(eff)}} \phi_1 + R_t^{\text{TPI}}(1 - \phi_1), & \text{if } N_{\text{TPI}} \leq N < N_{\text{test(eff)}} \\ R_t^{\text{test(ineff)}} \phi_2 + R_t^{\text{test(eff)}}(1 - \phi_2), & \text{if } N_{\text{test(eff)}} \leq N < N_{\text{test(ineff)}} \\ R_t \phi_3 + R_t^{\text{test(ineff)}}(1 - \phi_3), & \text{if } N_{\text{test(ineff)}} \leq N < N_{\text{no test}} \\ R_t, & \text{else,} \end{cases} \tag{40}$$

where the ϕ parameters of each convex combination depend on N :

$$\begin{aligned} \phi_1 &= \frac{N - N_{\text{TPI}}}{N_{\text{test(eff)}} - N_{\text{TPI}}}, \\ \phi_2 &= \frac{N - N_{\text{test(eff)}}}{N_{\text{test(ineff)}} - N_{\text{test(eff)}}}, \quad \text{and} \\ \phi_3 &= \frac{N - N_{\text{test(ineff)}}}{N_{\text{no test}} - N_{\text{test(ineff)}}}. \end{aligned} \tag{41}$$

Default reference values for the N -related set-points are $N_{\text{TPI}} = 20$, $N_{\text{test(eff)}} = 100$, and $N_{\text{test(ineff)}} = 500$ and $N_{\text{no test}} = 10000$ new daily cases per million. When we plot and refer to the gross reproduction number R_t , it is always the value obtained from Eq (40).

Observed reproduction number

In real-world settings, the full extent of the disease spread can only be observed through testing and contact tracing. While the *true* number of daily infections N is a sum of all new infections, the *observed* number of daily infections \hat{N}^{obs} is the number of new infections discovered by testing, tracing, and surveillance of the quarantined individuals' contacts. Thus, the observed number of daily infections is given by

$$\hat{N}^{\text{obs}}(t) = \underbrace{\left[\sum_{i,v} \rho E_i^v(t) \right]}_{\text{end of latency}} + \underbrace{\sum_{i,v} \frac{S_i^v(t) + V_i^v(t)}{M_i} \Phi_i(t)}_{\text{ext. influx}} \underbrace{\circledast \mathcal{K}(t)}_{\text{delay kernel}} \tag{42}$$

where \circledast denotes a convolution and \mathcal{K} an empirical probability mass function that models a variable reporting delay, inferred from German data. As the Robert-Koch-Institute (RKI), the official body responsible for epidemiological control in Germany [62], reports the date the test is performed, the delay until the appearance in the database can be inferred. The laboratories obtain 50% of the sample results on the next day, 30% the second day, 10% the third day, and further delays complete the remaining 10%, which for simplicity we will truncate at day four. Considering that an extra day is needed for reporting the laboratory results, the probability mass function for days 0 to 5 is given by $\mathcal{K} = [0, 0, 0.5, 0.3, 0.1, 0.1]$.

The spreading dynamics are usually characterized by the observed reproduction number \hat{R}_t^{obs} , an estimator of the effective reproduction number, calculated from the observed number of new cases $\hat{N}^{\text{obs}}(t)$. We use the definition underlying the estimates that are published by the RKI, which defines the reproduction number as the relative change of daily new cases

separated by 4 days (the assumed serial interval of COVID-19 [63])

$$\hat{R}_t^{\text{obs}} = \frac{\hat{N}^{\text{obs}}(t)}{\hat{N}^{\text{obs}}(t-4)}. \quad (43)$$

In contrast to the original definition of \hat{R}_t^{obs} [62], we do not need to remove real-world noise effects by smoothing this ratio. It should be noted that calling \hat{N}^{obs} the observed case numbers is somewhat misleading since we do not model the hidden figure explicitly. However, as this is expected only to change slowly, it is still sufficiently accurate to obtain the observed reproduction number from Eq (43).

Keeping a steady number of daily infections with a PD control approach

With increasing immunity from the progressing vaccination program, keeping the spread of COVID-19 under control will require less and less effort by society. We can use this positive effect to lower the infections by upholding the same NPIs or gradually lifting restrictions to keep daily case numbers or ICU occupancy constant.

We model the optimal lifting of restrictions in the latter strategy using a Proportional Derivative (PD) control approach. The gross reproduction number R_t is changed at every day of the simulation depending on either the daily case numbers \hat{N}^{obs} or the total ICU occupancy $\sum_{i,v} \text{ICU}_i^v$ such that the system is always driven towards a given set point. The change in R_t is negatively proportional to both the difference between the state and the setpoint as well as the change of that difference in time. The former dependence increases the number of infections if the case numbers drift down while the latter punishes rapid increases of the case numbers, keeping the system from overshooting the target value. We omit a dependence on the cumulative error, as is usually done in a PD controller, as that would enforce oscillations around the setpoint and because the PD has proven to be sufficient for our purposes.

Since both the case numbers and the ICU occupancy inherently only react to changes in R_t after a few days of delay, we can further improve the stability of the control by “looking into the future”. The full procedure for every day t of the simulation then follows:

1. Run the system for a time span T using the current R_t .
2. Quantify the relative error $\Delta(t+T)$ of the system state at the end by the difference between the observed case numbers or the total ICU occupancy and the chosen set point divided by said set point.
3. Calculate R_t for the next day according to

$$R_{t+1 \text{ day}} = R_t - \left(k_p \cdot \Delta(t+T) + k_d \cdot \frac{d\Delta}{dt}(t+T) \right),$$

where k_p and k_d denote constant control parameters listed in Table 6.

Table 6. The PD control parameters depending on the objective.

control problem	preview time span T	proportional k_p	derivative k_d
\hat{N}^{obs} (close to set point)	14 days	0.06	3.0
\hat{N}^{obs} (away from set point)	14 days	0.06	1.2
$\sum_{i,v} \text{ICU}_i^v$ (close to set point)	14 days	0.2	15.0
$\sum_{i,v} \text{ICU}_i^v$ (away from set point)	14 days	0.2	7.0

<https://doi.org/10.1371/journal.pcbi.1009288.t006>

4. Revert the system from the state at $t + T$ to $t + 1$ day and start again at 1.

We use the same control system to uphold the setpoint as we use to drive the system towards that state from the initial conditions. In a staged-control-like manner, we make the system more reactive to high slopes near the setpoint, i. e. increase k_d when within 10% of the target. In this way, the system can drive up quickly to the target while preventing overreactions to the gradual immunization changes while hovering at the fixed value.

Scenarios 2–4 in the main text consist of a chain of these control problems, changing from controlled case numbers to controlled ICU occupancy at one of the vaccination milestones (Fig 3).

Parameter choices

For the age stratification of the population and the ICU rates, we used numbers published for Germany (Table 4). We suppose that the quantitative differences to other countries are not so large that the result would differ qualitatively. When comparing ICU rates across countries, one has to bear in mind that the definition of what constitutes an intensive care unit can differ between countries. We chose our ICU limit of 65 per million as a conservative limit so that in Germany, around three-quarters of the capacity would still be available for non-COVID patients. This limit was reached during the second wave in Germany. Other countries in the EU might have fewer remaining beds for non-COVID patients at this limit, as Germany has a comparatively high *per capita* number of ICU beds available.

ICU-related parameters are calculated from 14043 hospitalizations reported by German institutions until October 26, 2020 Table 5, converted to transition rates from Table 1. All other epidemiological parameters, their sources, values, ranges, and units are listed in detail in Table 2.

The vaccine efficacy, as discussed previously, is modeled as a multiplicative factor of the non-vaccinated reference parameter. The dose-dependent multiplicative factor is chosen to be 90% in the default scenario, which is in the range of the 70 to 95% efficacy measured in phase 3 studies [57] of approved vaccines and in accordance with the 92% efficacy of the Pfizer vaccine found in a population study in Israel [23]. In addition, we analyzed different scenarios of vaccine uptake (namely, the overall compliance of people to get vaccinated according to the vaccination plan) because of its relevance to policymakers and different scenarios of the protection the vaccine grants against infections η . The latter has great relevance for assessing risks when evaluating restriction lifting.

Initial conditions

The initial conditions are chosen corresponding to the situation in Germany at the beginning of March 2021. We assume a seroprevalence of 10% because of post-infection immunity across all age groups, i.e., $R_i(0) = 0.1 \cdot M_i \forall i$. The vaccination at the beginning is according to the vaccination schedule introduced before, which leaves 5.1 million doses administered initially and an initial vaccination rate of 168 thousand doses per day. This compares to the 6.2 million total and the around 150 thousand daily administered doses at the time [26]. The initial number of daily new infections is at 200 per million, and the number of individuals treated in ICU is at 30 per million with an age distribution as observed during the first wave in Germany (taken from [47]). From these conditions and the total population sizes of the age groups (Table 4) we infer the initial size of each compartment.

Numerical calculation of solutions

The system of delay differential equations governing our model were numerically solved using a Runge-Kutta 4th order algorithm, implemented in Rust (version 1.48.0). The source code is available on GitHub https://github.com/Prieseemann-Group/covid19_vaccination.

Supporting information

S1 Fig. Sensitivity analysis centered at default parameters (solid black lines), for the fourth scenario from the main text. We vary central parameters of the model individually, while keeping all others at their respective default value. For assessing the sensitivity to the TTI efficacy we scale all the capacity limits N_{TTI} , $N_{test(eff)}$, $N_{test(ineff)}$ and $N_{no\ test}$ (see [Methods](#)) by a common ratio.
(TIF)

S2 Fig. Contact structure can have a significant impact on the population immunity threshold. We assume that infections are kept stable at 250 daily infections until all age groups have been vaccinated. Then most restrictions are lifted, leading to a wave if vaccine uptake has not been high enough (see [Fig 4A](#)). We measure the severity of the wave (quantified by the duration of full ICUs) for varying uptake and vaccine efficacies for different contact structures (see [Fig 7A–7C](#)). **A–C:** The duration of the wave (measured by the duration of full ICUs) depends on the vaccine uptake and on the effectiveness of the vaccine measured by its efficacy at preventing infection (shades of purple) and severe illness (vaccine efficacy, full vs dashed vs dotted). **D–F:** If some NPIs are kept in place (such that the gross reproduction number goes up to $R_t = 2.5$), ICUs would be prevented from overflowing even in some cases of lower vaccine effectiveness. If precautionary measures are dropped in all age groups, including schools (A,D) the required uptake to prevent a further severe wave is increased by about 10% when compared to our default scenario of some continued measures to reduce the potential contagious contacts in school settings (B,E) or to completely homogeneous contacts (C,F). Not all combinations of vaccine effectiveness are possible as the vaccine efficacy against severe illness is by definition larger as the protection against any infection at all.
(TIF)

S3 Fig. EU countries with different demographics have very similar dynamics—But the required vaccine uptake to guard against further severe waves is most sensitive to the initial seroprevalence. Extended version of [Fig 5](#), including more combinations of vaccine efficacies. **A–D:** If releasing all measures to pre-COVID contacts, keeping only some measures aiming to cup the reproduction number at 3.5. **E–H:** If releasing all measures to pre-COVID contacts, keeping only some measures aiming to cup the reproduction number at 3.5 and halving the contagiousness of contacts at school ages.
(TIF)

S4 Fig. Even with the emergence of the highly contagious B.1.1.7 variant vaccinations are a promising mid-term strategy against COVID-19. Staying at low case numbers can greatly increase the individual freedom, especially in the long-term. Schematic outlook into the effects of vaccination and the B.1.1.7 variant of SARS-CoV-2 on the societal freedom in the EU in 2021 compared to 2020 (see also the caption for [Fig 1A](#)). In 2020, seasonality effects and efficient test-trace-and-isolate (TTI) programs at low case numbers allowed for stable case numbers with only mild restrictions during summer, until about September. In 2021, vaccinations are expected to allow for greater freedom, but also a more contagious variant (B.1.1.7) is prevalent across the EU. Efficient TTI at low case numbers would thus help lifting major restrictions

earlier. The exact transition period between the wild type and B.1.1.7 (light purple shaded area) varies regionally.

(TIF)

S5 Fig. Lowering the case numbers without the most stringent restrictions opens a middle ground between freedom and fatalities and prevents a new wave in the long term. A–D:

Variation of the fourth scenario from the main text (see Fig 3), where moderate restrictions are kept in place in the long term (letting the gross reproduction number go up to 2.5, compared to 3.5 in the default scenarios). E–H: Variation of the fifth scenario from the main text (see Fig 2) avoiding the strict initial restrictions. Keeping the gross reproduction number at a moderate level (1.5) until the everyone above 60 has been offered vaccination allows to decrease case numbers steadily. Over the summer a slight gradual increase in the contacts is allowed and all NPIs expect for test-trace-and-isolate (TTI) and enhanced hygiene are lifted when everyone received the vaccination offer (increasing the gross reproduction number to 3.5). I: The variation of the fourth scenario initially allows for the same increase in freedom as all the main scenarios, but needs more restrictions in the long term. The variation of the fifth scenario calls for stricter NPIs in the mid-term, but grants high freedom after summer. J,K: Both proposals lead to low number of infections and fatalities. L: Projected vaccination rates (see Fig 2).

(TIF)

S6 Fig. Long-term control strategies (low vaccine uptake, 70% among the vaccinable population) from main text Figs 2 and 3. Scenarios using default protection against infection $\eta = 0.75$ and low vaccine uptake of 70% among the adult population.

(TIF)

S7 Fig. Long-term control strategies (default vaccine uptake, 80% among the vaccinable population) from main text Figs 2 and 3. Scenarios using default protection against infection $\eta = 0.75$ and default vaccine uptake of 80% among the adult population.

(TIF)

S8 Fig. Long-term control strategies (high vaccine uptake, 90% among the vaccinable population) from main text Figs 2 and 3. Scenarios using default protection against infection $\eta = 0.75$ and high vaccine uptake of 90% among the adult population.

(TIF)

S9 Fig. Mirror of Fig 2, using a homogeneous contact structure.

(TIF)

S10 Fig. Mirror of Fig 3, using a homogeneous contact structure.

(TIF)

S11 Fig. Mirror of S5 Fig, using a homogeneous contact structure.

(TIF)

S12 Fig. Mirror of Fig 2, using an empirical pre-COVID contact structure.

(TIF)

S13 Fig. Mirror of Fig 3, using an empirical pre-COVID contact structure.

(TIF)

S14 Fig. Mirror of S5 Fig, an empirical pre-COVID contact structure.

(TIF)

S1 Table. Parameters for the three main different vaccine uptake scenarios for Finland.

Uptakes and averages are to be understood across the eligible (16+) population. For German data see [Table 2](#) in the main text. Italian and Czech data are to be found in [S2](#) and [S3](#) Tables respectively.

(XLSX)

S2 Table. Parameters for the three main different vaccine uptake scenarios for Italy. The averages are to be understood across the eligible (16+) population. For German data see [Table 2](#) in the main text. Finnish and Czech data are to be found in [S1](#) and [S3](#) Tables respectively.

(XLSX)

S3 Table. Parameters for the three main different vaccine uptake scenarios for the Czech Republic. The averages are to be understood across the eligible (16+) population. For German data see [Table 2](#) in the main text. Finnish and Italian data are to be found in [S3](#) and [S2](#) Tables respectively.

(XLSX)

S1 Supplementary Note. Eigenvalues of the homogeneous contact matrix. Here we demonstrate a general case for the eigenvalues of a homogeneous contact matrix, for which every column accounts for the fraction age-groups represent respect to the total population.

(PDF)

Acknowledgments

We thank the Priesemann group for exciting discussions and for their valuable input. We thank Christian Karagiannidis for fruitful discussions about the age-dependent hospitalization, ICU and fatality rates.

Author Contributions

Conceptualization: Simon Bauer, Sebastian Contreras, Jonas Dehning, Alvaro Olivera-Nappa, Viola Priesemann.

Data curation: Simon Bauer, Matthias Linden.

Formal analysis: Simon Bauer, Sebastian Contreras, Jonas Dehning, Matthias Linden.

Funding acquisition: Viola Priesemann.

Investigation: Simon Bauer, Sebastian Contreras, Emil Iftekhar, Sebastian B. Mohr.

Methodology: Simon Bauer, Sebastian Contreras, Jonas Dehning, Matthias Linden, Viola Priesemann.

Project administration: Viola Priesemann.

Software: Simon Bauer.

Supervision: Viola Priesemann.

Validation: Simon Bauer, Sebastian Contreras, Jonas Dehning, Matthias Linden, Sebastian B. Mohr, Alvaro Olivera-Nappa, Viola Priesemann.

Visualization: Simon Bauer, Sebastian Contreras.

Writing – original draft: Simon Bauer, Sebastian Contreras, Jonas Dehning, Sebastian B. Mohr.

Writing – review & editing: Simon Bauer, Sebastian Contreras, Jonas Dehning, Emil Iftekhar, Sebastian B. Mohr, Alvaro Olivera-Nappa, Viola Priesemann.

References

1. Contreras S, Priesemann V. Risking further COVID-19 waves despite vaccination. *The Lancet Infectious Diseases*. 2021. [https://doi.org/10.1016/S1473-3099\(21\)00167-5](https://doi.org/10.1016/S1473-3099(21)00167-5) PMID: 33743848
2. Foy BH, Wahl B, Mehta K, Shet A, Menon GI, Britto C. Comparing COVID-19 vaccine allocation strategies in India: A mathematical modelling study. *International Journal of Infectious Diseases*. 2021; 103:431–438. <https://doi.org/10.1016/j.ijid.2020.12.075> PMID: 33388436
3. Moore S, Hill EM, Tildesley MJ, Dyson L, Keeling MJ. Vaccination and non-pharmaceutical interventions for COVID-19: a mathematical modelling study. *The Lancet Infectious Diseases*. 2021. [https://doi.org/10.1016/S1473-3099\(21\)00143-2](https://doi.org/10.1016/S1473-3099(21)00143-2) PMID: 33743847
4. Viana J, van Dorp CH, Nunes A, Gomes MC, van Boven M, Kretzschmar ME, et al. Controlling the pandemic during the SARS-CoV-2 vaccination rollout: a modeling study. *Nature communications*. 2021; 12(3674):1–15.
5. Bubar KM, Reinholt K, Kissler SM, Lipsitch M, Cobey S, Grad YH, et al. Model-informed COVID-19 vaccine prioritization strategies by age and serostatus. *Science*. 2021. <https://doi.org/10.1126/science.abe6959> PMID: 33479118
6. Wouters OJ, Shadlen KC, Salcher-Konrad M, Pollard AJ, Larson HJ, Teerawattananon Y, et al. Challenges in ensuring global access to COVID-19 vaccines: production, affordability, allocation, and deployment. *The Lancet*. 2021. [https://doi.org/10.1016/S0140-6736\(21\)00306-8](https://doi.org/10.1016/S0140-6736(21)00306-8) PMID: 33587887
7. Davies NG, Abbott S, Barnard RC, Jarvis CI, Kucharski AJ, Munday JD, et al. Estimated transmissibility and impact of SARS-CoV-2 lineage B.1.1.7 in England. *Science*. 2021. <https://doi.org/10.1126/science.abg3055> PMID: 33658326
8. Plante JA, Mitchell BM, Plante KS, Debbink K, Weaver SC, Menachery VD. The Variant Gambit: COVID's Next Move. *Cell Host & Microbe*. 2021. <https://doi.org/10.1016/j.chom.2021.02.020>
9. Van Egeren D, Novokhodko A, Stoddard M, Tran U, Zetter B, Rogers M, et al. Risk of rapid evolutionary escape from biomedical interventions targeting SARS-CoV-2 spike protein. *PLoS one*. 2021; 16(4): e0250780. <https://doi.org/10.1371/journal.pone.0250780> PMID: 33909660
10. Lavine JS, Bjornstad ON, Antia R. Immunological characteristics govern the transition of COVID-19 to endemicity. *Science*. 2021; 371(6530):741–745. <https://doi.org/10.1126/science.abe6522> PMID: 33436525
11. Petherick A, Goldszmidt RG, Andrade EB, Furst R, Pott A, Wood A. A Worldwide Assessment of COVID-19 Pandemic-Policy Fatigue. Available at SSRN 3774252. 2021.
12. Van Bavel JJ, Baicker K, Boggio PS, Capraro V, Cichocka A, Cikara M, et al. Using social and behavioural science to support COVID-19 pandemic response. *Nature Human Behaviour*. 2020; p. 1–12.
13. Dehning J, Zierenberg J, Spitzner FP, Wibral M, Neto JP, Wilczek M, et al. Inferring change points in the spread of COVID-19 reveals the effectiveness of interventions. *Science*. 2020. <https://doi.org/10.1126/science.abb9789> PMID: 32414780
14. Brauner JM, Mindermann S, Sharma M, Johnston D, Salvatier J, Gavenčičak T, et al. Inferring the effectiveness of government interventions against COVID-19. *Science*. 2020. <https://doi.org/10.1126/science.abd9338> PMID: 33323424
15. Priesemann V, Brinkmann MM, Ciesek S, Cuschieri S, Czypionka T, Giordano G, et al. Calling for pan-European commitment for rapid and sustained reduction in SARS-CoV-2 infections. *The Lancet*. 2020. [https://doi.org/10.1016/S0140-6736\(20\)32625-8](https://doi.org/10.1016/S0140-6736(20)32625-8) PMID: 33347811
16. Dorn F, Khailaie S, Stoeckli M, Binder SC, Lange B, Lautenbacher S, et al. The Common Interests of Health Protection and the Economy: Evidence from Scenario Calculations of COVID-19 Containment Policies. *medRxiv*. 2020; p. 2020.08.14.20175224.
17. Oliu-Barton M, Pradelski BS, Aghion P, Artus P, Kickbusch I, Lazarus JV, et al. SARS-CoV-2 elimination, not mitigation, creates best outcomes for health, the economy, and civil liberties. *The Lancet*. 2021. [https://doi.org/10.1016/S0140-6736\(21\)00978-8](https://doi.org/10.1016/S0140-6736(21)00978-8)
18. Contreras S, Dehning J, Loidolt M, Zierenberg J, Spitzner FP, Urrea-Quintero JH, et al. The challenges of containing SARS-CoV-2 via test-trace-and-isolate. *Nature communications*. 2021; 12(1):1–13. <https://doi.org/10.1038/s41467-020-20699-8> PMID: 33452267
19. Contreras S, Dehning J, Mohr SB, Spitzner FP, Priesemann V. Low case numbers enable long-term stable pandemic control without lockdowns. *medRxiv*. 2020.

20. Kretzschmar ME, Rozhnova G, van Boven M. Isolation and Contact Tracing Can Tip the Scale to Containment of COVID-19 in Populations With Social Distancing. *Frontiers in Physics*. 2021; 8. <https://doi.org/10.3389/fphy.2020.622485>
21. Godara P, Herminghaus S, Heidemann KM. A control theory approach to optimal pandemic mitigation. *PLOS ONE*. 2021; 16(2):1–16. <https://doi.org/10.1371/journal.pone.0247445> PMID: 33606802
22. Sharma M, Mindermann S, Rogers-Smith C, Leech G, Snodin B, Ahuja J, et al. Understanding the effectiveness of government interventions in Europe's second wave of COVID-19. medRxiv. 2021; p. 2021.03.25.21254330.
23. Dagan N, Barda N, Kepten E, Miron O, Perchik S, Katz MA, et al. BNT162b2 mRNA COVID-19 Vaccine in a Nationwide Mass Vaccination Setting. *New England Journal of Medicine*. 2021. <https://doi.org/10.1056/NEJMoa2101765>
24. Levine-Tiefenbrun M, Yelin I, Katz R, Herzal E, Golan Z, Schreiber L, et al. Initial report of decreased SARS-CoV-2 viral load after inoculation with the BNT162b2 vaccine. *Nature medicine*. 2021; 27(5):790–792. <https://doi.org/10.1038/s41591-021-01316-7> PMID: 33782619
25. Harris RJ, Hall JA, Zaidi A, Andrews NJ, Dunbar JK, Dabrera G. Effect of Vaccination on Household Transmission of SARS-CoV-2 in England. *New England Journal of Medicine*. 0;0(0):null.
26. Institute RK. COVID-19 Impfquoten-Monitoring in Deutschland (COVIMO) –1. Report; 2021. https://www.rki.de/DE/Content/InfAZ/N/Neuartiges_Coronavirus/Projekte_RKI/covimo_studie_bericht_1.pdf. Available from: https://www.rki.de/DE/Content/InfAZ/N/Neuartiges_Coronavirus/Projekte_RKI/covimo_studie_bericht_1.pdf?__blob=publicationFile.
27. O'Driscoll M, Ribeiro Dos Santos G, Wang L, Cummings DAT, Azman AS, Paireau J, et al. Age-specific mortality and immunity patterns of SARS-CoV-2. *Nature*. 2021; 590(7844):140–145. <https://doi.org/10.1038/s41586-020-2918-0> PMID: 33137809
28. Mistry D, Litvinova M, y Piontti AP, Chinazzi M, Fumanelli L, Gomes MF, et al. Inferring high-resolution human mixing patterns for disease modeling. *Nature communications*. 2021; 12(1):1–12. <https://doi.org/10.1038/s41467-020-20544-y> PMID: 33436609
29. RKI. Corona-Monitoring bundesweit (RKI-SOEP-Studie): Überblick zu ersten Ergebnissen; 2021. <https://www.rki.de/DE/Content/Gesundheitsmonitoring/Studien/lid/Ergebnisse.html?nn=14830934>. Available from: <https://www.rki.de/DE/Content/Gesundheitsmonitoring/Studien/lid/Ergebnisse.html?nn=14830934>.
30. Karagiannidis C, Windisch W, McAuley DF, Welte T, Busse R. Major differences in ICU admissions during the first and second COVID-19 wave in Germany. *The Lancet Respiratory Medicine*. 2021. [https://doi.org/10.1016/S2213-2600\(21\)00101-6](https://doi.org/10.1016/S2213-2600(21)00101-6) PMID: 33684356
31. Polack FP, Thomas SJ, Kitchin N, Absalon J, Gurtman A, Lockhart S, et al. Safety and Efficacy of the BNT162b2 mRNA COVID-19 Vaccine. *New England Journal of Medicine*. 2020; 383(27):2603–2615. <https://doi.org/10.1056/NEJMoa2034577> PMID: 33301246
32. Voysey M, Clemens SAC, Madhi SA, Weckx LY, Folegatti PM, Aley PK, et al. Safety and efficacy of the ChAdOx1 nCoV-19 vaccine (AZD1222) against SARS-CoV-2: an interim analysis of four randomised controlled trials in Brazil, South Africa, and the UK. *The Lancet*. 2021; 397(10269):99–111. [https://doi.org/10.1016/S0140-6736\(20\)32661-1](https://doi.org/10.1016/S0140-6736(20)32661-1) PMID: 33306989
33. Ministry of Health I. Effectiveness Data of the COVID-19 Vaccine Collected in Israel until 13.2.2021; <https://www.gov.il/en/departments/news/20022021-01>.
34. Petter E, Mor O, Zuckerman N, Oz-Levi D, Younger A, Aran D, et al. Initial real world evidence for lower viral load of individuals who have been vaccinated by BNT162b2. medRxiv. 2021.
35. Altmann DM, Boyton RJ, Beale R. Immunity to SARS-CoV-2 variants of concern. *Science*. 2021; 371(6534):1103–1104. <https://doi.org/10.1126/science.abg7404> PMID: 33707254
36. Wang P, Nair MS, Liu L, Iketani S, Luo Y, Guo Y, et al. Antibody resistance of SARS-CoV-2 variants B. 1.351 and B. 1.1. 7. *Nature*. 2021; p. 1–6.
37. Garcia-Beltran WF, Lam EC, St Denis K, Nitido AD, Garcia ZH, Hauser BM, et al. Multiple SARS-CoV-2 variants escape neutralization by vaccine-induced humoral immunity. *Cell*. 2021. <https://doi.org/10.1016/j.cell.2021.03.013>
38. Tarke A, Sidney J, Methot N, Yu ED, Zhang Y, Dan JM, et al. Impact of SARS-CoV-2 variants on the total CD4+ and CD8+ T cell reactivity in infected or vaccinated individuals. *Cell Reports Medicine*. 2021; p. 100355. <https://doi.org/10.1016/j.xcrm.2021.100355> PMID: 34230917
39. Hutt D. Why are Czechs among Europe's most sceptical over taking vaccines?; 2021. Available from: <https://www.euronews.com/2021/01/06/coronavirus-why-are-czechs-among-europe-s-most-sceptical-when-it-comes-to-vaccines>.
40. Mallapaty S. Can COVID vaccines stop transmission? Scientists race to find answers. *Nature*. 2021. PMID: 33608683

41. Hall VJ, Foulkes S, Saei A, Andrews N, Oguti B, Charlett A, et al. Effectiveness of BNT162b2 mRNA Vaccine Against Infection and COVID-19 Vaccine Coverage in Healthcare Workers in England, Multi-centre Prospective Cohort Study (the SIREN Study). Rochester, NY: Social Science Research Network; 2021. ID 3790399. Available from: <https://papers.ssrn.com/abstract=3790399>.
42. Dan JM, Mateus J, Kato Y, Hastie KM, Yu ED, Faliti CE, et al. Immunological memory to SARS-CoV-2 assessed for up to 8 months after infection. *Science*. 2021; 371 (6529). <https://doi.org/10.1126/science.abf4063> PMID: 33408181
43. DESTATIS. 14. koordinierte Bevölkerungsvorausberechnung für Deutschland (Coordinated Population Projection for Germany); 2019. <https://service.destatis.de/bevoelkerungspyramide/#!a=70,80&l=en&g>. Available from: <https://service.destatis.de/bevoelkerungspyramide/#!a=70,80&l=en&g>.
44. RKI. Digitales Impfquotenmonitoring zur COVID-19-Impfung; 2021. https://www.rki.de/DE/Content/InfAZ/N/Neuartiges_Coronavirus/Daten/Impfquoten-Tab.html. Available from: https://www.rki.de/DE/Content/InfAZ/N/Neuartiges_Coronavirus/Daten/Impfquoten-Tab.html.
45. Der Spiegel. Impfstoff für 50 Millionen bis Ende Juni; 2021. Available from: <https://www.spiegel.de/wirtschaft/soziales/corona-impfstoff-lieferungen-an-deutschland-vakzine-fuer-50-millionen-bis-ende-juni-a-c5a61e87-be51-4b79-8fd9-3be6d4201bee>.
46. Maier BF, Burdinski A, Rose AH, Schlosser F, Hinrichs D, Betsch C, et al. Potential benefits of delaying the second mRNA COVID-19 vaccine dose; 2021.
47. Schilling J, Lehfeld A, Schumacher D, Ullrich A, Diercke M, et al. Krankheitsschwere der ersten COVID-19-Welle in Deutschland basierend auf den Meldungen gemäß Infektionsschutzgesetz. *Journal of Health Monitoring*. 2020; 5(S11):2–20.
48. Intensivregister-Team am RKI IT. Tagesreport aus dem DIVI-Intensivregister; 2020. <https://doi.org/10.25646/7625>.
49. Karagiannidis C, Mostert C, Hentschker C, Voshaar T, Malzahn J, Schillinger G, et al. Case characteristics, resource use, and outcomes of 10 021 patients with COVID-19 admitted to 920 German hospitals: an observational study. *The Lancet Respiratory Medicine*. 2020; 8(9):853–862. [https://doi.org/10.1016/S2213-2600\(20\)30316-7](https://doi.org/10.1016/S2213-2600(20)30316-7) PMID: 32735842
50. Levin AT, Hanage WP, Owusu-Boaitey N, Cochran KB, Walsh SP, Meyerowitz-Katz G. Assessing the age specificity of infection fatality rates for COVID-19: systematic review, meta-analysis, and public policy implications. *European Journal of Epidemiology*. 2020. <https://doi.org/10.1007/s10654-020-00698-1> PMID: 33289900
51. Santos-Hövenner C, Busch MA, Koschollek C, Schlaud M, Hoebel J, Hoffmann R, et al. Seroepidemiological study on the spread of SARS-CoV-2 in populations in especially affected areas in Germany—Study protocol of the CORONA-MONITORING lokal study. *Journal of Health*. 2020.
52. Salje H, Kiem CT, Lefrancq N, Courtejoie N, Bosetti P, Paireau J, et al. Estimating the burden of SARS-CoV-2 in France. *Science*. 2020; 369(6500):208–211. <https://doi.org/10.1126/science.abc3517> PMID: 32404476
53. Millar JE, Busse R, Fraser JF, Karagiannidis C, McAuley DF. Apples and oranges: international comparisons of COVID-19 observational studies in ICUs. *The Lancet Respiratory Medicine*. 2020; 8(10):952–953. [https://doi.org/10.1016/S2213-2600\(20\)30368-4](https://doi.org/10.1016/S2213-2600(20)30368-4) PMID: 32835653
54. He X, Lau EHY, Wu P, Deng X, Wang J, Hao X, et al. Temporal dynamics in viral shedding and transmissibility of COVID-19. *Nature Medicine*. 2020; p. 1–4.
55. Pan F, Ye T, Sun P, Gui S, Liang B, Li L, et al. Time course of lung changes on chest CT during recovery from 2019 novel coronavirus (COVID-19) pneumonia. *Radiology*. 2020; p. 200370.
56. Ling Y, Xu SB, Lin YX, Tian D, Zhu ZQ, Dai FH, et al. Persistence and clearance of viral RNA in 2019 novel coronavirus disease rehabilitation patients. *Chinese medical journal*. 2020. <https://doi.org/10.1097/CM9.0000000000000774> PMID: 32118639
57. Mahase E. Covid-19: Where are we on vaccines and variants? *BMJ*. 2021; 372:n597. <https://doi.org/10.1136/bmj.n597> PMID: 33653708
58. Bernal JL, Andrews N, Gower C, Robertson C, Stowe J, Tessier E, et al. Effectiveness of the Pfizer-BioNTech and Oxford-AstraZeneca vaccines on covid-19 related symptoms, hospital admissions, and mortality in older adults in England: test negative case-control study. *bmj*. 2021; 373.
59. Haas EJ, Angulo FJ, McLaughlin JM, Anis E, Singer SR, et al K F. Impact and effectiveness of mRNA BNT162b2 vaccine against SARS-CoV-2 infections and COVID-19 cases, hospitalisations, and deaths following a nationwide vaccination campaign in Israel: an observational study using national surveillance data. *The Lancet*. 2021; 397(10287):1819–1829. [https://doi.org/10.1016/S0140-6736\(21\)00947-8](https://doi.org/10.1016/S0140-6736(21)00947-8) PMID: 33964222
60. Pritchard E, Matthews P, Stoesser N, et al. Impact of vaccination on new SARS-CoV-2 infections in the United Kingdom. *Nature Medicine*. 2021; p. 1546–170X. PMID: 34108716

61. Thompson MG, Burgess JL, Naleway AL, Tyner HL, Yoon SK, Meece J, et al. Interim estimates of vaccine effectiveness of BNT162b2 and mRNA-1273 COVID-19 vaccines in preventing SARS-CoV-2 infection among health care personnel, first responders, and other essential and frontline workers—eight US locations, December 2020–March 2021. *Morbidity and Mortality Weekly Report*. 2021; 70(13):495. <https://doi.org/10.15585/mmwr.mm7013e3> PMID: 33793460
62. an der Heiden M, Hamouda O. Schätzung der aktuellen Entwicklung der SARS-CoV-2- Epidemie in Deutschland—Nowcasting. *Epidemiologisches Bulletin*. 2020; 2020(17):10–15.
63. Lauer SA, Grantz KH, Bi Q, Jones FK, Zheng Q, Meredith HR, et al. The incubation period of coronavirus disease 2019 (COVID-19) from publicly reported confirmed cases: estimation and application. *Annals of internal medicine*. 2020. <https://doi.org/10.7326/M20-0504> PMID: 32150748
64. Bundesministerium für Gesundheit BAnz, Verordnung zum Anspruch auf Schutzimpfung gegen das Coronavirus SARS-CoV-2 (Coronavirus-Impfverordnung – CoronImpfV); 2021. Available from: <https://www.bundesregierung.de/resource/blob/975226/1851894/e195f7a8ee3e463e5947c8254b6be1d5/2021-02-08-impfverordnung-neu-data.pdf?download=1>.
65. Robert-Koch-Institut. Mitteilung der Ständigen Impfkommission am Robert-Koch-Institut. Beschluss der STIKO zur 2. Aktualisierung der COVID-19-Impfempfehlung und die dazugehörige wissenschaftliche Begründung; 2021. https://www.rki.de/DE/Content/Infekt/EpidBull/Archiv/2021/Ausgaben/05_21.pdf. Available from: https://www.rki.de/DE/Content/Infekt/EpidBull/Archiv/2021/Ausgaben/05_21.pdf?__blob=publicationFile.
66. Bar-On YM, Flamholz A, Phillips R, Milo R. Science Forum: SARS-CoV-2 (COVID-19) by the numbers. *Elife*. 2020; 9:e57309. <https://doi.org/10.7554/eLife.57309> PMID: 32228860
67. Li R, Pei S, Chen B, Song Y, Zhang T, Yang W, et al. Substantial undocumented infection facilitates the rapid dissemination of novel coronavirus (SARS-CoV-2). *Science*. 2020; 368(6490):489–493. <https://doi.org/10.1126/science.abb3221> PMID: 32179701
68. Linden M, Mohr SB, Dehning J, Mohring J, Meyer-Hermann M, Pigeot I, et al. Case numbers beyond contact tracing capacity are endangering the containment of COVID-19. *Dtsch Arztebl International*. 2020; 117(46):790–791. <https://doi.org/10.3238/arztebl.2020.0790> PMID: 33533714

INTERPLAY BETWEEN RISK PERCEPTION,
BEHAVIOR, AND COVID-19 SPREAD[†]

ABSTRACT

Pharmaceutical and non-pharmaceutical interventions (NPIs) have been crucial for controlling COVID-19. They are complemented by voluntary health-protective behavior, building a complex interplay between risk perception, behavior, and disease spread. We studied how voluntary health-protective behavior and vaccination willingness impact the long-term dynamics. We analyzed how different levels of mandatory NPIs determine how individuals use their leeway for voluntary actions. If mandatory NPIs are too weak, COVID-19 incidence will surge, implying high morbidity and mortality before individuals react; if they are too strong, one expects a rebound wave once restrictions are lifted, challenging the transition to endemicity. Conversely, moderate mandatory NPIs give individuals time and room to adapt their level of caution, mitigating disease spread effectively. When complemented with high vaccination rates, this also offers a robust way to limit the impacts of the Omicron variant of concern. Altogether, our work highlights the importance of appropriate mandatory NPIs to maximise the impact of individual voluntary actions in pandemic control.

[†] This chapter is identical to the publication [28]: Dönges, P., Wagner, J., Contreras, S., Iftexhar, E.N., Bauer, S., Mohr, S.B., Dehning, J., Calero Valdez, A., Kretzschmar, M., Mäs, M. and Nagel, K., Priesemann, V. 2022. Interplay between risk perception, behavior, and COVID-19 spread. *Frontiers in Physics*, 10. The article is published under the terms of a Creative Common License (<http://creativecommons.org/licenses/by/4.0/>). To this publication, I contributed equally with P. Dönges, J. Wagner, and E. N. Iftexhar. Roles: Conceptualization, Formal analysis, Investigation, Methodology, Visualization, Writing – original draft, Writing – review & editing, Supervision.

Cite as: Dönges, P., Wagner, J., Contreras, S., Iftexhar, E.N., Bauer, S., Mohr, S.B., Dehning, J., Calero Valdez, A., Kretzschmar, M., Mäs, M. and Nagel, K., Priesemann, V. 2022. Interplay between risk perception, behavior, and COVID-19 spread. Frontiers in Physics, 10. <https://doi.org/10.3389/fphy.2022.842180>



Interplay Between Risk Perception, Behavior, and COVID-19 Spread

Philipp Dönges^{1†}, Joel Wagner^{1†}, Sebastian Contreras^{1,2†}, Emil N. Iftekhhar^{1†}, Simon Bauer¹, Sebastian B. Mohr¹, Jonas Dehning¹, André Calero Valdez³, Mirjam Kretzschmar⁴, Michael Mäs⁵, Kai Nagel⁶ and Viola Priesemann^{1,7*}

¹Max Planck Institute for Dynamics and Self-Organization, Göttingen, Germany, ²Centre for Biotechnology and Bioengineering, Universidad de Chile, Santiago, Chile, ³Chair of Communication Science, RWTH Aachen University, Aachen, Germany, ⁴University Medical Center Utrecht, Utrecht University, Utrecht, Netherlands, ⁵Department of Sociology, Karlsruhe Institute of Technology, Karlsruhe, Germany, ⁶Chair of Transport Systems Planning and Transport Telematics, Technische Universität Berlin, Berlin, Germany, ⁷Institute for the Dynamics of Complex Systems, University of Göttingen, Göttingen, Germany

Pharmaceutical and non-pharmaceutical interventions (NPIs) have been crucial for controlling COVID-19. They are complemented by voluntary health-protective behavior, building a complex interplay between risk perception, behavior, and disease spread. We studied how voluntary health-protective behavior and vaccination willingness impact the long-term dynamics. We analyzed how different levels of mandatory NPIs determine how individuals use their leeway for voluntary actions. If mandatory NPIs are too weak, COVID-19 incidence will surge, implying high morbidity and mortality before individuals react; if they are too strong, one expects a rebound wave once restrictions are lifted, challenging the transition to endemicity. Conversely, moderate mandatory NPIs give individuals time and room to adapt their level of caution, mitigating disease spread effectively. When complemented with high vaccination rates, this also offers a robust way to limit the impacts of the Omicron variant of concern. Altogether, our work highlights the importance of appropriate mandatory NPIs to maximise the impact of individual voluntary actions in pandemic control.

Keywords: COVID-19, disease modeling, infodemic, human behavior, self-regulation, vaccine hesitancy, health policy and practice, Omicron variant (SARS-CoV-2)

OPEN ACCESS

Edited by:

Matjaž Perc,
University of Maribor, Slovenia

Reviewed by:

Gui-Quan Sun,
North University of China, China
Bosiljka Tadic,
Institut Jožef Stefan (IJS), Slovenia

*Correspondence:

Viola Priesemann
viola.priesemann@ds.mpg.de

[†]These authors have contributed
equally to this work

Specialty section:

This article was submitted to
Social Physics,
a section of the journal
Frontiers in Physics

Received: 23 December 2021

Accepted: 20 January 2022

Published: 15 February 2022

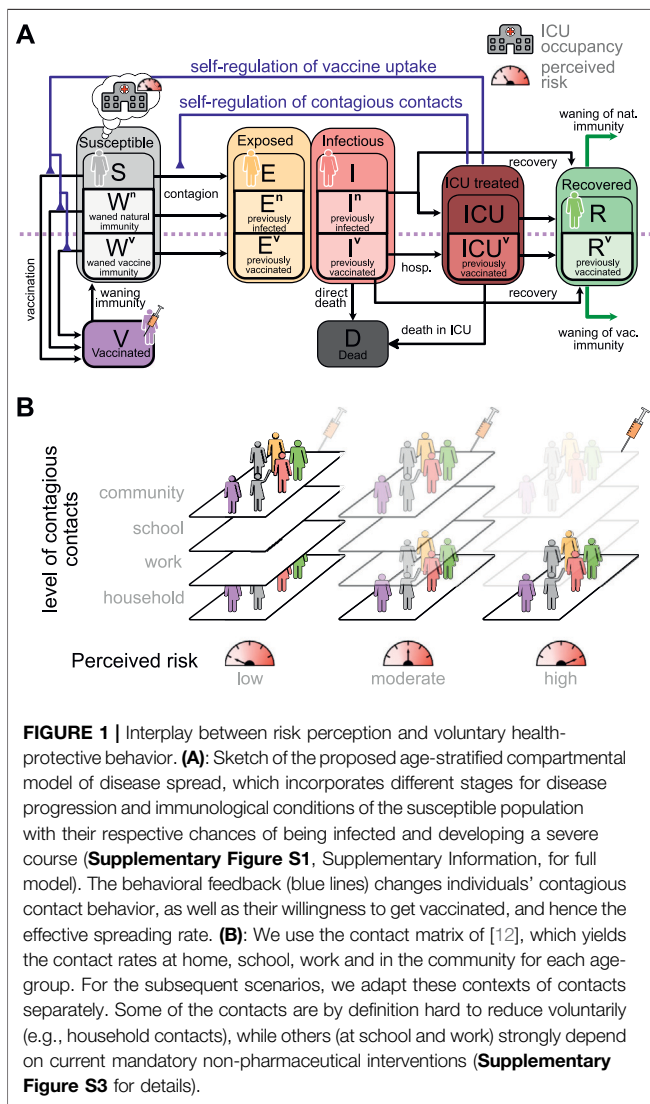
Citation:

Dönges P, Wagner J, Contreras S,
Iftekhhar EN, Bauer S, Mohr SB,
Dehning J, Calero Valdez A,
Kretzschmar M, Mäs M, Nagel K and
Priesemann V (2022) Interplay
Between Risk Perception, Behavior,
and COVID-19 Spread.
Front. Phys. 10:842180.
doi: 10.3389/fphy.2022.842180

1 INTRODUCTION

During the COVID-19 pandemic, the virus has played a central role in people's day-to-day conversations and the information they search for and consume [1]. The growing amount of news and specialized literature on COVID-19 can inform individual decisions in a wide range of situations and on various timescales [2]. For example, people decide multiple times every day how closely they follow mask-wearing regulations or meeting restrictions. However, if hesitant, they might take weeks or months to decide whether to accept a vaccine. These decisions impact the spreading dynamics of COVID-19 and ultimately determine the effectiveness of interventions and how smoothly we transit to SARS-CoV-2 endemicity.

While typical models of disease spread consider that individual behavior affects the spreading dynamics of an infectious disease, they often neglect that there is also a relation in the opposite causal direction. This feedback loop comprises that, e.g., mass media regularly updates individuals on the latest local developments of the pandemic, such as the current occupancy of intensive care units (ICUs). This information affects individuals' opinions and risk perceptions and, thus ultimately their actions [3]. For example, given high perceived risk, individuals reduce their non-essential contacts



beyond existing regulations and increase their willingness to accept vaccine offers accordingly, an effect observed in empirical research conducted with routine surveys in Germany [4] and other parts of the world [5–8]. However, to quantify the effect of individual voluntary actions on the dynamics of COVID-19, two questions remain open: 1) What is the relationship between risk perception and voluntary action, on the one hand, and the spread of the disease, on the other hand; and 2) what is the relative contribution of voluntary action when mandatory restrictions are in place?

In this work, we aim to quantify the impact of voluntary actions on disease spread while studying the questions mentioned above for the COVID-19 pandemic. 1) We analyze survey and COVID-19 vaccination data in European countries to uncover the relationship between the occupancy of ICUs—which determines the perceived risk—and voluntary immediate health-protective behavior as well as the willingness to get vaccinated. We then incorporate these effective feedback loops into a deterministic compartmental model (Figure 1A). 2) We

decompose the overall contact structure into contextual contacts (Figure 1B) and for each context define a range in which voluntary action can be adapted according to individual risk-perception, given the level of mandatory non-pharmaceutical interventions (NPIs). To that end, we use the functional form identified in 1) (Figure 2). We explore different intervention scenarios in the face of adverse seasonality [9–11], using as reference the winter 2021/2022 in central Europe. Our analysis confirms that both extremes (“freedom day” or stringent measures throughout) bear large harms in the long run. However, when measures leave space for voluntary actions, people’s adaptive behavior can efficiently contribute to breaking the wave and change the course of the pandemic.

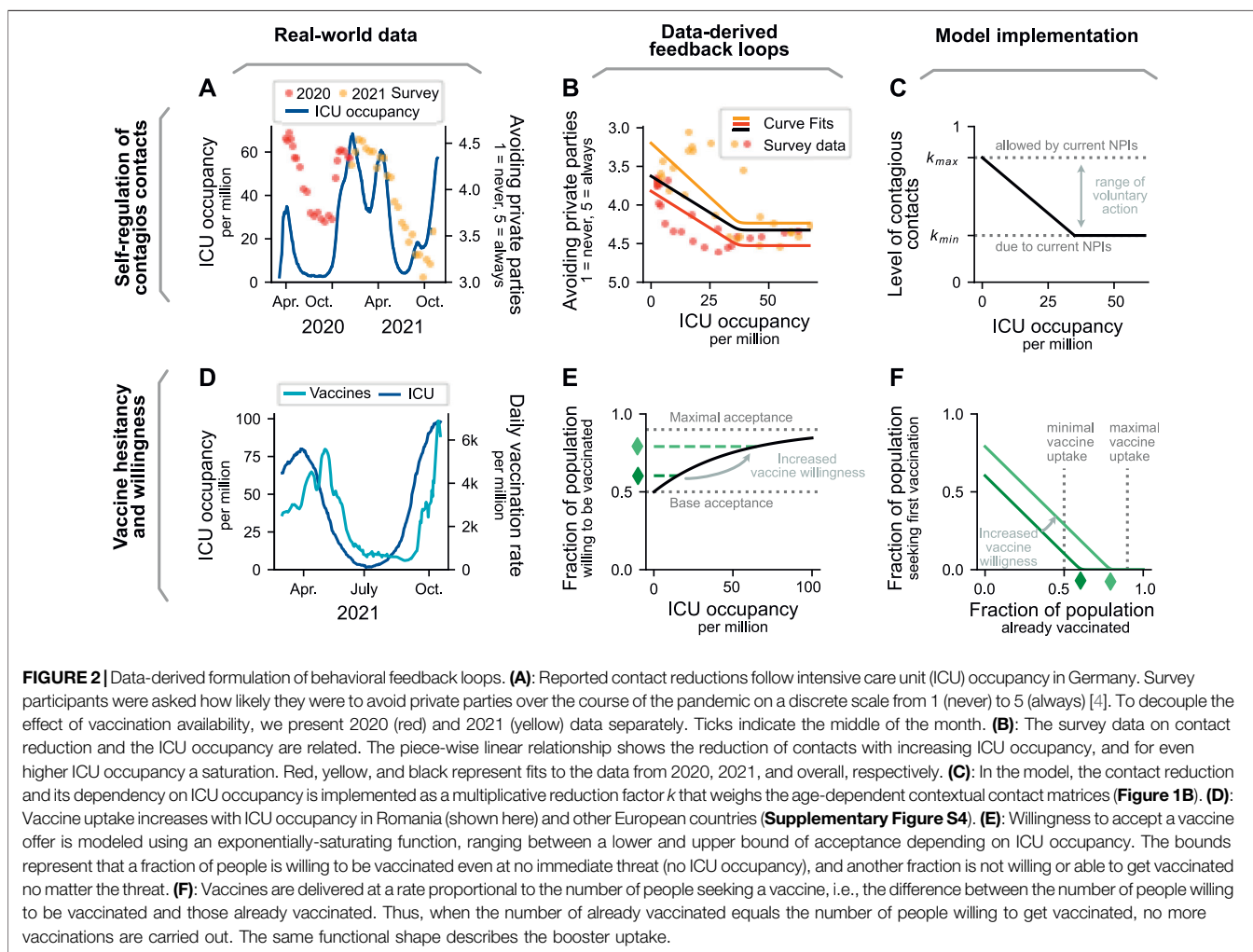
2 RESULTS

2.1 Data-Derived Behavioral Feedback Loops

Throughout this manuscript, we investigate how the interplay between information about the COVID-19 pandemic and its spreading dynamics is mediated by the perception of risk. Risk perception modulates both, 1) people’s immediate voluntary health-protective behavior, e.g., their level of contacts and their adherence to mask-wearing and hygiene recommendations, and 2) their willingness (or hesitancy) to receive vaccination (Figure 1). Individuals constantly receive information on the current COVID-19 incidence, ICU occupancy, and deaths (which are all closely related [13–15]) either via news outlets or because of reports about COVID-19 cases in their social circles. Hence, the risk they perceive depends on this evolving trend over time.

We tailor our approach to the situation of the COVID-19 pandemic, i.e., to a disease having the following characteristics: 1) high transmissibility, 2) relatively low infection fatality rate, 3) widespread vaccine hesitancy, 4) waning immunity, and 5) public attention and coverage. We differentiate from the approaches of [16–18] as we neither model the contagion of fear explicitly nor a direct coupling between incidence and fear. Instead, we assume that individuals build their perception of risk based on the ICU occupancy over time using a memory function, similar to the theoretical approach in [19, 20]. This is a sensible choice, as ICU occupancy signals 1) how likely governmental bodies are to re-implement emergency NPIs to prevent overwhelming healthcare facilities (and thereby limit individual freedoms), and 2) how likely it is that an individual’s close contacts (or their contacts) would have been severely ill. Besides, our modeling framework constitutes a methodological advancement from that presented in [17], as we provide a detailed description of all epidemiologically relevant disease states and several external effects influencing its spread, such as seasonality, contextual contact networks and NPIs.

We assume that individuals base their decisions about health-protective behavior on the recent developments of the pandemic. Following the ideas of Zauberman et al. about perception of time in decision-making [21], we consider that when individuals decide about behavior that only has immediate protective



effects, they consider only the current risk-level. For instance, when deciding whether or not to wear a mask in the supermarket on a given day, they only consider the most recently reported ICU occupancy. Decisions with longer-term protection, in contrast, are also based on a longer-term risk-assessment. When deciding whether or not to get a booster vaccine, for example, individuals do not only take into account the ICU-occupancy on the day of the decision but they are looking back at a longer period. We detail the assumptions about the perceived risk-level and the resulting health-protective behavior in the Methods section. In the following, we sketch the derivation of the feedback loops from this perceived risk to people's immediate voluntary health-protective behavior and willingness to get vaccinated.

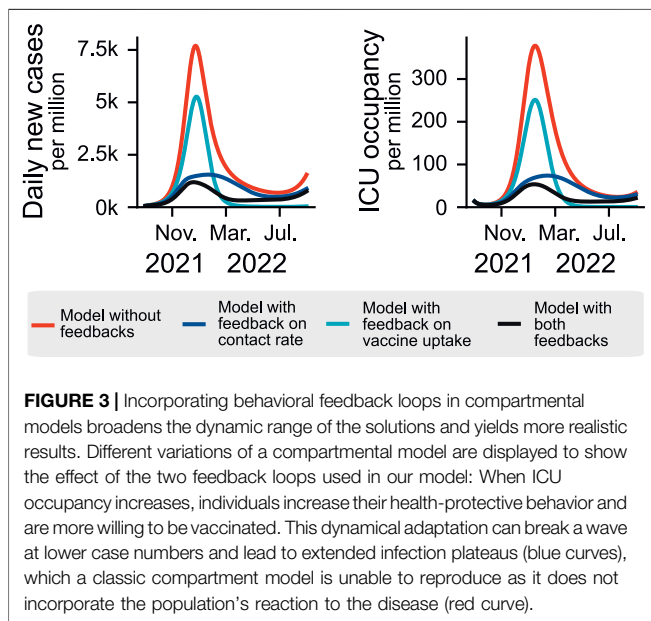
2.1.1 Feedback on Health-Protective Behavior

To determine the explicit relationship between the perceived level of risk and immediate voluntary health-protective behavior—which presents one of the feedback loops in our model—we exploit results from the German COSMO study, a periodic survey where participants are asked about their opinions and behavior regarding the COVID-19 pandemic and NPIs [4].

Their answers on adhering to health-protective behavior recommendations (avoiding private parties in this case) correlate with the ICU occupancy in Germany at the time (**Figure 2A**). However, at very high ICU occupancy, adoption of health-protective behavior seems to reach a plateau (**Figure 2B**); no further adoption seems to be feasible, arguably because those individuals willing to engage in health-protective behavior have done so already as far as they can, and those unwilling are insensitive to higher burden on ICUs. Hence, we fit a piece-wise linear function (with a rounded edge at the transition—called a softplus) to the COSMO data [Pearson correlation coefficient $r = 0.64$ for 2020–2021 (black), $r = 0.81$ for 2020 (red) and $r = 0.53$ for 2021 (yellow)] and use it for the feedback between information in terms of ICU occupancy and voluntary health-protective behavior (**Figure 2C** and Methods for details).

2.1.2 Feedback on Vaccination Behavior

The second feedback loop in our model describes the relationship between the level of perceived risk and vaccine hesitancy. To quantify it, we study the vaccination trends in different European countries and compare them with the trends in ICU occupancy



(**Supplementary Figure S4**, Supplementary Information). The case of Romania (**Figure 2D**) illustrates the relation very clearly: Vaccination rates follow the ICU occupancy with a delay of a few weeks. By analyzing the correlation between vaccination rate and ICU occupancy with a variable delay, we reach the highest Pearson correlation coefficient (0.96) with a delay of 25 days. However, the specific reaction delay and magnitude of the effect differs between countries (**Supplementary Figure S4**). In our model, we propose that as ICU occupancy increases so does the willingness to get vaccinated (i.e., higher probability of accepting a vaccine offer when ICU occupancy is high). As not everybody in the population is willing to accept a vaccine offer, the willing fraction of the population is a function that saturates below 1 (**Figure 2E**). With this formulation, vaccinations are only carried out if the fraction of the population willing to get vaccinated is larger than the fraction of currently vaccinated (**Figure 2F** and Methods for details).

Our model can capture two features observed in real-world vaccination programs. First, when case numbers are low and vaccine uptake high, rational agents might have insufficient incentives for getting vaccinated. Assuming a high perceived risk of vaccine side effects, the agents would thus decline vaccination when offered. The above is known as the free-rider problem in game theory and economics [22]. Second, the two feedback loops in our model and the incorporation of waning immunity allows us to observe different incidence curve shapes and replicate recurrent waves of infections. The above is a necessary validity check, as real-world outbreaks exhibit a large variety of incidence curve shapes [23]. These may ultimately unveil universal patterns of disease spread that are consistent across countries [24].

2.2 Behavioral Feedback Loops Yield More Realistic Results than Classical Models

Classical SEIR-like compartmental models have found wide application in the first stages of the COVID-19 pandemic. In

these models, the different stages of disease progression are represented by separate compartments and individuals transit from one to another at a given (and typically constant) transition rate. In that way, an infectious disease outbreak will proliferate if the spreading rate of the disease is larger than the recovery rate and if a large-enough fraction of the population is susceptible to being infected. However, these simple models often tend to overestimate the size of an infectious disease outbreak or all possible trajectories for the incidence trends [23], as they do not incorporate mechanisms of dynamical adaptation of restrictions [25] or, as studied in this paper, behavior.

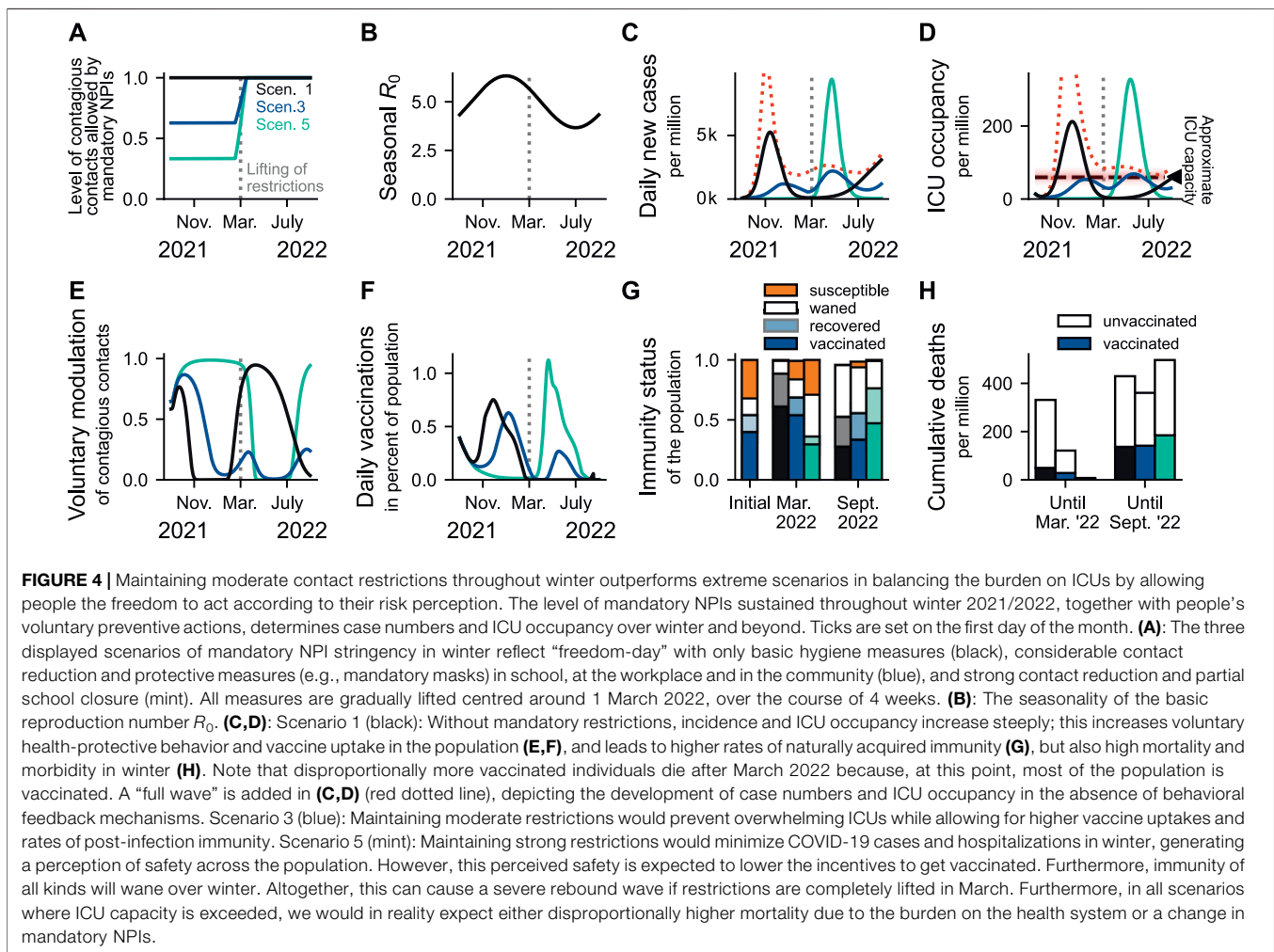
We observe that including the feedback loops described above reduces the peak in incidences and hospitalizations while keeping the timing of the wave almost unchanged (see **Figure 3**). More generally, these feedback loops break increasing and declining trends, resulting in long but flat infection plateaus or multiple waves. Compared to classical SEIR-like models, where two dynamical regimes are possible—exponential growth or decay of case numbers, when neglecting waning immunity—, our model captures a broader spectrum of dynamics by linking ICU occupancy with individuals' health-protective voluntary behavior and vaccine uptake.

2.3 Policies With Either too Weak or too Strong Interventions Throughout Winter Bear Higher Levels of Mortality and Morbidity

Using parameters obtained from surveys and other data sources (**Supplementary Table S3**, Supplementary Information), we analyze five scenarios of mandatory NPIs throughout winter (for all age-stratified results see **Supplementary Material**): 1) no NPIs at all, 2)-4) moderate NPIs and 5) strong NPIs (Methods for details). The stringency of the scenarios and the seasonal effects are depicted in **Figures 4A,B** and **Figures 5A,B**. As an example case, we assume a country with a total vaccination rate of 60% and a recovered fraction of 20%. Note that we include the possibility of overlaps between vaccinated and recovered. Thus, the total fraction of immune individuals does not add up to 80% but 68%. For more detail on the initial conditions, see **Supplementary Material, Supplementary Section S3.1**.

Without any mandatory NPIs throughout winter (Scenario 1, **Figure 4**, black lines), case numbers and hospitalizations will show a steep rise (**Figures 4C,D**). As a consequence, individuals voluntarily adapt their health-protective behavior and are more inclined to accept a vaccine offer (**Figures 4E–G**). Although this scenario features unrealistically high mortality and morbidity, modeling results in the absence of any behavior feedback mechanisms yield even higher levels (cf. **Figures 4C,D**, dotted red line).

In contrast, suppressing the seasonal wave through strong mandatory NPIs (Scenario 5, **Figure 4**, mint lines) and thereby maintaining low case numbers through winter only delays the wave to a later but inevitable date once restrictions



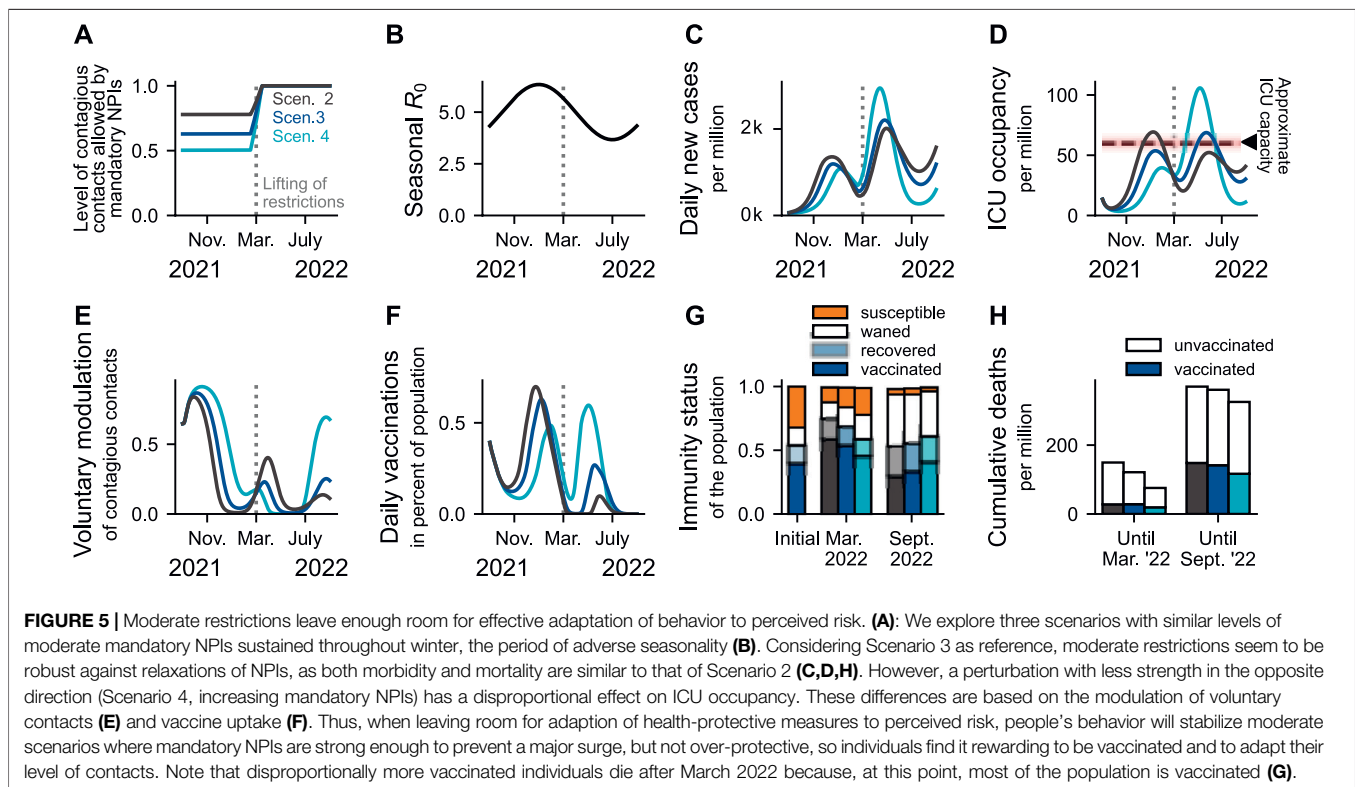
are lifted (**Figures 4C,D**). Low COVID-19 incidence throughout winter implies 1) low post-infection immunity, 2) little incentives for first or booster vaccination, 3) waning immunity, and 4) lower rates of “naturally” boosting immune memory upon re-exposure to the virus [26]. The resulting low immunity levels (**Figure 4G**) then fuel a higher rebound wave when restrictions are lifted in March 2022, despite favorable seasonality. Similar rebound waves have been observed for other seasonal respiratory viruses [27, 28].

Interestingly, the middle strategy, namely moderate NPIs during winter, prevents the high wave in winter as well as the rebound wave in spring that characterize the scenarios with no or with strong NPIs, respectively (Scenario 3, **Figure 4**, dark blue). Unlike in the extreme scenarios, the ICU capacity in Scenario 3 is not exceeded in any season, hence avoiding reduced health care quality and strong burden to health care workers. **Figure 4H** shows that the death toll in Scenario 3 is lower than in the other scenarios. In reality however, this difference would be much larger because Scenarios 1 and 5 surpass the assumed ICU capacity by far; that would imply disproportionately higher mortality, an effect we did not quantify in our model. Alternatively, emergency

mandatory NPIs would be introduced, which we do not model here.

2.4 Voluntary Actions can Dampen the Wave if Restrictions are Moderate

As presented in the previous section, extreme scenarios (Scenarios 1 and 5) bear high levels of morbidity and mortality. However, in scenarios with intermediate restriction levels (Scenarios 2–4, **Figure 5A**), voluntary preventive actions (**Figure 5E**) can compensate for slightly too low levels of mandatory NPIs, provided that these NPIs are strong enough to prevent a surge in COVID-19 incidence that might be too sudden or strong for individuals to voluntarily adopt health-protective behavior (**Figures 5C,D**). For example, while having different levels of mandatory NPIs, Scenarios 2 and 3 reach similar peaks in ICU occupancy (**Figure 5D**). Conversely, despite considering a proportional increase in the strength of NPIs (comparable to that from Scenario 2 to 3, **Figure 5A**), Scenario 4 is too protective: there are too few incentives to get vaccinated (**Figure 5F**) due to the low risk perception as well as too few infections (**Figure 5C**) and, hence, appropriate immunity



levels are not reached (Figure 5G). As a consequence, a disproportionately larger off-seasonal wave in spring overwhelms ICUs (Figure 5D). Noteworthy, even though the nominal mortality is the lowest for Scenario 4 (Figure 5H), this value does not account for triage-induced over-mortality or novel necessary NPIs that would be likely be imposed and is thus invalid.

2.5 Case Study: Emergence of the Omicron Variant of Concern and its Effect on Case Numbers

A risk that cannot be neglected is the emergence of SARS-CoV-2 variants of concern (VOC), such as the Omicron VOC. This variant is rapidly replacing the Delta VOC, thus posing an imminent risk. Although there is substantial uncertainty about its epidemiological features, preliminary evidence shows: Compared to the Delta VOC, Omicron exhibits 1) an increased risk of reinfection or break-through infection [29–31], 2) a substantial reduction in antibody neutralization [32–38], 3) a reduction in vaccine effectiveness against infection [31, 37, 39–44], and 4) faster spread [30, 31, 45, 46] mainly due to immune escape [47].

Given this evidence, we analyze the impacts of a potential full replacement of the dominant Delta VOC by the Omicron VOC by 15th of January 2022. We incorporate the protection against infection by booster doses. As example scenario, we start with Scenario 3 (moderate mandatory NPIs), as it resembles a typical development in Europe. We then analyze four different possible

reactions to the Omicron VOC, i.e., starting to switch from Scenario 3 to Scenarios 1, 3, 4, or 5 before it takes over (Figure 6A). We evaluate three possibilities regarding the booster vaccine-protection against infection, 50, 65, and 80% (relative to the protection granted for Delta). This is consistent with available evidence suggesting Omicron's immune escape to reduce vaccine effectiveness against symptomatic disease to about 73% for freshly mRNA-boosted individuals [32]. Furthermore, we explore two possibilities of severity of infections after previous immunization: Either efficacy against severe course remains the same as with Delta, both for the immunized and immune-naive persons (Figures 6B,E,H), or protection is five times better for the immunized (Figures 6C,F,I).

As expected, the enhanced transmissibility resulting from the partial escape of the Omicron VOC breaks the decreasing trend in case numbers observed for Scenarios 3, 4, and 5 from the moment where the replacement takes place (Figures 6A,D,G). This results in a substantial surge in daily new cases in all scenarios except for Scenario 5 (most restrictive). Regarding ICU occupancy, our results depend strongly on the assumed protection against infection by recent vaccination or boosters. When the protection against infection granted by recently administered vaccines is above 50%, both Scenarios 4 (which has a more strict testing policy and further reduced contacts compared to Scenario 3) and 5 (in addition, group sizes in school are reduced) yield optimistic results for ICU occupancy. If Omicron infections lead to much less severe course of the disease for immunized or convalescent individuals, then even Scenario 3 can avoid severely overfilling intensive care units. We have represented Scenario 1

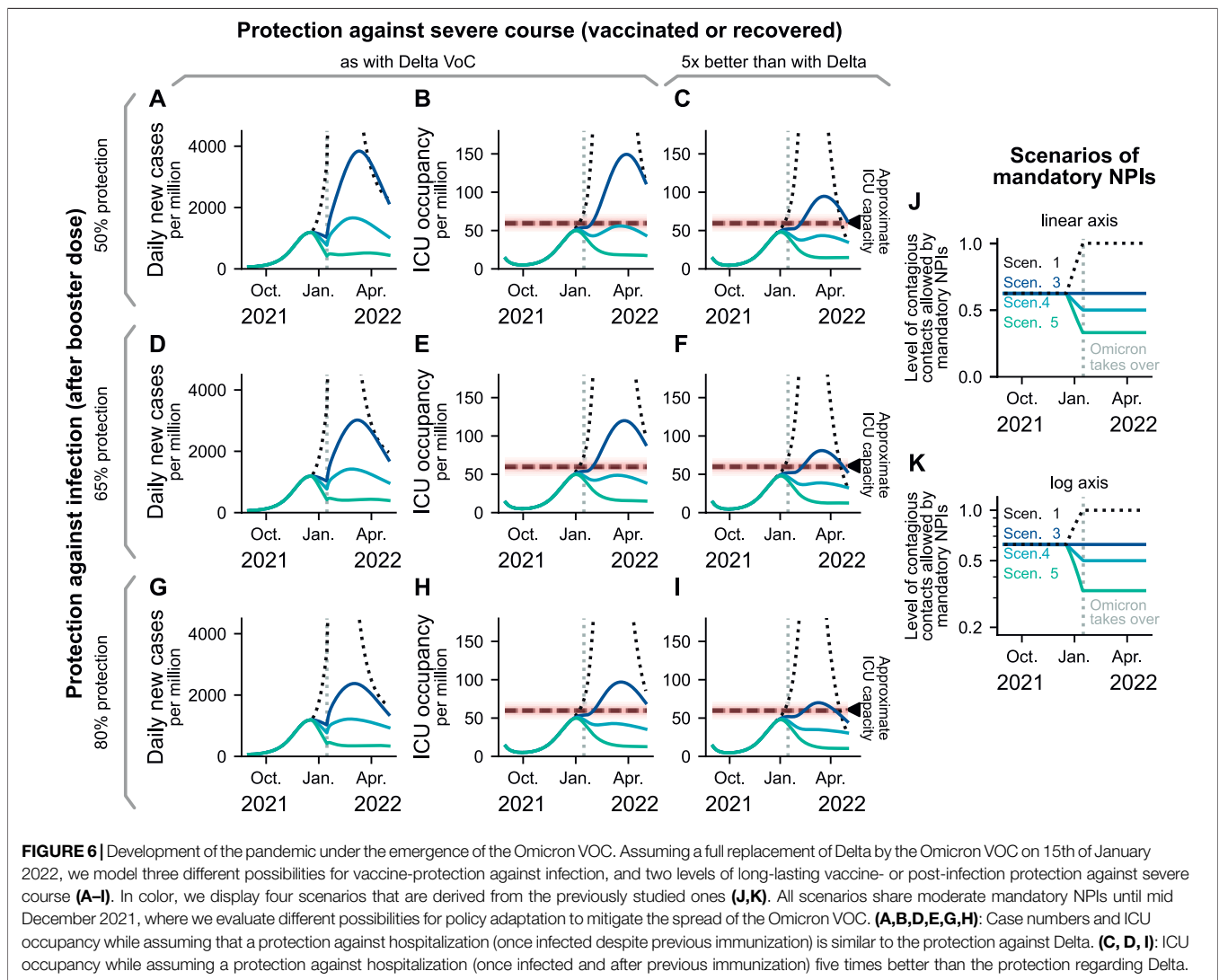


FIGURE 6 | Development of the pandemic under the emergence of the Omicron VOC. Assuming a full replacement of Delta by the Omicron VOC on 15th of January 2022, we model three different possibilities for vaccine-protection against infection, and two levels of long-lasting vaccine- or post-infection protection against severe course (A–I). In color, we display four scenarios that are derived from the previously studied ones (J,K). All scenarios share moderate mandatory NPIs until mid December 2021, where we evaluate different possibilities for policy adaptation to mitigate the spread of the Omicron VOC. (A,B,D,E,G,H): Case numbers and ICU occupancy while assuming that a protection against hospitalization (once infected despite previous immunization) is similar to the protection against Delta. (C, D, I): ICU occupancy while assuming a protection against hospitalization (once infected and after previous immunization) five times better than the protection regarding Delta.

(lifting all mandatory NPIs) with dashed lines, as it yields unrealistic results: Stricter NPIs would probably be reinstated if ICU occupancy becomes too high. The scenarios end in April, where we expect that an updated booster vaccine is developed and distributed. In that phase, lifting restrictions at the pace of vaccination and aiming for low case numbers would maximize freedom while minimizing mortality and morbidity [25, 48–50].

3 DISCUSSION

Modeling the interplay of human behavior and disease spread is one of the grand challenges of infectious disease modeling. While not being the first to model behavioral adaptation [17, 51–55], we incorporate data-driven insights into our modeling framework, inspiring the explicit functional dependency between risk and health-protective behavior as well as vaccine hesitancy in the context of the COVID-19 pandemic. Thereby, we can incorporate

self-regulation mechanisms into our scenario analysis, which best qualitatively describe what is to be expected in the future or in the event of the emergence of novel SARS-CoV-2 VOCs, such as the Omicron variant. We hence take a further step towards more empirically-grounded mathematical models.

Within our framework, a smooth transition to SARS-CoV-2 endemicity requires, besides a working and accepted vaccine, two ingredients. First, mandatory NPI levels should be high enough to prevent a surge in case numbers so fast that individuals could not react on time to prevent overwhelming ICUs. Second, mandatory NPIs should leave enough room so that individuals can effectively adopt voluntary preventive actions as a response to an increased perception of risk. Hence, governments must guarantee that the decision to, e.g., attend non-essential face-to-face activities that could be carried out remotely remains in the individual’s hands. Under such circumstances, voluntary actions can dampen the wave and prevent overwhelming ICUs (Scenarios 2 and 3, Figure 5). Otherwise, irresponsible or overprotective measures would result in a wave that could surpass the healthcare capacity

in the short term or when lifting all measures (Scenarios 1, 4, and 5, **Figures 4, 5**). In any case, people's awareness about the danger of a disease should ideally be driven by trust in scientific and governmental bodies instead of by the current burden to the healthcare system. Hence, it is crucial during a disease outbreak to engage in extensive, expert-guided, and audience-tailored risk communication [56] and to prevent the spread of mis- and disinformation that could damage general trust [57, 58].

Despite the empirical basis of our approach, the functional shape of the feedback mechanisms remains one of the main uncertainties in our model. The voluntary adoption of health-protective measures was inspired by survey data [4], and is thus bound to its limitations. Additionally, as ICU capacity was never extremely overwhelmed in Germany in the time frame of the COSMO survey, the study does not provide information on how people would act at very high levels of ICU occupancy; in principle, such emergency situations would trigger even stronger reactions in the population, and certainly also a change in NPI stringency (which we assumed to be constant throughout). Furthermore, when extrapolating our results to other countries, one should consider cultural differences or varying levels of trust in governmental bodies. Therefore, more empirical research to inform model assumptions and parameters remains crucial.

Vaccine uptake and coverage are critical parameters that determine mortality and morbidity levels. In line with what has been observed in high-income countries, we assume that vaccination rates are mostly limited by vaccine hesitancy instead of vaccine stocks or logistics. In that way, we can deal with emergent VOCs (as Omicron) with a healthy combination of mandatory NPIs aiming for low-case numbers while a working vaccine is developed and coverage is insufficient [25, 48] and by letting individuals decide on their own when the roll-out is complete. However, the core problem remains latent; wealthy countries concentrate resources while some countries cannot afford enough vaccines to protect even their population at risk [59]. As the latter countries are forced into accepting high-case numbers in order to keep their economies running, there are increased risks of breeding variants that could escape natural or vaccine-elicited protection [60]. Therefore, vaccine policy planning from an international perspective is critical for a smooth transition to SARS-CoV-2 endemicity.

Modeling the introduction and spread of different SARS-CoV-2 variants in a population is challenging. At the very least, modeling these dynamics would require having separate compartments for all the disease states of all circulating variants, disproportionately increasing the complexity of our model. In our approach, we take advantage of the extensive immune escape of the Omicron VOC to natural and vaccine-elicited neutralization [29, 31, 32, 45, 47], and assume that the replacement of Delta VOC occurs very quickly (i.e., basically instantaneously) in mid-January. This simplification is not too distant from reality; replacement of Delta and other predominant sublineages for Omicron took only a few weeks in several countries [61]. For the spread of Omicron, we use the same basic reproduction number as for Delta but instead consider most individuals previously immunized to have lost protection against

infection, i.e., they are moved to the susceptible pool (Methods for details). Thereby, we can capture the explosive spread of Omicron VOC without increasing the base transmissibility. We furthermore include that those people having received a booster vaccine maintain some protection against infection with Omicron, which, however, also wanes. These assumptions are consistent with a large Danish cohort of households, where the secondary attack rate among unvaccinated was slightly higher for Delta infections than for Omicron [47], and with extensive experimental and observational studies [32, 38, 62, 63]. Despite the approximation we did for the transition to the Omicron variant, the mid- and long-term dynamics of the Omicron VOC should be reflected well.

In our work, the level of mandatory NPIs dictates the minimum and maximum level of voluntary health-protective behavior that individuals may adapt. For each scenario, we assume one specific, static level of mandatory NPIs, which best resembles real-world observations on compulsory measures aiming to reduce the probability of contagion (i.e., mask-wearing mandates, immunity passports, meeting restrictions, among others) and testing policy (as described in Methods). However, this static level can lead to unrealistically high waves of incidence and ICU occupancy, which 1) have not been seen so far and 2) would undoubtedly trigger the implementation of additional restrictions to prevent a major collapse in the health system. Nonetheless, we decided to incorporate this static mandatory NPI level because it illustrates a worst-case trajectory of each scenario. Besides, due to *pandemic fatigue* [64], we would expect the effectiveness of interventions and thus the imposed change in health-protective behavior in the different mandatory NPI scenarios to decay over time.

In summary, the way governments approach a pandemic situation when vaccines are available will shape long-term transmission dynamics by influencing the magnitude of information-behavior feedback loops. We show that the latter play a major role during the transition from epidemicity to endemicity. Thus most importantly, the challenge for authorities is to find ways to engage individuals with vaccination programs and health-protective behavior without requiring high case numbers for that. Here, clear communication and trust continues to be essential [65].

4 METHODS

4.1 Model Overview

We use an age-stratified compartmental model with compartments for susceptible-exposed-infected-recovered (SEIR) as well as for fatalities (D), receiving treatment in an ICU (ICU), and vaccination (first time and booster vaccines) (V) (**Supplementary Figure S1**). We also include waning immunity and seasonality effects (**Figures 4, 5B**). To account for behavioral change induced by perceived risk of infection, we include a feedback loop between ICU occupancy, voluntary health-protective behavior and willingness to receive vaccination (**Figure 2** and **Supplementary Material**). Explicitly, we assume

that increases in ICU occupancy 1) decrease the contact rates among the population and thus the spreading rate of COVID-19 [4–7], and 2) increase vaccine acceptance among hesitant individuals [4, 8]. For the first feedback loop (voluntary health protective behavior), we assume that individuals adapt their contacts in different contexts depending on the risk they have perceived recently. The level of potentially contagious contacts is multiplied by a factor k that decreases with ICU occupancy between the minimum and maximum allowed by current mandatory NPIs (Figure 2C). Regarding the second feedback loop (related to vaccine uptake), we assume that a fraction of the population will always accept a vaccination offer, despite current ICU occupancy. From this minimum onward, vaccination willingness monotonically increases with ICU occupancy and saturates towards a maximum, accounting for a fraction of the population that will never accept the vaccine (Figure 2E). This means that we assume that there is a fraction in the population that is certainly not able or willing to be vaccinated. Given a fraction of people willing to be vaccinated, we determine the speed of the vaccination program using a linearly increasing function (Figure 2F). We model these two feedback loops to act on different timescales, as individuals can, e.g., decrease the number of contacts and contact intensity on a daily basis, while getting vaccinated takes longer. To capture this, we explicitly include memory kernels accounting for how individuals subjectively weigh events happening on different timescales when forming their perception of risk [21].

4.2 Memory on Perceived Risk

We assume that perceived risk regarding the disease depends on information about ICU occupancy that reaches individuals via media or affected social contacts. This perception of risk builds over time; people are not only aware of the occupancy numbers at the present moment but also of those in the recent past. To incorporate this into our model, we calculate the convolution of the ICU occupancy with a Gamma distribution (Supplementary Figure S2, Supplementary Information), effectively “weighting” the ICU occupancy numbers with their recency into a variable of risk perception which we call H_R . As a result, ICU occupancy numbers from a few days ago weigh more in people’s memory and thus influence voluntary health-protective behavior at the present moment more than ICU occupancy that lies further in the past. We use this concept of ICU occupancy “with memory” to design the functions of the feedback loops (Figures 2B,C,E,F). The effect of the parameters chosen for the Gamma distribution on the model results as well as of all other model parameters is quantified in the sensitivity analysis, Supplementary Section S4, Supplementary Information.

4.3 NPI- and Risk-Induced Change in Health-Protective Behavior

When analyzing the joint effect of mandatory NPIs and voluntary measures to mitigate the spread of COVID-19, we find a strong overlap between them; mandatory NPIs limit the range of the measures that individuals could voluntarily take to protect themselves and their loved ones. For example, when large

private gatherings are officially forbidden, individuals cannot voluntarily choose not to meet. Additionally, when the engagement of the population in voluntary protective measures is very large, certain mandatory NPIs would not be required. We model the combined effect of mandatory NPIs and voluntary adoption of health-protective behavior as a function $k_{\text{NPI, self}}(H_R)$. Using the baseline of mandatory NPIs as an input, this function calculates the level of voluntary preventive action in dependence of the perceived risk H_R . To be precise, the value of $k_{\text{NPI, self}}(H_R) \in [0, 1]$ represents the level to which (potentially contagious) contacts of an average individual are reduced (Figure 2C), a factor that is multiplied onto the entries of a contact matrix separated by contexts (Supplementary Figure S3, Supplementary Information). For example, adaption of voluntary mask-wearing or a direct reduction of gatherings decreases the level of potentially contagious contacts and, thereby, $k_{\text{NPI, self}}(H_R)$. Furthermore, we distinguish between contacts made at home, in schools, in workplaces or during communal activities. We weight all the interactions with different $k_{\text{NPI, self}}^\nu(H_R)$ with $\nu \in \{\text{Households, Schools, Workplaces, Communities}\}$ that act on contextual contact matrices C_{ij}^ν , see Supplementary Section S1.2 and Figure 1.

Inspired by the COSMO survey data [4] (Figure 2B), we suggest the following shape for $k_{\text{NPI, self}}^\nu(H_R)$: The level of (potentially) contagious contacts decreases linearly upon increases in the ICU-mediated perception of risk H_R below a threshold $H_R = H_{\text{max}}$, from which point on no further reduction is possible (Figure 2C). This might represent 1) a fraction of the population agnostic to measures or unwilling to comply, or 2) limitations of voluntary preventive action imposed by practical constraints related to the current level of imposed restrictions, for example, having to make contacts in one’s own household or having to go to work or school. We implement $k_{\text{NPI, self}}^\nu(H_R)$ as a softplus function, having a differentiable transition at H_{max} . Each function (for each scenario) is defined by 3 parameters H_{max} , $k_{\text{NPI, self}}^\nu(H_R = 0)$, and $k_{\text{NPI, self}}^\nu(H_R = H_{\text{max}})$. $H_{\text{max}} = 37$ is obtained by the fit to the COSMO data shown in Figure 2 (black line) and used for the two other fits shown in Figure 2 (red and yellow lines) as well as for the behavior parametrizations for the different scenarios (Supplementary Figure S3, Supplementary Information).

4.4 Different Mandatory NPI Scenarios

We choose to simulate five different scenarios, each having a different level of overall stringency. In the following we briefly describe the scenarios:

Scenario 1 (“Freedom day”): All mandatory restrictions are lifted, resulting in a factor of $k_{\text{NPI, self}}^\nu(H_R = 0) = 1 \forall \nu$. However, if ICU occupancy increases, we leave room for individuals’ voluntary action based on perceived risk to reduce viral transmission: $k_{\text{NPI, self}}^\nu(H_R > 0) < 1$. We assume that communal activities and workplaces leave more room for voluntary preventive action than households and schools because of the possibility of working from home, avoiding non-essential gatherings etc. This difference is depicted in Supplementary Figure S3.

TABLE 1 | Different scenarios of mandatory NPIs. Listed are descriptions of the general measures imposed in each scenario as well as the input parameters to the function $k_{NPI, self}^*(H_R)$ that modulates the spread. The parameters act as multiplicative factors onto infection terms in our model, thus high parameter values (close to 1) translate to little reduction in infections and low parameters (close to 0) translate to strong reductions in infections. For each cell, the first parameter translates to a reduction at high ICUs ($k_{NPI, self}^*(H_R = H_{max})$) and the second parameter to the corresponding reduction at empty ICUs ($k_{NPI, self}^*(H_R = 0)$), between which we linearly interpolate (**Supplementary Figure S3**).

Sc.	Name	Description of measures	$k_{Households}$	$k_{Schools}$	$k_{Workplaces}$	$k_{Communities}$
1	“freedom day”	no mandatory measures	0.8–1	0.8–1	0.6–1	0.6–1
2	moderate NPIs A	increased stringency affecting risk of transmission in schools	0.8–1	0.25–0.5	0.5–0.9	0.5–0.9
3	moderate NPIs B	mild NPIs + reduction of transmission at workplaces	0.8–1	0.25–0.5	0.25–0.5	0.5–0.9
4	moderate NPIs C	moderate NPIs + enforcement of restrictions in communal activities	0.8–1	0.1–0.25	0.25–0.5	0.25–0.5
5	strong NPIs	strong NPIs + further restrictions wherever possible	0.8–1	0.1–0.25	0.25–0.5	0.1–0.2

Scenario 2 (Moderate NPIs A): Easy-to-follow measures are kept in place and potentially contagious contacts at school are reduced to $k_{NPI, self}^{School}(H_R = 0) = 0.5$.

Scenario 3 (Moderate NPIs B): Further measures at work (e.g., home office or testing) reduce $k_{NPI, self}^{Workplaces}(H_R = 0) = 0.5$.

Scenario 4 (Moderate NPIs C): Further reduction in potentially contagious school contacts and restrictions affecting communal contacts reduce $k_{NPI, self}^{School}(H_R = 0) = 0.25$ and $k_{NPI, self}^{Communities}(H_R = 0) = 0.5$.

Scenario 5 (Strong NPIs): Communal activities are further reduced to $k_{NPI, self}^{Communities}(H_R = 0) = 0.2$.

Table 1 lists all values for the different scenarios and contexts of interaction between individuals. The reduction of household contacts is assumed to remain the same for all scenarios. Note that, as the stringency of measures increases, room for voluntary adoption of health-protective behavior usually decreases: To give an example, without mandatory measures the level of contact reduction in communal activities lies in the range 1–0.6, whereas in a scenario with strong mandatory NPIs it lies in the range 0.2–0.1. The difference between the two bounds effectively measures the room for voluntary actions (0.4 for freedom day vs. 0.1 for strong NPIs). An exception are school contacts in which moderate restriction scenarios (2 and 3) display a wider range of possible voluntary action than the freedom day scenario. As health-protective behavior among children could be encouraged but not imposed, their adherence to rules constitutes a voluntary act.

4.5 Modeling the Introduction and Spread of the Omicron VOC

Modeling the introduction and spread of the Omicron VOC requires modifications to the model compartments, transition rates, and parameters. In particular, these modifications allow us to explore the effects of Omicron’s 1) extensive immune escape and 2) potential reduced risk for severe course of the disease. We implemented the introduction of Omicron VOC as a total replacement of the previously dominating Delta VOC on 15 Jan 2022. At that moment, we rearrange the distribution of individuals between the “waned” and “immune” compartments, increase the rate of waning immunity to account for Omicron’s immune escape, and

reduce the probability of having a severe course. Explicitly, before the introduction of the Omicron VOC, the immune population is tracked in additional pseudo-compartments V^o , R^o , $R^{v,o}$ with a faster waning rate. In that way, there are always less individuals in V^o , R^o , $R^{v,o}$ than in V , R , R^v . At the time of variant replacement, $V - V^o$, $R - R^o$, $R^v - R^{v,o}$ individuals are moved from the vaccinated and recovered compartments to the respective waned compartments; individuals previously protected against Delta would now be susceptible to Omicron. We model booster-vaccination protection against infection following a leaky scheme, thus boosted individuals have a probability of η of being entirely protected. With probability $1 - \eta$, individuals remain in their current compartment but are tracked as if the vaccine had worked successfully.

DATA AVAILABILITY STATEMENT

The original contributions presented in the study are included in the article/**Supplementary Material**. Source code for data generation and analysis is available online on GitHub https://github.com/Priesemann-Group/covid19_infoXpand_feedbackloop. Further inquiries can be directed to the corresponding author.

AUTHOR CONTRIBUTIONS

Conceptualization: PD, JW, SC, SB, JD, VP. Methodology: PD, JW, SC, SB, SM, EI, VP. Software: PD, JW. Formal analysis: PD, JW, SC, SB. Writing—Original Draft: all authors. Writing—Review and Editing: all authors. Visualization: PD, JW, SC. Supervision: SC, MK, MM, KN, AC, VP.

FUNDING

Open Access publication has been enabled by the Max-Planck-Society. Authors with affiliation “1” acknowledge support from the Max-Planck-Society. SC acknowledges support from the Centre for Biotechnology and Bioengineering—CeBiB (PIA project FB0001, ANID, Chile). SB and SM were financially supported by the German Federal

Ministry of Education and Research (BMBF) as part of the Network University Medicine (NUM), project egePan, funding code: 01KX2021. AC received funding from the Digital Society research program funded by the Ministry of Culture and Science of the German State of North Rhine-Westphalia. MK acknowledges support from the Netherlands Organisation for Health Research and Development (ZonMw), funding code: 91216062, and from the European Union's Horizon 2020 research and innovation program under grant agreement No 101003480 (Project CORESMA). KN acknowledges support by the German Federal Ministry of Education and Research (BMBF) for the MODUS-COVID project, funding code: 01KX2022A.

REFERENCES

- Casero-Ripolles A. Impact of COVID-19 on the media System. Communicative and Democratic Consequences of News Consumption during the Outbreak. *Epi* (2020) 29. doi:10.3145/epi.2020.mar.23
- Kim HK, Ahn J, Atkinson L, Kahlor LA. Effects of COVID-19 Misinformation on Information Seeking, Avoidance, and Processing: A Multicountry Comparative Study. *Sci Commun* (2020) 42:586–615. doi:10.1177/1075547020959670
- Ferrer RA, Klein WM. Risk Perceptions and Health Behavior. *Curr Opin Psychol* (2015) 5:85–9. doi:10.1016/j.copsyc.2015.03.012
- Betsch C, Wieler LH, Habersaat K. Monitoring Behavioural Insights Related to Covid-19. *The Lancet* (2020) 395:1255–6. doi:10.1016/s0140-6736(20)30729-7
- Imbriano G, Larsen EM, Mackin DM, An AK, Luhmann CC, Mohanty A, et al. Online Survey of the Impact of Covid-19 Risk and Cost Estimates on Worry and Health Behavior Compliance in Young Adults. *Front Public Health* (2021) 9:157. doi:10.3389/fpubh.2021.612725
- Perrotta D, Grow A, Rampazzo F, Cimentada J, Del Fava E, Gil-Clavel S, et al. Behaviours and Attitudes in Response to the Covid-19 Pandemic: Insights from a Cross-National Facebook Survey. *EPJ Data Sci* (2021) 10:17–3. doi:10.1140/epjds/s13688-021-00270-1
- Druckman JN, Klar S, Krupnikov Y, Levendusky M, Ryan JB. Affective Polarization, Local Contexts and Public Opinion in America. *Nat Hum Behav* (2021) 5:28–38. doi:10.1038/s41562-020-01012-5
- Salali GD, Uysal MS. Effective Incentives for Increasing Covid-19 Vaccine Uptake. *Psychol Med* (2021) 1–3. doi:10.1017/s0033291721004013
- Gavenciak T, Monrad JT, Leech G, Sharma M, Mindermann S, Brauner JM, et al. Seasonal Variation in Sars-Cov-2 Transmission in Temperate Climates. *medRxiv* (2021). doi:10.1101/2021.06.10.21258647
- Moriyama M, Hugentobler WJ, Iwasaki A. Seasonality of Respiratory Viral Infections. *Annu Rev Virol* (2020) 7:83–101. doi:10.1146/annurev-virology-012420-022445
- Sajadi MM, Habibzadeh P, Vintzileos A, Shokouhi S, Miralles-Wilhelm F, Amoroso A. Temperature and Latitude Analysis to Predict Potential Spread and Seasonality for COVID-19. Available at SSRN 3550308 (2020).
- Mistry D, Litvinova M, y Piontti AP, Chinazzi M, Fumanelli L, Gomes MF, et al. Inferring High-Resolution Human Mixing Patterns for Disease Modeling. *Nat Commun* (2021) 12:1–12. doi:10.1038/s41467-020-20544-y
- Olivieri A, Palù G, Sebastiani G. Covid-19 Cumulative Incidence, Intensive Care, and Mortality in Italian Regions Compared to Selected European Countries. *Int J Infect Dis* (2021) 102:363–8. doi:10.1016/j.ijid.2020.10.070
- Bravata DM, Perkins AJ, Myers LJ, Arling G, Zhang Y, Zillich AJ, et al. Association of Intensive Care Unit Patient Load and Demand with Mortality Rates in Us Department of Veterans Affairs Hospitals during the Covid-19 Pandemic. *JAMA Netw Open* (2021) 4:e2034266. doi:10.1001/jamanetworkopen.2020.34266
- Linden M, Mohr SB, Dehning J, Mohring J, Meyer-Hermann M, Pigeot I, et al. Case Numbers beyond Contact Tracing Capacity Are Endangering the Containment of COVID-19. *Dtsch Arztebl Int* (2020) 117:790–1. doi:10.3238/arztebl.2020.0790
- Epstein JM, Parker J, Cummings D, Hammond RA. Coupled Contagion Dynamics of Fear and Disease: Mathematical and Computational Explorations. *PLoS One* (2008) 3:e3955. doi:10.1371/journal.pone.0003955
- Epstein JM, Hatna E, Crodelle J. Triple Contagion: a Two-Fears Epidemic Model. *J R Soc Interf* (2021) 18:20210186. doi:10.1098/rsif.2021.0186
- Bauch CT. Imitation Dynamics Predict Vaccinating Behaviour. *Proc R Soc B* (2005) 272:1669–75. doi:10.1098/rspb.2005.3153
- d'Onofrio A, Manfredi P. Information-related Changes in Contact Patterns May Trigger Oscillations in the Endemic Prevalence of Infectious Diseases. *J Theor Biol* (2009) 256:473–8.
- d'Onofrio A, Manfredi P, Salinelli E. Vaccinating Behaviour, Information, and the Dynamics of Sir Vaccine Preventable Diseases. *Theor Popul Biol* (2007) 71:301–17.
- Zauberman G, Kim BK, Malkoc SA, Bettman JR. Discounting Time and Time Discounting: Subjective Time Perception and Intertemporal Preferences. *J Marketing Res* (2009) 46:543–56. doi:10.1509/jmkr.46.4.543
- Bauch CT, Bhattacharyya S. Evolutionary Game Theory and Social Learning Can Determine How Vaccine Scars Unfold. *Plos Comput Biol* (2012) 8:e1002452. doi:10.1371/journal.pcbi.1002452
- Tkachenko AV, Maslov S, Wang T, Elbana A, Wong GN, Goldenfeld N. Stochastic Social Behavior Coupled to Covid-19 Dynamics Leads to Waves, Plateaus, and an Endemic State. *eLife* (2021) 10:e68341. doi:10.7554/eLife.68341
- Dankulov MM, Tadic B, Melnik R. Worldwide Clustering and Infection Cycles as Universal Features of Multiscale Stochastic Processes in the Sars-Cov-2 Pandemic. *medRxiv* (2021). doi:10.1101/2021.12.20.21268095
- Bauer S, Contreras S, Dehning J, Linden M, Iftekhar E, Mohr SB, et al. Relaxing Restrictions at the Pace of Vaccination Increases freedom and Guards against Further Covid-19 Waves. *Plos Comput Biol* (2021) 17:e1009288. doi:10.1371/journal.pcbi.1009288
- Brown EL, Essigmann HT. Original Antigenic Sin: the Downside of Immunological Memory and Implications for Covid-19. *Msphere* (2021) 6:e00056–21. doi:10.1128/mSphere.00056-21
- Gomez GB, Mahé C, Chaves SS. Uncertain Effects of the Pandemic on Respiratory Viruses. *Science* (2021) 372:1043–4. doi:10.1126/science.abh3986
- Sanz-Muñoz I, Tamames-Gómez S, Castrodeza-Sanz J, Eiros-Bouza JM, de Lejarazu-Leonardo RO. Social Distancing, Lockdown and the Wide Use of Mask; a Magic Solution or a Double-Edged Sword for Respiratory Viruses Epidemiology? *Vaccines* (2021) 9:595. doi:10.3390/vaccines9060595
- Viana R, Moyo S, Amoako DG, Tegally H, Scheepers C, Lessells RJ, et al. Rapid Epidemic Expansion of the Sars-Cov-2 Omicron Variant in Southern Africa. *Nature* (2021). doi:10.1038/d41586-021-03832-5
- Pulliam JR, van Schalkwyk C, Govender N, von Gottberg A, Cohen C, Groome MJ, et al. Increased Risk of Sars-Cov-2 Reinfection Associated with Emergence of the Omicron Variant in south africa. *medRxiv* (2021). doi:10.1101/2021.11.11.21266068
- Ferguson N, Ghani A, Cori A, Hogan A, Hinsley W, Volz E. Report 49: Growth, Population Distribution and Immune Escape of the Omicron in england. *Imperial College London* (2021). doi:10.25561/93038
- Cele S, Jackson L, Khoury DS, Khan K, Moyo-Gwete T, Tegally H, et al. Omicron Extensively but Incompletely Escapes Pfizer Bnt162b2 Neutralization. *Nature* (2021). doi:10.1038/s41586-021-04387-1

ACKNOWLEDGMENTS

We thank Prof. Dr. Cornelia Betsch, her colleagues and her team for publicly sharing survey data of the COVID-19 Snapshot Monitoring (COSMO) study, which enabled a quantitative approach otherwise not possible.

SUPPLEMENTARY MATERIAL

The Supplementary Material for this article can be found online at: <https://www.frontiersin.org/articles/10.3389/fphy.2022.842180/full#supplementary-material>

33. Wilhelm A, Widera M, Grikscheit K, Toptan T, Schenk B, Pallas C, et al. Reduced Neutralization of Sars-Cov-2 Omicron Variant by Vaccine Sera and Monoclonal Antibodies. *medRxiv* (2021). doi:10.1101/2021.12.07.21267432
34. Cameroni E, Bowen JE, Rosen LE, Saliba C, Zepeda SK, Culap K, et al. Broadly Neutralizing Antibodies Overcome Sars-Cov-2 Omicron Antigenic Shift. *Nature* (2021) 1–9. doi:10.1038/s41586-021-04386-2
35. Roessler A, Riepler L, Bante D, von Laer D, Kimpel J. Sars-cov-2 B. 1.1. 529 Variant (Omicron) Evades Neutralization by Sera from Vaccinated and Convalescent Individuals. *medRxiv* (2021). doi:10.1101/2021.12.08.21267491
36. Hoffmann M, Krüger N, Schulz S, Cossmann A, Rocha C, Kempf A, et al. The Omicron Variant Is Highly Resistant against Antibody-Mediated Neutralization—Implications for Control of the Covid-19 Pandemic. *Cell* (2021). doi:10.1016/j.cell.2021.12.032
37. Gardner BJ, Kilpatrick AM. Estimates of Reduced Vaccine Effectiveness against Hospitalization, Infection, Transmission and Symptomatic Disease of a New Sars-Cov-2 Variant, Omicron (B. 1.1. 529), Using Neutralizing Antibody Titers. *medRxiv* (2021). doi:10.1101/2021.12.10.21267594
38. Pérez-Then E, Lucas C, Monteiro VS, Miric M, Brache V, Cochon L, et al. Immunogenicity of Heterologous Bnt162b2 Booster in Fully Vaccinated Individuals with Coronavac against Sars-Cov-2 Variants delta and Omicron: The dominican republic Experience. *medRxiv* (2021). doi:10.1101/2021.12.27.21268459
39. Gruell H, Vanshylla K, Tober-Lau P, Hillus D, Schommers P, Lehmann C, et al. Mrna Booster Immunization Elicits Potent Neutralizing Serum Activity against the Sars-Cov-2 Omicron Variant. *Nat. Med.* (2022). doi:10.1038/s41591-021-01676-0
40. Kuhlmann C, Mayer CK, Claassen M, Maponga TG, Sutherland AD, Suliman T, et al. Breakthrough Infections with Sars-Cov-2 Omicron Variant Despite Booster Dose of Mrna Vaccine. Available at SSRN 3981711 (2021).
41. Nemet I, Kliker L, Lustig Y, Zuckerman N, Erster O, Cohen C, et al. Third Bnt162b2 Vaccination Neutralization of SARS-CoV-2 Omicron Infection. *New Engl J Med* (2021). doi:10.1056/nejmc2119358
42. Basile K, Rockett RJ, McPhie K, Fennell M, Johnson-Mackinnon J, Agius J, et al. Improved Neutralization of the Sars-Cov-2 Omicron Variant after Pfizer-Biontech Bnt162b2 Covid-19 Vaccine Boosting. *bioRxiv* (2021). doi:10.1101/2021.12.12.472252
43. Garcia-Beltran WF, St Denis KJ, Hoelzemer A, Lam EC, Nitido AD, Sheehan ML, et al. mRNA-based COVID-19 Vaccine Boosters Induce Neutralizing Immunity Against SARS-CoV-2 Omicron Variant. *Cell* (2022). doi:10.1016/j.cell.2021.12.033
44. Andrews N, Stowe J, Kirsebom F, Toffa S, Rieckard T, Gallagher E, et al. Effectiveness of Covid-19 Vaccines against the Omicron (B. 1.1. 529) Variant of Concern. *medRxiv* (2021). doi:10.1101/2021.12.14.21267858
45. Torjesen I. Covid Restrictions Tighten as Omicron Cases Double Every Two to Three Days. *BMJ* (2021) 375. doi:10.1136/bmj.n3051
46. Barnard RC, Davies NG, Pearson CA, Jit M, John W, Edmunds WJ. Projected epidemiological consequences of the Omicron SARS-CoV-2 variant in England. *medRxiv* (2021). doi:10.1101/2021.12.15.21267858
47. Lyngse FP, Mortensen LH, Denwood MJ, Christiansen LE, Møller CH, Skov RL, et al. Sars-cov-2 Omicron Voc Transmission in Danish Households. *medRxiv* (2021). doi:10.1101/2021.12.27.21268278
48. Contreras S, Dehning J, Mohr SB, Bauer S, Spitzner FP, Priesemann V. Low Case Numbers Enable Long-Term Stable Pandemic Control without Lockdowns. *Sci Adv* (2021) 7:eabg2243. doi:10.1126/sciadv.abg2243
49. Oliu-Barton M, Pradelski BSR, Aghion P, Artus P, Kickbusch I, Lazarus JV, et al. SARS-CoV-2 Elimination, Not Mitigation, Creates Best Outcomes for Health, the Economy, and Civil Liberties. *The Lancet* (2021) 397:2234–6. doi:10.1016/s0140-6736(21)00978-8
50. Czypionka T, Iftekhar EN, Prainsack B, Priesemann V, Bauer S, Calero Valdez A, et al. The Benefits, Costs and Feasibility of a Low Incidence Covid-19 Strategy. *The Lancet Reg Health - Europe* (2022) 13:100294. doi:10.1016/j.lanepe.2021.100294
51. Funk S, Salathé M, Jansen VAA. Modelling the Influence of Human Behaviour on the Spread of Infectious Diseases: a Review. *J R Soc Interf* (2010) 7:1247–56. doi:10.1098/rsif.2010.0142
52. Verelst F, Willem L, Beutels P. Behavioural Change Models for Infectious Disease Transmission: a Systematic Review (2010-2015). *J R Soc Interf* (2016) 13:20160820. doi:10.1098/rsif.2016.0820
53. Weston D, Hauck K, Amlöt R. Infection Prevention Behaviour and Infectious Disease Modelling: a Review of the Literature and Recommendations for the Future. *BMC public health* (2018) 18:336–16. doi:10.1186/s12889-018-5223-1
54. Bedson J, Skrip LA, Pedi D, Abramowitz S, Carter S, Jalloh MF, et al. A Review and Agenda for Integrated Disease Models Including Social and Behavioural Factors. *Nat Hum Behav* (2021) 1–13. doi:10.1038/s41562-021-01136-2
55. Buonomo B, Della Marca R. Effects of Information-Induced Behavioural Changes during the Covid-19 Lockdowns: the Case of Italy. *R Soc Open Sci* (2020) 7:201635. doi:10.1098/rsos.201635
56. Priesemann V, Balling R, Bauer S, Beutels P, Valdez AC, Cuschieri S, et al. Towards a European Strategy to Address the Covid-19 Pandemic. *The Lancet* (2021) 398:838–9. doi:10.1016/s0140-6736(21)01808-0
57. Cinelli M, Quattrocioni W, Galeazzi A, Valensise CM, Brugnoli E, Schmidt AL, et al. The Covid-19 Social media Infodemic. *Sci Rep* (2020) 10:16598–10. doi:10.1038/s41598-020-73510-5
58. Banerjee D, Meena K. Covid-19 as an “Infodemic” in Public Health: Critical Role of the Social media. *Front Public Health* (2021) 9:231. doi:10.3389/fpubh.2021.610623
59. Contreras S, Olivera-Nappa Á, Priesemann V. Rethinking Covid-19 Vaccine Allocation: it Is Time to Care about Our Neighbours. *The Lancet Reg Health - Europe* (2022) 12, 100277. doi:10.1016/j.lanepe.2021.100277
60. Thompson RN, Hill EM, Gog JR. SARS-CoV-2 Incidence and Vaccine Escape. *Lancet Infect Dis* (2021) 21:913–4. doi:10.1016/s1473-3099(21)00202-4
61. Ritchie H, Mathieu E, Rodés-Guirao L, Appel C, Giattino C, Ortiz-Ospina E, et al. *Coronavirus Pandemic (Covid-19)*. Our World in Data (2020). Available at: <https://ourworldindata.org/coronavirus>.
62. Viana J, van Dorp CH, Nunes A, Gomes MC, van Boven M, Kretzschmar ME, et al. Controlling the Pandemic during the SARS-CoV-2 Vaccination Rollout. *Nat Commun* (2021) 12:3674–15. doi:10.1038/s41467-021-23938-8
63. Lu L, Mok BW-Y, Chen L-L, Chan JM-C, Tsang OT-Y, Lam BH-S, et al. Neutralization of SARS-CoV-2 Omicron Variant by Sera from BNT162b2 or Coronavac Vaccine Recipients. *Clinical Infectious Diseases* (2021). doi:10.1093/cid/ciab1041
64. Petherick A, Goldszmidt R, Andrade EB, Furst R, Hale T, Pott A, et al. A Worldwide Assessment of Changes in Adherence to Covid-19 Protective Behaviours and Hypothesized Pandemic Fatigue. *Nat Hum Behav* (2021) 5: 1145–60. doi:10.1038/s41562-021-01181-x
65. Iftekhar EN, Priesemann V, Balling R, Bauer S, Beutels P, Calero Valdez A, et al. A Look into the Future of the COVID-19 Pandemic in Europe: an Expert Consultation. *Lancet Reg Health - Europe* (2021) 8:100185. doi:10.1016/j.lanepe.2021.100185

Conflict of Interest: The authors declare that the research was conducted in the absence of any commercial or financial relationships that could be construed as a potential conflict of interest.

The handling editor declared a past co-authorship with several of the authors EI, SB, SM, AV, MK, VP.

Publisher’s Note: All claims expressed in this article are solely those of the authors and do not necessarily represent those of their affiliated organizations, or those of the publisher, the editors and the reviewers. Any product that may be evaluated in this article, or claim that may be made by its manufacturer, is not guaranteed or endorsed by the publisher.

Copyright © 2022 Dönges, Wagner, Contreras, Iftekhar, Bauer, Mohr, Dehning, Calero Valdez, Kretzschmar, Mäs, Nagel and Priesemann. This is an open-access article distributed under the terms of the Creative Commons Attribution License (CC BY). The use, distribution or reproduction in other forums is permitted, provided the original author(s) and the copyright owner(s) are credited and that the original publication in this journal is cited, in accordance with accepted academic practice. No use, distribution or reproduction is permitted which does not comply with these terms.

MODEL-BASED ASSESSMENT OF SAMPLING
PROTOCOLS FOR INFECTIOUS DISEASE GENOMIC
SURVEILLANCE[†]

ABSTRACT

Genomic surveillance of infectious diseases allows monitoring circulating and emerging variants and quantifying their epidemic potential. However, due to the high costs associated with genomic sequencing, only a limited number of samples can be analysed. Thus, it is critical to understand how sampling impacts the information generated. Here, we combine a compartmental model for the spread of COVID-19 (distinguishing several SARS-CoV-2 variants) with different sampling strategies to assess their impact on genomic surveillance. In particular, we compare adaptive sampling, i.e., dynamically reallocating resources between screening at points of entry and inside communities, and constant sampling, i.e., assigning fixed resources to the two locations. We show that adaptive sampling uncovers new variants up to five weeks earlier than constant sampling, significantly reducing detection delays and estimation errors. This advantage is most prominent at low sequencing rates. Although increasing the sequencing rate has a similar effect, the marginal benefits of doing so may not always justify the associated costs. Consequently, it is convenient for countries with comparatively few resources to operate at lower sequencing rates, thereby profiting the most from adaptive sampling. Finally, our methodology can be readily adapted to study undersampling in other dynamical systems.

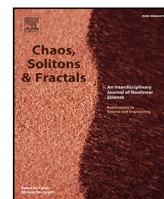
[†] This chapter is identical to the publication [28]. This article was published in *Chaos, Solitons & Fractals* 167, Contreras, S., Oróstica, K.Y., Daza-Sanchez, A., Wagner, J., Dönges, P., Medina-Ortiz, D., Jara, M., Verdugo, R., Conca, C., Priesemann, V. and Olivera-Nappa, Á.. *Model-based assessment of sampling protocols for infectious disease genomic surveillance*, p.113093. Copyright Elsevier (2023). Roles: Conceptualization, Methodology, Software, Validation, Formal analysis, Investigation, Writing – original draft, Writing – review & editing, Visualization.

Cite as: Contreras, S., Oróstica, K.Y., Daza-Sanchez, A., Wagner, J., Dönges, P., Medina-Ortiz, D., Jara, M., Verdugo, R., Conca, C., Priesemann, V. and Olivera-Nappa, Á., 2023. Model-based assessment of sampling protocols for infectious disease genomic surveillance. Chaos, Solitons & Fractals, 167, p.113093. <https://doi.org/10.1016/j.chaos.2022.113093>



Contents lists available at ScienceDirect

Chaos, Solitons and Fractals

journal homepage: www.elsevier.com/locate/chaos

Model-based assessment of sampling protocols for infectious disease genomic surveillance

Sebastian Contreras^{a,*}, Karen Y. Oróstica^b, Anamaria Daza-Sanchez^c, Joel Wagner^a, Philipp Dönges^a, David Medina-Ortiz^d, Matias Jara^e, Ricardo Verdugo^b, Carlos Conca^{c,e}, Viola Priesemann^{a,f,**}, Álvaro Olivera-Nappa^{d,g,***}

^a Max Planck Institute for Dynamics and Self-Organization, Am Faßberg 17, 37077 Göttingen, Germany

^b Instituto de Investigación Interdisciplinaria, Vicerrectoría Académica, Universidad de Talca, Talca, Chile

^c Centre for Biotechnology and Bioengineering, Universidad de Chile, Santiago, Chile

^d Departamento de Ingeniería en Computación, Universidad de Magallanes, Punta Arenas, Chile

^e Departamento de Ingeniería Matemática, Universidad de Chile, Santiago, Chile

^f Institute for the Dynamics of Complex Systems, University of Göttingen, Göttingen, Germany

^g Departamento de Ingeniería Química, Biotecnología y Materiales, Universidad de Chile, Santiago, Chile

ARTICLE INFO

Dataset link: https://github.com/Priesemann-Group/sampling_for_genomic_surveillance

Keywords:

Genomic surveillance
COVID-19
SARS-CoV-2
Dynamical systems
Sampling
Undersampling

ABSTRACT

Genomic surveillance of infectious diseases allows monitoring circulating and emerging variants and quantifying their epidemic potential. However, due to the high costs associated with genomic sequencing, only a limited number of samples can be analysed. Thus, it is critical to understand how sampling impacts the information generated. Here, we combine a compartmental model for the spread of COVID-19 (distinguishing several SARS-CoV-2 variants) with different sampling strategies to assess their impact on genomic surveillance. In particular, we compare *adaptive sampling*, i.e., dynamically reallocating resources between screening at points of entry and inside communities, and *constant sampling*, i.e., assigning fixed resources to the two locations. We show that adaptive sampling uncovers new variants up to five weeks earlier than constant sampling, significantly reducing detection delays and estimation errors. This advantage is most prominent at low sequencing rates. Although increasing the sequencing rate has a similar effect, the marginal benefits of doing so may not always justify the associated costs. Consequently, it is convenient for countries with comparatively few resources to operate at lower sequencing rates, thereby profiting the most from adaptive sampling. Finally, our methodology can be readily adapted to study undersampling in other dynamical systems.

1. Introduction

Genomic sequencing tools help to characterise and keep track of the genetic properties of pathogens causing infectious diseases and strongly contribute to evidence-based decision-making in public health [1,2]. High-throughput, next-generation sequencing technologies (NGS) have substantially reduced sequencing costs over the past 15 years [3], thereby bringing them closer to routine clinical and public health practices [4]. An important example is the genomic surveillance of infectious diseases, where the mutational dynamics of a particular pathogen (and variants thereof) are tracked and quantified [5]. In the context of the COVID-19 pandemic, genomic surveillance has unveiled the rapid evolution of SARS-CoV-2 and signalled the emergence of

variants with increased transmissibility and partial immune escape (e.g., those labelled as Variants of Concern VoC) [6–11].

The snapshots provided by genomic surveillance serve three primary purposes [12,13]; (i) to signal the introduction of novel variants to a country through surveillance at points of entry (POEs) or detect emerging variants within the communities, (ii) to quantify the fraction of the total cases detected in community transmission that these variants caused (thereby enabling the quantification of their spreading rate [7,8]), and (iii) to design and tailor diagnosis and therapeutic alternatives (e.g., drugs and vaccines). However, how reliable this information is depends on (i) the quality of the *sampling protocol*, i.e., the strategy to select which PCR-positive samples would be sent for

* Corresponding author.

** Corresponding author at: Max Planck Institute for Dynamics and Self-Organization, Am Faßberg 17, 37077 Göttingen, Germany.

*** Correspondence to: Centre for Biotechnology and Bioengineering, Universidad de Chile, Beauchef 851, Santiago 8370448, Chile.

E-mail addresses: sebastian.contreras@ds.mpg.de (S. Contreras), viola.priesemann@ds.mpg.de (V. Priesemann), aolivera@ing.uchile.cl (Á. Olivera-Nappa).

<https://doi.org/10.1016/j.chaos.2022.113093>

Received 14 July 2022; Received in revised form 20 December 2022; Accepted 28 December 2022

Available online 3 January 2023

0960-0779/© 2022 Elsevier Ltd. All rights reserved.

genomic sequencing [13], and (ii) the total number of samples analysed per week (i.e., the *sequencing rate*).

Although official recommendations state that sampling protocols should be coordinated, adaptive, representative, and serve differential purposes [13,14], the guidelines to achieve these goals lack a quantitative analysis of the benefits that these concepts bring. Moreover, the optimal strategy is not universal but is expected to depend on a country’s resource availability. Despite decreasing costs for NGS, the economic barriers raised by the high equipment and training costs remain prohibitory for low-to-middle income countries [5,6,15–19]. Therefore, exploring how different sampling protocols for genomic surveillance determine the information we gather can help these nations to optimise resource allocation.

In our work, we propose a hybrid (deterministic/stochastic) model-based approach to assess the effectiveness of sampling protocols for genomic surveillance on a country-level scale. We focus on answering how to allocate limited sequencing resources best to ensure the early detection of variants, in a setting where: (i) sequencing capacity is limited, (ii) new variants are imported and enter the system through the POEs, as an external input, and (iii) sampling is representative and corrects for potential heterogeneities in the population. First, we simulate the ground truth dynamics for the simultaneous spread of several SARS-CoV-2 variants using a deterministic differential equations model. Then, we build a stochastic framework to emulate sampling over temporal trends, enabling us to assess the performance of arbitrarily complex sampling protocols. In particular, we compare *adaptive* sampling (dynamically reallocating resources between screening at points of entry and communities according to new variants’ detection) and *constant* sampling (sequencing a fixed number of samples from each source). We assess the performance of each strategy through their (i) variant detection delay (time between the introduction and first detection of a variant in community transmission), and (ii) how well these can approximate the ground truth dynamics by estimating the share of the total cases that each of these represent (and thereby inform inference models). Besides, our approach constitutes a methodological advance that can be readily adapted to model sampling in other systems far from equilibrium. Altogether, we provide new quantitative insights to optimise sampling protocols for genomic surveillance and evidence for the benefits of using adaptive sampling, especially in countries with limited sequencing capacity.

2. Methods overview

2.1. Hybrid approach to simulate genomic surveillance in realistic settings

To assess and compare the performance of adaptive and constant sampling protocols, we need to test them under the same conditions. Besides, to determine which one approximates the true underlying dynamics better, we need to (approximately) know the system’s state at each time (i.e., its ground truth). As that is not possible in real settings, we propose a model-based hybrid approach: First, we formulate a deterministic mathematical model to represent the simultaneous spread of several SARS-CoV-2 variants in a closed population and thereby produce the ground truth of our system, i.e., the variant-resolved COVID-19 incidence over time. Second, we compare different protocols to determine the origin of samples that will be sent for sequencing (i.e., sampling protocols). Finally, we evaluate the performance of each protocol by quantifying (i) how well the share of new COVID-19 cases caused by each variant at a given time is represented and (ii) the delay between the true introduction of a new variant and its first detection in community transmission (hereafter *detection delay*).

In the following, we introduce general aspects of the model for disease spread, the numerical experiments and scenarios that we propose, and the implementation of sampling for genomic surveillance. Full details can be found in Methods, Section 5.

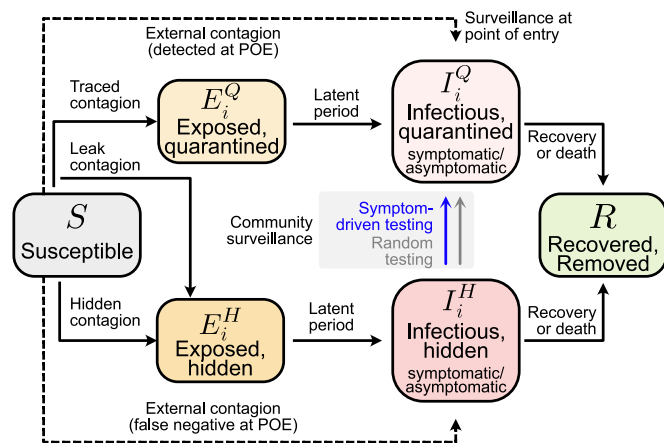


Fig. 1. Flowchart of the complete model. The solid blocks in the diagram represent different SEIR compartments for both hidden and quarantined individuals. Hidden cases are further divided into symptomatic and asymptomatic carriers. Solid lines represent the natural progression of the infection (contagion, latent period, and recovery). Dashed lines account for the external influx of infections, while testing is represented by arrows moving individuals from the hidden to the quarantined infectious compartment. Quarantined compartments, which contribute less to the spreading of the disease, are coloured with paler shades. (For interpretation of the references to colour in this figure legend, the reader is referred to the web version of this article.)

2.2. Model overview

We study the spread of COVID-19 using a deterministic ordinary differential equations (ODE) susceptible–exposed–infectious–recovered (SEIR) compartmental model, where several SARS-CoV-2 variants can spread simultaneously. In our model (adapted from [20,21] and schematised in Fig. 1), we distinguish between two contributions of infections: hidden and quarantined. Hidden infections are those where the infector is unaware of being infectious. Therefore, hidden chains propagate unnoticed in the communities until detected via testing. On the other hand, quarantined infectious individuals can also infect others due to imperfect isolation and limited compliance. However, quarantined infections spread at a much lower rate than hidden infections. We assume that individuals are equally susceptible to all SARS-CoV-2 variants before they had any infection, and after recovery, they obtain cross-immunity against infection. Hence, there is not explicit immune-escape in the timeframe considered.

From the point of view of most (in particular small) countries, new SARS-CoV-2 variants were often introduced from abroad over the course of the COVID-19 pandemic. To reflect that in the model, we include a non-zero influx $\Phi_i(t)$ of new cases that acquired the virus variant i abroad, reentering our system through points of entry (POEs). These imported variants, labelled as variants of concern (VoCs) abroad, subsequently spread in the communities. In addition, to increase our model’s flexibility, we distinguish between symptomatic and asymptomatic infections and allow for potentially different asymptomatic ratios and test sensitivity across variants. Finally, since testing is explicitly considered in our model, we can estimate the “observed” new COVID-19 cases detected via PCR testing (and the collection of samples that can be selected for sequencing). Although we know, by construction, which SARS-CoV-2 variant caused each case, this information is only revealed in each sampling strategy if the sample is selected for sequencing.

2.3. Scenarios for the baseline spreading dynamics

We formulate different scenarios for the baseline spreading dynamics of COVID-19 at a country-scale, thereby evaluating different patterns for the theoretical waves of incidence. We assume that variants can only be imported from abroad, and that they are introduced to

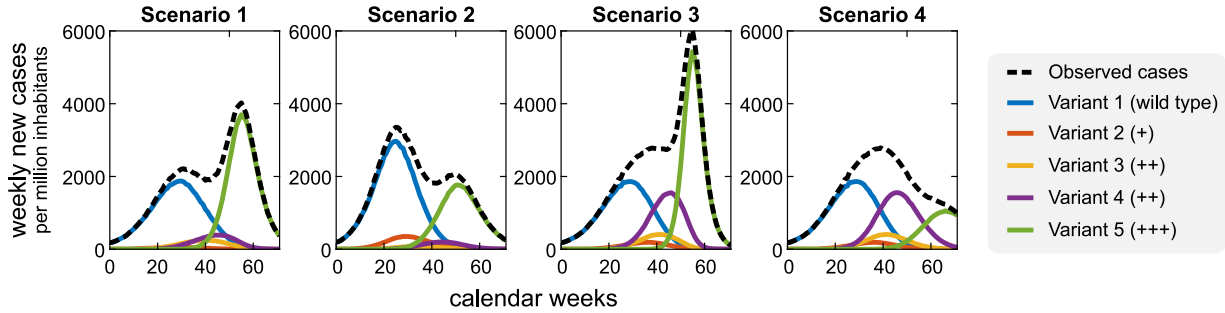


Fig. 2. Scenarios considered for waves of incidence. To evaluate sampling strategies, we define a set of scenarios that differ in the transmissibility and time of introduction of a new variant, represented by different colours (variants’ spreading parameters are reported in Table 1). Without genomic surveillance, policymakers would only observe the bulk trend of PCR-positive COVID-19 new cases (dashed line) without noticing new variants’ emergence and replacement dynamics. In the figure legend, “+” represents increased transmissibility compared to that of the wild type. Scenario 1: double peak (second higher), two dominant variants. Scenario 2: double peak (first higher), two dominant variants. Scenario 3: double peak (second higher), three dominant variants. Scenario 4: single peak, three dominant variants. A systematic analysis of wave patterns is provided in Supplementary Materials, Section S2. (For interpretation of the references to colour in this figure legend, the reader is referred to the web version of this article.)

Table 1
Influx parameters and differential transmissibility of (theoretical) SARS-CoV-2 variants across scenarios.

Variant	Scenario	ϕ_i^{\max}	a_i	b_i	T^{in} [days]	R_0^i
1	1	1000	3	4	-5	1.5
	2					1.6
	3					1.5
	4					1.5
2	1	1500	4	5	50	1.5
	2				30	1.8
	3				75	1.75
	4				75	1.75
3	1	1000	3	6	75	1.8
	2				100	2
	3				100	2
	4				100	2
4	1	1500	3	5	125	2
	2				150	2.5
	3				125	2.25
	4				125	2.25
5	1	500	2	5	200	3
	2				150	3
	3				250	4.5
	4				250	3.5

the system through the POEs (and represent this as an external input to the system of ODEs). As a general rule, in each scenario, we set (1) initial conditions, (2) time of introduction of each variant, and (3) transmissibility of each variant (through their adjusted reproduction number R_0^i). Note that the R_0^i values capture both the variant base transmissibility and the reductions induced by non-pharmaceutical interventions (NPIs) and hygiene measures. Thus, R_0^i are lower than typically reported base reproduction numbers for SARS-CoV-2 variants (Tables 1 and 2). We initialise our system with a single variant in the population and introduce the following ones as an influx to the system acting at different times, defined per scenario. After solving the system of ODEs that define our model, we estimate the “observed” cases at POEs and communities, and accumulate them to obtain weekly trends (typical temporal resolution for sequencing rates).

We use our model to answer the following question: Given a specific sampling protocol for genomic surveillance (adaptive or constant sampling), how long will it take until we detect a newly introduced variant in community transmission? To that end, we study a system where one variant is dominant, and a second one (with higher transmissibility) enters the system at a given time. We systematically explore different combinations of transmissibility and time of introduction, generating continuous wave patterns. The results are summarised in Supplementary Section S2. Additionally, we decided to illustrate our methodology by studying four markedly different scenarios, summarised in Fig. 2

and Table 1. We choose the scenarios in Fig. 2 motivated by typical wave patterns observed during the COVID-19 pandemic (e.g., [20]). In particular, scenarios 1 and 2 represent a situation where only two variants drive the wave, and other VoCs do not reach a significant share of the observed cases at any point (e.g., the wild type and Alpha waves in 2020/2021). Scenario 3 shows a situation where the “taking over” of a second variant is replaced by a third, much more transmissible variant (as the emergence of the Omicron VoC in 2021 [8,13]), leading to a markedly higher second peak. The last scenario (4) illustrates the situation where a single peak wave in observed cases hides multiple peaks of different variants. Note that different variants in this context do not refer to a particular VoC, but to a determined configuration of transmissibility and time of introduction, which can vary across scenarios (as described in Table 1).

2.4. Constant and adaptive sampling protocols

After estimating and discretising the weekly “observed” trends of new COVID-19 cases at POEs and communities, we sort them according to the variant they represent (see Fig. 3). Of the resulting vector S of length $[N_{(i)}^{X, \text{obs}}(t)]$ (with $X \in \{\text{POE, COM}\}$) representing the eligible positive samples collected in week t , we select $K_X(t)$ entries to be sequenced, thereby revealing their label (i.e., the variant i to which they belong). This is done by drawing $K_X(t)$ random numbers between 1 and $[N_{(i)}^{X, \text{obs}}(t)]$, and identifying to what variant the corresponding entries in S belong. We repeat the sampling stage several times to obtain meaningful statistics. As the overall sequencing rate K is constant, we must ensure that $K_{\text{POE}}(t) + K_{\text{COM}}(t) = K$.

As described above, we test two alternative sampling protocols for genomic surveillance: (i) *constant* sampling, i.e., destining a fixed amount of sequencing capacities to samples collected at POEs and communities, and (ii) *adaptive* sampling, i.e., dynamically reallocating sequencing capacity between POEs and communities. Reallocation of sequencing capacity in the adaptive protocol is determined by the following criterion: First, as we assume that after detecting a variant at POEs other cases would probably have bypassed the entry screening and thus be already spreading in the population, parts of the sequencing capacity at POEs should be reallocated to surveillance in communities. Second, if the variant the fraction of the total cases represented by a given variant (hereafter, *variant share* f_i) estimated from the community contagion (f_i^{COM}) does not change much over time (i.e., that $|f_i(t) - f_i(t-1)| \leq \epsilon$ arbitrarily small), the variant replacement dynamics have reached an equilibrium. In that case, the baseline sequencing capacity at POEs should be reinstated. We provide a detailed description of the mathematical formulation of the protocols (e.g., the equilibrium criteria for equilibrium in variant shares in the adaptive case) and parameter values in the Methods section, Sections 5.7 and 5.8.

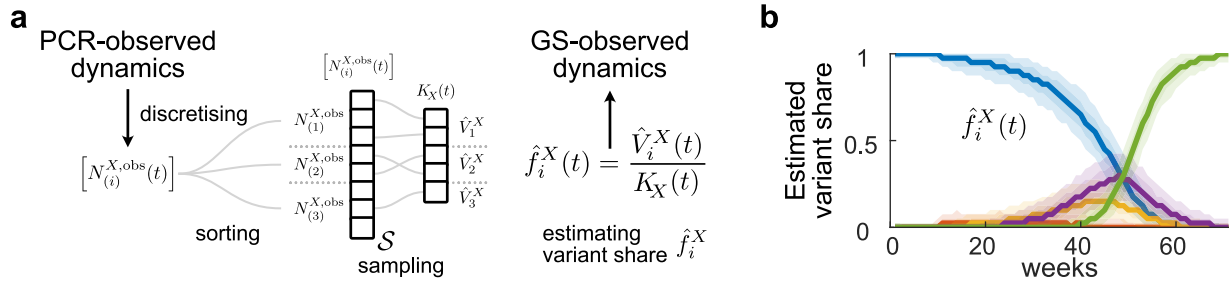


Fig. 3. Description of the genomic surveillance framework implemented in this work. a: We discretise the “observed” weekly new COVID-19 cases, understood as a collection of PCR-positive samples eligible for genomic surveillance (GS), and sort them according to the variant that caused them to create a vector S of labels. We then select $K_X(t)$ (X : point of entry or community) random samples from this pool of tests (i.e., entries of S) and reveal their label. We count the number of times that a variant i was detected this week, $\hat{V}_i^X(t)$, and estimate the share that they represent of total cases $\hat{f}_i^X(t)$, defined as the quotient $\hat{V}_i^X(t)/K_X(t)$. Finally, we repeat the random selection of samples an arbitrary number of times using different random seeds and study the resulting distributions (example in b).

Table 2
Model parameters.

Parameter	Meaning	Value (default)	Range	Units	Source
M	Population size	1 000 000		people	–
R_0^i	NPI-corrected reproduction number variant i	4	See Table 1	–	[22–24]
ν	Registered contacts (quarantined)	0.075		–	[20]
ϵ	Lost contacts (quarantined)	0.05		–	[20]
γ	Recovery/removal rate	0.10	0.08–0.12	day ⁻¹	[25,26]
ξ_i	Asymptomatic ratio for variant i	0.32	0.15–0.43	–	[27,28]
λ_s	Symptom-driven testing rate	0.25	0–1	day ⁻¹	Assumed
λ_r	Random testing rate	0.0	0.0–0.1	day ⁻¹	Assumed
η_i	Test sensitivity to variant i	0.9		–	Assumed
Φ_i	External influx of variant i	–	0–10	cases day ⁻¹	Assumed
ρ	Exposed-to-infectious rate	0.25		day ⁻¹	[29,30]
s_α	Stiffness adaptive response (α)	5		–	Assumed
s_ζ	Stiffness adaptive response (ζ)	1		–	Assumed
$A_{1/2}$	Middle point sigmoidal response (α)	0.25		–	Assumed
$\Theta_{1/2}$	Middle point sigmoidal response (ζ)	10		–	Assumed
a_0	Scaling factor (α)	5		–	Assumed
$\Delta K_{\text{COM}}^{\text{max}}$	Max adaptation of community surveillance	10		–	Assumed
$K_{\text{COM}}^{\text{max/min}}$	Max/min value for community surveillance	–	60%–95% $K_{\text{COM}}^{\text{base}}$	–	Assumed

3. Results

3.1. Adaptive sampling protocols significantly reduce variant detection delays and estimation errors

We assess the efficacy of the sampling protocols described above across scenarios, repeating the random selection of samples $m = 100$ times. We find that an adaptive protocol significantly reduces the (expected) detection delay compared to a protocol with constant sampling. Besides, the overall delay distribution in the former is narrower than in the latter. While this result is consistent across scenarios (see Fig. 4), the reduction in dispersion achieved through an adaptive protocol is secondary to increasing the sequencing rate K .

Depending on the value of K , an adaptive protocol can detect a variant in community transmission a couple of weeks earlier than a constant sampling protocol. Although we focus on and emphasise improvements regarding the time of variant detection, an adaptive sampling protocol also improves the accuracy of the estimated trends for variant shares (see Supplementary Material, Section S4).

3.2. The marginal benefits of increasing the sequencing rate decline quickly

We now analyse the expected detection delay D for both adaptive and constant sampling protocols in all scenarios, as a function of the sequencing rate K . We observe that settings with low base sequencing rates would substantially profit from increasing it, by means of reducing the detection delay more steeply when adding an extra unit of K . However, such improvement quickly reaches a plateau; further reductions of the expected detection delay would require major increases in K (cf.

Fig. 5). In other words, these improvements would cost a much higher price.

The sharp decrease in the detection delay D when increasing K resembles an exponential decay. For analytical purposes only, we fit an exponential function to the empirical trends for the median detection delay in Fig. 5. The equation for the exponential fit is given by

$$D(K) = D_0 \exp\left(-\frac{K - K_0}{K_{\text{ref}}}\right) + D_\infty, \quad (1)$$

where D_0 represents the expected delay for the minimum sampling K_0 , K_{ref} is a reference sequencing rate, and D_∞ represents the minimum delay we can reach. Fitted trends agree well with our simulations for both adaptive and constant sampling protocols (cf. the overlap between solid and dashed lines in Figs. 5 and S2). We also performed this experiment for the constant sampling protocol (see Supplementary Fig. S2). While both graphics look very alike, there are marked differences between the two. For example, differences in the average detection delay for both protocols can be as large as five weeks when the sequencing rate K is low and quickly decline as we increase the sequencing rate K (Fig. 6). However, the benefits of using an adaptive protocol also depend on the number of co-circulating variants; if there are several variants in the pool of infections, improvements by using an adaptive sampling persist to higher sequencing rates (Fig. 6).

In the following section, we use the analytical approximation we propose for the expected variant detection delay to generalise our results to an economic perspective.

3.3. Economic assessment of strategies for genomic surveillance

As the early detection of variants in community transmission allows policymakers to timely implement measures to mitigate their impact,

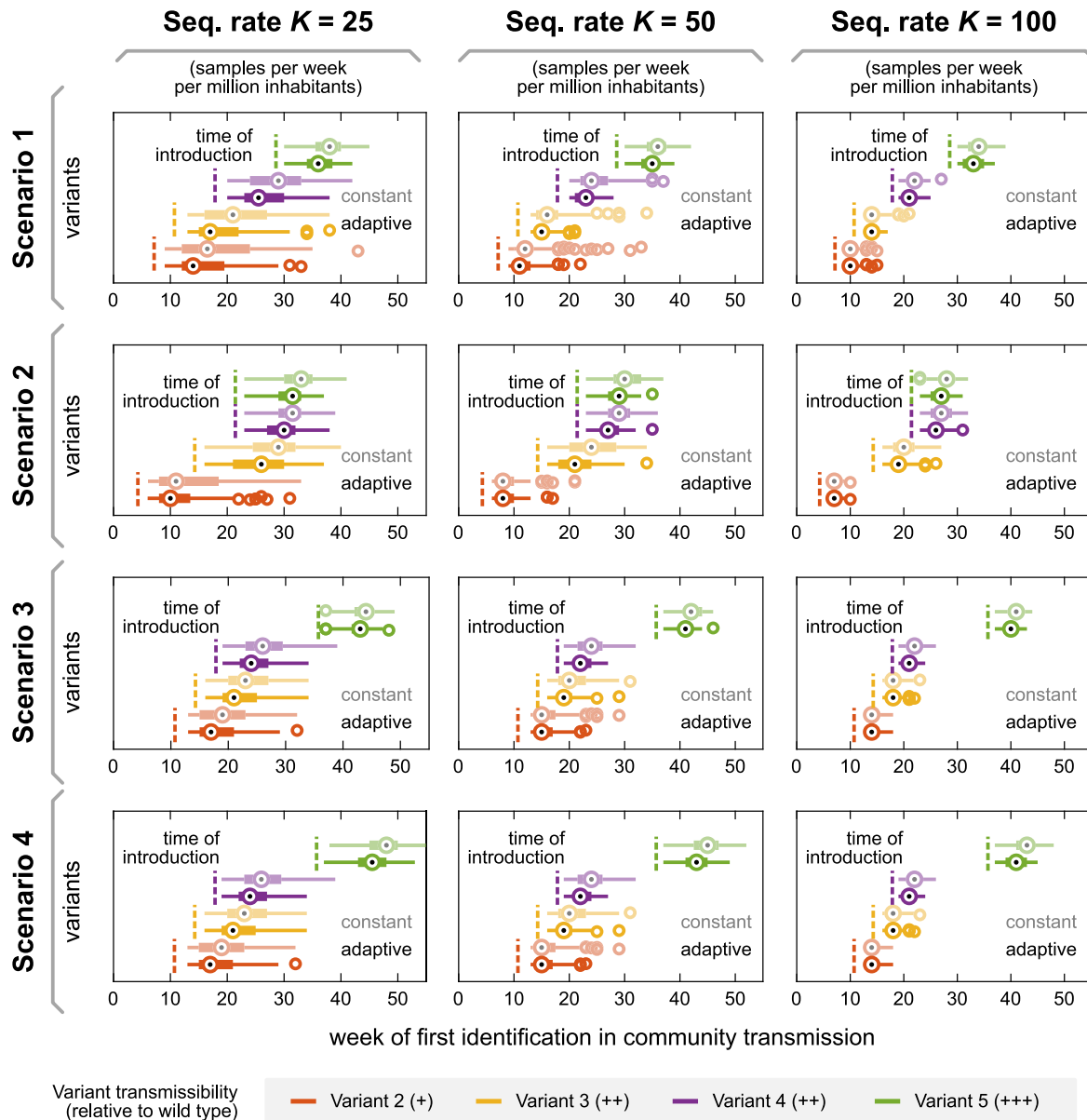


Fig. 4. Variant detection time across scenarios for different sampling protocols and sequencing rates. An **adaptive** sampling protocol for genomic surveillance (i.e., dynamically reallocating sampling resources between POEs and community) reduces the time between variant introduction (dashed line) and the first detection in community transmission significantly when compared to a protocol with **constant** sampling in POEs and community (solid vs. faded, see statistical significance levels in Tabs. S1 and S2, and description of both strategies in Section “Constant and adaptive sampling protocols” and Methods). Variants are colour-coded as in Fig. 2, and “+” represents their increased transmissibility compared to the wild type. Here, boxplots represent results using different random seeds for the sampling stage ($m = 100$ realisations). Besides reducing the expected time of first detection, an adaptive protocol also reduces the variance of the distribution. However, this effect is secondary to increasing the sequencing rate K , which can reduce both median times and variability more drastically. Black dots represent medians, boxes the interquartile range of the distribution (upper quartile: 0.75 quantile, lower quartile: 0.25 quantile), and whiskers its range excluding outliers. Outliers (represented as circles) are defined as elements more than 1.5 interquartile ranges above the upper quartile or below the lower quartile. (For interpretation of the references to colour in this figure legend, the reader is referred to the web version of this article.)

reducing the detection delay would benefit all actors in society. In economic terms, this defines an *utility* function $U(D)$ that increases as we reduce D . As per the observations in the previous section, we know that D decreases when we increase the number of samples analysed K . The question is then how much extra benefit an extra unit of K would produce, i.e., what is the *marginal utility* of increasing K . Speaking against increasing K , the *marginal costs* of increasing it should grow linearly while well below the sequencing capacity limit given by country-specific infrastructure ($K_{country}^{lim}$) and should strongly increase when approaching it. Assuming that the variant detection delay profiles remain unchanged across countries, we can study the optimal number of sequences that should be analysed per week. In other words, the

sequencing rate from which the marginal benefits reached by increasing K would not justify the required costs.

Using the mathematical formulation for the marginal utility and costs presented in Supplementary Section S1 (Supplementary Eqs. (2) and (3)), we schematise the criteria for economically-optimal sequencing in two types of countries (Fig. 7a). On the one hand, countries with high installed sequencing capacities $K_{country}^{lim}$ can increment the number of samples they analyse per week without incurring in higher additional costs. On the other hand, countries with less sequencing infrastructure or specialised workforce will see their costs increase disproportionately larger for lower K , finding their sequencing optimum K_1^{lim} at fewer samples per week. In that case, instead of searching to increase K beyond K_1^{lim} , these countries would find it more rewarding

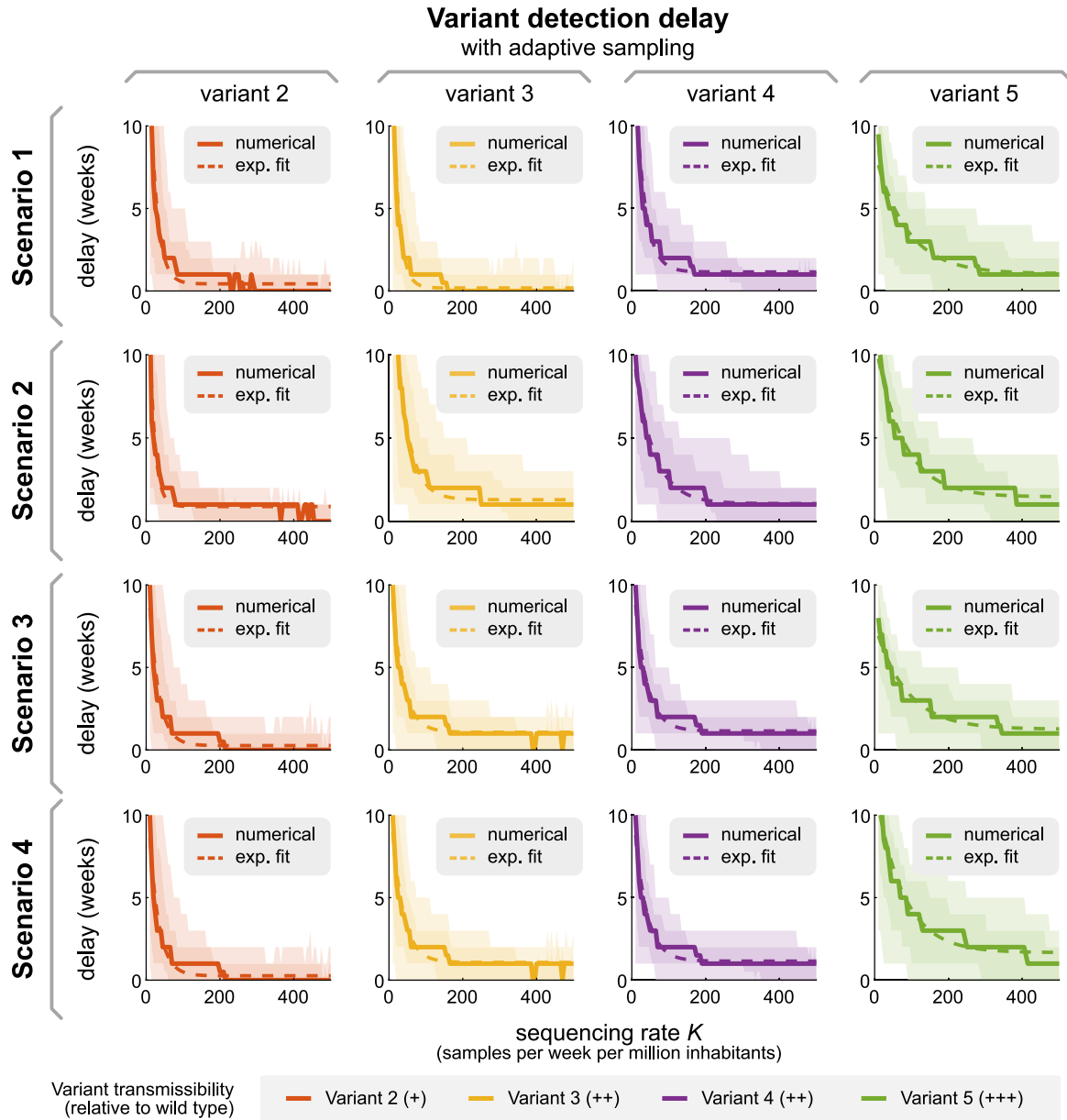


Fig. 5. Across scenarios, increasing the sequencing rate K strongly decreases the detection delay for all variants. Solid lines represent the median delay between true introduction and first detection of different SARS-CoV-2 variants across scenarios, and dashed lines represent proposed exponential function (cf. Eq. (1)). Shaded areas denote sample variability (dark: 68%, light: 95%). Results for a constant sampling protocols are provided in Supplementary Fig. S2.

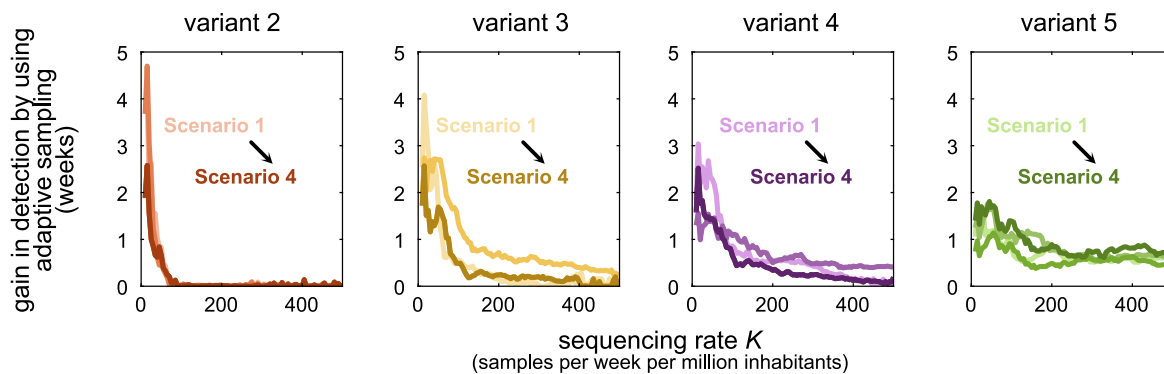


Fig. 6. Across scenarios, the gains of using an adaptive sampling protocol instead of constant sampling are higher for lower values of K . Although the overall dependency on K is similar for both sampling protocols, i.e., both decay exponentially, differences in the detection delay obtained by each (averaged across realisations) are markedly stronger for lower K in all scenarios. Furthermore, how quickly this difference vanishes when increasing K also seems to depend on the number of variants spreading simultaneously. Note that scenarios 3 and 4 only differ in the parametrisation of the last variant (5) (see Table 1), and thus coincide for variants 2–4.

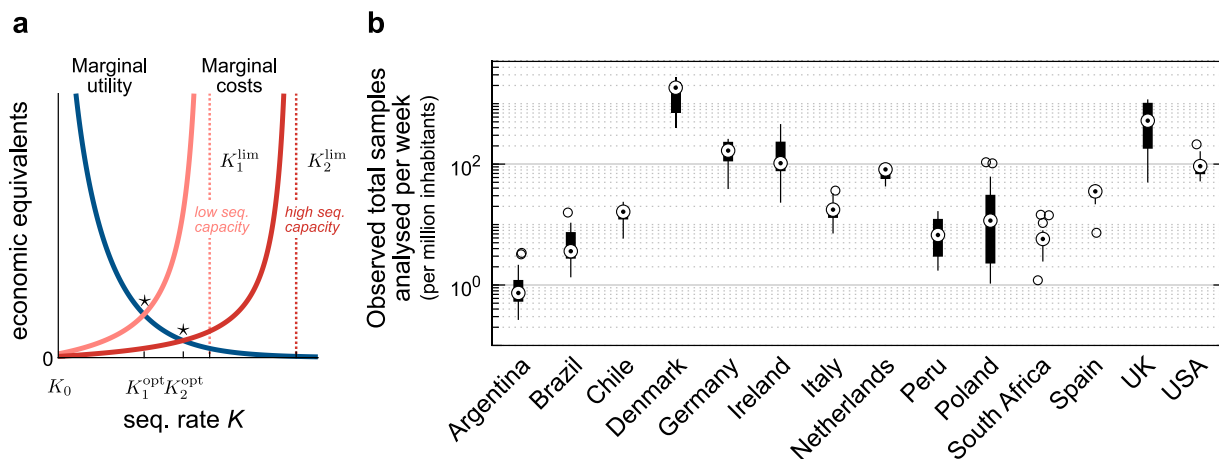


Fig. 7. Cost-benefit analysis of increasing the sequencing rate in countries with different sequencing capacity. a: Based on economic terms, countries with less installed sequencing capacity K^{lim} will see their operational cost escalate considerably at a lower number of sequences analysed per week (K), finding their operational optima at lower values. b: Observed weekly sequencing rate K^{obs} for different countries worldwide, normalised per million inhabitants. The logarithmic scale used to represent the y axis facilitates comparing observed sequencing rates across countries, where differences can be of orders of magnitude. Boxplots describe the K^{obs} values observed between Feb. 2nd, and Jun. 4th, 2022.

to reallocate those resources into other active interventions, such as subsidies for lockdowns and the distribution of hygiene materials to the general population. While these economic principles are clear, how much improvements in reducing D are valued in a given country needs to be quantified in economic terms by local policymakers.

Analysing real-world data of the observed sequencing rates K in countries worldwide, we see a sizeable week-to-week variability (see Fig. 7b). For example, countries in the global north have higher observed sequencing rates and dispersion overall (week-to-week variations in K). This can be due to the protocols they follow for sequencing; rather than being the installed capacity $K_{\text{country}}^{\text{lim}}$ which limits the rate, they aim to send a fixed fraction of the observed new cases for sequencing [31].

4. Discussion

In our manuscript, we used a hybrid model-based approach combining deterministic ODE models with a stochastic sampling framework to assess the effectiveness of different sampling protocols for genomic surveillance. Our quantitative insights support the benefits of using adaptive sampling, where sequencing efforts are reallocated between surveillance at points of entry (POEs) and communities according to the progression of the disease. We showed that adaptive sampling protocols outperform protocols where a constant amount of sequencing capacity is allocated to POE and community samples. These results hold across incidence wave patterns (scenarios and systematic analysis, cf. Supplementary Section S2) and values for the sequencing rate K .

Compared with a constant sampling protocol, adaptive sampling can reduce the expected detection delay of introduced variants by a couple of weeks at the same sequencing rate K , especially when operating at low sequencing rates. Timely detecting a new variant is critical to mitigating its potential impacts, especially for diseases that spread fast. For example, considering the doubling time of Omicron VoC infections (between 1.5 and 3 days in its initial stages [24]), detecting its introduction two weeks later (i.e., ~ 5 doubling times later) implies dealing with an incidence $\sim 30x$ larger. Therefore, using an adaptive protocol allows policymakers to react earlier to emerging public health threats, thereby facilitating containment through test-trace-and-isolate [20,21] and minimising disruptions to everyday life and economies [32,33]. We also showed that K is the strongest determinant for reducing the detection delay D . In fact, D declines exponentially when increasing K . However, this also implies that the benefits earned by expanding K by an extra unit decline similarly and would soon not justify the high costs incurred. Thus, there is a cost-effective optimal K , which depends on

the installed sequencing capacity of a given country $K_{\text{country}}^{\text{lim}}$ and how local policymakers weigh reductions in D in economic terms.

Despite decreasing sequencing costs induced by technological advancements, genomic surveillance is still costly as it requires specialised equipment, high-performance computing capability, and specialist personnel. Thus, it raises economic barriers that not all countries can circumvent [5,6,15–19]. This translates to little elasticity to changing the sequencing rate K , and inspired our assumption of setting it constant. For example, in Chile, despite the governmental and private investments in genomic surveillance, the sequencing rate is around 400 samples per week (i.e., 20 samples per million inhabs.), at least two orders of magnitude lower than the UK's surveillance program, with a sequencing rate larger than 10% of their positive weekly tests ([6,31,34], and Fig. 7b). Therefore, most decisions have been based on trends of the current reproduction number, which, however, does not capture the spreading dynamics of VoCs [35–39]. The situation is similar in other countries in LATAM and the global south, where countries have not reached a sequencing rate of 1% of their positive tests [31]. Overall, sequencing rates and genomic surveillance programmes are markedly different between high and low-income countries, where the sequences reported by the former are 12 times higher than the latter. Furthermore, the ratio of confirmed cases sequenced by high-income countries is 16 times higher than that of low-income countries (4.36% and 0.27%, respectively) [6]. This again highlights the economic determinants of success in pandemic control [40–44].

Following the same line of thought, we formulate our model assuming that the sequencing capacity is the limiting factor for surveillance and apply it to study how different sampling protocols (i.e., distributions of this capacity between points of entry and communities) can help to reduce the variant detection delay. This restricts our analysis to settings where variants enter the system through defined points, and sampling protocols guarantee representativeness and correct for potential heterogeneities among the population. Examples of that are small countries with singular points of entry or isolated communities within a country [8,45]. An equally important question in settings with more sequencing capacity is how much sequencing is required to correctly estimate the share of the total cases corresponding to a given variant. This question is thoroughly studied in [46], where the authors determine, for different scales, the required number of sequences to be analysed to estimate the share of cases belonging to each variant. This question is critical to determine whether a newly detected variant is taking over and should be considered a VoC. However, as we study a setting resembling a small country where variants are introduced from abroad, it falls outside the scope of this paper.

Our deterministic model for disease spread has certain limitations. For example, we do not include age structure in our model, as we do not intend to quantify the impacts in morbidity/mortality that different variants may cause. We also do not include vaccination or waning immunity, as these are unessential within the time frame we analyse. In fact, in the timeframe we study here, more than 90% of the population had only one infection, and only a tiny fraction had two or more. Furthermore, although vaccination effectively reduces morbidity and mortality rates from COVID-19, the effect that this process generates on the transmissibility of a given variant, especially Omicron, is relatively small (e.g., [47–49]). Therefore, vaccination was not considered an essential variable in this modelling. There is also no spatial resolution in the model (as in, e.g., [38,50]) as we assume sampling to be representative, and these would only affect wave patterns (which do not compromise our results). Besides, we excluded contact tracing from our model; samples collected within the same infection chain are likely caused by the same SARS-CoV-2 variant (thus, including them would induce selection biases in our analyses). Finally, for simplicity, we assume that genomic surveillance does not affect variant transmissibility while, in real settings, information about a new variant is likely to trigger new interventions. However, this is straightforward to incorporate by including a feedback loop between the estimated variant share \hat{f}_i and the overall spreading rate (as, e.g., in [51–53]), and does not play a role in the metrics we analyse (i.e., detection delay and mismatch between estimations and ground truth). Nonetheless, the model is simple enough to serve our objective fully: To produce quantitative insights on the performance of different sampling protocols for genomic surveillance in detecting introduced variants and reducing the uncertainty of their inference with the available resources.

Similar sampling approaches to ours can, in principle, be applied to many other physical problems. Limited sampling poses a challenge when trying to access properties of various complex dynamical systems [54,55]. Furthermore, undersampling may introduce systematic bias to observations that need to be corrected [56–58]. This can happen, for example, when assessing *collective* properties, like graph structures in a network or activity clusters spanning large fractions of the system. In the case of detecting SARS-CoV-2 variants, such undersampling bias is not expected because the random selection of a PCR-positive sample is representative. Here, the core challenge is economical; how much we can sample depends on the resources destined for genomic surveillance. Thus, it is crucial to implement methods to maximise the information gathered with the available resources. Our work demonstrates the benefits of using adaptive sampling in genomic surveillance and quantifies the improvements reached by increasing the installed sequencing capacity to reduce the detection delay of newly introduced variants. Besides, the proposed methodology can readily be adapted to study other dynamical systems far from equilibrium or arbitrarily complex sampling protocols. This is crucial to assess current protocols and design contingency plans for current and future global health emergencies, especially in settings where resources are limited.

5. Methods

5.1. Spreading dynamics

We propose a modified SEIR-type model to adequately capture COVID-19 spread, where infected individuals can be either symptomatic or asymptomatic, and their infection can be caused by several co-circulating SARS-CoV-2 variants. They belong to hidden (E_i^H, I_i^H) or quarantined (E_i^Q, I_i^Q) pools of infections, thus creating in total one compartment of susceptible individuals (S), two compartments of exposed individuals (E_i^H, E_i^Q), three compartments of infectious individuals ($I_i^{H,s}, I_i^{H,a}, I_i^Q$), and one compartment for recovered/removed individuals (R). Model compartments, transitions between them, and testing mechanisms are illustrated in Fig. 1.

New infections are asymptomatic with a variant-specific ratio ξ_i , the remaining infections are symptomatic. In all compartments, individuals are removed at a rate γ because of recovery or death (see Table 2 for all parameters). In the hidden pools, the disease spreads according to the population's contact patterns and the base transmissibility of the variants. Here, we parameterise the spreading rate of SARS-CoV-2 variants through their NPI-corrected reproduction number R_0^i . In this parameter, we combine the base spreading properties of the variant (as per their base reproduction number) with typical levels of contact reductions induced by moderate restrictions. This reproduction number R_0^i reflects the disease spread in the general population without the testing-induced isolation of individuals, nor current immunity levels. Additionally, the hidden pool receives a mobility-induced influx $\Phi_i(t)$ of new infections. Cases are removed from the hidden pool (i) when detected by testing and put into the quarantined pool I_i^Q , or (ii) due to recovery or death.

The quarantined exposed and infectious pools (E_i^Q, I_i^Q) contain those infected individuals who have been tested positive as well as their positively tested contacts. Infectious individuals in I_i^Q are (imperfectly) isolated; we assume their contacts have been reduced to a fraction $(\nu + \epsilon)$ of the ones they had in pre-COVID-19 times, of which only ν are captured by the tracing efforts of the health authorities. As traced cases generated by isolated individuals would be of the same SARS-CoV-2 variant, we do not include them into the pool of tests potentially sent for sequencing. The remaining fraction of produced infections, ϵ , are missed and act as an influx to the hidden pools (E_i^H). Therefore, the overall reproduction number in the I_i^Q pool is $(\nu + \epsilon)R_0$. See Table 3 for all model variables.

5.2. Testing strategies

We consider symptom-driven testing and random testing:

Symptom-driven testing is here defined as applying tests to individuals presenting symptoms of COVID-19. In this context, it is important to note that non-infected individuals can have symptoms similar to those of COVID-19, as many symptoms are rather unspecific. Although symptom-driven testing suffers less from imperfect specificity, it can only uncover symptomatic cases that are willing to be tested (see below). Here, *symptomatic, infectious individuals* are transferred from the hidden to the traced pool at rate λ_s .

Random testing is here defined as applying tests to individuals irrespective of their symptom status or whether they belong to the contact chain of other infected individuals. In our model, random testing transfers infected individuals from the hidden to the quarantined infectious pools with a fixed rate λ_r , irrespective of whether or not they are showing symptoms.

5.3. Model equations

$$\frac{dS}{dt} = -\underbrace{\gamma \frac{S}{M} \sum_{i=1}^k R_0^i I_i^H}_{\text{hidden contagion}} - \underbrace{\gamma \frac{S}{M} \sum_{i=1}^k (\epsilon + \nu) R_0^i I_i^Q}_{\text{quarantined contagion}} - \underbrace{\frac{S}{M} \sum_{i=1}^k \Phi_i(t)}_{\text{ext. influx}}, \quad (2)$$

$$\frac{dE_i^Q}{dt} = \underbrace{\gamma \frac{S}{M} \nu R_0^i I_i^Q}_{\text{observed contagion}} - \underbrace{\rho E_i^Q}_{\text{end of latency}}, \quad (3)$$

$$\frac{dE_i^H}{dt} = \underbrace{\gamma \frac{S}{M} R_0^i I_i^H}_{\text{hidden contagion}} + \underbrace{\gamma \frac{S}{M} \epsilon R_0^i I_i^Q}_{\text{leak contagion}} - \underbrace{\rho E_i^H}_{\text{end of latency}}, \quad (4)$$

$$\frac{dI_i^Q}{dt} = \underbrace{\rho E_i^Q - \gamma I_i^Q}_{\text{spreading dynamics}} + \underbrace{(\lambda_s + \lambda_r) \eta_i I_i^{H,s}}_{\text{testing, symptomatic}} + \underbrace{\lambda_r \eta_i I_i^{H,a}}_{\text{testing}}$$

$$+ \underbrace{\frac{S}{M} \Phi_i(t)}_{\text{ext. influx (POE detected)}}, \tag{5}$$

$$\frac{dI_i^{H,s}}{dt} = \underbrace{\xi_i \rho E_i^H - \gamma I_i^{H,s}}_{\text{spreading dynamics}} - \underbrace{(\lambda_s + \lambda_r) \eta_i I_i^{H,s}}_{\text{testing}} + \underbrace{\xi_i (1 - \eta_i) \frac{S}{M} \Phi_i(t)}_{\text{ext. influx (false negative at POE)}}, \tag{6}$$

$$\frac{dI_i^{H,a}}{dt} = \underbrace{(1 - \xi_i) \rho E_i^H - \gamma I_i^{H,a}}_{\text{spreading dynamics}} - \underbrace{\lambda_r \eta_i I_i^{H,a}}_{\text{testing}} + \underbrace{(1 - \xi_i) (1 - \eta_i) \frac{S}{M} \Phi_i(t)}_{\text{ext. influx (false negative at POE)}}, \tag{7}$$

$$\frac{dR}{dt} = \gamma \underbrace{\sum_{i=1}^k (I_i^Q + I_i^{H,a} + I_i^{H,s})}_{\text{recovered/removed individuals}}. \tag{8}$$

5.4. Initial conditions

Let x be the vector collecting the variables of all different pools:

$$x = [S, E_i^Q, E_i^H, I_i^Q, I_i^{H,s}, I_i^{H,a}, R]. \tag{9}$$

We assume a population size of $M = 10^6$ individuals, such that $\sum_i x_i = M$. We initialise all scenarios with only one variant (the wild type), and the following settings: $E_i^Q(0) = 50$, $E_i^H(0) = 1050$, $I_i^Q(0) = 100$, $I_i^{H,s}(0) = 250$, $I_i^{H,a}(0) = 750$, (for $i = 1$), and $S(0) = 997800$.

5.5. Modelling the influx of infections and the introduction of new variants

In our model, we incorporate a mechanism for externally acquired infections, i.e., individuals belonging to the population, but acquiring the virus (and variants thereof) overseas. Explicitly, they appear as an influx $\Phi_i(t)$, which we model as the overlap of different gamma-distributed pulses and constant contributions of “old” variants. Mathematically, the influx (as a vector of size k) is given by

$$\Phi(t) = \sum_{i=1}^k e_i \Phi_i^{\max} \Gamma(a_i, b_i)(t) + \Phi_{\text{base}} \frac{\sum_{i=1}^k e_i \mathbb{1}(T_i^{\text{in}} + \Delta_{\text{time}} \leq t \leq T_{i+1}^{\text{in}} + 2\Delta_{\text{time}})}{1 + \sum_{i>1}^k \mathbb{1}(T_i^{\text{in}} + \Delta_{\text{time}} \leq t \leq T_{i+1}^{\text{in}} + 2\Delta_{\text{time}})}, \tag{10}$$

where e_i are canonical unit vectors, a_i and b_i shape and scale parameters for the Gamma distribution, Φ_{base} the baseline influx of infections, T_i^{in} the time of introduction of the i ’th variant to the system, and Δ_{time} represents the time window where an old variant continues appearing in the influx. Values for variant-specific parameters across scenarios are given in Table 1.

5.6. Central epidemiological parameters that can be observed

In the real world, disease spread can only be observed through testing and contact tracing. While the *true* number of daily infections N is a sum of all new infections in the hidden and traced pools, the *observed* number of daily infections \hat{N}^{obs} is the number of new infections discovered by testing, tracing, and monitoring of the contacts of those individuals in the quarantined infectious pool I_i^Q , delayed by a variable reporting time. This includes internal contributions as well as contributions from testing and tracing:

$$N_i = \underbrace{\gamma k_i R_0^i \frac{S}{M} I_i^H}_{\text{hidden contagion}} + \underbrace{\gamma (v + \epsilon) R_0^i \frac{S}{M} I_i^Q}_{\text{observed contagion}} + \underbrace{\frac{S}{M} \Phi_i(t)}_{\text{ext. influx}} \tag{11}$$

$$\hat{N}_{\text{com},i}^{\text{obs}} = \left[\underbrace{\lambda_s I_i^{H,s}}_{\text{sympt. test}} + \underbrace{\lambda_r I_i^H}_{\text{rand. test}} \right] \otimes \mathcal{K}, \tag{12}$$

$$\hat{N}_{\text{POE},i}^{\text{obs}} = \left[\underbrace{\eta_i \Phi_i(t)}_{\text{test at POE}} \right] \otimes \mathcal{K}, \tag{13}$$

where \otimes denotes a convolution and \mathcal{K} an empirical probability mass function that models a variable reporting delay, inferred from German data (as the RKI reports the date the test is performed, the delay until the appearance in the database can be inferred): The total delay between testing and reporting a test corresponds to one day more than the expected time the laboratory takes for obtaining results, which is defined as follows: from testing, 50% of the samples would be reported the next day, 30% the second day, 10% the third day, and further delays complete the remaining 10%, which for simplicity we will truncate at day four. Considering the extra day needed for reporting, the probability mass function for days 0 to 5 would be given by $\mathcal{K} = [0, 0, 0.5, 0.3, 0.1, 0.1]$.

5.7. Modelling sampling protocols

As described earlier, we compare two sampling protocols for genomic surveillance throughout the manuscript, constant sampling and adaptive sampling. For the first case, we assume that the number of samples collected at POEs and communities remains constant so that K_{POE} and K_{COM} are constant. In contrast, an adaptive sampling protocol prioritises samples collected at POEs or communities depending on the genomic surveillance findings of the previous weeks. While markedly different, both start from the same baseline $K_{\text{POE}}(t = 0) = [0.6 K]$, and have the same thresholds $K_{\text{COM}}^{\min} = 0.6 K$ and $K_{\text{COM}}^{\max} = [0.95 K]$ (although these are meaningful only for the adaptive case). In the following section, we describe the adaptive sampling protocol in detail (see Table 3).

5.8. Adaptive sampling strategy for genomic surveillance

As described previously and in [13], genomic surveillance serves two objectives depending on where samples were collected. On the one hand, if samples are collected at POEs, these signal the introduction of novel variants to the country, and provide an alert of what we should look for in community transmission. On the other hand, samples collected from community transmission provide information on the local features of the spread of such variants, their mutational signatures, and their reproduction numbers. Let K be the total amount of samples that can be sequenced per week (i.e., the sequencing rate), and $K_{\text{COM}}(t)$ and $K_{\text{POE}}(t)$ be the amount of these that were taken from community contagion and at POEs, respectively, at time t . Then, $K = K_{\text{COM}}(t) + K_{\text{POE}}(t)$. In the adaptive sampling, we allow $K_{\text{COM}}(t)$ and $K_{\text{POE}}(t)$ to change over time depending on our estimations for the variant share at POEs and within the community, \hat{f}_i^{POE} and \hat{f}_i^{COM} . Thus, we define two quantities that will help us decide when to reallocate resources:

$$\Lambda(t) = \max_i \{ \hat{f}_i^{\text{POE}}(t - 1) - \hat{f}_i^{\text{COM}}(t - 1) \}, \tag{14}$$

$$\Theta(t) = \max_i \left\{ \frac{\partial \hat{f}_i^{\text{COM}}}{\partial t}(t - 1) \right\}, \tag{15}$$

where ∂ denotes a discrete derivative. When $\Lambda(t)$ is large, variants being introduced to the country are not yet markedly spreading in the community. When $\Theta(t)$ is large, the replacement dynamics are far from equilibrium — in either way, we require more sequencing in the community. We use a logistic function to smooth the response, and two auxiliary variables:

$$\alpha(\Lambda) = \alpha_0 \frac{\exp(s_\alpha(\Lambda - \Lambda_{1/2}))}{1 + \exp(s_\alpha(\Lambda - \Lambda_{1/2}))}, \tag{16}$$

$$\zeta(\Theta) = \frac{1}{1 + \exp(s_\zeta(\Theta - \Theta_{1/2}))}. \tag{17}$$

so that

$$\frac{\partial K_{\text{COM}}}{\partial t} = [(\alpha(\Lambda) - \zeta(\Theta)) \Delta k_{\text{max}}]. \tag{18}$$

Table 3
Model variables.

Variable	Meaning	Units	Explanation
S	Susceptible pool	people	Non-infected people that may acquire the virus.
E_i^Q	Exposed pool (quarantined)	people	Total quarantined exposed people.
E_i^H	Exposed pool (hidden)	people	Total non-traced, non-quarantined exposed people.
$I_i^{H,s}$	Infectious pool (hidden, symptomatic)	people	Non-traced, non-quarantined people who are symptomatic.
$I_i^{H,a}$	Infectious pool (hidden, asymptomatic)	people	Non-traced, non-quarantined people who are asymptomatic.
I_i^H	Infectious pool (hidden)	people	Total non-traced, non-quarantined infectious people. $I_i^H = I_i^{H,s} + I_i^{H,a}$.
I_i^Q	Infectious pool (quarantined)	people	Total quarantined infectious people.
N_i	New infections (Total, variant i)	cases day ⁻¹	Given by: $N = \gamma k_i R_0 I_i^H + \gamma(v + \epsilon) R_0^i I_i^Q + \frac{\delta}{M} \Phi_i(t)$.
$\hat{N}_{(i)}^{\text{obs}}$	Observed new infections (influx to traced pool, variant i)	cases day ⁻¹	Daily new cases, observed from the quarantined pool; delayed because of imperfect reporting.
K_{POE}	Sequencing rate for samples collected at POEs	samples week ⁻¹	Number of POE samples sequenced per million inhabitants and per week.
K_{COM}	Sequencing rate for samples collected from community contagion	samples week ⁻¹	Number of community samples sequenced per million inhabitants and per week.
D	Variant detection delay	weeks	Time between variant introduction and first detection.

However, as K_{COM} is bounded between a minimum and maximum value, the effective correction could be lowered to ensure that the following inequality holds

$$K_{\text{COM}}^{\min} \leq K_{\text{COM}}(t) \leq K_{\text{COM}}^{\max}. \quad (19)$$

CRedit authorship contribution statement

Sebastian Contreras: Conceptualization, Methodology, Software, Validation, Formal analysis, Investigation, Writing – original draft, Writing – review & editing, Visualization. **Karen Y. Oróstica:** Conceptualization, Validation, Investigation, Writing – original draft, Writing – review & editing. **Anamaria Daza-Sanchez:** Conceptualization, Investigation, Writing – original draft, Writing – review & editing. **Joel Wagner:** Writing – review & editing. **Philipp Dönges:** Methodology, Writing – review & editing. **David Medina-Ortiz:** Software. **Matias Jara:** Software, Validation. **Ricardo Verdugo:** Writing – review & editing. **Carlos Conca:** Conceptualization, Supervision. **Viola Priesemann:** Conceptualization, Writing – review & editing, Supervision. **Álvaro Olivera-Nappa:** Conceptualization, Supervision.

Declaration of competing interest

The authors declare the following financial interests/personal relationships which may be considered as potential competing interests: VP is currently active in various groups to advise the government.

Data availability

Numerical experiments and data analysis of ODEs was performed using MATLAB R2021a and the DMAKit Python library [59]. Code and datasets generated are available in the following github repository: http://github.com/Priesemann-Group/sampling_for_genomic_surveillance.

Acknowledgements

We thank the Priesemann group for exciting discussions and for their valuable input.

Funding

SC, JW, PD, and VP received support from the Max-Planck-Society (Max-Planck-Gesellschaft MPRG-Priesemann). SC, JW, PD, and VP received funding by the German Federal Ministry for Education and Research for the RESPINOW project (031L0298). KYO and RV funding by ANID Chile, projects Rapid-Covid COVID0961 and Anillo ACT210085. AS-D, CC, and AO-N acknowledge funding by the Centre for Biotechnology and Bioengineering — CeBiB (PIA project FB0001, ANID, Chile). DM-O received support from Universidad de Magallanes (MAG-2095 project).

Appendix A. Supplementary data

Supplementary material related to this article can be found online at <https://doi.org/10.1016/j.chaos.2022.113093>.

References

- [1] Stärk Katharina DC, Pekala Agnieszka, Muellner Petra. Use of molecular and genomic data for disease surveillance in aquaculture: Towards improved evidence for decision making. *Prevent Vet Med* 2019;167:190–5.
- [2] Muellner P, Stärk KDC, Dufour S, Zadoks RN. 'Next-generation' surveillance: An epidemiologists' perspective on the use of molecular information in food safety and animal health decision-making. *Zoonoses Public Health* 2016;63(5):351–7.
- [3] Slatko Barton E, Gardner Andrew F, Ausubel Frederick M. Overview of next-generation sequencing technologies. *Curr Protoc Mol Biol* 2018;122(1):e59.
- [4] Besser John, Carleton Heather A, Gerner-Smidt Peter, Lindsey Rebecca L, Trees Eija. Next-generation sequencing technologies and their application to the study and control of bacterial infections. *Clin Microbiol Infect* 2018;24(4):335–41.
- [5] Armstrong Gregory L, MacCannell Duncan R, Taylor Jill, Carleton Heather A, Neuhaus Elizabeth B, Bradbury Richard S, Posey James E, Gwinn Marta. Pathogen genomics in public health. *N Engl J Med* 2019;381(26):2569–80.
- [6] Chen Zhiyuan, Azman Andrew S, Chen Xinhua, Zou Junyi, Tian Yuyang, Sun Ruijia, Xu Xiangyanyu, Wu Yani, Lu Wanying, Ge Shijia, et al. Global landscape of SARS-CoV-2 genomic surveillance and data sharing. *Nature Genet* 2022;54(4):499–507.
- [7] Obermeyer Fritz, Jankowiak Martin, Barkas Nikolaos, Schaffner Stephen F, Pyle Jesse D, Yurkovetskiy Leonid, Bosso Matteo, Park Daniel J, Babadi Mehrta, MacInnis Bronwyn L, et al. Analysis of 6.4 million SARS-CoV-2 genomes identifies mutations associated with fitness. *Science* 2021;abm1208.
- [8] Oróstica Karen Y, Contreras Sebastian, Mohr Sebastian B, Dehning Jonas, Bauer Simon, Medina-Ortiz David, Iftekhar Emil N, Mujica Karen, Covarrubias Paulo C, Ulloa Soledad, et al. Mutational signatures and transmissibility of SARS-CoV-2 Gamma and Lambda variants. 2021, arXiv preprint arXiv:2108.10018.
- [9] Zhu Na, Zhang Dingyu, Wang Wenling, Li Xingwang, Yang Bo, Song Jingdong, Zhao Xiang, Huang Baoying, Shi Weifeng, Lu Roujian, et al. A novel coronavirus from patients with pneumonia in China, 2019. *N Engl J Med* 2020.

- [10] Shu Yuelong, McCauley John. GISAID: Global initiative on sharing all influenza data – from vision to reality. *Eurosurveillance* 2017;22(13).
- [11] Wu Fan, Zhao Su, Yu Bin, Chen Yan-Mei, Wang Wen, Song Zhi-Gang, Hu Yi, Tao Zhao-Wu, Tian Jun-Hua, Pei Yuan-Yuan, et al. A new coronavirus associated with human respiratory disease in China. *Nature* 2020;579(7798):265–9.
- [12] Oude Munnink Bas B, Worp Nathalie, Nieuwenhuijse David F, Sikkema Reina S, Haagmans Bart, Fouchier Ron AM, Koopmans Marion. The next phase of SARS-CoV-2 surveillance: real-time molecular epidemiology. *Nat Med* 2021;27(9):1518–24.
- [13] Oróstica Karen Y, Contreras Sebastian, Sanchez-Daza Anamaria, Fernandez Jorge, Priesemann Viola, Olivera-Nappa Álvaro. New year, new SARS-CoV-2 variant: Resolutions on genomic surveillance protocols to face Omicron. *Lancet Reg Health–Am* 2022;7.
- [14] World Health Organization, et al. Guidance for surveillance of SARS-CoV-2 variants: interim guidance, 9 August 2021. Technical report, World Health Organization; 2021.
- [15] Brito Anderson F, Semenova Elizaveta, Dudas Gytis, Hassler Gabriel W, Kalinich Chaney C, Kraemer Moritz UG, Ho Jose, Tegally Houriiyah, Githinji George, Agoti Charles N, et al. Global disparities in SARS-CoV-2 genomic surveillance. 2021, Medrxiv.
- [16] Cyranoski David. Alarming COVID variants show vital role of genomic surveillance. *Nature* 2021;589(7842):337–8, Bandiera_abtest: a Cg_type: News Number: 7842 Publisher: Nature Publishing Group.
- [17] Malick MShahen S, Fernandes Helen. The genomic landscape of SARS-CoV-2: Surveillance of variants of concern. *Adv Mol Pathol* 2021.
- [18] Bartlow Andrew W, Middlebrook Earl A, Romero Alicia T, Fair Jeanne M. How cooperative engagement programs strengthen sequencing capabilities for biosurveillance and outbreak response. *Front Public Health* 2021;9:163.
- [19] Helmy Mohamed, Awad Mohamed, Mosa Kareem A. Limited resources of genome sequencing in developing countries: challenges and solutions. *Appl Transl Genom* 2016;9:15–9.
- [20] Contreras Sebastian, Dehning Jonas, Mohr Sebastian B, Bauer Simon, Spitzner F Paul, Priesemann Viola. Low case numbers enable long-term stable pandemic control without lockdowns. *Sci Adv* 2021;7(41):eabg2243.
- [21] Contreras Sebastian, Dehning Jonas, Loidolt Matthias, Zierenberg Johannes, Spitzner F Paul, Urrea-Quintero Jorge H, Mohr Sebastian B, Wilczek Michael, Wibrall Michael, Priesemann Viola. The challenges of containing SARS-CoV-2 via test-trace-and-isolate. *Nature Commun* 2021;12(1):1–13.
- [22] Zhao Shi, Lin Qianyin, Ran Jinjun, Musa Salihu S, Yang Guangpu, Wang Weiming, Lou Yijun, Gao Daozhou, Yang Lin, He Daihai, Wang Maggie H. Preliminary estimation of the basic reproduction number of novel coronavirus (2019-nCoV) in China, from 2019 to 2020: A data-driven analysis in the early phase of the outbreak. *Int J Infect Dis* 2020;92:214–7.
- [23] Davies Nicholas G, Abbott Sam, Barnard Rosanna C, Jarvis Christopher I, Kucharski Adam J, Munday James D, Pearson Carl AB, Russell Timothy W, Tully Damien C, Washburne Alex D, Wenseleers Tom, Gimma Amy, Waites William, Wong Kerry LM, Zandvoort Kevin van, Silverman Justin D, Group1 CMMID COVID-19 Working, Consortium COVID-19 Genomics UK (COG-UK), Diaz-Ordaz Karla, Keogh Ruth, Eggo Rosalind M, Funk Sebastian, Jit Mark, Atkins Katherine E, Edmunds W John. Estimated transmissibility and impact of SARS-CoV-2 lineage B.1.1.7 in England. *Science* 2021.
- [24] Torjesen Ingrid. Covid restrictions tighten as omicron cases double every two to three days. *BMJ* 2021;375.
- [25] He Xi, Lau Eric H Y, Wu Peng, Deng Xilong, Wang Jian, Hao Xinxin, Lau Yiu Chung, Wong Jessica Y, Guan Yujuan, Tan Xinghua, et al. Temporal dynamics in viral shedding and transmissibility of COVID-19. *Nat Med* 2020;1–4.
- [26] Pan Feng, Ye Tianhe, Sun Peng, Gui Shan, Liang Bo, Li Lingli, Zheng Dandan, Wang Jiazheng, Hesketh Richard L, Yang Lian, et al. Time course of lung changes on chest CT during recovery from 2019 novel coronavirus (COVID-19) pneumonia. *Radiology* 2020;200370.
- [27] Lavezzo Enrico, Franchin Elisa, Ciavarella Constanze, Cuomo-Dannenburg Gina, Barzon Luisa, Del Vecchio Claudia, Rossi Lucia, Manganelli Riccardo, Loregian Arianna, Navarin Nicolò, et al. Suppression of COVID-19 outbreak in the municipality of Vo, Italy. *Nature* 2020.
- [28] Wilhelm Alexander, Widera Marek, Grikscheit Katharina, Toptan Tuna, Schenk Barbara, Pallas Christiane, Metzler Melinda, Kohmer Niko, Hoehl Sebastian, Helfritz Fabian A, Wolf Timo, Goetsch Udo, Ciesek Sandra. Reduced neutralization of SARS-CoV-2 omicron variant by vaccine sera and monoclonal antibodies. 2021, MedRxiv.
- [29] Bar-On Yonon M, Flamholz Avi, Phillips Rob, Milo Ron. Science Forum: SARS-CoV-2 (COVID-19) by the numbers. *Elife* 2020;9:e57309.
- [30] Li Ruiyun, Pei Sen, Chen Bin, Song Yimeng, Zhang Tao, Yang Wan, Shaman Jeffrey. Substantial undocumented infection facilitates the rapid dissemination of novel coronavirus (SARS-CoV-2). *Science* 2020;368(6490):489–93.
- [31] Brito Anderson F, Semenova Elizaveta, Dudas Gytis, Hassler Gabriel W, Kalinich Chaney C, Kraemer Moritz UG, Ho Jose, Tegally Houriiyah, Githinji George, Agoti Charles N, Matkin Lucy E, Whittaker Charles, Horden Benjamin P, Sintchenko Vitali, Zuckerman Neta S, Mor Orna, Blankenship Heather M, de Oliveira Tulio, Lin Raymond TP, Siqueira Marilda Mendonça, Resende Paola Cristina, Vasconcelos Ana Tereza R, Spilki Fernando R, Aguiar Renato Santana, Alexiev Ivailo, Ivanov Ivan N, Philipova Ivva, Carrington Christine VF, Sahadeo Nikita SD, Gurry Céline, Maurer-Stroh Sebastian, Naidoo Dhamari, von Eije Karin J, Perkins Mark D, van Kerkhove Maria, Hill Sarah C, Sabino Ester C, Pybus Oliver G, Dye Christopher, Bhatt Samir, Flaxman Seth, Suchard Marc A, Grubaugh Nathan D, Baele Guy, Faria Nuno R. Global disparities in SARS-CoV-2 genomic surveillance. 2021, 2021.08.21.21262393, MedRxiv.
- [32] Cypionka Thomas, Iftekhar Emil N, Prainsack Barbara, Priesemann Viola, Bauer Simon, Valdez Andre Calero, Cuschieri Sarah, Glaab Enrico, Grill Eva, Krutzinna Jenny, et al. The benefits, costs and feasibility of a low incidence COVID-19 strategy. *Lancet Reg Health-Eur* 2022;13:100294.
- [33] Prati Gabriele, Mancini Anthony D. The psychological impact of COVID-19 pandemic lockdowns: a review and meta-analysis of longitudinal studies and natural experiments. *Psychol Med* 2021;51(2):201–11.
- [34] COVID The. An integrated national scale SARS-CoV-2 genomic surveillance network. *Lancet Microbe* 2020;1(3):e99.
- [35] Contreras Sebastián, Biron-Lattes Juan Pablo, Villavicencio H Andrés, Medina-Ortiz David, Llanovarcad-Kawles Nyna, Olivera-Nappa Álvaro. Statistically-based methodology for revealing real contagion trends and correcting delay-induced errors in the assessment of COVID-19 pandemic. *Chaos Solitons Fractals* 2020;139:110087.
- [36] Contreras Sebastián, Villavicencio H Andrés, Medina-Ortiz David, Saavedra Claudia P, Olivera-Nappa Álvaro. Real-time estimation of Rt for supporting public-health policies against COVID-19. *Front Public Health* 2020;8:556689.
- [37] Medina-Ortiz David, Contreras Sebastián, Barrera-Saavedra Yasna, Cabas-Mora Gabriel, Olivera-Nappa Álvaro. Country-wise forecast model for the effective reproduction number R t of coronavirus disease. *Front Phys* 2020;8:304.
- [38] Freire-Flores Danton, Llanovarcad-Kawles Nyna, Sanchez-Daza Anamaria, Olivera-Nappa Álvaro. On the heterogeneous spread of COVID-19 in Chile. *Chaos Solitons Fractals* 2021;150:111156.
- [39] Sanchez-Daza Anamaria, Medina-Ortiz David, Olivera-Nappa Alvaro, Contreras Sebastian. COVID-19 modeling under uncertainty: Statistical data analysis for unveiling true spreading dynamics and guiding correct epidemiological management. In: Modeling, control and drug development for COVID-19 outbreak prevention. Cham: Springer International Publishing; 2022, p. 245–82.
- [40] Contreras Sebastian, Olivera-Nappa Álvaro, Priesemann Viola. Rethinking COVID-19 vaccine allocation: it is time to care about our neighbours. *Lancet Reg Health-Eur* 2022;12.
- [41] Smith James A, Judd Jenni. COVID-19: Vulnerability and the power of privilege in a pandemic. *Health Promot J Aust* 2020;31(2):158.
- [42] Petherick Anna, Goldszmidt Rafael, Andrade Eduardo B, Furst Rodrigo, Hale Thomas, Pott Annalena, Wood Andrew. A worldwide assessment of changes in adherence to COVID-19 protective behaviours and hypothesized pandemic fatigue. *Nat Hum Behav* 2021;5(9):1145–60.
- [43] Mena Gonzalo E, Martinez Pamela P, Mahmud Ayesha S, Marquet Pablo A, Buckee Caroline O, Santillana Mauricio. Socioeconomic status determines COVID-19 incidence and related mortality in Santiago, Chile. *Science* 2021;372(6545):eabg5298.
- [44] Snowden Lonnie R, Graaf Genevieve. COVID-19, social determinants past, present, and future, and African Americans' health. *J Racial Ethn Health Dispar* 2021;8(1):12–20.
- [45] González-Puelma Jorge, Aldridge Jacqueline, de Oca Marco Montes, Pinto Mónica, Uribe-Paredes Roberto, Fernandez-Goycoolea Jose, Alvarez-Saravia Diego, Álvarez Hermy, Encina Gonzalo, Weitzel Thomas, Weitzel Thomas, Muñoz Rodrigo, Muñoz Rodrigo, Olivera-Nappa Álvaro, Pantano Sergio, Pantano Sergio, Navarrete Marcelo A. Mutation in a SARS-CoV-2 haplotype from sub-antarctic Chile reveals new insights into the spike's dynamics. *Viruses* 2021.
- [46] Wohl Shirlee, Lee Elizabeth C, DiPrete Bethany L, Lessler Justin. Sample size calculations for variant surveillance in the presence of biological and systematic biases. 2022, MedRxiv.
- [47] Woodbridge Yonatan, Amit Sharon, Huppert Amit, Kopelman Naama M. Viral load dynamics of SARS-CoV-2 Delta and Omicron variants following multiple vaccine doses and previous infection. *Nature Commun* 2020;13(6706).
- [48] Kissler Stephen M, Fauver Joseph R, Mack Christina, Tai Caroline G, Breban Mallory I, Watkins Anne E, Samant Radhika M, Anderson Deverick J, Metti Jessica, Khullar Gaurav, et al. Viral dynamics of SARS-CoV-2 variants in vaccinated and unvaccinated persons. *N Engl J Med* 2021;385(26):2489–91.
- [49] Singanayagam Anika, Haggi Seran, Dunning Jake, Madon Kieran J, Crone Michael A, Koycheva Aleksandra, Derqui-Fernandez Nieves, Barnett Jack L, Whitfield Michael G, Varro Robert, et al. Community transmission and viral load kinetics of the SARS-CoV-2 delta (b. 1.617. 2) variant in vaccinated and unvaccinated individuals in the UK: a prospective, longitudinal, cohort study. *Lancet Infect Dis* 2021.
- [50] Contreras Sebastián, Villavicencio H Andrés, Medina-Ortiz David, Biron-Lattes Juan Pablo, Olivera-Nappa Álvaro. A multi-group SEIRA model for the spread of COVID-19 among heterogeneous populations. *Chaos Solitons Fractals* 2020;136:109925.

- [51] Contreras Sebastian, Dönges Philipp, Wagner Joel, Bauer Simon, Mohr Sebastian B, Dehning Jonas, Iftekhar Emil N, Kretzschmar Mirjam, Maes Michael, Nagel Kai, Valdez André Calero, Priesemann Viola. The winter dilemma. 2021, arXiv preprint [arXiv:2110.01554](https://arxiv.org/abs/2110.01554).
- [52] Dönges Philipp, Wagner Joel, Contreras Sebastian, Iftekhar Emil N, Bauer Simon, Mohr Sebastian B, Dehning Jonas, Calero Valdez André, Kretzschmar Mirjam, Mäs Michael, Nagel Kai, Priesemann Viola. Interplay between risk perception, behavior, and COVID-19 spread. *Front Phys* 2022;10.
- [53] Bauer Simon, Contreras Sebastian, Dehning Jonas, Linden Matthias, Iftekhar Emil, Mohr Sebastian B, Olivera-Nappa Alvaro, Priesemann Viola. Relaxing restrictions at the pace of vaccination increases freedom and guards against further COVID-19 waves. *PLoS Comput Biol* 2021;17(9):e1009288.
- [54] Levina Anna, Priesemann Viola. Subsampling scaling. *Nature Commun* 2017;8(1):1–9.
- [55] Wilting Jens, Priesemann Viola. Inferring collective dynamical states from widely unobserved systems. *Nature Commun* 2018;9(1):1–7.
- [56] Priesemann Viola, Munk Matthias HJ, Wibrál Michael. Subsampling effects in neuronal avalanche distributions recorded in vivo. *BMC Neurosci* 2009;10(1):1–20.
- [57] Wilting Jens, Priesemann Viola. 25 Years of criticality in neuroscience—established results, open controversies, novel concepts. *Curr Opin Neurobiol* 2019;58:105–11.
- [58] Levina Anna, Priesemann Viola, Zierenberg Johannes. Tackling the subsampling problem to infer collective properties from limited data. *Nat Rev Phys* 2022;1–15.
- [59] Medina-Ortiz David, Contreras Sebastián, Quiroz Cristofer, Asenjo Juan A, Olivera-Nappa Álvaro. Dmakit: a user-friendly web platform for bringing state-of-the-art data analysis techniques to non-specific users. *Inf Syst* 2020;93:101557.

Part III

DISCUSSION AND OUTLOOK

*The deeper understanding Faust sought
 Could not from the Devil be bought.
 But now we are told
 By theorists bold
 All we need know is R_0 [89, 90]*

Robert May, 1936–2020

9.1 A TALE OF TIPPING POINTS

When an infectious disease emerges, a reasonable question to ask is whether it can be eradicated or if it comes to stay. Traditionally, one would say: If the basic reproduction number R_0 of the disease is larger than one, there will be exponential growth until reaching $1 - 1/R_0$ of the population (i.e., the point where the effective reproduction number equals one, $R_{\text{eff}} = R_0 \frac{S}{N} = 1$). From that point on, collective immunity will protect as a shield susceptible individuals from being infected through what we call "herd" or "population" immunity. However, can it be that R_0 is all we need to know? Inspired by Robert May's limerick, can a single parameter fully capture the complexity of disease spread? In general, the answer is "no" [89, 90]. So, beyond R_0 , what more is there to know?

In this manuscript, we study the effect of different sources of complexity on disease spread, searching to provide a better characterization of the determinants of stability. To that end, we modified SIR-like models and explored the dynamics resulting from adding non-pharmaceutical interventions, vaccination, and behavioral feedback loops. Although Chapters 4–8 already include dedicated Discussion sections, here we discuss further the physical dimension of our findings and the implications that these have across fields.

9.1.1 *TTI-induced tipping points*

Beyond the tipping point at $R_0 = 1$, we identified two new tipping points in TTI-stabilized systems of disease spread [20, 28], defined by the critical hidden reproduction number R_{crit}^H (equivalently, the critical fraction of contagious contacts k_t^{crit}) and the TTI capacity limit. These tipping points separate regions of conditional stability; if the behavior-driven hidden reproduction number R_t^H surpasses R_{crit}^H (e.g., due to a sudden behavioral change), or the number of observed cases surpasses the TTI capacity (e.g., due to a sudden influx),

stability is lost. From that point on, we observe two modes of exponential growth joined by a faster-than-exponential phase. Regaining control once crossing the first tipping point is challenging; we not only need to adjust the interventions or induce behavioral changes that result in a reduction of R_t^H to values below R_{crit}^H , but also need to lower the incidence to values that are within the handling capacity of health authorities (i.e., below the TTI capacity limit). Here, regaining control denotes a hysteresis loop and can be costly, and there are many analogies to climate-change-induced tipping points (e.g., in [91]). However, as the model in Chapter 4 is linear almost everywhere, only changes in stability could occur; linear systems cannot have limit cycles (as discussed in Chapter 2). Nonetheless, as demonstrated in Section 3.4.3, non-linear variations of this simple model that include TTI as a feedback loop can feature sustained oscillations.

Although the importance of R_{crit}^H is evident, calculating it can be challenging. In Section 3.4, we analytically explored the determinants of R_{crit}^H , and provided formulas to estimate it in special cases (e.g., when isolation is perfect $-\epsilon = 0$). In the general case, R_{crit}^H can be numerically calculated if all other spreading parameters are known. As discussed in Chapter 4, an informed guess on spreading parameters yield reasonable results for R_{crit}^H in the context of stability analysis.

9.1.2 *New mechanistic insights to empirical evidence*

There is empirical evidence for transitions between modes of exponential growth in COVID-19 data for different waves and countries [20, 92, 93]. Our theoretical framework provides a mechanistic pathway to observing this transition between modes of exponential growth or decay in SIR-like models. We illustrate that in the example in Fig. 9.1 (adapted from Contreras et al. [28]). Assuming a behavioral change that drives R_t^H to a value over R_{crit}^H , we observe three markedly different stages in the evolution of case numbers (Fig. 9.1a). First, before the change, case numbers were stable, and thus, the reproduction number $R = 1$. Immediately after the behavioral change, R increases to a first (slow) mode of exponential growth (Fig. 9.1b), which for the parameter values analyzed looks almost exponential. However, after surpassing the TTI capacity, the spread self-accelerates, showing a phase of faster-than-exponential spread. Here, R changes from its first mode to another, faster mode of exponential growth, at which it settles (Fig. 9.1b). We can numerically obtain both asymptotic modes of disease spread using the largest eigenvalue of the linearized system. Regarding eigenvalues, the experiment here corresponds to the path marked with numbers in Fig. 9.1c. Analyzing time series for COVID-19 incidence across countries, we hypothesize that the TTI-induced tipping point was crossed by autumn 2020 (cf. to Fig. 6, Chapter 5 and Fig. S5 in Contreras et al. [20]). However, while we observe the faster-than-exponential transition from stable case numbers to exponential growth, we cannot assure a causal relationship.

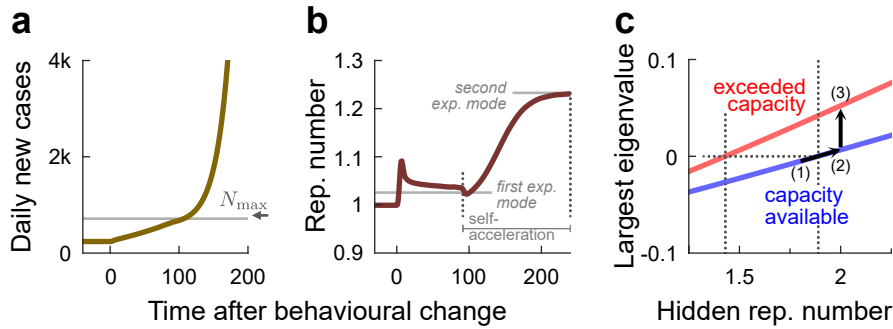


Figure 9.1: **Our model offers a mechanism for different exponential asymptotic modes of exponential growth.** We illustrate the latter by starting from a system at equilibrium and increasing R_t^H to a value slightly above R_{crit}^H . **a:** Three markedly different regimes can be observed: a first mode of exponential growth (almost linear), self-acceleration, and a second mode of exponential growth. These are reflected as plateaus in the observed reproduction number **(b)**. **c:** The trajectory in the example is explained by changes in the largest eigenvalue of the system; below TTI capacity, the largest eigenvalue is on the blue curve, and above, on the red. Figure adapted from [28].

Following the above, could there be more paths to an uncontrolled spread? In the end, the primary requisite for disease spread (from a mean-statistics perspective) is an effective reproduction number larger than one, i.e., that each case effectively infects, on average, more than one other individual. Furthermore, the effective reproduction number can cross the threshold in the event of adverse seasonality or through permanent behavioral changes among the population [13, 14, 22, 24]. The dynamics of combining these two elements in compartmental models are rich and diverse, featuring period-doubling cascades to chaos and parameter sensitivity in epidemiologically feasible parameter ranges [21, 25].

9.2 ENDEMICITY AS A SOCIAL AGREEMENT

Models including waning immunity and human behavior provide a fresh interpretation of the endemic level of a disease, which is not only determined by the spreading parameters but instead emerges as a social agreement [17]. Here, the endemic fixed point (stable or not) captures both properties of the disease (e.g., the basic reproduction number, lasting of immunity, seasonal forcing, severity, and infection fatality risk) and of the population where it spreads (e.g., the mandatory mitigation measures, the contributions to the perceived risk, the memory time, the baseline vaccine hesitancy). Some diseases will be perceived as typical and do not trigger much of a reaction by the general population (e.g., seasonal influenza before the COVID-19 pandemic), and this leads to the paradox of endemic diseases costing orders of magnitude more than rapidly eradicated epidemics [17].

In Chapter 7, we implemented a data-inspired effective bridge between opinion and contact behavior. Using answers from a recurrent survey on COVID-19 behavior [94], we studied how the answers to "how likely are you to avoid private parties" changed over time and compared them to the COVID-19-related hospital burden at the time. This relationship was piece-wise linear (Chapter 7, Fig.2A–C). We then incorporated it into the force of infection so that protective behavior (or mitigation) would not only be characterized by a parameter (e.g., the behavior-driven hidden reproduction number R_t^H) but would also have a mechanism.

Having a mechanism instead of a single parameter for human behavior (e.g., feedback loop vs R_t^H) widens the dynamics that even simple models can represent, as, for example, period doubling cascades to chaos [24, 25]. Simple models that include behavioral feedback and seasonality also show complex dynamics, as demonstrated by Wagner [21], who reported phase-locking, parameter sensitivity, and chaos in an epidemiologically feasible regime. This result challenges the common perception of endemic diseases as steady and predictable.

Both pharmaceutical and non-pharmaceutical interventions can impact a disease's endemic state. In Chapter 7, we saw that after a winter of overprotective restrictions, there was an off-seasonal "rebound" wave (cf. to Scenario 5 in Fig. 4, Chapter 7). Here, the lack of natural infections and incentives to get vaccinated caused the overall immunity to drop, i.e., an *excess susceptibility* among the population. Intuitively, the more susceptibility accumulates in the population, the higher the rebound wave. However, what are the determinants of the rebound waves after a lockdown? First, immunity drops are highly non-linear; we saw that scenarios having slightly fewer restrictions had an over-proportional improvement (cf. to Scenarios 3 and 4 in Fig. 5, Chapter 7). Second, as seasonality modulates the base spread of diseases [19, 95, 96], the moment at which we lift restrictions (and its phase towards adverse seasonality) should have a larger impact. Third, the contributions to the behavioral/mitigation feedback, e.g., when multiple pathogens spread simultaneously and are coupled through the perception of risk.

Indeed, lockdown duration and the time of lifting restrictions (phase towards seasonality) had the strongest effect on rebound waves [55]. Furthermore, these two concepts dominated over other spreading parameters. As long as the reproduction number is high enough to cause a population-scale epidemic and the duration of lockdown is larger than the average duration of immunity, the effect of other parameters such as the recovery rate, spreading rate, waning immunity rate, or latent period is secondary. However, some resonance effects could emerge when considering very short lockdowns (as the "circuit breakers" in Chapter 5). Resonance has also been reported in contact patterns [84] and due to the spacing of mass events such as the UEFA Euro 2020 football championship [88].

Perturbations to the endemic state of a disease can also be caused indirectly by other diseases. Again using COVID-19 as a working example, interventions aiming to curb its spread affected the endemic levels of other diseases. Non-

specific NPIs that affected the contact rates (e.g., lockdowns and curfews [20, 97, 98]) reduced the effective R of COVID-19 but also that of influenza and RSV. Unlike COVID-19 (in most cases), these diseases had a reproduction number below one even in the most adverse seasonality. Hence, the waves were canceled [99–101]. The suppression of these waves caused not only a drop in the rates of naturally acquired immunity but also an excess susceptibility among the population due to waning immunity and vital dynamics (e.g., babies not being exposed to RSV). Complex dynamics can also arise in a multi-pathogen system when, for example, analyzing the simultaneous spread of various diseases coupled through interventions or fear [55].

Altogether, the transition from epidemicity to endemicity in infectious diseases results from the complex interplay between the properties of the disease and the society where it spreads. With this work, we have provided new modeling insights that challenge the perception of endemic diseases as stable or regular cycles.

9.3 ON THE USE OF COMPARTMENTAL MODELS IN DISEASE SPREAD

Why if, as discussed in Chapter 3, contagion is stochastic by nature, are deterministic models one of the most common choices when modeling disease spread? In most cases, when outbreaks reach a population scale, stochastic effects average out, and the mean statistics can be well described by differential equation models as those derived from the pioneering work of Kermack and McKendrick [73]. In this manuscript and related research, we have developed several extensions of the SIR model, including i) additional compartments, to represent TTI [20, 28], to capture heterogeneities and structure in the population [11, 54, 77], and to model the simultaneous spread of different variants [47]), and ii) additional mechanisms, as the behavioral feedback loops and seasonality [11, 102], and the delayed contact tracing in the DDE model in Section 3.4.3.3. Differential equation models are very helpful to obtain analytical insights on the determinants of control and to estimate the mean statistics of an outbreak, e.g., the tipping points described in Chapters 4 and 5, and to describe the evolution of case numbers when incidences are high (e.g., in [78, 103]). However, by construction, these models cannot capture certain expected phenomena such as extinction or super-spreading events in outbreaks.

Population averages obscure the effects of heterogeneity, e.g., highly connected nodes in a contact network which can generate super-spreading events [104]. In particular, individual variation in infectiousness can drastically impact the emergence of infectious diseases, i.e., the probability of an outbreak to succeed [105]. If R_0 instead of being understood as a parameter of a deterministic model but as the mean value of the statistical distribution of individual infectiousness (quantified as the number of offspring infections generated in a fully susceptible population), the initial stages of an outbreak can be described by stochastic processes. Suppose the mean of the distribution is the same and larger than one. On the one hand, outbreaks of diseases whose distributions of infectiousness have heavier tails (i.e., where most of the spread is generated

in super-spreading events) are likelier to die out [105]. On the other hand, besides being likelier to die out naturally, outbreaks of diseases with a broad distribution of individual infectiousness are more sensitive to contact bans and other interventions, as these truncate the individual reproduction number distribution. COVID-19 is a highly overdispersed disease [106], therefore it is no surprise that interventions limiting the number of non-repetitive contacts were more effective than expected [107]. At this point, it results evident to see that there is no magic number from which an outbreak is considered to settle into the population so that stochastic effects average out we can thus change to mean-field description of disease spread. Bridging the scales that both these models can represent depends from disease to disease and remains an open problem in the community.

Agent-Based simulations allow for a more detailed description of the mechanics of contagion through, e.g., incorporating rules of interaction between agents and different contexts plus day/night dynamics [108, 109]. While these models need many parameters to be fitted, the parameters are intuitive and easier to determine in studies. However, Agent Based Model (ABM)s are computation-intensive, as simulation complexity and times scale heavily with the number of agents. Furthermore, the level of detail to be incorporated starts getting arbitrary, and the models are far too complex to allow for a deep understanding of the emergent dynamics. Nonetheless, they are fantastic for understanding emerging phenomena in the microstructure, which can be translated as effective mechanisms in mean-field models (as our feedback loop in [11]). Bobashev et al. [110] proposed a hybrid approach that combines ABMs to start the simulation, and when case numbers cross a threshold incidence, the simulation drifts to an equation-based ODE model. Through this method, they managed to substantially reduce computation costs and capture network properties into the observed dynamics of the ODE model.

As described in Chapter 3, a major drawback of ODE compartmental models is the coupling through first-order kinetics, which translate to an exponential distribution of the residence time in the compartment. Adding more compartments, the exponential distribution can be shifted to an Erlang one at no cost—however, without any noticeable effect in the qualitative dynamics observed (cf. to Section S1.8 in [20] Supplementary Material). Other modifications can be achieved by incorporating mechanistic dependency on the parameters, which can be a function of time or state variables (e.g., feedback loops).

Back to TTI models, Sturniolo et al. [111] demonstrated that an SEIR-TTI model can also capture the relevant features of an outbreak at much less computational cost than ABMs. Consistently, our description of the stability landscape in TTI-stabilized disease spread is in good agreement with other simulation and modeling studies (e.g., ABM with realistic contact structure [29, 112]), stochastic transmission models [113, 114], and other mean-field models with tractable equations [30, 31, 115, 116].

9.4 OUR RESULTS IN CONTEXT: TEN PRINCIPLES FOR DISEASE MITIGATION AND CONTROL

Aiming to better bridge the translation of our results to public health practice, here we summarize their implications into *ten principles*. These principles build on the physics of contagion explored in Chapter 3, and particularly on the findings presented in this manuscript.

Point 1: Mind the tipping points

As discussed previously, the controllability of an outbreak depends not only on the properties of the disease but also on the properties of the population it spreads. Different contact behaviors and cultural patterns can favor or challenge the spread of infectious diseases at the base level. From that point on, interventions move this threshold between controlled and uncontrolled spread and expand the stable regime, allowing for larger hidden reproduction numbers R_t^H so that the new transition is at $R_t^H = R_{crit}^H > 1$. One way to expand the stable regime is through the incorporation of TTI (cf. to Chapters 4 and 5).

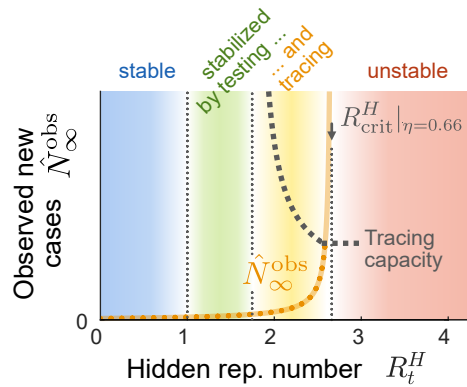


Figure 9.2: **Point 1: Mind the tipping points.** TTI-stabilized systems of disease spread allow for constant case numbers at values of the hidden reproduction number larger than one. This stability can be lost through two tipping points; R_t^H surpassing the critical value R_{crit}^H , or case numbers surpassing the tracing capacity. Figure adapted from [28].

Point 2: Exploit the tipping points

Including NPI largely broadens the possible dynamical regimes observable in simple SIR models. For example, in a linear SIR-TTI model with an external influx, we can observe sub-linear, linear, exponential, and faster-than-exponential variations in case numbers [20, 28, 92]. In particular, between the tipping points described in Point 1 and Chapters 4 and 5, we observe a stable equilibrium at low case numbers, where TTI contains local spread and thereby allows for

more freedom (i.e., larger R_t^H). Exploiting the tipping points is thus planning interventions that will enable us to operate in this regime.

The implications for public health are immense; we provide mathematical representations to plan not only the target incidence levels but also its stability before perturbations. The dynamic system response can also be used to raise early signals; we demonstrated that loss of stability in TTI-stabilized systems looks deceptively linear before self-accelerating. In the end, this dynamic equilibrium is a matter of balance.

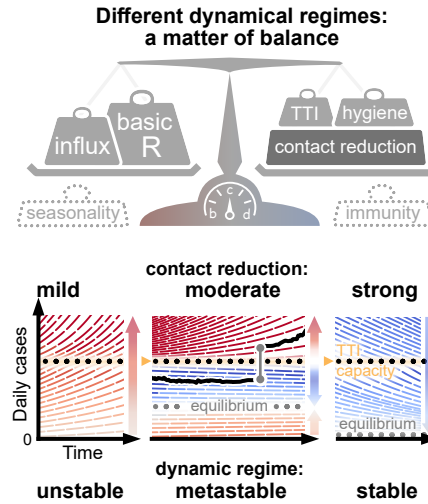


Figure 9.3: **Point 2: Exploit the tipping points.** Between the tipping points described in Point 1, case numbers will approach the stable equilibrium at low case numbers, where TTI promptly breaks chains of hidden contagion and allows for more freedom without costs in stability. Figure adapted from [20].

Point 3: Anticipate your distance to the tipping points

The number of observed cases in equilibrium $\hat{N}_\infty^{\text{obs}}$ is proportional to the influx of infections, but also simultaneously to the inverse of the distance to the tipping point (determined by R_{crit}^H , or equivalently by k_t^{crit} , see equation 1 in Chapter 5): the application of the equations shows that the further away we are, the safer. As schematized in Fig. 9.4, the following applies: i) small increases in the contact level near the tipping point will lead to a considerable increase in $\hat{N}_\infty^{\text{obs}}$ (a). ii) Reducing the influx of infections reduces the number of infections but does not affect the tipping point (b). iii) Only changes in testing and self-reporting, contact tracing, hygiene, and contact patterns, can lead to changes in the tipping point (c and Chapter 3). Altogether, operating at a controlled distance to the tipping point can thus help to create robust mitigation plans.

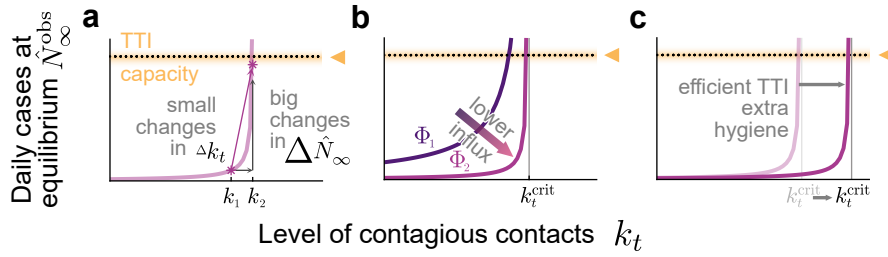


Figure 9.4: **Point 3: Mind the gap between current and critical values for k_t^{crit} (or equivalently R_{crit}^H).** The metastable equilibrium has the same qualitative behavior as systems operating close to criticality (e.g., [43, 45]). **a:** Close to the critical level of contagious contacts k_t^{crit} (equivalently, R_{crit}^H), small changes in k_t generate big changes in $\hat{N}_\infty^{\text{obs}}$. **b:** At a fix value for k_t , reducing the influx reduces $\hat{N}_\infty^{\text{obs}}$, but does not modify k_t^{crit} , which is only affected by structural changes in TTI or other interventions. Figure adapted from [20].

Point 4: Hit early

In the event of an outbreak, early action is crucial [17]. The reasons for this are twofold. First, disease spread (at this stage) is likely to be exponential [20, 28, 92]. Second, as discussed in Sec. 9.1, remaining TTI capacity can mask a much larger mode of exponential growth, which only becomes evident after the spread self-accelerates. Both reasons point to the convenience of stopping an outbreak earlier.

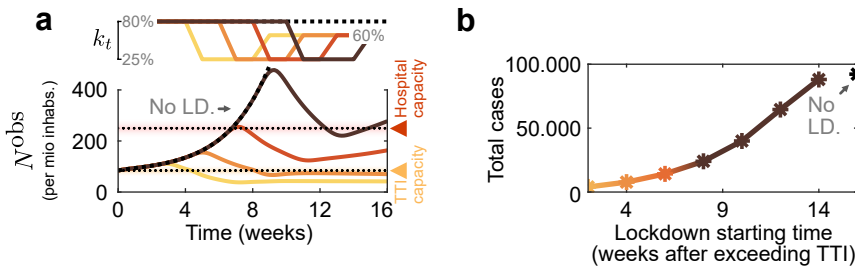


Figure 9.5: **Point 4: Hit early.** **a:** The time at which the same intervention is enacted determines whether it will be sufficient for containment. **b:** Acting late can be as bad as not acting. Figure adapted from [20].

Point 5: Hit hard

In the event of an outbreak, interventions need to be sufficiently strong to counteract the spread of the disease and reduce case numbers. In physical terms, the control parameter (here the hidden reproduction number R_t^H or the level of contagious contacts k_t) needs to be reduced to a point where the largest eigenvalue of the system is negative for a period such that incidence is lowered to a target level. Interventions need to be successful in that regard, given the

costs they imply and the impression they produce among the population; the most vital determinant of their success is people’s compliance with them. In the framework of **TTI**, interventions need to lower the incidence to the levels where we can profit from the conditionally stable regime at low case numbers.

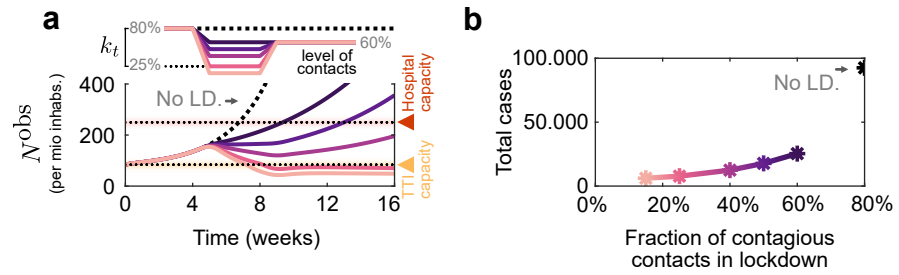


Figure 9.6: **Point 5: hit hard.** **a:** The strength of an intervention determines whether case numbers can be lowered to a point where **TTI** can be efficient. **b:** Stronger lockdowns manage to reduce the total count of cases more drastically, but all slow down the spread. Figure adapted from [20]

Point 6: Plan your interventions

Once you hit, you have to release – interventions will progressively lose adherence, individuals get mentally and economically fatigued by the burden imposed by interventions [34], and ultimately will adapt to the new levels of risk in a dynamical way [11]. Interventions need to be planned to be effective, as short as possible and discussed openly with the population [117–120].

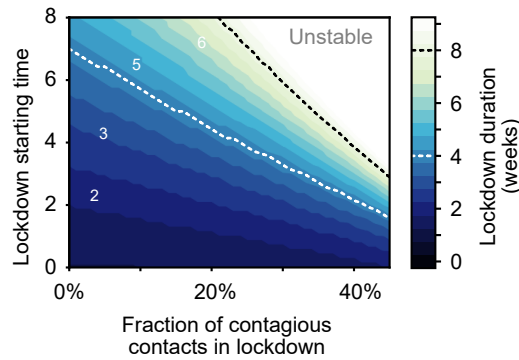


Figure 9.7: **Point 6: Plan your interventions.** The minimal duration and strength required for a lockdown to be effective can be calculated numerically. However, these estimates are rather optimistic, as they do not include the potential loss of adherence or pandemic fatigue that both populations and economies would feel [34]. Figure adapted from [20]

Point 7: Characterize the levels of mixing in the population

As discussed previously, one of the determinants of stability in a system with different pools of infection (e.g., hidden and traced pools in Chapters 4 and 5) was the interaction between them. In a way, it was sufficient to lose stability in one of the pools to lose it in the whole system; the system is as stable as its most unstable component. Putting this statement in epidemiological terms, a population is as well prepared for a pandemic as are its least favored social groups. In our TTI models, cultural factors, such as the possibility to isolate and the compliance to isolation (characterized by parameters ν and ϵ , respectively representing the secondary attack rate and the "leak" of infections), directly challenged containment by reducing R_{crit}^H . In other words, the larger these parameters, the narrower the zone of conditional stability in the parameter space. This effect has been reported in other models considering different levels of mixing in the population, e.g., [121–123]. Preliminary, we have found similar effects relating to household distributions in a country with structural disadvantages for containment (cf. to Fig. 9.8).

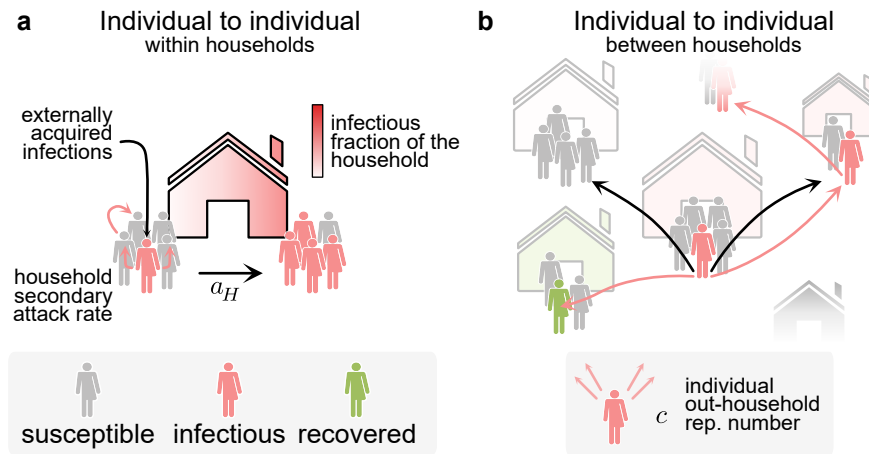


Figure 9.8: **Point 7: Characterize the levels of mixing in the population. a:** Once infections are imported into the household, the spreading dynamics are different; isolation measures are harder to impose, and the spread is bound to the household size. The secondary attack rate a_H captures both properties of the virus (as base transmissibility) and socioeconomic properties of the household. **b:** Individuals can infect households, depending on how connected they are. Figure belongs to a manuscript in preparation, thus rights are reserved.

Point 8: There is not a single "herd immunity"

There is not a single herd immunity; thus, reaching the desired shielding effect in the population may take longer than expected. The idea behind herd immunity is that, at a given point, immune individuals (either by recovering or being vaccinated) would impede disease spread as a shield just by blocking the

chain of contagion. This assumes that the disease had spread homogeneously over the population and that all our contacts somehow respect this proportion of susceptible and recovered individuals. We know that, in real networks, this is not the case. People tend to form clusters of matching behaviors and ideas and, if required, rearrange their contact networks to meet only those with matching patterns. Some examples of that are political opinions, beliefs, and sexual orientation. In the context of the COVID-19 pandemic (and of general epidemics), this also meant clusterization of individuals with, e.g., matching protective behaviors or the same opinion about the vaccine. This heterogeneity is critical; even in the case of, from an average perspective, achieving herd immunity, susceptible bubbles will prevail and could fuel further waves or drive a collapse of the hospital capacity. Models need to account for this (e.g., [54] including an explicit "never vaccinated" compartment). In the event of vaccines not granting full protection against infection, diseases with marked seasonality, rapidly mutating pathogens, or quickly decaying immunity, herd immunity might not be possible at all.

Nonetheless, under the hypotheses of homogeneity, the herd immunity threshold is represented by $1 - \frac{1}{R_0}$. However, the time we would require to achieve it can differ. Assuming a vaccine with perfect protection against infection rolled out at a constant rate of ϕ [% of the population/week], the time required to reach the herd immunity threshold through vaccination would simply be $t_v = \frac{1}{\phi} \left(1 - \frac{1}{R_0}\right)$. Even in a scenario with an all-or-nothing vaccine with partial immunity, t_v is just fractions of a year (cf. to Chapter 6).

We can also estimate the time required to reach herd immunity by natural means if stabilizing at a given incidence, e.g., hospital capacity (cf. to Chapter 5). First, the level at which incidence needs to be stabilized is determined by the infection hospitalization risk, typical residence time in the hospital, and the hospital capacity as:

$$N_{\text{Hosp}}^{\text{obs}} \times \text{Hosp. Risk} \times \text{Res. Time} \approx \text{Hosp. Capacity.}$$

Then, we can estimate the time t_{Hosp} required to reach the target immunity level (i.e., $\left(1 - \frac{1}{R_0}\right)$) as

$$\frac{N_{\text{Hosp}}^{\text{obs}} \times t_{\text{Hosp}}}{\text{Total Population}} \approx \left(1 - \frac{1}{R_0}\right).$$

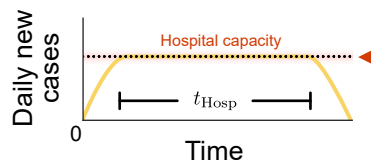


Figure 9.9: **Point 8: There is no single herd immunity.** Here we schematize the time required to reach theoretical herd immunity through natural infection, stabilizing around hospital capacity.

Given that the residence time can be up to months for the severely diseased, this alternative is less appealing. Furthermore and again, the above considers i) homogeneous mixing in the population, ii) a fully protective vaccine, and iii) no variants of the pathogen with immune escape will emerge. The latter is not always the case...

Point 9: Look out for variants

The game of life occurs at all scales. As pathogens are subject to selective pressures (e.g., partial immunity in the host), variants will emerge—the question is just when. With every new person infected (in fact, every time that—for the case of virus—replication occurs), pathogens have a chance to mutate and evolve[124]. New viral variants can take over the previous dominating lineages if equipped with a faster replication, partial immune escape, producing less symptomatic disease, or having longer incubation periods. However, in the absence of genomic surveillance, the emergence, replacement, and simultaneous spread of variants can be masked under the same spreading parameters (cf. to discussions in Chapter 8 and Oróstica et al. [40]). Genomic surveillance programs are thus fundamental for long-lasting disease control.

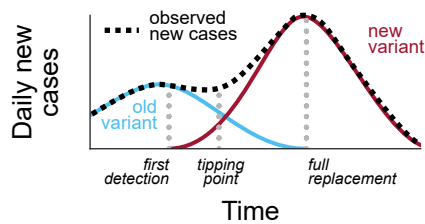


Figure 9.10: **Point 9: Look out for variants.** Genomic surveillance of infectious disease allows for detecting the variant replacement dynamic and reducing the delay between the true emergence/introduction of a variant and the time when their epidemiological consequences are noticeable. Figure adapted from [40].

Point 10: It is not over for us until it is over for all

Although evident in normal times, in the event of an emergency, it is common to make decisions only aiming to maximize the likelihood of survival (or minimizing the discomfort) of ourselves and the ones we care about. This had happened at all scales, from people buying more than they needed [125] to countries hoarding vaccines and medical supplies due to their stronger economies [126, 127]. In our globalized, interconnected world, leaving the least favored behind will only squander progress; variants escaping the current vaccine-elicited immunity can be generated and imported, thereby also losing the gains. Fighting a pandemic requires a global perspective, not only local action, as it can only be over when it is over for us all.

9.5 FUTURE RESEARCH DIRECTIONS

Although many questions were answered with our work, it opened new and interesting ones. Below, we present some questions in the context of the topics explored in this work, classified according to the preliminary time required to find answers to them.

9.5.1 *Short-term research projects*

Regarding test-trace-and-isolate **TTI** policies, given the rich data that has become available during the pandemic, can we find evidence of crossing a **TTI**-induced tipping point in COVID-19 data? This question can be better answered using Bayesian inference models, as that of [88, 103], eventually incorporating behavior through feedback loops as in Chapter 7.

From the theoretical point of view, what are the dynamical regimes observable in a simple **TTI** model with seasonality, where all timescales are similar? (i.e., infectious period \sim contact tracing delay \sim seasonal frequency)? As presented in Section 3.5.1, these models feature delay-induced oscillations through a Hopf bifurcation. There is evidence that systems including mitigation feedback (which can also lead to sustained oscillations through a Hopf bifurcation) present phase-locking and period-doubling cascades to chaos when including seasonality [21, 24, 25]. Therefore, exploring a variation of the minimal **SIR-TTI** model in Section 3.4.3.3 to include seasonality can show new unexpected phenomena.

Another theoretical question that follows the above relates to incorporating behavior through a mitigation feedback in a minimal **SIR-TTI** model. Why is this interesting and promising? As demonstrated in Section 3.4.3.5 for the **SIR-TTI** model and in [21, 25] for a mitigation-feedback model, each mechanism can trigger a Hopf bifurcation. Can it be that, for given hidden reproduction numbers R_t^H , two pairs of characteristic exponents (with different frequencies) coexist? In that case, a co-dimension-two double Hopf bifurcation would emerge as reported in [57] and references therein.

Another, more interesting, way to incorporate human behavior in the **TTI** framework is through "selective" compliance: what if an individual's response to **TTI** (i.e., self-reporting intention and following isolation rules) depended on the perceived risk? Here, we expect another level of complexity, as R_{crit}^H would not be a constant. A model like this could provide more insights into the emergence of endemicity (or just steady levels in case numbers) as a social agreement between risks and freedoms.

Selective compliance can also be translated to dynamic levels of vaccine hesitancy, which can challenge mid-term planning, especially if aiming to lift restrictions at the pace of vaccination. In Chapter 6, we incorporated the possibility of individuals declining a vaccine when offered but assumed that those who would accept the vaccine would do it as scheduled. However, what if, e.g., given an optimistic forecast pointing to declining infections made people less willing to accept a vaccine offer so that there is more susceptibility in the

population than planned? How can we design plans that are robust to these deviations? Once again, simple models incorporating information-dependent vaccination feature rich dynamics, including endemic equilibrium (in diseases that without this dependency would be eradicated) and sustained oscillations through Hopf bifurcations [128].

A major research direction relates to the dynamics of co-circulating diseases when NPIs targeting one of them are in place. How do these NPIs acting over one disease affect the endemic cycle of others? How do these react when lifting the restrictions? Models with several variants or pathogens feature rich dynamics, as synchronization/de-synchronization of wave patterns following the lifting of restrictions [55] and even chaos when externally forced with seasonality [129]. Coupling diseases through fear and mitigation feedback can provide further insights into the emergence of the endemic equilibrium as a social agreement. We will explore this research question in the context of the RESPINOW BMBF-funded consortia (www.respinow.de/en/) in the upcoming years.

Last but not least, one of the major open challenges in disease modeling is capturing properties of the microstructure (e.g., contact networks, spatial heterogeneity, household structures) in simple ODE compartmental models. Is it possible to summarize all these agent-level properties into effective transfer functions that can be incorporated into ODE models for disease spread? Can we expand the theoretical foundations to achieve more realistic dynamics in disease spread model? Advances in this direction will not only advance the state-of-the-art in modeling but also help to increase the reliability of our models.

9.5.2 *Long-term research projects*

The main uncertainty and most fascinating mechanism we studied throughout this manuscript is human behavior, particularly, how we adapt our behavioral patterns (e.g., decisions in routine actions) based on the information we receive and our opinion about it. When individuals are faced with (partial) information about a widely unobserved dynamical system and have to make decisions (which ultimately may affect the system itself), what are the rules? From a long-term perspective, my research aim is to understand how decision-making works in situations where information is partial and the readout of a dynamical system with potentially complex dynamics, e.g., pandemics or climate crises. This requires bridging the fields of psychology [130], epidemiology [9], and physics (neuroscience and network sciences) to capture the drivers and consequences of such decisions. In the context of an emergency, e.g., a pandemic, the complexity in the decisions of "whom to protect", or, in other words, "whom do we care about", separate acts of social altruism from those of mere survival. Understanding the triggers and boundaries of each can provide new metrics of social stability and signal its tipping to social collapse (e.g., riots, plundering, panic buying, hate crime) and social fragmentation. Individual decisions in this context are not only a result of the spread of information (as, e.g., in [131]), but also responding to the levels of risks coupled with disease

dynamics through non-trivial feedback loops. I want to explore the drivers and consequences of decision-making under uncertainty coupled with complex dynamical systems and create a novel modeling framework to study the mean statistical descriptors and phase transitions in such a system.

From a practical point of view, given the current developments in climate crises, war, and political instability, discovering the physical principles that govern decision-making under uncertainty when information is an observed variable resulting from a complex dynamical system is critical. Furthermore, to offer better preparedness for future global health threats, we need to imagine the unimaginable. For example, what if diseases spread over a virtual network (e.g., infectious ideas leading to fanaticism or harming mental health)? How would containment be possible in a world with climate change-induced intermittent logistic disruptions, migrations, and hate? What kind of new pathogens (and spreading mechanisms) can we imagine (e.g., fungi)? Preliminary and complete answers to these questions could be needed sooner than later.

9.6 CLOSING REMARKS

We can find complex dynamics in the spread of infectious diseases. This work expands the state-of-the-art by describing two new tipping points in [TTI](#)-stabilized models and exploring the stability and bifurcations of their equilibria, besides applying them to offer viable alternatives for pandemic control. This contributes to and complements the growing body of literature on the physics of infectious diseases; finding new physics here can inspire new physics elsewhere. In fact, there are marked parallelisms between disease spread and spreading in other well-studied systems, e.g., in neural systems [[45](#), [132–134](#)]. We discussed the advantages of operating close to criticality (instability, in our context), as it maximizes freedom, and provided different arguments why social systems would tend to operate close to this regime as an implicit and self-organized social pact [[17](#), [135](#)].

Incorporating the complexity of human behavior into disease spread models continues to be an open problem [[8](#), [9](#)]; the capricious way we make up our minds has overarching impacts on the outcomes and predictability of real-world spreading phenomena. Instead of this being a defeating and irrevocable truth, it is a message of hope; *the solution is in our hands*. Interventions in the future should aim to harvest this potential for collective action and give us all the chance to do good.

BIBLIOGRAPHY

- [1] Zhen Wang, Chris T Bauch, Samit Bhattacharyya, Alberto d’Onofrio, Piero Manfredi, Matjaž Perc, Nicola Perra, Marcel Salathé, and Dawei Zhao. “Statistical physics of vaccination.” In: *Physics Reports* 664 (2016), pp. 1–113.
- [2] Sebastian Contreras, Jonas Dehning, and Viola Priesemann. “Describing a landscape we are yet discovering.” In: *AStA Advances in Statistical Analysis* (2022), pp. 1–4. DOI: <https://doi.org/10.1007/s10182-022-00449-5>.
- [3] Hans Heesterbeek, Roy M Anderson, Viggo Andreasen, Shweta Bansal, Daniela De Angelis, Chris Dye, Ken TD Eames, W John Edmunds, Simon DW Frost, Sebastian Funk, et al. “Modeling infectious disease dynamics in the complex landscape of global health.” In: *Science* 347.6227 (2015), aaa4339.
- [4] Sebastian Funk, Shweta Bansal, Chris T Bauch, Ken TD Eames, W John Edmunds, Alison P Galvani, and Petra Klepac. “Nine challenges in incorporating the dynamics of behaviour in infectious diseases models.” In: *Epidemics* 10 (2015), pp. 21–25.
- [5] James O Lloyd-Smith, Sebastian Funk, Angela R McLean, Steven Riley, and James LN Wood. “Nine challenges in modelling the emergence of novel pathogens.” In: *Epidemics* 10 (2015), pp. 35–39.
- [6] Ricard Solé, Josep Sardanyés, and Santiago F Elena. “Phase transitions in virology.” In: *Reports on Progress in Physics* 84.11 (2021), p. 115901.
- [7] Joshua S Weitz, Sang Woo Park, Ceyhun Eksin, and Jonathan Dushoff. “Awareness-driven behavior changes can shift the shape of epidemics away from peaks and toward plateaus, shoulders, and oscillations.” In: *Proceedings of the National Academy of Sciences* 117.51 (2020), pp. 32764–32771.
- [8] Sebastian Funk, Marcel Salathé, and Vincent AA Jansen. “Modelling the influence of human behaviour on the spread of infectious diseases: a review.” In: *Journal of the Royal Society Interface* 7.50 (2010), pp. 1247–1256.

- [9] Piero Manfredi and Alberto D’Onofrio. *Modeling the interplay between human behavior and the spread of infectious diseases*. Springer Science & Business Media, 2013.
- [10] AK Misra, Anupama Sharma, and JB Shukla. “Modeling and analysis of effects of awareness programs by media on the spread of infectious diseases.” In: *Mathematical and Computer Modelling* 53.5-6 (2011), pp. 1221–1228.
- [11] Philipp Dönges et al. “Interplay Between Risk Perception, Behavior, and COVID-19 Spread.” In: *Frontiers in Physics* 10 (2022). ISSN: 2296-424X. DOI: [10.3389/fphy.2022.842180](https://doi.org/10.3389/fphy.2022.842180). URL: <https://www.frontiersin.org/article/10.3389/fphy.2022.842180>.
- [12] P Rohani, CJ Green, NB Mantilla-Beniers, and BT Grenfell. “Ecological interference between fatal diseases.” In: *Nature* 422.6934 (2003), pp. 885–888.
- [13] Joshua M Epstein, Jon Parker, Derek Cummings, and Ross A Hammond. “Coupled contagion dynamics of fear and disease: mathematical and computational explorations.” In: *PLoS One* 3.12 (2008), e3955.
- [14] Joshua M Epstein, Erez Hatna, and Jennifer Crodelle. “Triple contagion: a two-fears epidemic model.” In: *Journal of the Royal Society Interface* 18.181 (2021), p. 20210186.
- [15] Alexandra Teslya, Thi Mui Pham, Noortje G Godijk, Mirjam E Kretzschmar, Martin CJ Bootsma, and Ganna Rozhnova. “Impact of self-imposed prevention measures and short-term government-imposed social distancing on mitigating and delaying a COVID-19 epidemic: A modelling study.” In: *PLoS medicine* 17.7 (2020), e1003166.
- [16] Karen Y Oróstica, Sebastian Contreras, Sebastian B Mohr, Jonas Dehning, Simon Bauer, David Medina-Ortiz, Emil N Iftekhar, Karen Mujica, Paulo C Covarrubias, Soledad Ulloa, et al. “Mutational signatures and transmissibility of SARS-CoV-2 Gamma and Lambda variants.” In: *arXiv preprint arXiv:2108.10018* (2021).
- [17] Graham F Medley and Anna Vassall. “When an emerging disease becomes endemic.” In: *Science* 357.6347 (2017), pp. 156–158.
- [18] Nicholas C Grassly and Christophe Fraser. “Seasonal infectious disease epidemiology.” In: *Proceedings of the Royal Society B: Biological Sciences* 273.1600 (2006), pp. 2541–2550.

- [19] Sonia Altizer, Andrew Dobson, Parvies Hosseini, Peter Hudson, Mercedes Pascual, and Pejman Rohani. “Seasonality and the dynamics of infectious diseases.” In: *Ecology letters* 9.4 (2006), pp. 467–484.
- [20] Sebastian Contreras, Jonas Dehning, Sebastian B Mohr, Simon Bauer, F Paul Spitzner, and Viola Priesemann. “Low case numbers enable long-term stable pandemic control without lockdowns.” In: *Science advances* 7.41 (2021), eabg2243.
- [21] Joel Wagner. “On stability, synchronisation and chaos in SIR-like disease models.” Bachelor’s Thesis. Georg-August-Universität Göttingen, Göttingen, Germany, 2022.
- [22] Nico Stollenwerk, Stefano Spaziani, Javier Mar, Irati Eguiguren Arrizabalaga, Damián Knopoff, Nicole Cusimano, Vizda Anam, Akhil Shrivastava, and Maíra Aguiar. “Seasonally forced SIR systems applied to respiratory infectious diseases, bifurcations, and Chaos.” In: *Computational and Mathematical Methods 2022* (2022).
- [23] Miquel Oliu-Barton, Bary SR Pradelski, Philippe Aghion, Patrick Artus, Ilona Kickbusch, Jeffrey V Lazarus, Devi Sridhar, and Samantha Vanderslott. “SARS-CoV-2 elimination, not mitigation, creates best outcomes for health, the economy, and civil liberties.” In: *The Lancet* 397.10291 (2021), pp. 2234–2236.
- [24] Sileshi Sintayehu Sharbayta, Bruno Buonomo, Alberto d’Onofrio, and Tadesse Abdi. “Period doubling induced by optimal control in a behavioral SIR epidemic model.” In: *Chaos, Solitons & Fractals* 161 (2022), p. 112347.
- [25] Alberto d’Onofrio and Piero Manfredi. “Information-related changes in contact patterns may trigger oscillations in the endemic prevalence of infectious diseases.” In: *Journal of Theoretical Biology* 256.3 (2009), pp. 473–478.
- [26] Allison E Aiello, Rebecca M Coulborn, Vanessa Perez, and Elaine L Larson. “Effect of hand hygiene on infectious disease risk in the community setting: a meta-analysis.” In: *American journal of public health* 98.8 (2008), pp. 1372–1381.
- [27] Lorna Fewtrell, Rachel B Kaufmann, David Kay, Wayne Enanoria, Laurence Haller, and John M Colford. “Water, sanitation, and hygiene interventions to reduce diarrhoea in less developed countries: a systematic review and meta-analysis.” In: *The Lancet infectious diseases* 5.1 (2005), pp. 42–52.

- [28] Sebastian Contreras, Jonas Dehning, Matthias Loidolt, Johannes Zierenberg, F Paul Spitzner, Jorge H Urrea-Quintero, Sebastian B Mohr, Michael Wilczek, Michael Wibral, and Viola Priesemann. “The challenges of containing SARS-CoV-2 via test-trace-and-isolate.” In: *Nature communications* 12.1 (2021), pp. 1–13.
- [29] Cliff C Kerr, Dina Mistry, Robyn M Stuart, Katherine Rosenfeld, Gregory R Hart, Rafael C Núñez, Jamie A Cohen, Prashanth Selvaraj, Romesh G Abeysuriya, Michał Jastrzębski, et al. “Controlling COVID-19 via test-trace-quarantine.” In: *Nature communications* 12.1 (2021), p. 2993.
- [30] Mirjam E. Kretzschmar, Ganna Rozhnova, and Michiel van Boven. “Isolation and Contact Tracing Can Tip the Scale to Containment of COVID-19 in Populations With Social Distancing.” English. In: *Frontiers in Physics* 8 (2021). ISSN: 2296-424X. DOI: [10.3389/fphy.2020.622485](https://doi.org/10.3389/fphy.2020.622485). URL: <https://www.frontiersin.org/articles/10.3389/fphy.2020.622485/full> (visited on 03/18/2021).
- [31] Christophe Fraser, Steven Riley, Roy M Anderson, and Neil M Ferguson. “Factors that make an infectious disease outbreak controllable.” In: *Proceedings of the National Academy of Sciences* 101.16 (2004), pp. 6146–6151.
- [32] Johannes Brug, Arja R Aro, and Jan Hendrik Richardus. “Risk perceptions and behaviour: towards pandemic control of emerging infectious diseases: international research on risk perception in the control of emerging infectious diseases.” In: *International Journal of Behavioral Medicine* 16 (2009), pp. 3–6.
- [33] Svenn-Erik Mamelund, Jessica Dimka, and Nan Zou Bakkeli. “Social disparities in adopting non-pharmaceutical interventions during COVID-19 in Norway.” In: *Journal of Developing Societies* 37.3 (2021), pp. 302–328.
- [34] Anna Petherick, Rafael Goldszmidt, Eduardo B Andrade, Rodrigo Furst, Thomas Hale, Annalena Pott, and Andrew Wood. “A worldwide assessment of changes in adherence to COVID-19 protective behaviours and hypothesized pandemic fatigue.” In: *Nature Human Behaviour* 5.9 (2021), pp. 1145–1160.
- [35] Wen-Ying Sylvia Chou and Alexandra Budenz. “Considering emotion in COVID-19 vaccine communication: addressing vaccine hesitancy and fostering vaccine confidence.” In: *Health communication* 35.14 (2020), pp. 1718–1722.

- [36] Sebastian Contreras and Viola Priesemann. “Risking further COVID-19 waves despite vaccination.” In: *The Lancet Infectious Diseases* (2021). DOI: [https://doi.org/10.1016/S1473-3099\(21\)00167-5](https://doi.org/10.1016/S1473-3099(21)00167-5).
- [37] David A Steinhauer and JJ Holland. “Rapid evolution of RNA viruses.” In: *Annual Reviews in Microbiology* 41.1 (1987), pp. 409–431.
- [38] Stephen S Morse. *Factors in the emergence of infectious diseases*. Springer, 2001.
- [39] Gregory L Armstrong, Duncan R MacCannell, Jill Taylor, Heather A Carleton, Elizabeth B Neuhaus, Richard S Bradbury, James E Posey, and Marta Gwinn. “Pathogen genomics in public health.” In: *New England Journal of Medicine* 381.26 (2019), pp. 2569–2580.
- [40] Karen Y Oróstica, Sebastian Contreras, Anamaria Sanchez-Daza, Jorge Fernandez, Viola Priesemann, and Álvaro Olivera-Nappa. “New year, new SARS-CoV-2 variant: Resolutions on genomic surveillance protocols to face Omicron.” In: *The Lancet Regional Health–Americas* 7 (2022).
- [41] Yuelong Shu and John McCauley. “GISAID: Global initiative on sharing all influenza data—from vision to reality.” In: *Euro-surveillance* 22.13 (2017), p. 30494.
- [42] Anna Levina and Viola Priesemann. “Subsampling scaling.” In: *Nature communications* 8.1 (2017), pp. 1–9.
- [43] Jens Wilting and Viola Priesemann. “Inferring collective dynamical states from widely unobserved systems.” In: *Nature communications* 9.1 (2018), pp. 1–7.
- [44] Viola Priesemann, Matthias HJ Munk, and Michael Wibral. “Subsampling effects in neuronal avalanche distributions recorded in vivo.” In: *BMC neuroscience* 10.1 (2009), pp. 1–20.
- [45] Jens Wilting and Viola Priesemann. “25 years of criticality in neuroscience—established results, open controversies, novel concepts.” In: *Current opinion in neurobiology* 58 (2019), pp. 105–111.
- [46] Anna Levina, Viola Priesemann, and Johannes Zierenberg. “Tackling the subsampling problem to infer collective properties from limited data.” In: *Nature Reviews Physics* (2022), pp. 1–15.

- [47] Sebastian Contreras, Karen Y Oróstica, Anamaria Daza-Sanchez, Joel Wagner, Philipp Dönges, David Medina-Ortiz, Matias Jara, Ricardo Verdugo, Carlos Conca, Viola Priesemann, et al. “Model-based assessment of sampling protocols for infectious disease genomic surveillance.” In: *Chaos, Solitons & Fractals* 167 (2023), p. 113093.
- [48] Mohamed Helmy, Mohamed Awad, and Kareem A Mosa. “Limited resources of genome sequencing in developing countries: challenges and solutions.” In: *Applied & translational genomics* 9 (2016), pp. 15–19.
- [49] Anderson F Brito, Elizaveta Semenova, Gytis Dudas, Gabriel W Hassler, Chaney C Kalinich, Moritz UG Kraemer, Joses Ho, Hourriyah Tegally, George Githinji, Charles N Agoti, et al. “Global disparities in SARS-CoV-2 genomic surveillance.” In: *Medrxiv* (2021).
- [50] Zhiyuan Chen, Andrew S Azman, Xinhua Chen, Junyi Zou, Yuyang Tian, Ruijia Sun, Xiangyanyu Xu, Yani Wu, Wanying Lu, Shijia Ge, et al. “Global landscape of SARS-CoV-2 genomic surveillance and data sharing.” In: *Nature genetics* 54.4 (2022), pp. 499–507.
- [51] David Cyranoski. “Alarming COVID variants show vital role of genomic surveillance.” en. In: *Nature* 589.7842 (Jan. 2021). Bandiera_abtest: a Cg_type: News Number: 7842 Publisher: Nature Publishing Group, pp. 337–338. DOI: [10.1038/d41586-021-00065-4](https://doi.org/10.1038/d41586-021-00065-4). URL: <https://www.nature.com/articles/d41586-021-00065-4> (visited on 07/13/2021).
- [52] M Shaheen S Malick and Helen Fernandes. “The Genomic Landscape of SARS-CoV-2: Surveillance of Variants of Concern.” In: *Advances in Molecular Pathology* (2021).
- [53] Andrew W Bartlow, Earl A Middlebrook, Alicia T Romero, and Jeanne M Fair. “How Cooperative Engagement Programs Strengthen Sequencing Capabilities for Biosurveillance and Outbreak Response.” In: *Frontiers in Public Health* 9 (2021), p. 163.
- [54] Simon Bauer, Sebastian Contreras, Jonas Dehning, Matthias Linden, Emil Iftekhar, Sebastian B Mohr, Alvaro Olivera-Nappa, and Viola Priesemann. “Relaxing restrictions at the pace of vaccination increases freedom and guards against further COVID-19 waves.” In: *PLoS computational biology* 17.9 (2021), e1009288.

- [55] Philipp Dönges. “Complex Interactions of Viral Strains under Behavioral Feedback and Cross-Immunity.” Masters’s Thesis. Georg-August-Universität Göttingen, Göttingen, Germany, 2022.
- [56] Steven H Strogatz. “Nonlinear Dynamics and Chaos: With Applications to Physics, Biology, Chemistry, and Engineering.” In: (2018). DOI: <https://doi.org/10.1201/9780429492563>.
- [57] Gábor Orosz. “Hopf bifurcation calculations in delayed systems.” In: *Periodica Polytechnica Mechanical Engineering* 48.2 (2004), pp. 189–200.
- [58] Alan S Perelson. “Modelling viral and immune system dynamics.” In: *Nature reviews immunology* 2.1 (2002), pp. 28–36.
- [59] Alan L Rothman et al. “Dengue: defining protective versus pathologic immunity.” In: *The Journal of clinical investigation* 113.7 (2004), pp. 946–951.
- [60] Rachel Brazil. “How your first brush with COVID warps your immunity.” In: *Nature* 613.7944 (Jan. 2023), pp. 428–430. DOI: [10.1038/d41586-023-00086-1](https://doi.org/10.1038/d41586-023-00086-1). URL: <https://doi.org/10.1038/d41586-023-00086-1>.
- [61] Yair Goldberg, Micha Mandel, Yinon M Bar-On, Omri Bodenheimer, Laurence S Freedman, Eric Haas, Ron Milo, Sharon Alroy-Preis, Nachman Ash, and Amit Huppert. “Waning immunity of the BNT162b2 vaccine: A nationwide study from Israel.” In: *medRxiv* (2021).
- [62] Edward M Hill, Stavros Petrou, Simon de Lusignan, Ivelina Yonova, and Matt J Keeling. “Seasonal influenza: Modelling approaches to capture immunity propagation.” In: *PLoS computational biology* 15.10 (2019), e1007096.
- [63] Santiago F Elena, Ricard V Solé, and Josep Sardanyés. “Simple genomes, complex interactions: epistasis in RNA virus.” In: *Chaos: An Interdisciplinary Journal of Nonlinear Science* 20.2 (2010), p. 026106.
- [64] Michael G Ison, Larisa V Gubareva, Robert L Atmar, John Treanor, and Frederick G Hayden. “Recovery of drug-resistant influenza virus from immunocompromised patients: a case series.” In: *The Journal of infectious diseases* 193.6 (2006), pp. 760–764.
- [65] Christine M Hunt, James M McGill, Marchelle I Allen, and Lynn D Condreay. “Clinical relevance of hepatitis B viral mutations.” In: *Hepatology* 31.5 (2000), pp. 1037–1044.

- [66] Graciela Andrei and Robert Snoeck. “Herpes simplex virus drug-resistance: new mutations and insights.” In: *Current opinion in infectious diseases* 26.6 (2013), pp. 551–560.
- [67] Ewen Callaway. “What Omicron’s BA.4 and BA.5 variants mean for the pandemic.” In: *Nature* 606.7916 (June 2022), pp. 848–849. DOI: [10.1038/d41586-022-01730-y](https://doi.org/10.1038/d41586-022-01730-y). URL: <https://doi.org/10.1038/d41586-022-01730-y>.
- [68] Fritz Obermeyer, Martin Jankowiak, Nikolaos Barkas, Stephen F Schaffner, Jesse D Pyle, Leonid Yurkovetskiy, Matteo Bosso, Daniel J Park, Mehrtash Babadi, Bronwyn L MacInnis, et al. “Analysis of 6.4 million SARS-CoV-2 genomes identifies mutations associated with fitness.” In: *Science* (2021), abm1208.
- [69] Lee Benson, Ross S Davidson, Darren M Green, Andrew Hoyle, Mike R Hutchings, and Glenn Marion. “When and why direct transmission models can be used for environmentally persistent pathogens.” In: *PLoS Computational Biology* 17.12 (2021), e1009652.
- [70] Freja Nordsiek, Eberhard Bodenschatz, and Gholamhossein Bagheri. “Risk assessment for airborne disease transmission by polypathogen aerosols.” In: *PLoS One* 16.4 (2021), e0248004.
- [71] Gholamhossein Bagheri, Birte Thiede, Bardia Hejazi, Oliver Schlenczek, and Eberhard Bodenschatz. “An upper bound on one-to-one exposure to infectious human respiratory particles.” In: *Proceedings of the National Academy of Sciences* 118.49 (2021), e2110117118.
- [72] Robert S McLeod, Christina J Hopfe, Eberhard Bodenschatz, Heinz-Jörn Moriske, Ulrich Pöschl, Tunga Salthammer, Joachim Curtius, Frank Helleis, Jennifer Niessner, Caroline Herr, et al. “A multi-layered strategy for COVID-19 infection prophylaxis in schools: A review of the evidence for masks, distancing, and ventilation.” In: *Indoor air* 32.10 (2022), e13142.
- [73] William Ogilvy Kermack and Anderson G McKendrick. “A contribution to the mathematical theory of epidemics.” In: *Proceedings of the royal society of london. Series A, Containing papers of a mathematical and physical character* 115.772 (1927), pp. 700–721.
- [74] Anamaria Sanchez-Daza, David Medina-Ortiz, Alvaro Olivera-Nappa, and Sebastian Contreras. “COVID-19 Modeling Under

- Uncertainty: Statistical Data Analysis for Unveiling True Spreading Dynamics and Guiding Correct Epidemiological Management.” In: *Modeling, Control and Drug Development for COVID-19 Outbreak Prevention*. Cham: Springer International Publishing, 2022, pp. 245–282. ISBN: 978-3-030-72834-2. DOI: [10.1007/978-3-030-72834-2_9](https://doi.org/10.1007/978-3-030-72834-2_9). URL: https://doi.org/10.1007/978-3-030-72834-2_9.
- [75] Kate M Bubar, Kyle Reinholt, Stephen M Kissler, Marc Lipsitch, Sarah Cobey, Yonatan H Grad, and Daniel B Larremore. “Model-informed COVID-19 vaccine prioritization strategies by age and serostatus.” In: *Science* (2021).
- [76] Sam Moore, Edward M Hill, Michael J Tildesley, Louise Dyson, and Matt J Keeling. “Vaccination and non-pharmaceutical interventions for COVID-19: a mathematical modelling study.” In: *The Lancet Infectious Diseases* (2021). DOI: [https://doi.org/10.1016/S1473-3099\(21\)00143-2](https://doi.org/10.1016/S1473-3099(21)00143-2).
- [77] Sebastián Contreras, H Andrés Villavicencio, David Medina-Ortiz, Juan Pablo Biron-Lattes, and Álvaro Olivera-Nappa. “A multi-group SEIRA model for the spread of COVID-19 among heterogeneous populations.” In: *Chaos, Solitons & Fractals* 136 (2020), p. 109925. ISSN: 0960-0779. DOI: <https://doi.org/10.1016/j.chaos.2020.109925>.
- [78] Danton Freire-Flores, Nyna Llanovarcad-Kawles, Anamaria Sanchez-Daza, and Álvaro Olivera-Nappa. “On the heterogeneous spread of COVID-19 in Chile.” In: *Chaos, Solitons & Fractals* 150 (2021), p. 111156.
- [79] Otilia Boldea, Amir Alipoor, Sen Pei, Jeffrey Shaman, and Ganna Rozhnova. “Age-specific transmission dynamics of SARS-CoV-2 during the first two years of the pandemic.” In: *arXiv preprint arXiv:2212.13470* (2022).
- [80] Mohamed El Khalifi and Tom Britton. “Extending SIRS epidemics to allow for gradual waning of immunity.” In: *arXiv preprint arXiv:2211.09062* (2022).
- [81] Davin Lunz, Gregory Batt, and Jakob Ruess. “To quarantine, or not to quarantine: A theoretical framework for disease control via contact tracing.” In: *Epidemics* 34 (2021), p. 100428.
- [82] Hildeberto Jardón-Kojakhmetov, Christian Kuehn, Andrea Pugliese, and Mattia Sensi. “A geometric analysis of the SIR, SIRS and

- SIRWS epidemiological models.” In: *Nonlinear Analysis: Real World Applications* 58 (2021), p. 103220.
- [83] Jan C Budich and Emil J Bergholtz. “Synchronization in epidemic growth and the impossibility of selective containment.” In: *Mathematical Medicine and Biology: A Journal of the IMA* 38.4 (Oct. 2021), pp. 467–473. ISSN: 1477-8602. DOI: [10.1093/imamb/dqab013](https://doi.org/10.1093/imamb/dqab013). eprint: <https://academic.oup.com/imamb/article-pdf/38/4/467/41324957/dqab013.pdf>. URL: <https://doi.org/10.1093/imamb/dqab013>.
- [84] Johannes Zierenberg, F Paul Spitzner, Viola Priesemann, Martin Weigel, and Michael Wilczek. “How contact patterns destabilize and modulate epidemic outbreaks.” In: *arXiv preprint arXiv:2109.12180* (2021).
- [85] Federico Vazquez. “Opinion dynamics on coevolving networks.” In: *Dynamics On and Of Complex Networks, Volume 2: Applications to Time-Varying Dynamical Systems* (2013), pp. 89–107.
- [86] Nathalie Stroeymeyt, Anna V Grasse, Alessandro Crespi, Danielle P Mersch, Sylvia Cremer, and Laurent Keller. “Social network plasticity decreases disease transmission in a eusocial insect.” In: *Science* 362.6417 (2018), pp. 941–945.
- [87] Alun L Lloyd and Robert M May. “Spatial heterogeneity in epidemic models.” In: *Journal of theoretical biology* 179.1 (1996), pp. 1–11.
- [88] Jonas Dehning, Sebastian B. Mohr, Sebastian Contreras, Philipp Dönges, Emil N. Iftexhar, Oliver Schulz, Philip Bechtle, and Viola Priesemann. “Impact of the Euro 2020 championship on the spread of COVID-19.” In: *Nature Communications* 14.1 (2023), p. 122. ISSN: 2041-1723. DOI: [10.1038/s41467-022-35512-x](https://doi.org/10.1038/s41467-022-35512-x). URL: <https://doi.org/10.1038/s41467-022-35512-x>.
- [89] Roy M Anderson and Robert M May. “Population biology of infectious diseases: Part I.” In: *Nature* 280.5721 (1979), pp. 361–367.
- [90] Chris T Bauch. “Estimating the COVID-19 R number: a bargain with the devil?” In: *The Lancet Infectious Diseases* 21.2 (2021), pp. 151–153.
- [91] Peter Ditlevsen and Susanne Ditlevsen. “Warning of a forthcoming collapse of the Atlantic meridional overturning circulation.” In: *Research Square* (2022), rs.3.rs-2034845.

- [92] Induja Pavithran and RI Sujith. “Extreme COVID-19 waves reveal hyperexponential growth and finite-time singularity.” In: *Chaos: An Interdisciplinary Journal of Nonlinear Science* 32.4 (2022), p. 041104.
- [93] Matthias Linden, Sebastian B. Mohr, Jonas Dehning, Jan Mohring, Michael Meyer-Hermann, Iris Pigeot, Anita Schöbel, and Viola Priesemann. “Case numbers beyond contact tracing capacity are endangering the containment of COVID-19.” In: *Dtsch Arztebl International* 117.46 (2020), pp. 790–791. DOI: [10.3238/arztebl.2020.0790](https://doi.org/10.3238/arztebl.2020.0790).
- [94] Cornelia Betsch, Lothar H Wieler, and Katrine Habersaat. “Monitoring behavioural insights related to COVID-19.” In: *The Lancet* 395.10232 (2020), pp. 1255–1256.
- [95] Miyu Moriyama, Walter J Hugentobler, and Akiko Iwasaki. “Seasonality of respiratory viral infections.” In: *Annual review of virology* 7 (2020).
- [96] Tomáš Gavenčiak, Joshua Teperowski Monrad, Gavin Leech, Mrinank Sharma, Sören Mindermann, Jan Marcus Brauner, Samir Bhatt, and Jan Kulveit. “Seasonal variation in SARS-CoV-2 transmission in temperate climates.” In: *medRxiv* (2021). DOI: [10.1101/2021.06.10.21258647](https://doi.org/10.1101/2021.06.10.21258647). eprint: <https://www.medrxiv.org/content/early/2021/06/13/2021.06.10.21258647.full.pdf>. URL: <https://www.medrxiv.org/content/early/2021/06/13/2021.06.10.21258647>.
- [97] Mrinank Sharma et al. “Understanding the effectiveness of government interventions in Europe’s second wave of COVID-19.” en. In: *medRxiv* (Mar. 2021), p. 2021.03.25.21254330. DOI: [10.1101/2021.03.25.21254330](https://doi.org/10.1101/2021.03.25.21254330). URL: <https://www.medrxiv.org/content/10.1101/2021.03.25.21254330v1> (visited on 06/01/2021).
- [98] Jan M. Brauner et al. “Inferring the effectiveness of government interventions against COVID-19.” en. In: *Science* (2020). ISSN: 0036-8075, 1095-9203. DOI: [10.1126/science.abd9338](https://doi.org/10.1126/science.abd9338). URL: <https://science.sciencemag.org/content/early/2020/12/15/science.abd9338> (visited on 01/30/2021).
- [99] Jong-Hun Kim, Yun Ho Roh, Jong Gyun Ahn, Min Young Kim, Kyungmin Huh, Jaehun Jung, and Ji-Man Kang. “Respiratory syncytial virus and influenza epidemics disappearance in Korea

- during the 2020–2021 season of COVID-19.” In: *International Journal of Infectious Diseases* 110 (2021), pp. 29–35.
- [100] Philip N Britton, Nan Hu, Gemma Saravanos, Jane Shrapnel, Jake Davis, Tom Snelling, Jacqui Dalby-Payne, Alison M Kesson, Nicholas Wood, Kristine Macartney, et al. “COVID-19 public health measures and respiratory syncytial virus.” In: *The Lancet Child & Adolescent Health* 4.11 (2020), e42–e43.
- [101] Zhe Zheng, Virginia E Pitzer, Eugene D Shapiro, Louis J Bont, and Daniel M Weinberger. “Estimation of the timing and intensity of reemergence of respiratory syncytial virus following the COVID-19 pandemic in the US.” In: *JAMA network open* 4.12 (2021), e2141779–e2141779.
- [102] Sebastian Contreras et al. “The winter dilemma.” In: *arXiv preprint arXiv:2110.01554* (2021). arXiv: [2110.01554](https://arxiv.org/abs/2110.01554) [q-bio.PE].
- [103] Jonas Dehning, Johannes Zierenberg, F Paul Spitzner, Michael Wibral, Joao Pinheiro Neto, Michael Wilczek, and Viola Priesemann. “Inferring change points in the spread of COVID-19 reveals the effectiveness of interventions.” In: *Science* (2020).
- [104] Maksim Kitsak, Lazaros K Gallos, Shlomo Havlin, Fredrik Liljeros, Lev Muchnik, H Eugene Stanley, and Hernán A Makse. “Identification of influential spreaders in complex networks.” In: *Nature physics* 6.11 (2010), pp. 888–893.
- [105] James O Lloyd-Smith, Sebastian J Schreiber, P Ekkehard Kopp, and Wayne M Getz. “Superspreading and the effect of individual variation on disease emergence.” In: *Nature* 438.7066 (2005), pp. 355–359.
- [106] Akira Endo, Sam Abbott, Adam J Kucharski, Sebastian Funk, and Others. “Estimating the overdispersion in COVID-19 transmission using outbreak sizes outside China.” In: *Wellcome Open Research* 5.67 (2020), p. 67.
- [107] Kim Sneppen, Bjarke Frost Nielsen, Robert J Taylor, and Lone Simonsen. “Overdispersion in COVID-19 increases the effectiveness of limiting nonrepetitive contacts for transmission control.” In: *Proceedings of the National Academy of Sciences* 118.14 (2021), e2016623118.
- [108] Liliana Perez and Suzana Dragicevic. “An agent-based approach for modeling dynamics of contagious disease spread.” In: *International journal of health geographics* 8.1 (2009), pp. 1–17.

- [109] Cliff C Kerr, Robyn M Stuart, Dina Mistry, Romesh G Abey-suriya, Katherine Rosenfeld, Gregory R Hart, Rafael C Núñez, Jamie A Cohen, Prashanth Selvaraj, Brittany Hagedorn, et al. “Covasim: an agent-based model of COVID-19 dynamics and interventions.” In: *PLOS Computational Biology* 17.7 (2021), e1009149.
- [110] Georgiy V Bobashev, D Michael Goedecke, Feng Yu, and Joshua M Epstein. “A hybrid epidemic model: combining the advantages of agent-based and equation-based approaches.” In: *2007 winter simulation conference*. IEEE. 2007, pp. 1532–1537.
- [111] Simone Sturniolo, William Waites, Tim Colbourn, David Manheim, and Jasmina Panovska-Griffiths. “Testing, tracing and isolation in compartmental models.” In: *PLoS computational biology* 17.3 (2021), e1008633.
- [112] Adam J Kucharski et al. “Early dynamics of transmission and control of COVID-19 : a mathematical modelling study.” In: *The lancet infectious diseases* (2020).
- [113] Joel Hellewell et al. “Feasibility of controlling COVID-19 outbreaks by isolation of cases and contacts.” In: *The Lancet Global Health* (2020).
- [114] Mirjam E Kretzschmar, Ganna Rozhnova, Martin CJ Bootsma, Michiel van Boven, Janneke HHM van de Wiggert, and Marc JM Bonten. “Impact of delays on effectiveness of contact tracing strategies for COVID-19: a modelling study.” In: *The Lancet Public Health* 5.8 (2020), e452–e459.
- [115] Luca Ferretti, Chris Wymant, Michelle Kendall, Lele Zhao, Anel Nurtay, Lucie Abeler-Dörner, Michael Parker, David Bonsall, and Christophe Fraser. “Quantifying SARS-CoV-2 transmission suggests epidemic control with digital contact tracing.” In: *Science* 368.6491 (2020).
- [116] Peter Ashcroft, Sonja Lehtinen, and Sebastian Bonhoeffer. “Test-trace-isolate-quarantine (TTIQ) intervention strategies after symptomatic COVID-19 case identification.” In: *PloS one* 17.2 (2022), e0263597.
- [117] Emil Nafis Iftekhar et al. “A look into the future of the COVID-19 pandemic in Europe: an expert consultation.” In: *The Lancet Regional Health - Europe* 8 (2021), p. 100185. ISSN: 2666-7762. DOI: <https://doi.org/10.1016/j.lanep.2021.100185>. URL:

<https://www.sciencedirect.com/science/article/pii/S2666776221001629>.

- [118] Viola Priesemann, Melanie M Brinkmann, Sandra Ciesek, Sarah Cuschieri, Thomas Czypionka, Giulia Giordano, Deepti Gurdasani, Claudia Hanson, Niel Hens, Emil Iftekhar, et al. “Calling for pan-European commitment for rapid and sustained reduction in SARS-CoV-2 infections.” In: *The lancet* 397.10269 (2021), pp. 92–93.
- [119] Viola Priesemann et al. “Calling for pan-European commitment for rapid and sustained reduction in SARS-CoV-2 infections.” In: *The Lancet* (2020).
- [120] Viola Priesemann, Rudi Balling, Melanie M Brinkmann, Sandra Ciesek, Thomas Czypionka, Isabella Eckerle, Giulia Giordano, Claudia Hanson, Zdenek Hel, Pirta Hotulainen, et al. “An action plan for pan-European defence against new SARS-CoV-2 variants.” In: *The Lancet* 397.10273 (2021), pp. 469–470.
- [121] Frank Ball, Denis Mollison, and Gianpaolo Scalia-Tomba. “Epidemics with two levels of mixing.” In: *The Annals of Applied Probability* (1997), pp. 46–89.
- [122] Thomas House and Matt J Keeling. “Deterministic epidemic models with explicit household structure.” In: *Mathematical biosciences* 213.1 (2008), pp. 29–39.
- [123] T House and MJ Keeling. “Household structure and infectious disease transmission.” In: *Epidemiology & Infection* 137.5 (2009), pp. 654–661.
- [124] Robin N Thompson, Edward M Hill, and Julia R Gog. “SARS-CoV-2 incidence and vaccine escape.” In: *The Lancet Infectious diseases* 21.7 (2021), pp. 913–914.
- [125] Steven Taylor. “The psychology of pandemics.” In: *Annual review of clinical psychology* 18 (2022), pp. 581–609.
- [126] Sam Moore, Edward M Hill, Louise Dyson, Michael J Tildesley, and Matt J Keeling. “Retrospectively modeling the effects of increased global vaccine sharing on the COVID-19 pandemic.” In: *Nature Medicine* (2022), pp. 1–8.
- [127] Sebastian Contreras, Álvaro Olivera-Nappa, and Viola Priesemann. “Rethinking COVID-19 vaccine allocation: it is time to care about our neighbours.” In: *The Lancet Regional Health–Europe* 12 (2022).

- [128] Alberto d’Onofrio, Piero Manfredi, and Ernesto Salinelli. “Vaccinating behaviour, information, and the dynamics of SIR vaccine preventable diseases.” In: *Theoretical population biology* 71.3 (2007), pp. 301–317.
- [129] Masashi Kamo and Akira Sasaki. “The effect of cross-immunity and seasonal forcing in a multi-strain epidemic model.” In: *Physica D: Nonlinear Phenomena* 165.3-4 (2002), pp. 228–241.
- [130] Leonid I Perlovsky. “Toward physics of the mind: Concepts, emotions, consciousness, and symbols.” In: *Physics of Life Reviews* 3.1 (2006), pp. 23–55.
- [131] Dmitriy Tsarev, Anastasiia Trofimova, Alexander Alodjants, and Andrei Khrennikov. “Phase transitions, collective emotions and decision-making problem in heterogeneous social systems.” In: *Scientific reports* 9.1 (2019), p. 18039.
- [132] Roxana Zeraati, Viola Priesemann, and Anna Levina. “Self-organization toward criticality by synaptic plasticity.” In: *Frontiers in Physics* 9 (2021), p. 619661.
- [133] Johannes Zierenberg, Jens Wilting, and Viola Priesemann. “Homeostatic Plasticity and External Input Shape Neural Network Dynamics.” In: *Physical Review X* 8.3 (July 2018), p. 031018.
- [134] Jens Wilting and Viola Priesemann. “25 years of criticality in neuroscience—established results, open controversies, novel concepts.” In: *Current opinion in neurobiology* 58 (2019), pp. 105–111.
- [135] Dirk Helbing, Dirk Brockmann, Thomas Chadeaux, Karsten Donnay, Ulf Blanke, Olivia Woolley-Meza, Mehdi Moussaid, Anders Johansson, Jens Krause, Sebastian Schutte, et al. “Saving human lives: What complexity science and information systems can contribute.” In: *Journal of statistical physics* 158 (2015), pp. 735–781.